PcrA function in plasmid replication

Thesis submitted in accordance with the requirements of the

University College London, UCL

Liisa Tellervo Chisty

Student No. 831056

Ph.D. thesis for programme in Structural, Chemical and Computational Biology

Division of Physical Biochemistry

National Institute for Medical Research

Mill Hill

London

NW7 1AA

I, Liisa Tellervo Chisty, confirm that the work presented in this thesis is my own. Where information has been derived from other sources, I confirm that this has been indicated in the thesis.

_____

Acknowledgements

Firstly, I would like to thank my primary supervisor, Dr. Martin Webb, for his patience, guidance and shared knowledge during my PhD. Also, I would like to thank my co-supervisor, Dr. Justin Molloy, for his support during my PhD and especially for the practical help with TIRF microscopy and analysis of the single molecule data.

I would like to thank my thesis committee that included Dr. Martin Webb, Dr. Justin Molloy and Prof. Bonnie Wallace for their advice at different stages of my PhD.

I would like to thank everybody in the Webb lab for encouragement and support and for making various biosensors required during the experiments.

I would like to thank my sons, Aaron and Musa, for their unconditional love and understanding. I would also like to thank my parents and family for their care and love.

I would like to dedicate this thesis to my sons, Aaron and Musa.

Abstract

PcrA is a DNA helicase involved in unwinding plasmids as a part of a complex in asymmetric rolling-circle replication of certain plasmids carrying antibiotic resistance genes. PcrA translocates on single stranded DNA by coupling ATP hydrolysis to movement on DNA. Initiator protein, RepD is required to nick supercoiled plasmid site-specifically and open an ssDNA stretch that PcrA can bind. The presence of RepD is needed throughout plasmid unwinding to maintain processivity.

Using fluorescent-based techniques, PcrA helicase mechanistic functions and interactions with different components of the replication complex were examined at the ensemble and single molecule level. The development of ensemble techniques included labelling of PcrA with environment sensitive fluorophores such as the coumarin derivative, MDCC. Using MDCC-PcrA(K138C) a translocation assay was developed, which determined that PcrA translocates two times faster on dC (500 bases s^{-1}) than on dT oligos (240 bases s^{-1}). MDCC-PcrA(E449C) was used to investigate the PcrA and RepD interaction. The signal observed with this and other labelled PcrA mutants indicated that the 2B subdomain of PcrA is likely to be interaction site between PcrA and RepD. MDCC-PcrA(E449C) enabled the determination of PcrA kinetics with the initiation complex and showed that ATP-PcrA binds differently to PcrA to RepD-DNA complex as compared to apo PcrA, possibly indicating that ATP binding stabilises PcrA in a specific conformation when binding to RepD-DNA.

A single-molecule assay was developed to study individual surface-bound PcrA helicases unwinding full length plasmids by total internal reflection fluorescence microscopy. PcrA unwinds plasmid with the average rate of 40-50 bp s^{-1} showing 10-fold variation between the individual helicases. The experiments indicated that the unwinding starts almost immediately after addition of ATP. The single molecule experiments with fluorophore-labelled biotinylated PcrA so clear indication that PcrA unwinds

plasmids as a monomer with processivity over 3000 base pairs. The comparison of the ssDNA translocation rate and dsDNA unwinding rates showed a significant difference between the two forms of translocation, which indicated PcrA to be a passive helicase. This means that PcrA is not actively destabilising the hydrogen bonding between DNA bases but taking advantage of the thermal fluctuation between the base pairs and so leading to separation of component DNA strands.

Abbreviations

AAA+	ATPases Associated with various cellular Activities
ADP	Adenosine disphosphate
ASPT	Automatic Single Particle Tracking
ATP	Adenosine triphosphate
bioPcrA	Biotinylated PcrA
bp	Base pair
Cy3B-bioPcrA	Cy3B-labelled biotinylated PcrA(E449C)
Cy3B-SSB	Cy3B-labelled SSB(W88C)
Da	Dalton
dA_x	Deoxyadenosine oligo of x number of dA bases
dC_x	Deoxycytodine oligo of x number of dC bases
DCC	IDCC,*N*-[2-(iodoacetamido)ethyl]-7-diethylaminocoumarin-3-carboxamide
DCC-SSB	IDCC-labelled SSB(G26C)
dG_x	Deoxyguanosine oligo of x number of dG bases
DNA	Deoxyribonucleic acid
dT_x	Deoxythymidine oligo of x number of dT bases
DTNB	Dithionitrobenzoic acid, Ellman's reagent
dsDNA	Double stranded DNA
EDTA	Ethylenediaminetetraacetic acid
EMCCD	Electron multiplying charge coupled device
FPLC	Fast protein liquid chromatography
FRET	Förster resonance energy transfer
HPLC	High performance liquid chromatography
ICR	Inverted complementary repeat
IPTG	Isopropyl-beta-D-thiogalactopyranoside
MDCC	*N*-[2-(1-maleimidyl)ethyl]-7-diethylaminocoumarin-3-carboxamide
MDCC-PBP	MDCC-labelled PBP(A197C)
MS photobleaching	Multiple step photobleaching
NA	Numerical aperture
NHS	*N*-hydroxysuccimide ester
nt	Nucleotide
NTP	Nucleotide triphosphate
P_i	Inorganic phosphate
PBP	Phosphate binding protein
PCR	Polymerase chain reaction
PcrA	Plasmid copy number reduction A (a helicase)
PEG	Polyethylene glycol
RNA	Ribonucleic acid
SEC-MALS	Size exclusion chromatography- multi angle light scattering
SEM	Standard error of the mean
SFDA	Single Fluorophore Detection Algorithm
SS photobleaching	Single step photobleaching
ssDNA	Single stranded DNA
SSB	Single stranded DNA binding protein
ssiA/B	Single stranded origin of replication of RSF1010 plasmid
SSO	Single stranded origin of replication
TIRFM	Total internal reflection fluorescence microscopy

Table of Contents

Table of Figures

Table of Tables

Introduction

1.1. DNA replication

All genetic material required for inheritance of any one character of an organism is carried as genes, which are made of deoxyribonucleic acid (DNA). DNA is formed of two polynucleotide chains made from four bases: thymine (T), adenine (A), cytosine (C) and guanine (G). These are paired with each other by hydrogen bonding to form a double helical structure. The A bases pair with T bases through two hydrogen bonds and the G bases pair with C bases through three hydrogen bonds (A·T and G·C base pairs). The structure of DNA was discovered by Watson and Crick in the 1950s [1, 2]. The base-pairing principle of DNA itself suggested how genetic material may be duplicated from one generation to the next by possible synthesis of the new strands from the two old strands [3]. Since the discovery of the DNA structure, the DNA replication was shown to be semiconservative, whereby the new DNA is formed from one old and one newly replicated DNA strand, in which the new strand has been copied from the old.

DNA replication can be divided into three distinct phases, which are initiation, DNA synthesis and termination. All three steps require the replication machinery formed of specific proteins and enzymes (Figure 1). In bacteria, where the genomic DNA replication is best understood, DNA replication is initiated by multimeric origin-binding proteins that recognise a unique DNA sequence called the origin of replication. They bind to it and melt the double-stranded DNA (dsDNA). Most genomic DNA has multiple origins of replication, where the replication can be initiated simultaneously. Typically, the origins of replication are AT rich. This is thought to be a requirement for initiation to be energy efficient as the A·T base pairing has two hydrogen bonds whereas the G·C base pairs have three. Melting of DNA allows a helicase and other replication complex proteins to bind, unwind DNA, and start the synthesis of new complementary strands. In *Escherichia*

coli, the origin of replication is DNA segment of ~240 bp called *oriC*. The *oriC* is recognised by DnaA protein, which facilitates the initial melting of dsDNA. The further separation of dsDNA is performed by a hexameric ring helicase, DnaB. DnaB helicase utilises ATP to move on DNA in a 5'-to-3' direction. The replication starts on both strands' in 5'-to-3' direction forming a replication bubble. Figure 1 shows one side of the replication bubble. Similar process takes places on the other side of replication bubble. This means that the genomic DNA replication is bidirectional. A topoisomerase enzyme moves in front of the replication fork removing the supercoiling of the DNA. Single-stranded DNA binding protein (SSB) binds the single-stranded DNA (ssDNA), produced by the helicase, to prevent them from reannealing or forming secondary structures. RNA polymerases called primases synthesise ~10 nucleotide RNA primers of for DNA polymerases. All DNA polymerases are able to only synthesise DNA in 5'-to-3' direction and require a primer with a free 3' end of DNA to begin the synthesis of the new daughter strands. The leading strand synthesis requires only one primer. The replication of lagging strand runs in an opposite direction (Figure 1) and is synthesised discontinuously in segments due to DNA polymerase property of synthesising DNA only 5'-to-3' direction. Hence, lagging strand synthesis requires many primers. The DNA segments produced in lagging strand synthesises are called Okazaki fragments. The Okazaki fragments are between 1000 to 2000 bases long in *E. coli* and in comparison to eukaryotes these are longer as the Okazaki fragments are 100 to 200 bases long in eukaryotes [4, 5]. In *E. coli,* the leading and lagging strands are primarily synthesised by DNA polymerase III. The RNA primers are removed and the gaps are filled by the DNA polymerase I as it also has 5'-to-3' exonuclease activity. The Okazaki fragments are then joined together by DNA ligase.

Most of the early information of DNA replication comes from work done in bacteria such as *E. coli* and the eukaryotic DNA replication, which is significantly more complex, contains all the components mentioned here for bacterial replication. For example, the eukaryotic DNA polymerases α and δ correspond to bacterial DNA polymerases I and III. The unravelling of DNA replication machinery through research is a great example of how bacterial

work has simplified the study of an essential process taking place in all organisms.

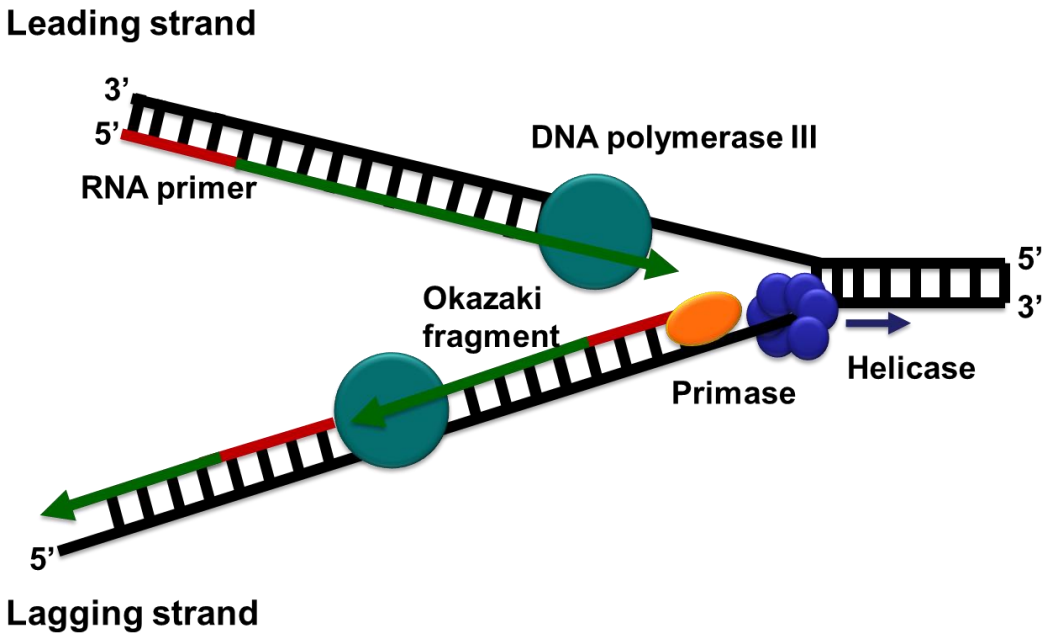

Figure 1. Cartoon representation of one of the replication forks of replication bubble during DNA replication.

Cartoon shows one of the replication forks in replication bubble during DNA replication. The DNA polymerase III (turquoise sphere) is the main replicative polymerase moving in 3'-to-5' direction. The components ssDNA strands of the dsDNA are separated by DNA helicase (blue hexamer), which moves in 5'-to- 3' direction on the ssDNA. Primase (orange oval shape) synthesises RNA primers that enable the DNA polymerase III to synthesise the leading and the lagging strand. Lagging strand synthesis requires multiple primers and is replicated in sequences called Okazaki fragments. The RNA primers are removed by DNA polymerase I using its endonuclease activity and the gap is filled by the 5-to-3' polymerase activity of the same enzyme. The fragments produced are ligated together by DNA ligase.

1.2. DNA and RNA helicases

This thesis investigates and discusses the function and biochemical characteristics of a bacterial DNA helicase, PcrA, belonging to superfamily I. Helicases are ubiquitous enzymes found in bacteria to multicellular eukaryotes, and are also encoded by viral genomes. They are involved in most of the cellular functions involving nucleic acid processing such as DNA replication, recombination, repair and transcription. Helicases are NTP-driven enzymes, able to separate dsDNA into single strands. Helicases are divided into six superfamilies (SF1 to SF6) according to their sequence similarity, structure and function [6]. More broadly, helicases are divided in are to two groups based on their structure. These are the monomeric (albeit some active as dimers) or hexameric helicases. Helicases can also be classed depending on whether they translocate on ssDNA or dsDNA. Most helicases function as part of larger molecular machines such as the DNA replication machinery, which includes initiator proteins, DNA polymerases and SSB [6, 7]. These proteins may interact directly with the helicase or the interaction may be facilitated or stabilised by DNA or other accessory proteins, which may also affect the activity or functionality of the helicase.

In humans, helicases have been found to be involved in many disorders such as Werner syndrome, Bloom's syndrome and Rothmund-Thomson syndrome [8-10]. These disorders are caused by faults in the function of the RecQ family helicases (belonging to SF2) that are vital in genome stability from microorganisms to higher eukaryotes [10-12]. Many of the diseases involving helicases show increased cancer rates, which can be expected as many of the helicases function in DNA replication and repair [13, 14]. This is the case with Werner and Bloom's syndromes patients, who have a predisposition to sarcomas and premature aging.

1.2.1. Structural similarities between the six helicase superfamilies

The mechanisms of DNA translocation and unwinding may vary considerably between the different helicase superfamilies. However, there are several fundamental features shared by all helicases [6], the main requirement being the actual ability to unwind DNA. The structural similarities are mainly contained in their ATPase core structure and sequence, which resemble the RecA ATPase core that has RecA-like/AAA+ domain, which plays an important role in energy transduction of converting ATP hydrolysis to movement [6, 15]. RecA protein is a DNA translocase protein, which couples ATP hydrolysis to binding and formation of filaments on ssDNA [16]. Many enzymes with DNA translocation activity have high structural resemblance to RecA and so are named RecA-like. AAA+ stands for the ATPases Associated with various cellular Activities domain, which also include the classical Walker A (motif I) and B (motif II) motifs involved in ATP hydrolysis. These motifs interact with the Mg·ATP/ADP. The Walker A motif is classically defined as a GxxxxGKT/S [17], whereby the amino group of lysine interacts with phosphates of Mg·ATP/ADP and the hydroxyl group of threonine ligates the Mg^{2+} ion.

The RecA central ATPase domain consists of twisted beta sheet with several β-strands joined by α-helices [18].The number of ATP-hydrolysing domains varies between the monomeric/dimeric and hexameric helicases. Figure 2 shows a cartoon presentation of the structures of monomeric and hexameric helicases and gives examples of individual helicases belonging to each type. Monomeric/dimeric helicase have two RecA-like/AAA+ subdomains in each monomer/subunit (SF1 and SF2 helicases) [19-28], whereas hexameric helicases have one RecA-like/AAA+ subdomain per subunit (SF3 to SF6 helicases) [6, 29-35].

The presence of a RecA-like/AAA+ subdomain in an enzyme is not the only requirement for correct classification of a DNA binding enzyme as a helicase. Initially, many DNA translocases containing RecA-like/AAA+ motifs were grouped as helicases. However, these enzymes lack the DNA

unwinding function and are not true helicases [6]. Many of the known helicases also contain the 'arginine finger' on one of the RecA-like subdomains (motif IV) [15]. PcrA helicase has been used as to demonstrate how this arginine finger plays an important role in the ATP hydrolysis by interacting with γ phosphate of the ATP [21, 36]. The release of the γ phosphate from the arginine after the hydrolysis leads to separation of the motor domains (1A and 2A domains). This is vital step for the PcrA movement and for the DNA strand displacement or DNA duplex destabilisation.

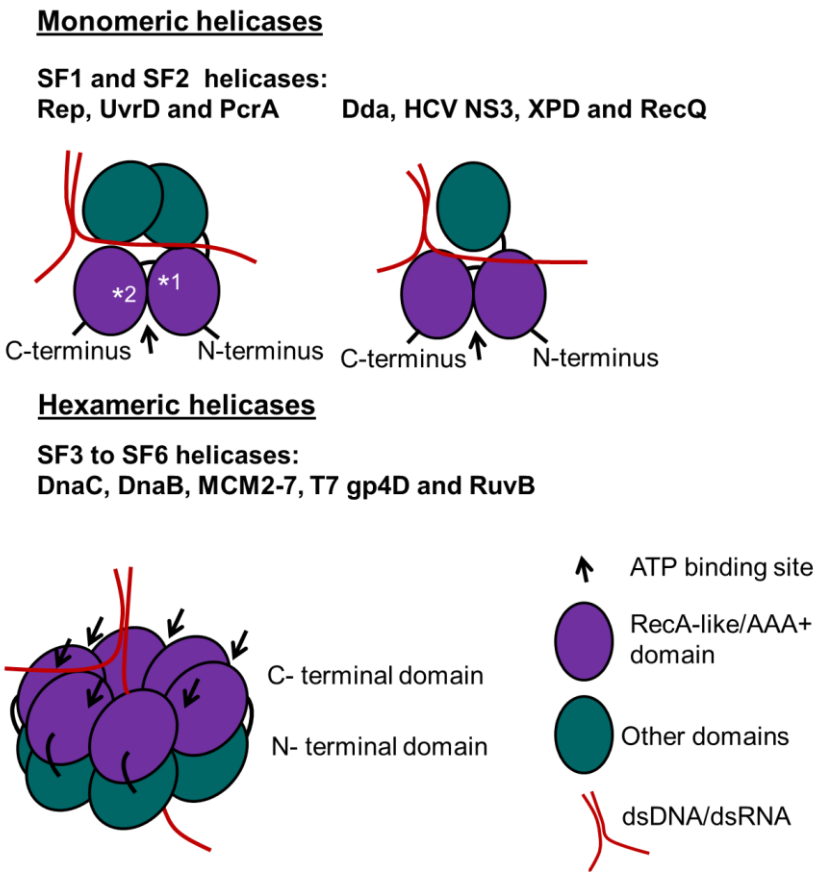

Figure 2. The RecA-like/AAA+ subdomains in monomeric and hexameric helicases.

The RecA-like/AAA+ domains couple the nucleotide hydrolysis to movement on DNA in all helicases and DNA translocases The monomeric/dimeric helicases have two RecA-like/AAA+ subdomains per subunit, whereas the hexameric helicases have one RecA-like/AAA+ subdomain per subunit. The direction of the DNA translocation isn't shown in this diagram as this varies between helicases. *1, indicates the approximate location of the Walker A (motif I) and the Walker B (motif II) motifs on the AAA+ domains. The Walker B motif interacts with the Mg^{2+} ion required for ATP hydrolysis. *2, indicates the location of the motif IV (arginine finger). [6, 19-23, 25-34]

1.2.2. Superfamily 1 and 2 helicases and PcrA-SF 1 helicase

The superfamily 1 helicases together with those from superfamily 2 are the largest and the most extensively studied groups of helicases. The oligomeric state of SF1 and SF2 helicases has been disputed in the past but generally they are considered to be monomeric or dimeric and all have some form of DNA translocation functionality as a monomer [6, 37-41]. The large number of known SF2 helicases reflects the large number of cellular processes they are involved in. A well characterised example of SF2 helicases is the non-structural protein 3 (NS3) helicase of the hepatitis C virus that unwinds RNA-DNA duplexes. The crystal structure of the NS3 helicase showed a three domain structure with two RecA-like domains, equivalent to the 1A and 2A domains of SF1 helicases, which form a nucleotide binding pocket between them and function as motor domains [23, 24]. The two RecA-like domains and the third core domain together form a groove for ssDNA binding. The NS3 has also been crystallised in complex with SSB protein on a ssDNA template indicating possible direct interaction of the two proteins [23].

E. coli helicases UvrD and Rep also belong to SF1 and share high structural and functional similarity with PcrA. Due to their sequence and structural similarity, they are often used as a comparison for PcrA. UvrD and Rep both have the same domains as PcrA and go through similar structural changes when binding to DNA (Figure 3) [19, 20]. The sequence similarity between PcrA and UvrD is 42% and 37% between PcrA and Rep [19] SF1 family helicases share many defined motifs that are not found in other superfamily helicases [19, 20, 42-45]. They can translocate unidirectionally either in the 3-to-5’ or 5-to-3’ direction. Figure 3 shows the conserved sequence motifs of SF1 helicases and the alignments of these motifs on the substrate bound ‘closed’ conformation of UvrD. This figure also includes the closest known eukaryotic helicase to PcrA, the Srs2 helicase from *Saccharomyces cerevisiae* [43]. Most of the conserved sequence motifs are in domains 1A and 2A, which are the motor domains of SF1 and many other helicases. They facilitate the conversion of energy from ATP hydrolysis into

movement on ssDNA and unwinding of dsDNA. These include the already mentioned Walker A and B domains and the motif IV, the 'arginine-finger' in the Section 1.2.1. Also, further conserved motifs are found in dsDNA and ssDNA binding sites in domains 2B and 1B. The motif IVa is unique to SF1 helicases and contains conserved binding sites for ssDNA [44].

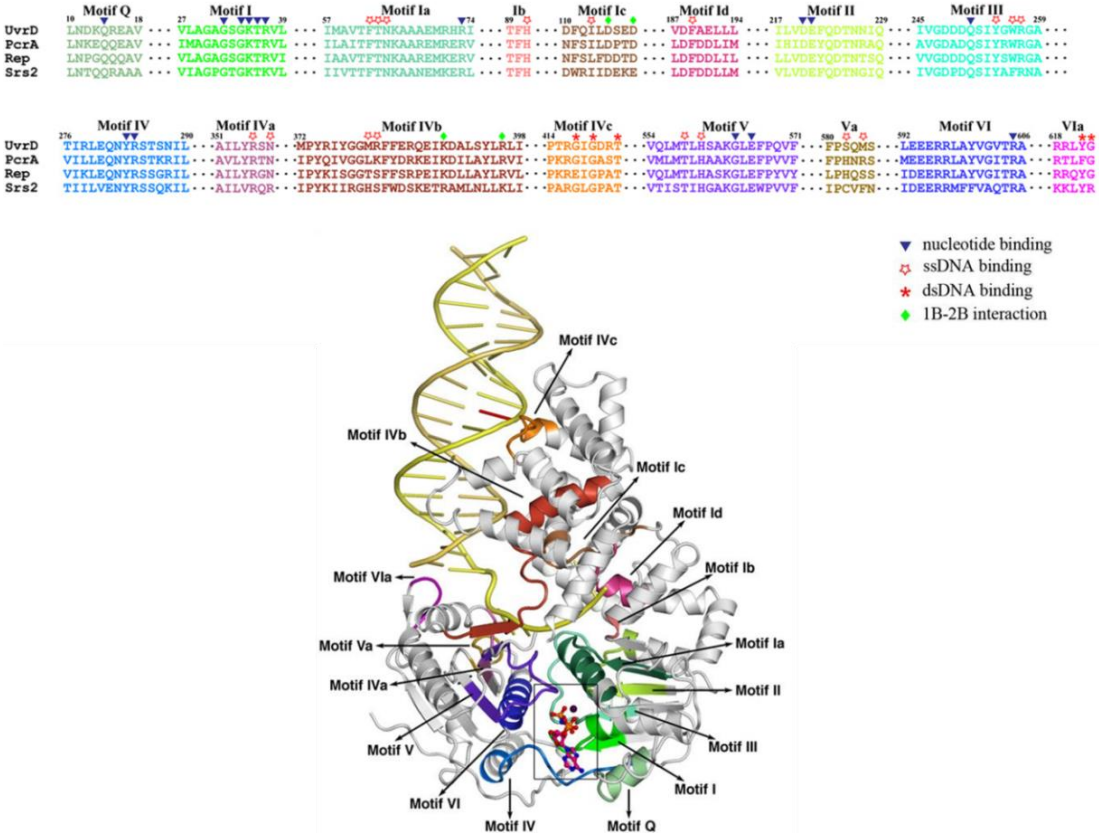

Figure 3. SF1 family helicase motifs.

Sequence alignment displaying motifs of the most studied SF1 helicases, and motifs displayed on UvrD 3D structure (The sequence colours match the colours on the structure). ATP is highlighted by a square around it. Motif I is the Walker A motif and motif II is the Walker B motif, which interacts with the Mg^{2+} ion (black sphere). The motif IV contains the highly conserved "arginine finger" required for ATP hydrolysis. Adapted from Lee *et al.* (2006) *Cell* 127(7):1349-1360. [19].

PcrA (plasmid copy number reduction A), a member of the SF1 helicases, is the main focus of this project. PcrA is an essential protein found in Gram-positive bacteria [46-50]. PcrA and other SF1 helicases were determined to have a four subdomain structure by X-ray crystallography [19,

21, 22, 44]. The domains are named 1A, 2A, 1B and 2B and are shown in Figure 4 [22, 36]. Similarly to other helicases, PcrA uses ATP to translocate on ssDNA and unwind dsDNA [51]. The binding site for ATP is in a cleft between domains 1A and 2A. The crystal structures of PcrA bound to a non-hydrolysable ATP analogue, AMP PNP, and apo PcrA indicate a ~30° conformational change where the 1A and 2A domains come together, thus “trapping” the nucleotide. The 1A and 2A domains are responsible for ATP hydrolysis and coupling of the hydrolysis to movement on DNA. They are often called the motor domains and share structural similarity with RecA-like proteins and functional similarity with other ATPases [52] as discussed in the previous section.

The PcrA binding to DNA leads to ~140° rotation of the 2B domain over the 1B domain (Figure 4). Often the apo PcrA state in the crystal structure is called the “open” form and the folded state in the substrate bound crystal structure is called the “closed” form. The ssDNA interacts with PcrA at the surfaces on 1A, 2A and 1B domains, and 2B subdomain also has a possible dsDNA interface.

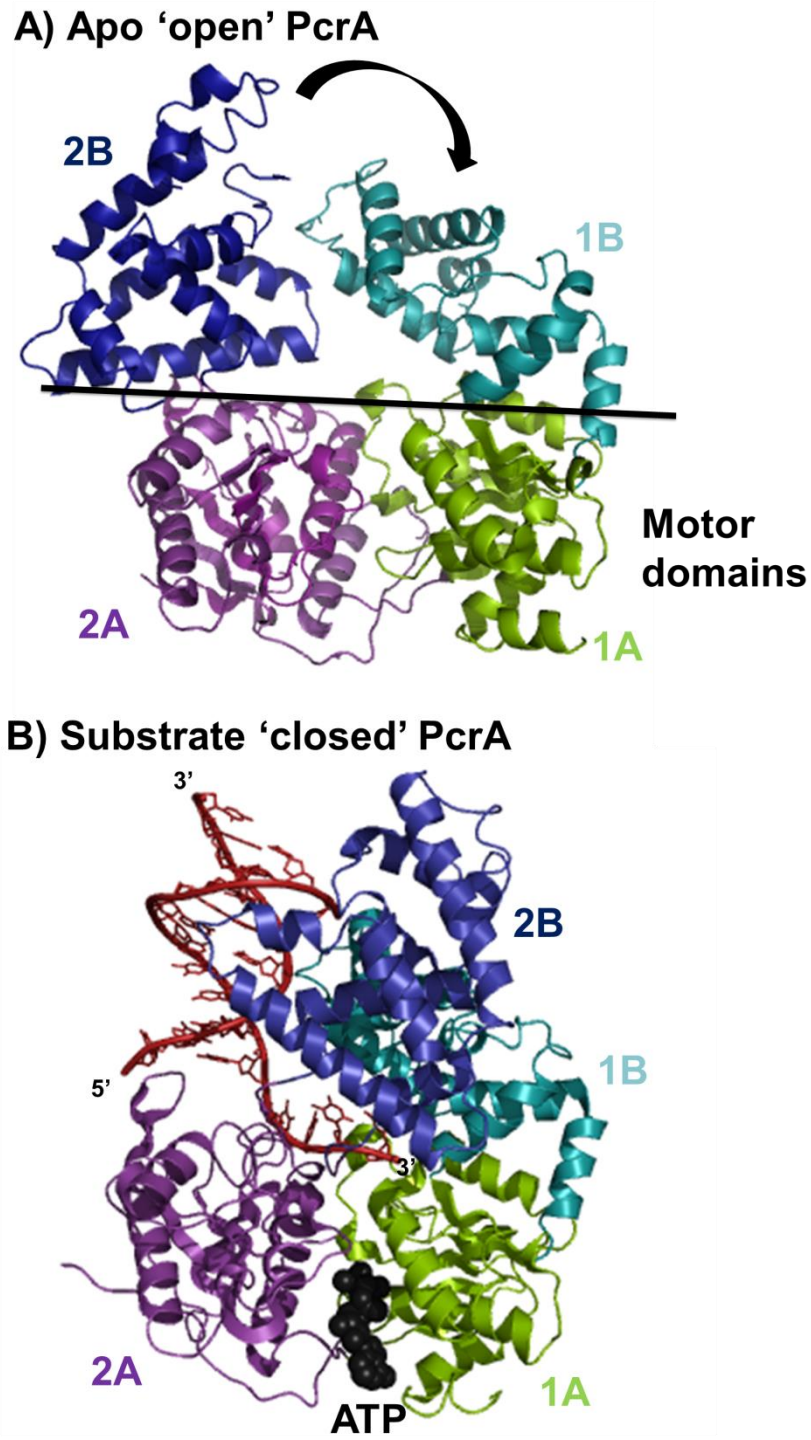

Figure 4. PcrA crystal structure with and without DNA and ATP-analogue.

A) PcrA at the 'open' conformation without substrates. B) PcrA structure when bound to ATP and DNA, 'closed' conformation. The DNA duplex (red) has 3' ssDNA overhang for PcrA binding. When the PcrA binds the DNA duplex, the 2B domain folds over 1B domain causing a ~140° rotation change. The ATP analogue is AMP PNP. The coordinates for the image were taken from PDB files 1PJR and 3PJR and visualised using PyMol (http://www.pymol.org/).

1.2.3. PcrA DNA translocation model

PcrA translocates in 3'-to-5' direction on ssDNA by the model shown in Figure 5, which was deduced from the available crystal structures for PcrA [36, 53, 54]. The model proposes that a monomer of PcrA moves along DNA by changes in a series of base-binding pockets across the protein, using one ATP per base moved/unwound. ATP hydrolysis and the movement on ssDNA are facilitated by the 1A and 2A domains closing and opening (tightening and loosening the grip) on ssDNA (Figure 5B). The movement of the PcrA destabilises the DNA fork junction and so separates the dsDNA (The active and passive movement of helicases is introduced in Section 1.2.5). Before ATP binding the 1A domain has tighter binding to ssDNA and 1A and 2A domains are further apart. The ATP binding to PcrA causes the 1A and 2A subdomains becoming closer together and 2A subdomain tighter binding to ssDNA. ATP hydrolysis to ADP leads to separation of 1A and 2A domains apart and PcrA is held on the DNA by the tighter binding by 1A domain. This leads to PcrA moving one base forward in 3'-to-5' direction on ssDNA [55, 56].

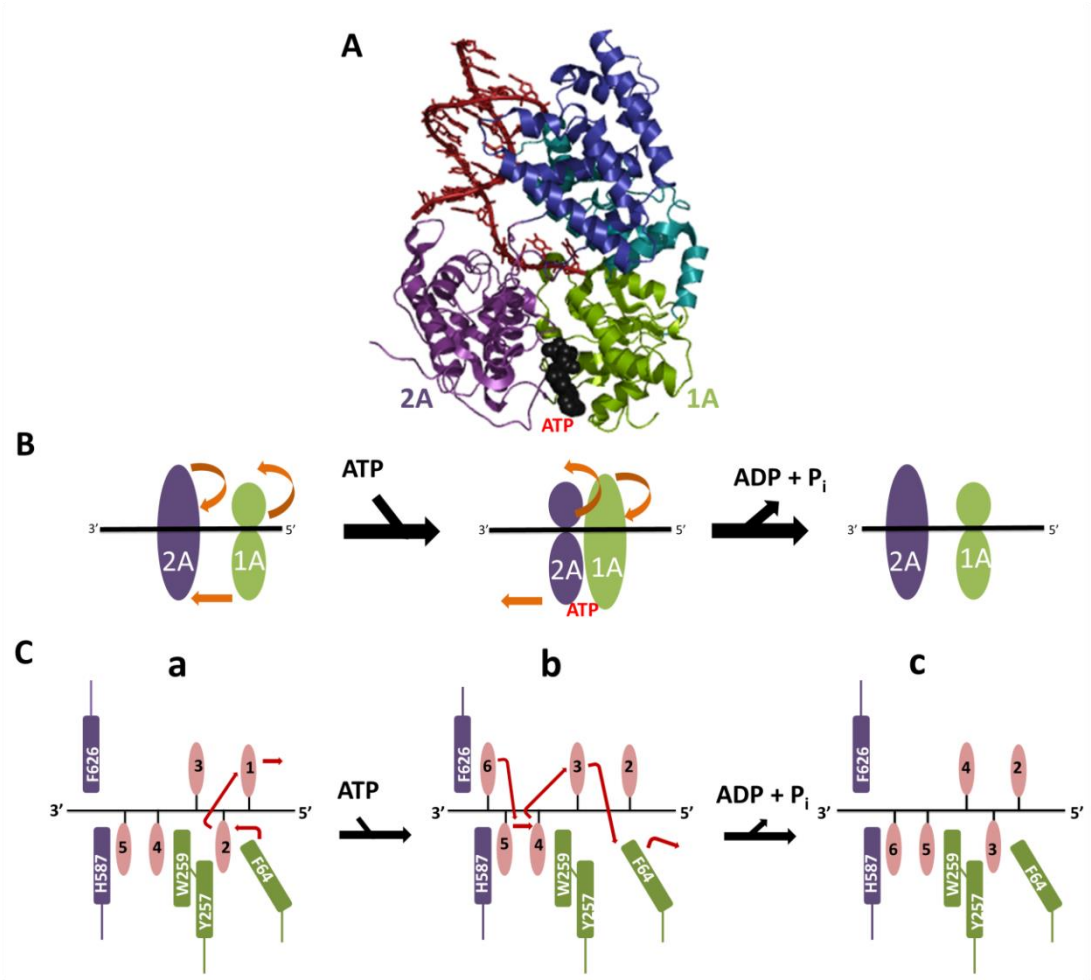

Figure 5. Model of PcrA translocation on DNA.

A) Crystal structure of substrate bound PcrA. B) PcrA 1A and 2A subdomain structural movements coupled to movement on ssDNA. In this model, one ATP is hydrolysed per base moved/unwound. The eclipses represent the tightening and loosening of the grip of PcrA 1A and 2A domains on ssDNA. C) Individual residues indicated to interact with the bases of the ssDNA. [36]

1.2.4. Helicase superfamilies 3 to 6

All SF3 to SF6 helicases are ring-shaped hexamers or double-hexamers (12 subunits) [6]. Each subunit contains one RecA-like/AAA+ containing domain with one ATP binding pockets. The individual subunits have negative co-operativity in binding and hydrolysing ATP. Several models have been suggested for the ATP hydrolysis from highly ordered to stochastic or random ATP hydrolysis [6]. Figure 6 shows several suggested ATP hydrolysis models for hexameric helicases. Generally, the hexameric

helicases translocate and unwind DNA faster than monomeric helicases. SF3 helicases have four conserved motifs and all translocate in 3'-to-5' direction. An example of a SF3 helicase is the human papilloma virus E1 that has been crystallised in complex with DNA and ADP [57]. This structure has given clues to how ring-shaped helicases may couple ATP hydrolysis with the translocation on DNA, as all six subunits had a nucleotide bound, but three different conformations were present. This indicated a possible sequential-block ATP hydrolysis model, where the ATP bound subunits are adjacent to each other forming "a block". This block then moves sequentially around the hexamer ring as the ATP hydrolysis is coupled to movement on ssDNA resulting in unwinding of dsDNA.

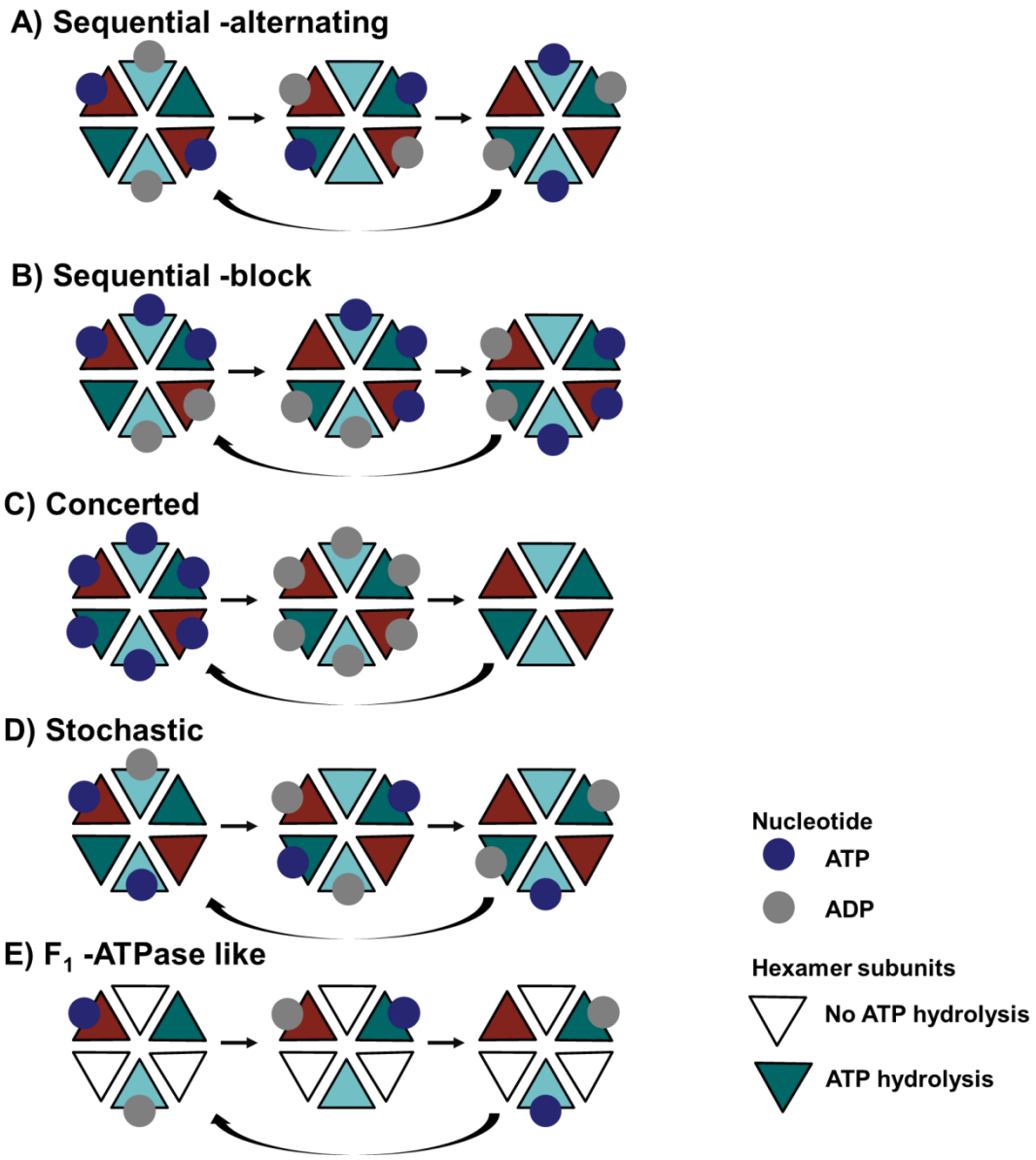

Figure 6. ATP hydrolysis models for hexameric helicases (SF3-SF6).

A) Sequential-alternating model, where opposite subunits are hydrolysing ATP synchronously to each other whereas B) Sequential-block, where the subunits are synchronised in block in terms of their ATP hydrolysis cycle. C) Concerted model, where all subunits are hydrolysing ATP synchronously. D) Stochastic where the subunits hydrolyse ATP random order. E) F1-ATPase like where only every second subunit is hydrolysis ATP.

SF4 helicases all translocate in 5'-to-3' direction and share five conserved sequence motifs (H1, H1a, H2, H3 and H4) of which H3 and H4 are SF4 specific [6]. The H1 and H2 motifs are equivalent to the Walker A and B motifs also found in SF3 helicases. These motifs are vital for interaction with the nucleotide. The most extensively studied SF4 helicase is the bacteriophage T7 gp4 helicase for which an atomic-resolution structure exists [58]. T7 gp4 has primase and helicase domains connected by a linker. T7 gp4 has been suggested to hydrolyse ATP sequentially by alternating the subunits with ATP, ADP and empty [32]. SF5 helicases are closely related to SF4 helicases. Example of superfamily 5 helicases is the Rho helicase that is responsible for transcription termination in bacteria by unwinding the RNA from RNA-DNA duplexes.

SF6 helicases include the minichromosome maintenance (MCM) protein complex that is thought to be the main replicative helicase in eukaryotes. The MCM2-7 complex has been shown to be essential for replication initiation and elongation [6, 59]. Crystal structures of the eukaryotic MCM helicase domain have not been obtained and most structural information is from archaeal MCM that differs from the eukaryotic MCM by being a homohexamer. Eukaryotic MCM is formed of heterohexamers made up of related, but not identical polypeptides.

1.2.5. Helicase movement on DNA

When studying a helicase at biochemical level several aspects of its movement on DNA are important [6]. These include rate, directionality, processivity, step size and whether helicase unwinds DNA actively or passively. The rate is a measurement of the speed the helicase moves on ssDNA, which is called translocation on ssDNA (bases s^{-1}) or the measurement of the rate of DNA strand separation (base pairs s^{-1}). These rates may vary for different helicase and can be affected by interaction with accessory factors. Both, translocation and unwinding rates may be tightly coupled to the ATPase rate. Helicase movement on DNA is usually

unidirectional, proceeding in either the 3´-to-5´ or 5´-to-3´ directions. The directionality of helicase can be changed or restricted by the interaction with accessory factors such as other proteins. Helicase step size is a measure of the number of base pairs the helicase moves during single catalytic cycle. This is often seen as the movement during single ATP hydrolysis cycle. Processivity of helicases is a measure of how many bases helicase can unwind before stalling or dissociating from DNA. This can vary greatly between helicases from few base pairs to thousands of base pairs. Processivity can also be improved by helicase interaction with other proteins or specific DNA sequences.

Another fundamental question concerning a helicase mechanism is whether it separates dsDNA into ssDNA by actively or passively breaking the base pairing. In an active mechanism, helicase movement forces the two strands apart, for example, using a wedge domain coupled to ATP hydrolysis that produces a combination of force and movement [60]. In a passive mechanism, thermal fluctuations in the degree of pairing at of the dsDNA fork allow the helicase to translocate; hence, the helicase must await fortuitous separation, which may slow its progress. Comparison of helicase properties when moving along dsDNA compared with those when it moves along ssDNA have been proposed [61] as a way to determine to what extent unwinding is an active process or a passive ‘by-product’ of the translocation mechanism [60]. According to this model, helicases that have similar rates of unwinding dsDNA and translocation on ssDNA are considered active, whereas those with slower unwinding rates on dsDNA than ssDNA translocation rates are termed passive. In practice, it would be expected that a range of intermediate levels is also likely. An example of a helicase that has been considered essentially optimally active is Dda belonging to the SF2 helicases [62]. Dda has been shown to have the rate of unwinding (V_{un}) of 257 +/- 42 bp s^{-1} and the rate of ssDNA translocation (V_{trans}) of 267 +/- 15 nt s^{-1}. These give a value of 0.96 for the V_{un}/V_{trans}. For optimally active helicases the V_{un}/V_{trans} value is close to 1, whereas helicases with the V_{un}/V_{trans} value close to 0 are seen as passive helicases.

1.3. Replication of circular bacterial plasmids

Plasmid replication and control of its frequency are important for maintaining a stable copy number of plasmids in the host cell [63, 64]. If plasmids are replicated too frequently, the high requirement of substrates and energy will become a burden and result in a slower growing and weaker host cell. If the plasmid replication is infrequent and slow, the plasmids may be lost entirely from the host or its daughter cells at cell division. This may result in plasmid-containing cells being be outgrown by plasmid-free bacteria, leading to loss of often beneficial genetic properties such as antibiotic resistance genes [63]. The plasmid replication processes have been divided into three main types, which are theta replication, strand displacement and rolling circle plasmid replication [64]. Irrespective of the exact mechanism, replication occurs in three stages - initiation, extension and termination. Theta and strand displacement replication initiations involve opening of the strands, followed by RNA priming and can be uni- or bidirectional, but both form a replication bubble, which is visible under electron microscopy as theta-like structures [65]. The rolling circle replication is asynchronous and the initiation of replication involves cleavage of one of the DNA strands to generate a 3′-OH end typically resulting in a unidirectional replication (Figure 7).

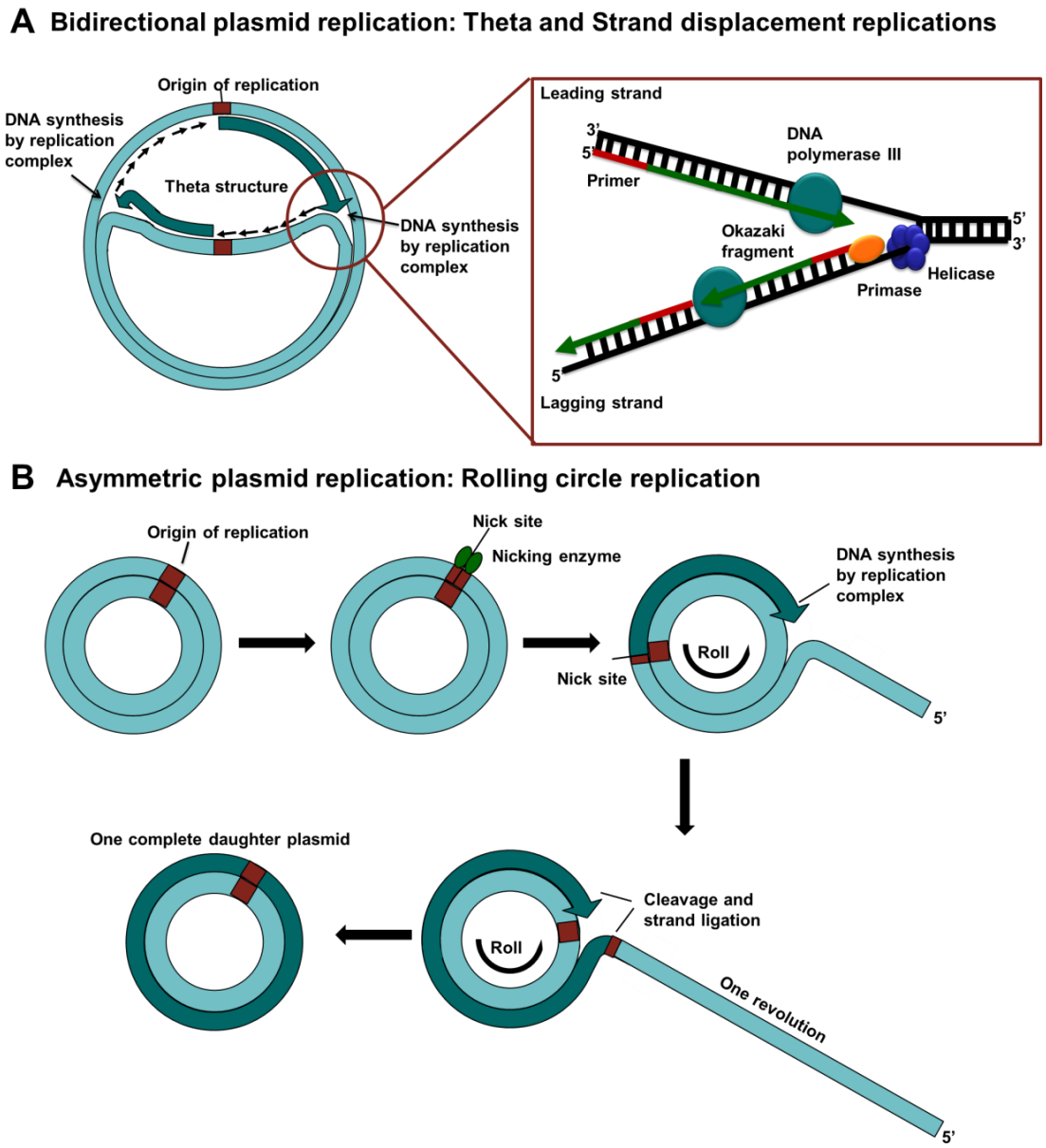

Figure 7. The different forms of plasmid replication.

A) Bidirectional plasmid replication. Theta replication may be unidirectional or bidirectional depending on the plasmid in question. B) Unidirectional rolling circle plasmid replication. The nicked strand is the (+)-strand.

Theta plasmid replication mechanism involves melting of the complementary strands at the origin of replication, synthesis of RNA primer and initiation of the DNA synthesis covalently from the primer [64]. It is common in Gram-negative bacteria but has also been found in Gram-positive bacteria. The synthesis by theta mechanism can be bidirectional, but in most cases it is unidirectional. When In unidirectional replication, the

leading strand is replicated continuously without the discontinuous replication of the lagging strand. Opening of the strands is catalysed by specific initiators (Rep and DnaA proteins) and/or by transcription by RNA primer. The plasmid unwinding is performed by the main replicative helicase such as DnaB in *E. coli*. Termination of theta replication is often achieved by sequences specific DNA-protein complexes. One of the most extensively studied examples of the theta replication is the ColE1 replication in *E. coli* (Figure 8A). ColE1 replication requires melting of the *ori* sequence, which requires DNA polymerase I, RNA polymerase and RNAse H and synthesis of a RNA primer DNA gyrase and topoisomerase (Figure 8A)[64, 66-68]. ColE1 plasmid has a copy number control mechanism (~20 copies per cell), which involves two RNA substrates, RNAI and RNAII, and Rop (or Rom) protein. RNAII is a primer RNA (over 500 bases), which is nicked by the RNase H to generate the free 3'-OH group required by the DNA polymerase for the synthesis of a new complementary strand. The RNAI is shorter (~108 bases) with complementary sequence with RNAII. Its binding to RNAII prevents the initiation of replication by prevention of RNAII binding to *ori*. The RNAI-RNAII complex is further stabilised by Rop protein binding. Many other plasmids are also known to replicative by theta mechanism including the R1, pAMβ1, ColE2 and ColE3 plasmids [64, 69, 70]. They all require a Rep initiator protein encoded from the plasmid, but may also use many of the components of the genomic DNA replication.

A Initiation of theta plasmid replication: ColE1 plasmid

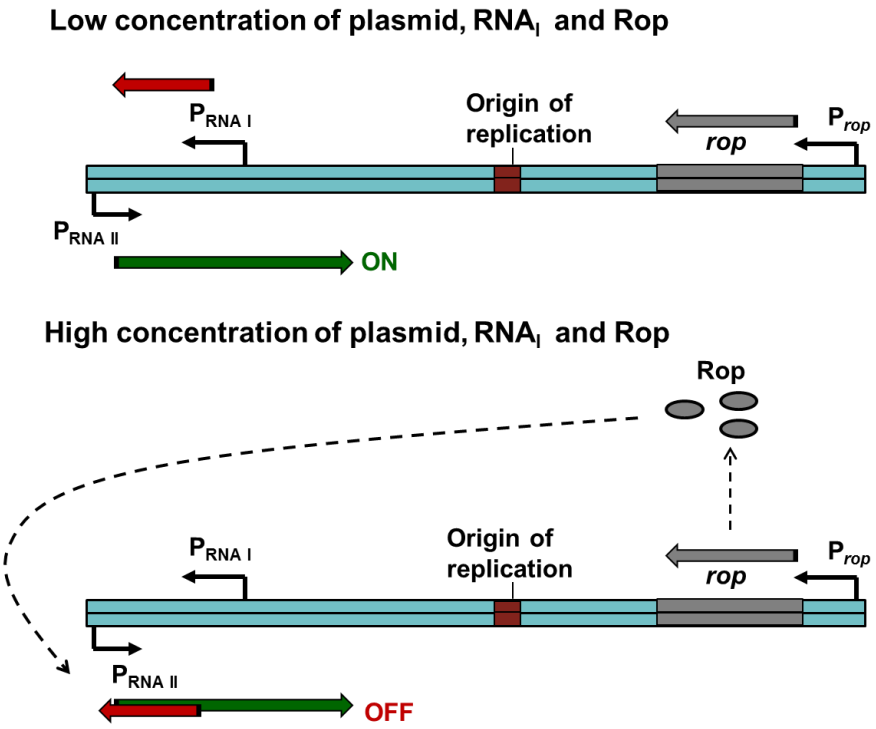

B Initiation of strand displacement plasmid replication: RSF1010 plasmid

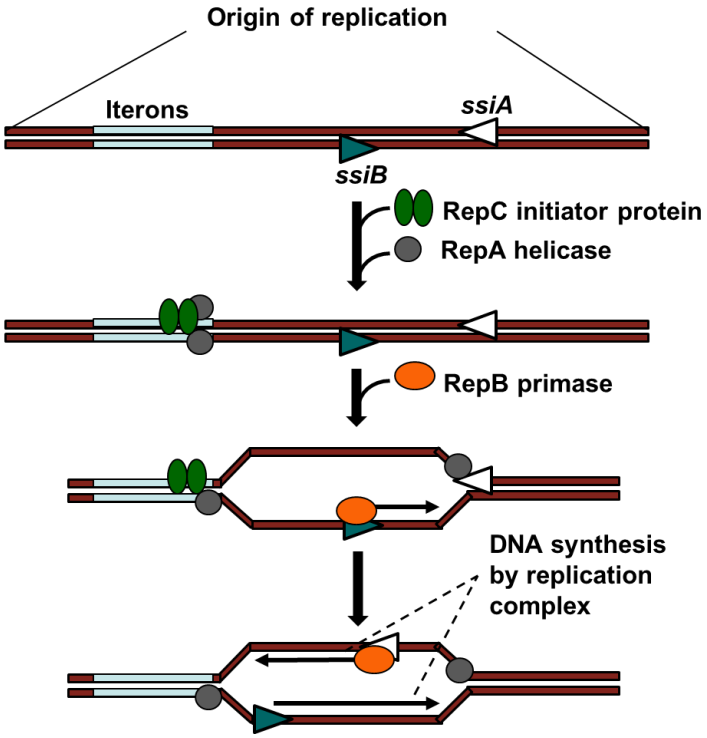

Figure 8. Initiation of ColE1 and RSF1010 plasmids.

A) Initiation of ColE1 plasmid replication and control of plasmid copy number. ColE1 plasmid number is tightly controlled by the presence of RNAI and RNAII and their interaction. If RNAII is transcribed and cleaved by RNase H, it can initiate the replication by providing a primer for the DNA polymerase I. If RNAI is transcribed at high concentrations it will bind to RNAII, forming an RNAI-RNAII complex. This complex is stabilised by Rop protein, preventing the RNAII from initiating the replication. If RNAI concentration is low, RNAII is free to initiate plasmid replication. B) Initiation of RSF1010 plasmid replication. This requires three plasmid encoded proteins, RepA, RepB and RepC. RepC melts the dsDNA at the iterons. RepA unwinds the dsDNA throughout the process of plasmid replication. The exposure of *ssiA* and *ssiB* elements as ssDNA enables RepB priming for processive plasmid replication.

Strand displacement plasmid replication has been mostly studied in IncQ (incompatibility group Q) plasmids such as the RSF1010 plasmid in *E. coli* [64]. The replication requires three plasmid encoded proteins, RepA helicase, RepB primase and RepC initiator protein (Figure 8B) [64, 65, 71]. The origin of replication of the RSF1010 plasmid contains iterons with self-complementary sequences, AT-rich sequence, GC-rich sequence and *ssiA* and *ssiB* elements. The initiation of replication of RSF1010 starts by the RepC binding to the iterons and AT-rich sequences preceding the iterons. RepC together with RepA melt the dsDNA. The *ssiA* and *ssiB* function as a priming region and once exposed as ssDNA are primed by the RepB. These primers are then used by DNA polymerase III to bidirectionally synthesise the complementary DNA strands. The RepA helicase is responsible for the unwinding of the entire plasmid and functions in the 5'-to-3' direction. The 5'-to-3' direction movement by RepA implies that it unwinds while being bound to the displaced strand. As the three initiator proteins are plasmid encoded, the host RNA polymerase and other components of the DNA replication machinery are not required. This makes the RSF1010 a rather promiscuous plasmid and enables it to possess a broad host range. The termination of strand displacement replication is achieved by specific DNA-protein interactions.

The third type of plasmid replication is the rolling circle replication, which is the subject of study in this thesis [64, 72]. Rolling circle replication is

asymmetric, whereby the leading and lagging strand are synthesised one after the other. The rolling circle replication was discovered as the replication mechanism of ssDNA phage genomes of ϕX174 and M13, which are both native to *E. coli* [73]. The significant differences for the rolling circle replication as compared to theta and strand displacement replication are the RNA priming requirement for the latter two and the strictly unidirectional DNA synthesis of rolling circle replication. In rolling circle replication, the DNA unwinding is performed by a helicase that is not the primary replicative helicase. For example, the replicative helicase in *Bacillus subtilis* is DnaC helicase and the T181-family plasmids are unwound by the PcrA helicase [50, 74]. Rolling circle replication has been identified in various Gram-positive and Gram-negative bacteria as well as *Archaea* [75-77]. In *E. coli* for example, UvrD helicase dependent plasmid replication applies the rolling circle mechanism [78], which uses the nicked free 3'-OH end of the lagging strand for DNA polymerase III synthesis of the leading strand of T181-family plasmids. The termination is not well understood, but requires sequence specific DNA-protein complex formation. The focus of this work is the function of PcrA helicase in the replication of pT181 and pC221 plasmids through asymmetric rolling circle replication (discussed further in the next section).

1.4. PcrA function

1.4.1. Asymmetric rolling circle plasmid replication and PcrA

PcrA helicase is responsible for DNA unwinding in asymmetric rolling circle plasmid replication of T181-family plasmids that carry antibiotic resistance genes in Gram-positive bacteria [47, 64]. Figure 9 summarises this replication by PcrA and initiator protein Rep. Asymmetric replication means that the (+)-strand and the (-)-strand of the plasmid are not copied simultaneously. Here, the leading strand refers to the strand that is replicated first using the parental (-)-strand as a template. The lagging strand synthesis refers to replication second strand using the parental (+)-strand as a template. PcrA was discovered in *Staphylococcus aureus* where a

conditional mutation of the *pcrA* gene led to a reduction in plasmid copy number [79, 80]. Plasmid replication by PcrA requires a dimeric initiator protein Rep encoded by the plasmid DNA. In these studies the Rep initiator protein is the RepD from *S. aureus* carried by the pC221 plasmid *in vivo* [72]. Rep nicks dsDNA at a specific sequence in the double stranded origin (DSO) called *ori* [81-83] (Step 1, Figure 9). The origin of replication for RepD, *Ori*D, is formed of three inverted complementary repeats (ICRI-III) (Figure 10A). Rep makes a single-stranded nick on the (+)-strand and binds the nicked 5' end of the DNA strand by forming covalent bond at the tyrosine residue of one of the monomers of the dimer (Figure 10B). The nicking reaction and bond formation is achieved by a series of transesterifications, where the phosphodiester bond between bases is broken and another is formed between the 5'end of DNA and the active tyrosine on Rep. This releases supercoiling and opens a section of ssDNA to which PcrA can bind and begin unwinding the dsDNA (Step 2 and 3, Figure 9). Rep binding and nicking is highly sequence specific and Rep is only able to initiate one round of plasmid replication as it dissociates in an inactive form at the end of plasmid replication [84, 85]. Rep remains part of the replication complex until the whole plasmid is unwound [82]. While PcrA unwinds the plasmid, the leading strand is simultaneously replicated by a DNA polymerase III reading the (-)-strand (Step 4, Figure 9). Once the replication machinery reaches the DSO, Rep recognises it and terminates leading strand elongation. This leads to dissociation of PcrA and DNA polymerase III (Step 5, Figure 9). Rep performs strand exchange through a series of transesterifications that result in a complete plasmid, which is supercoiled by DNA gyrase [86](Step 6, Figure 9). Rep dissociates in an inactive form with a covalently bound small ssDNA left from the strand exchange [84].

The lagging strand is replicated by DNA polymerase from the SSO using the (+)-strand as a template (single strand origin of replication). During leading strand synthesis (template (-)-strand), the (+)-strand is protected by SSB proteins. This project uses the *S. aureus* Rep protein called RepD and *Bacillus stearothermophilus* PcrA, which are able unwind plasmid lengths of DNA *in vitro* [87].

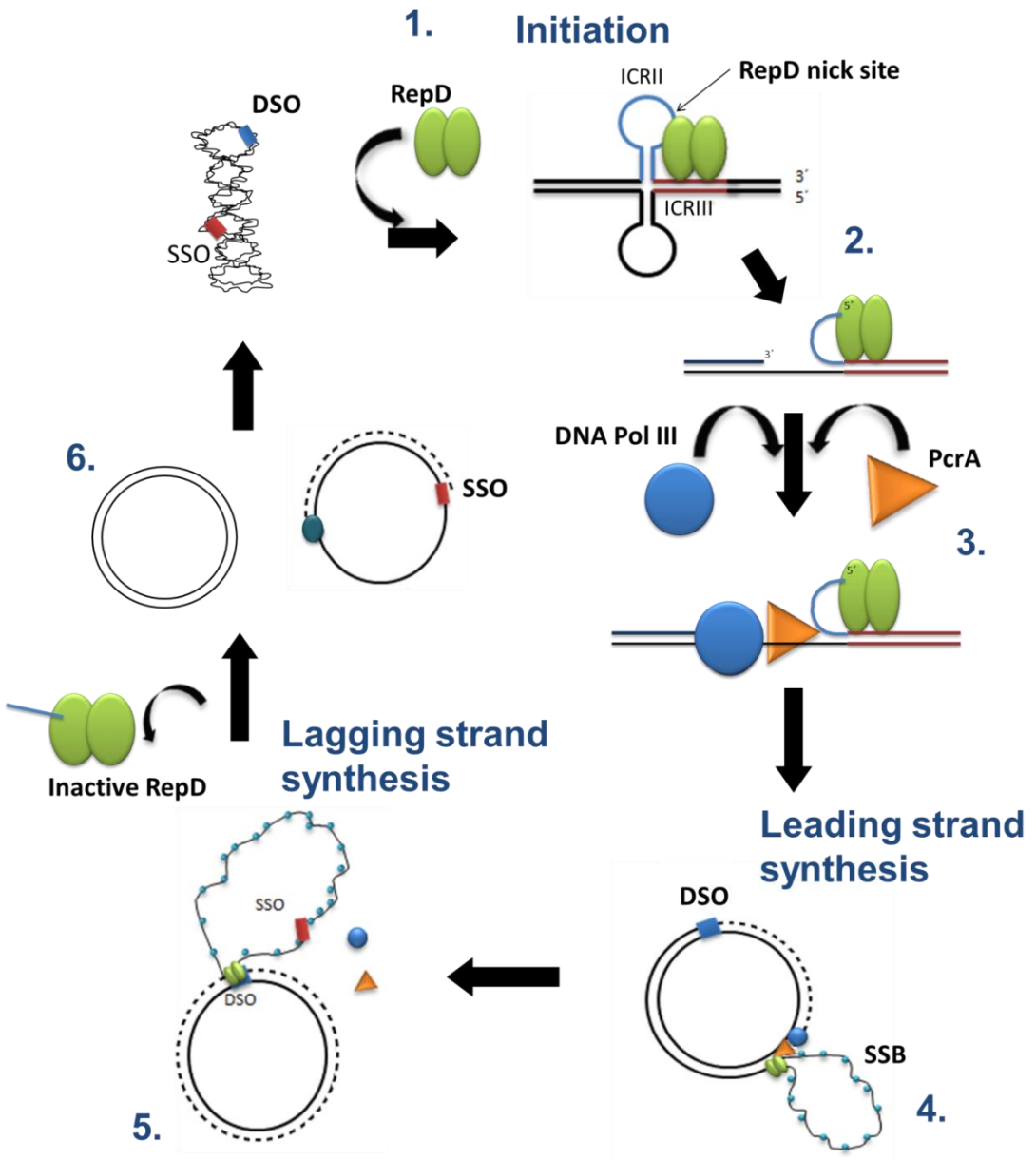

Figure 9. Asymmetric rolling circle replication of T181-family plasmids.

1. RepD sequence specific loading onto the DSO of the supercoiled plasmid. 2. RepD nicks the *oriD* sequence releasing the super coiling and forms a covalent bond to the 5' end of the (+)-lagging strand. 3. PcrA and DNA polymerase III are recruited to the replication complex. They both bind to, and translocate on, the (-)-strand. 4. Leading replication: PcrA unwinds dsDNA followed by DNA polymerase III. The single stranded (+)-strand is covered by SSB proteins (small cyan spheres). 5. Once the replication complex reaches the DSO it replicates a few bases over the DSO and RepD performs the strands exchange. PcrA and DNA polymerase III dissociate from the complex. The leading (-)-strand replication is completed and inactive RepD is released. 6. The lagging (+)-strand is synthesised from a SSO by a DNA polymerase I. The complete daughter plasmids are supercoiled by DNA gyrase.

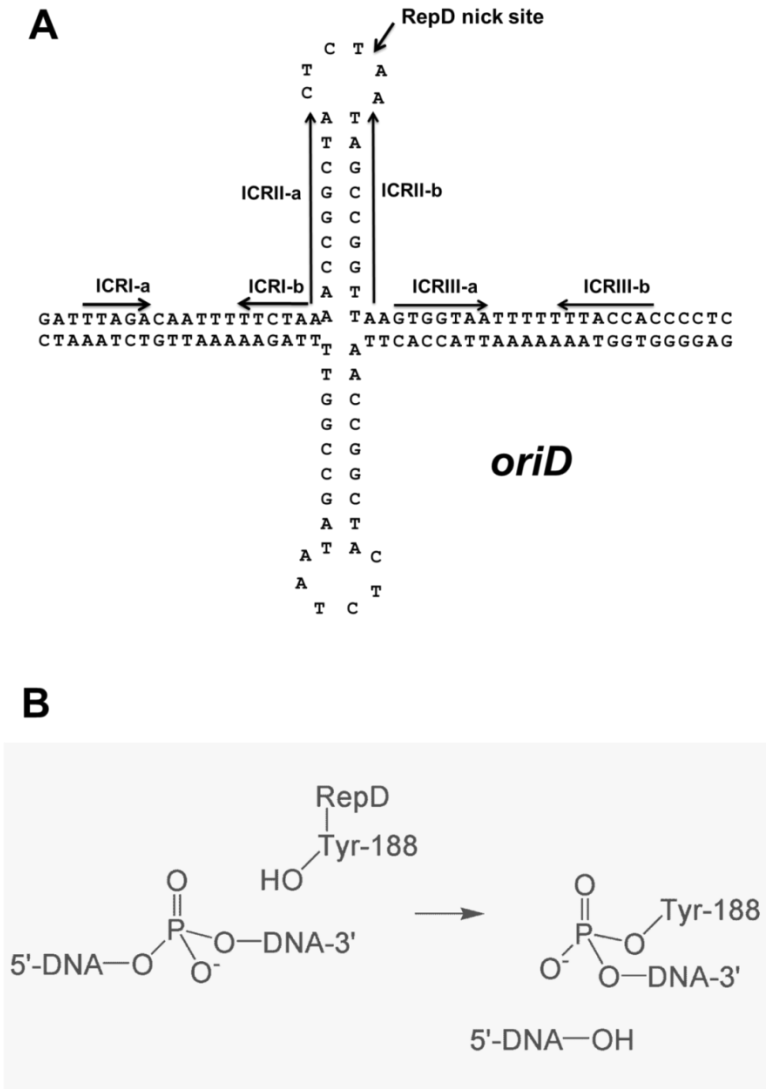

Figure 10. Initiation of plasmid unwinding at the origin of replication by RepD.

A) *OriD* sequence and its postulated secondary structure. B) RepD nicking reaction and covalent bond formation with DNA. RepD nicking includes a transesterification where on phosphodiester bond is broken between the DNA bases and another one is formed between the 5'end of nicked DNA and reactive tyrosine (Tyr-188) of the RepD. [85, 86]

1.4.2. *In vitro* studies of the molecular motor PcrA and initiator protein RepD

PcrA is one of the most studied helicases and its function has been investigated in detail, but a proven model for DNA unwinding has been hard to produce [6, 7, 36, 49]. Most evidence supports the idea that PcrA is functional as a monomer, but it has been suggested that it may function as dimer [37]. The main mechanistic functions of PcrA are ATP hydrolysis,

translocation on ssDNA and unwinding of dsDNA [51, 54]. PcrA is not known to bind dsDNA without a ssDNA overhang and is only able to translocate on ssDNA. The *in vitro* ssDNA translocation rate has been shown to be ~80 bases s^{-1} at 20°C and it hydrolyses 1 ATP per base translocated [51].

In vitro experiments show that PcrA cannot unwind even short DNA duplexes on its own and requires the presence of initiator protein RepD for processive DNA unwinding [83, 87, 88]. The compatibility of RepD and PcrA has been suggested as one of the regulating factors for the spread of antibiotic resistance carrying plasmids between bacterial species. Hence, probing this interaction may further our understanding of plasmid replication and the spread of antibiotic resistance in bacteria. The interaction surfaces between PcrA and RepD is not known. As has been shown using the plasmid unwinding assay developed in the Webb lab, PcrA and RepD are able to unwind plasmid lengths of dsDNA as long as ATP is present [87, 89]. The rate of plasmid unwinding in these experiments is ~30 bp s^{-1} at 30°C. The rate of genomic DNA synthesis for *S. aureus* DNA polymerase III holoenzyme has been measured as ~700 bp s^{-1} *in vitro* [90], hence implying that the rate of plasmid unwinding could be increased or DNA polymerase synthesis may be decreased to synchronise the speed of DNA unwinding and DNA synthesis. This has been shown to be the case in *E. coli,* where the DnaB helicase speed has been shown to be reduced by the interaction with DNA polymerases to allow enough time for the maintenance of the replication fork [91].

Once RepD nicks *oriD*, it remains as a part of the unwinding/replication complex until the (-)-strand is fully unwound/replicated [85]. RepD has been shown to bind all the ICRI-III sequences, but nicks it only at ICRII [92]. The rate of RepD nicking of pCER*oriD* plasmid has been determined as > 25 s^{-1} [93]. Fluorescence based assays have been developed to study RepD dependent DNA unwinding by PcrA on DNA structures that mimic the *oriD* .This assay has shown that RepD does not need to be covalently bound to the DNA to facilitate the RepD dependent unwinding as the nicking deficient RepD was able to induce processive DNA

unwinding [93]. Of course, RepD nicking is a requirement for plasmid unwinding as it enables PcrA binding to ssDNA. The RepD nicking rate of *oriD*-mimic DNA junctions has been determined as ~1 s^{-1} indicating the supercoiled plasmid is significantly better substrate for RepD nicking than linear DNA [93].

1.4.3. PcrA function in DNA repair and RecA filament removal

PcrA functions in the replication of a certain family of plasmids carrying initiator protein and antibiotic resistance genes. This function itself is important in the transfer of DNA between individual bacteria and between different bacterial species, thus the ability to recruit an endogenous helicase during the replication of plasmid DNA is beneficial for the organism. In other words, an organism having a helicase able to unwind exogenous DNA has been positively selected through natural selection. This is unlikely to be PcrA helicases' only function as the replication of plasmids isn't essential for survival of the organism but the presence of PcrA is [50]. There have been several publications with experimental evidence suggesting a possible role for PcrA in DNA repair [50, 94, 95]. This could involve removing "road blocks" from DNA that may introduce DNA abnormalities and stall DNA replication, for example DNA-binding proteins or secondary DNA structures formed on ssDNA.

PcrA *E. coli* orthologue UvrD and homologous Rep helicases have been used to compare their possible functions in DNA repair. All three helicases, PcrA, UvrD and Rep, share a function of replicating exogenous DNA; UvrD unwinds Gram-negative rolling circle plasmids, Rep unwinds bacteriophage M13 and ΦX174 DNA and PcrA replicates Gram-positive rolling circle plasmids [47, 78, 96], but most have also been shown to have function in other endogenous cellular processes. Several points from previous work, which indicate this, are discussed here. As mentioned before, Gram-negative bacteria *E. coli* helicases Rep and UvrD share high sequence similarity with PcrA and are also structurally and functionally very

much alike (Figure 3). However, PcrA deletion is lethal to an organism, whereas deletion of Rep or UvrD is not lethal [50]. Deletion of both Rep and UvrD simultaneously is detrimental for the *E. coli*, thus it has been suggested that they are together functionally equivalent to PcrA [97]. It has also been shown that the Rep helicase and UvrD are not functionally equivalent to each other. UvrD is known for its function in UV damage repair and mismatch repair by activation of MutL [98]. UvrD *E. coli* mutants have been shown to be hyper-recombinogenic, indicating a function in DNA repair [99]. The UV repair in *E. coli ΔuvrD* can be rescued by expression of PcrA. Rep helicase has been shown to take part in genome replication in *E. coli* and interact with the replicative helicase DnaB [100].

In vitro UvrD has been shown to perform RecA filament removal [101]. RecA filaments are an important part of homologous recombination mediated DNA repair as they bind to ssDNA after double stranded DNA break and scan for homologous sequences to enable the break to be repaired [102-105]. The control of RecA filament formation and removal is vital for the cell and an organisms' survival, requiring a control step that is able to remove unwanted RecA filaments and prevent unnecessary recombination. Similarly to the *E. coli* UvrD, the closest eukaryotic PcrA orthologue, the *S. cerevisiae* Srs2 helicase, is involved in Rad51 filament removal, which is functionally equivalent to *E. coli* RecA filaments [43, 106]. PcrA deletion has been shown to lead to hyper-recombinogenic cells and the lethality of the *prcA* deletion can be overcome by deletion of *recFOR* genes [50, 97]. *RecFOR* genes express proteins that mediate the loading of RecA on to ssDNA during recombination [107]. *In vitro* evidence also showed that PcrA was able to remove toxic RecA filament structures [95]. These mutants were unable to unwind the DNA, but were able to remove RecA proteins either by translocating on ssDNA or possibly reeling it. In the experiments by Anand *et al.* (2007) ATP hydrolysis also seems unnecessary for PcrA-mediated removal of RecA from DNA. This is quite surprising as translocation on ssDNA requires ATP. Further, experiments by the same group also state that DNA unwinding and ATP hydrolysis may take part in RecA removal [95].

A single molecule assay by Park *et al.* (2010) using FRET showed PcrA removing RecA filaments [94]. In these experiments, the PcrA was shown preferentially to bind to the DNA junction. An oscillating FRET signal was observed in the presence of ATP. This was thought to correspond to the PcrA being adhered to the fork junction and reeling the ssDNA in a 3'-to-5'direction, hereby removing RecA filaments.

1.5. Fluorescence

Many fluorescent-based techniques have been developed for studying cellular structure and function, as well as interactions of molecules in biological systems. Fluorescence is also important in the detection and quantitation of nucleic acids and proteins in gel electrophoresis, microarrays and fluorescence spectroscopy. Understanding how fluorescence takes place is vital for the development of these techniques. Many aspects of fluorescence and its uses were reviewed in Lakowicz J.R. (2006) [108]. Fluorescence is a process where a fluorophore absorbs light at a certain wavelength, which forms an energetically excited state that is released as emission at a different wavelength. The electron in its excited state has different paths to return back to the unexcited state that depend upon the exact nature of the fluorophore and its surroundings. If the deactivation of the excited state takes place by loss of energy by emission of photons, the process is known as fluorescence. This is schematically illustrated in a Jablonski diagram (Figure 11), proposed by Alexander Jablonski in 1930s [109]. The other main deactivation process that may occur is internal conversion followed by vibrational relaxation, which is also non-radiative loss of energy to surroundings as heat or intersystem crossing to the triplet state and it is known as phosphorescence. Before excitation by absorption of light the molecule is in the ground state (S_0). The absorption of energy leads to excitation of electrons to higher energy and vibrational states (S_1). This occurs on a time scale of 10^{-15} seconds. Before returning to ground state the electrons move to lower vibrational states, which occur on a time scale of 10^{-14} to 10^{-11} seconds. The relaxation through fluorescence is on a time scale of 10^{-9} to 10^{-7} seconds. For many of the fluorescence based methods used in experiments, such as presented in this thesis, the triplet state emitted as phosphorescence is undesirable as it doesn't contribute to the fluorescent signal and occurs on a longer time scale of 10^{-3} to 10^{2} seconds, which may be too slow for detection of enzyme mechanics.

Fluorophores absorb light at a specific range of wavelengths with a characteristic peak at a maximum excitation and emit light at the specific range of wavelengths with a peak of emission maximum. For example, Cy3B maleimide has an absorption maximum of 549 nm and emission maximum of 570 nm. The absorbed light has higher energy than the emitted light, as some of the absorbed energy is lost to the system and by other non-radiative relaxation pathways. This phenomenon is known as the Stokes shift. Structurally, fluorophores are usually aromatic compounds with one or multiple carbon rings containing conjugated double bonds. Aromatic fluorophores are small in size ranging from a few hundred Daltons to a maximum of ~1000 Daltons (MDDC – 382 Da and Cy-dyes ~800 Da) when compared to fluorescent proteins like GFP, which is ~26 kDa.

The efficiency of fluorescence emission can be expressed through the quantum yield (ϕ), which defines quantitatively the probability of the excited state being deactivated by fluorescence rather than any other mechanism. This can be calculated by: ϕ = number of photons emitted/number of photons absorbed. The quantum yield always has a value below 1. Other factors that affect the fluorescence characteristics are the extinction coefficient, which determines how much light the fluorophore is able to absorb, and the fluorescence lifetime of the fluorophore (duration of the excited state). These factors can be affected by most environmental factors, which include the type of solvent, ionic strength, temperature and pH of an aqueous solution. The change in quantum yield of a fluorophore due to a change in its environment can be used as a probe of conformational changes near the fluorophore attachment point.

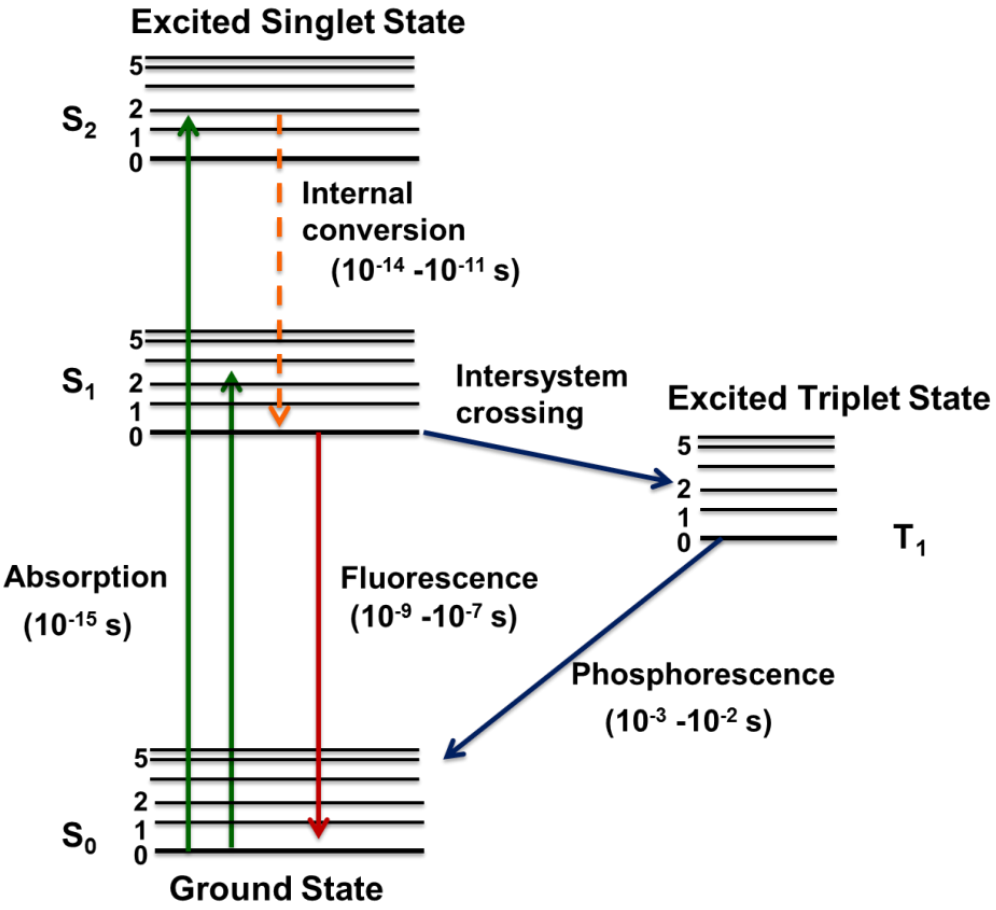

Figure 11. Jablonski diagram of absorbance, fluorescence and phosphorescence.

1.5.1. Förster resonance energy transfer

If two fluorophores are in close proximity and at a correct angle to each other energy transfer can take place, if the donor fluorophore has an emission spectrum that overlaps with the excitation spectrum of another fluorophore (acceptor). The energy is transferred in a non-radiative manner to the acceptor [110-112], which is then excited and emits the energy transferred as fluorescence. This is called Förster or fluorescence resonance energy transfer (FRET) and the efficiency of the energy transfer (E_{FRET}) is dependent on the distance and the orientation of the donor and acceptor fluorophores. The E_{FRET} can be written as shown in Equation 1.

Equation 1:

$$E_{FRET} = \frac{1}{1 + R^6/R^6_0}$$

In Equation 1, R is the inter-dye distance and R_0 is the Förster radius at which E_{FRET} is 0.5. The E_{FRET} has a value between 0 and 1. The Jablonski diagram for FRET is shown in Figure 12. For Cy3 and Cy5 dyes the R_0 is ~5.5 nm and typically FRET is seen to observable up to distance of 10 nm between acceptor and donor, but often in experimental set ups it is significantly less than 10 nm. Following distance changes between two molecules using FRET is possible by labelling the molecules with fluorophores suitable for FRET. It is often enough to determine the intensities of donor and acceptor fluorophores at different reaction states for correct measurement of FRET efficiency and its variation due to changes in the reaction.

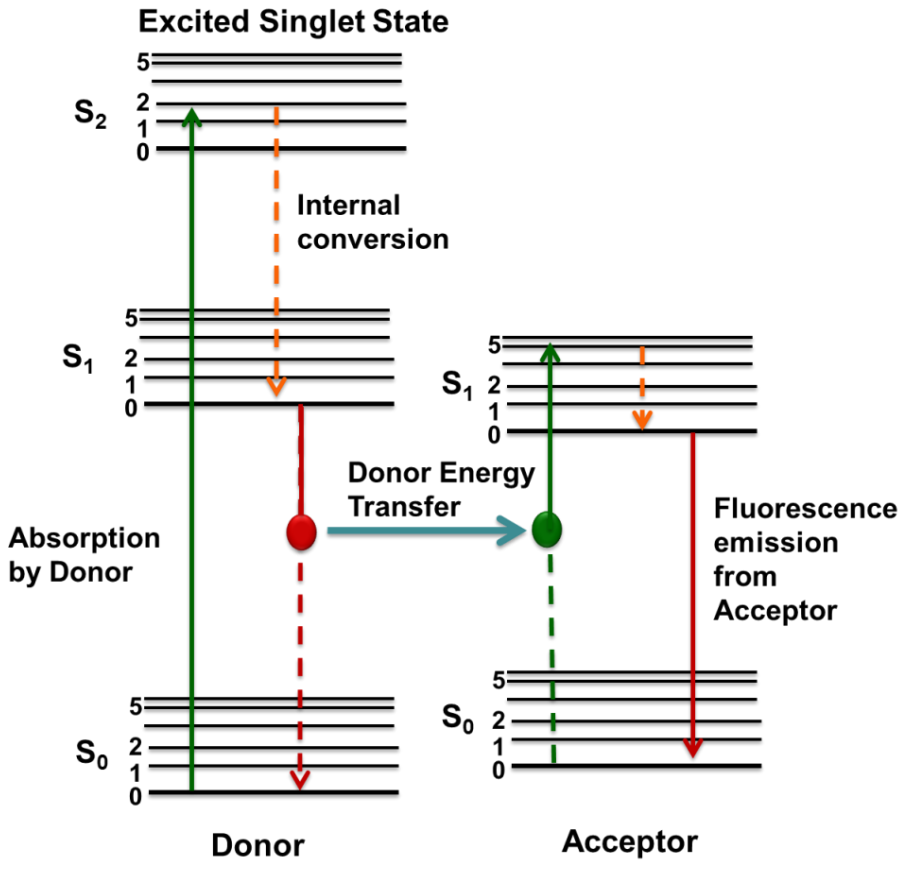

Figure 12. Jablonski diagram for Förster resonance energy transfer.

1.5.2. Anisotropy

Fluorescence anisotropy is the property of a fluorophore to absorb polarised light (photons) at a particular range of angles. If the fluorophore does not move/rotate, the photons emitted are also polarised. In biochemistry, anisotropy uses fluorophores such as fluorescein attached to the ligand or protein and relies on the existence of transition dipoles for absorption and emission lying along the specific direction of the fluorophore (Figure 13). These transition dipoles are used to excite randomly oriented molecules in the solution with polarised light. The emission of the molecules is measured and some of the excited molecules become depolarised as the molecules "tumble" in solution. This depolarisation can be calculated by measuring the intensity of parallel and perpendicular light and is expressed as anisotropy (*r*). Equation 2 can be used to calculate anisotropy, where $I_{\parallel}$ is the intensity of parallel light and $I_{\perp}$ is the intensity of perpendicular light. The rate of "tumbling" is dependent on the size of the molecule or complex and so, when a ligand is bound by protein its tumbling is slowed down, which can be observed as a change in anisotropy. The rate of tumbling is not only dependent on the size of the molecule, but is also affected by the linker that connects the reactive group to the fluorophore. If the linker allows for a larger movement of the fluorophore, larger tumbling can be expected, which is observed as low anisotropy.

Equation 2:

$$\text{Anisotropy (r)} = \frac{I_{\parallel} - I_{\perp}}{I_{\parallel} + 2I_{\perp}}$$

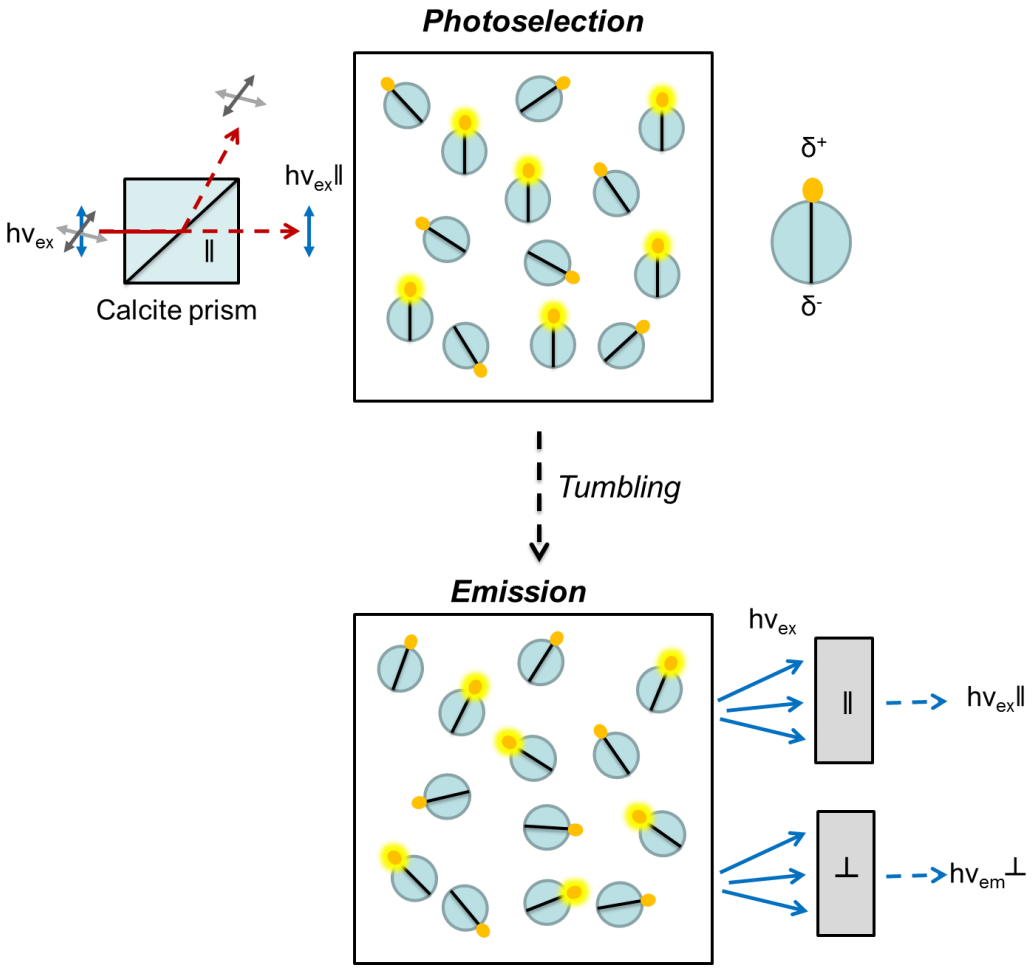

Figure 13. Fluorescence anisotropy.

Vertical polarisation (‖) of excited light is achieved by passing the excitation light through a calcite prism. Only fluorophores with the excitation transition dipoles parallel to the excitation plane are excited in a process called 'photoselection'. Fluorophores in the excited state are able to tumble in solution within their fluorescence lifetime. Emission is measured at the appropriate wavelength for the fluorophore through polarizers that are parallel (‖) and perpendicular (⊥) to the plane of the excitation. Fluorescence anisotropy is calculated using Equation 2. The observed rate of tumbling is dependent on the size of the macromolecule and the linker on the fluorophore. If tumbling is fast, low anisotropy is observed and vice versa.

1.5.3. Utilisation of fluorescence to study protein function

Fluorescence is used in many assays and applications. It can be used *in vitro* to investigate enzyme binding to its ligand or to fluorescently label molecules in a cell. To study protein interactions and enzyme kinetics, the

use of fluorophores as reporters of the reaction is advantageous due to their sensitivity and rapid response. The time scale of the main steps of excitation and emission of fluorophores are given in Figure 11 and often occur at a nanosecond timescale, making them fast enough to investigate biological processes that are often significantly slower. Fluorescent labelling can be highly sensitive and enables the observation of reaction components at nanomolar concentration and individual fluorophores can be observed in single molecule assays.

The three of the main fluorescent properties of fluorophores used in assays to study biological processes are fluorescence intensity, fluorescence anisotropy/polarisation and FRET. The fluorescence intensity can be used by labelling the ligand or protein in question with fluorophores that respond to environmental changes via their quantum yield. The change in quantum yield can be observed as either decreased or increased fluorescent signal when two molecules interact. FRET can be used by measuring the FRET efficiency of FRET labelled molecules as discussed in the previous Section 1.5.1.

1.5.4. Attachment of extrinsic fluorescent probes to biomolecules

The use of fluorophores for *in vitro* assays requires a form of attachment of the fluorophore to the desired molecule. Molecules like DNA and nucleotides like ATP with fluorophore modification can be obtained relatively easily as many can be purchased commercially. Attaching a fluorophore to the molecule may affect the native form of binding and processing of these molecules by sterically hindering binding or enhancing the binding by increasing the substrate affinity. When experiments are designed using fluorophores this is something that is to be taken into account.

Another option is the fluorescent labelling of the enzyme. Depending on the function of the enzyme this can make the signals harder to understand, as enzymes are often able to perform several chemical

functions and may interact with multiple components in the reaction. The fluorescent labelling of proteins can be achieved by several methods, but typically requires modifications to be made *in vitro* and rely on expression and purification of mutant protein. Many methods have been published for attaching a fluorophore onto a protein. The NHS-ester attached fluorophores react with amine groups. There may be many amine groups in one protein molecule. Another method is the use of maleimide/iodoacetamide chemistry. These groups can be attached to the desired fluorophore and sometimes bought commercially. Iodoacetamide and maleimide are selectively reactive with the –SH groups of cysteine residues. Many other forms of labelling of peptides and proteins have been and are being developed, for example inteins [113] and bromomaleimides [114].

Orthogonal nonsense suppressor tRNA labelling strategies involve introduction of unnatural amino acids into proteins, which can then be used to attach modifications site specifically [115]. This method is called unnatural amino acid mutagenesis (UAAM) and over 100 different unnatural amino acids have been introduced into proteins using this method [115]. UAAM uses engineered aminoacyl-tRNA synthetase that incorporates an unnatural amino acid at an amber (nonsense) codon. For example, this can be the p-azido-L-phenylalanine, which is sensitive to UV light and at exposure to wavelengths below 310 nm, photo crosslinks with amines [116]. This method can be used for *in vivo* and *in vitro* labelling.

Maleimide/iodoacetamide coupling chemistry is often seen as the most well established and highly selective method of protein labelling. For coupling with maleimides, cysteine residues must be located at the surface of the protein to allow accessibility. If environment sensitive fluorophores are used, the conformational change in protein must change the environment of the fluorophore, hence the cysteine often has to be located close to the interaction or reaction site to have an effect on the environment of the fluorophore when the molecule interacts or catalyses a reaction.

1.5.5. Fluorescent biosensors

Many fluorescence based biosensors have been developed to study enzyme function and kinetics and protein-ligand/protein-protein interactions due to their advantageous properties. These include the fluorescent signal that does not affect the system being studied, user safety and ease of disposal as compared to radioactive labels and most importantly real time measurement of the reaction [117, 118]. Examples of such biosensors include genetically encoded biosensors that contain the GFP or its derivatives coupled to a target protein [117]. These enable the observation of protein localisation and possible interaction *in vivo*. This method requires the production of a construct with GFP and its successful transfection and expression in the cell. Another, relatively common group of biosensor constructs are the aptamers [119]. These are peptide or nucleic acid based molecules that have highly specific binding to a molecule of interest such as ATP.

Another type are the reagentless biosensors [118]. They are protein-based, sometimes enzymes, with site-specific fluorophore modification to report on specific reaction or interaction. They can be produced to high purity and in high amount in *E. coli* and labelled with suitable fluorophore(s) after purification *in vitro*. Good examples of reagentless protein-based biosensors are the P_i biosensor MDCC-PBP/6ATR-PBP (fluorophore-labelled phosphate binding protein) [120], ssDNA biosensor DCC-SSB [89] and ADP biosensor MDCC-ParM [121]. These biosensors can be applied to many biological systems *in vitro* and some *in vivo*, but the main use has been *in vitro*. The introduction of reagentless biosensors into cells is complicated and often requires techniques such as microinjection that can be time consuming and cause damage to the cell. Typically, the fluorescent biosensors are made from enzymes that have a high affinity to the ligand of interest. For labelling, environment sensitive fluorophores, such as the coumarins, are used and introduced through genetic modification of the enzyme. The native residue is mutated into a cysteine residue that is reactive with a maleimide or iodoacetamide attached through a linker to the fluorophore. Genetic

modification is often required for enhancing the selectivity of the biosensor, where an amino acid is changed site-specifically at the reaction site of enzyme so that it changes the affinity of the enzyme to its substrate or substrate-type, for example ADP over ATP in case of the Rhodamine-ParM [122, 123].

1.6. Rapid reaction techniques

Rapid reaction techniques are biochemical *in vitro* techniques that include methods which can be used to observe biological processes in real time. This is required as many biological processes occur on the millisecond time scale. The observation of a reaction that is at steady-state only allows the rate constant of the rate limiting step to be measured. Rapid reaction techniques enable the analysis of chemical steps of reactions, enabling determination of individual rate constants, which can be highly informative of the biological process in question [124, 125]. Several methods have been developed for the measurement of rapid kinetics and they can be divided broadly into rapid mixing and relaxation based techniques.

The rapid mixing techniques include methods that use specially designed apparatuses, which use the flow of solutions to push and rapidly mix the reaction in the observation chamber. These include methods such as stopped-flow (discussed individually in the next section), quenched flow and photolysis of caged compounds (Figure 14). Photolysis uses caged compounds that can be photo activated by a fast pulse of light. For the helicase assay a caged form of ATP can be used, which is released by a light pulse. Once the ATP is available the helicase can start to unwind the DNA.

The quenched flow is built so that two reactants are rapidly mixed together and pushed into “aging tube”. The aging tube length can be varied to enable measurements of reactions at specific time points after mixing. The reaction is then quenched to stop the reaction using stop solutions of acid or quenchers like EGTA and EDTA that remove the metal ions from the

enzymes. The reactions are collected and run on HPLC or analysed by other suitable methods to separate the reactants and the products. For example, running samples on 1% agarose gel was used to separate nicked and un-nicked plasmid to measure RepD plasmid nicking rate [93]. Quenched flow can be seen as more labour intensive than stopped-flow, but it is highly valuable when no signal can be observed or interpreted using other methods and enables measurement of the formation or breakage of covalent bonds.

Reactions that take place faster than what can be measured using rapid mixing techniques can be measured using relaxation techniques. Here a rapid change to the equilibrium of a system is induced and the effect of this change is observed. This can be achieved by rapidly changing the temperature or pressure of the reaction [124, 126, 127].

All the above techniques require a suitable optical signal to be produced, which can be based on radioactivity or fluorescence. Sometimes, intrinsic chromophores can be used and these include the tryptophans and tyrosines of proteins. Often, extrinsic chromophores such as environmentally sensitive fluorophores are the preferred choice, as they offer a larger range of excitation and emission wavelengths with better fluorescence quantum yields [128].

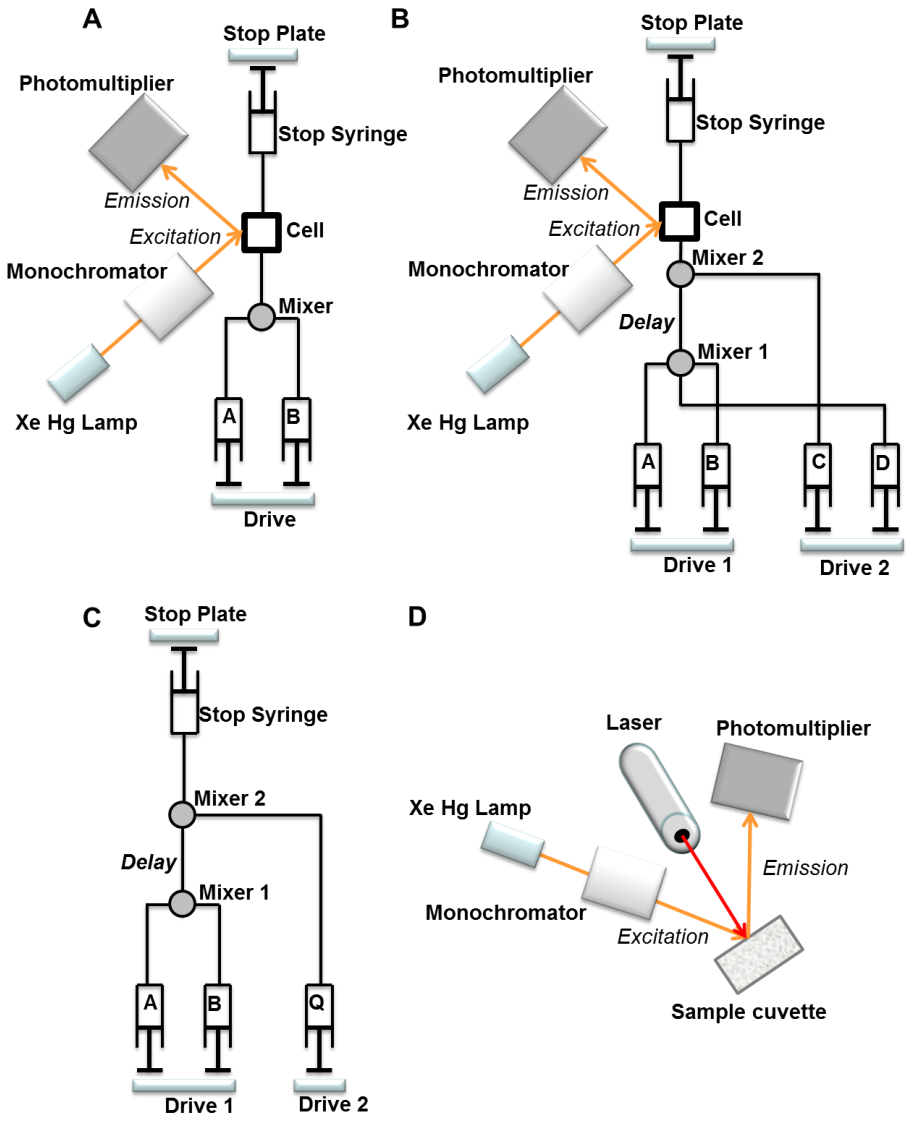

Figure 14. Rapid mixing techniques.

A) Stopped-flow apparatus with single-mixing set-up. The reactants are placed into syringes A and B and mixed together in the mixing chamber. The reaction is observed in the observation chamber. The drives and stop plate have tight control over the volumes pushed out from the syringes. B) Stopped-flow apparatus with double-mixing set-up. The first reactants are mixed from syringe A and B in mixing chamber 1. The delay or duration of the first mixing can be controlled before this solution is mixed with a third reactant from syringe C. The entire reaction is then pushed into the observation chamber by buffer/reaction mixture from syringe D. C) Quenched flow set-up. In quenched flow experiments two reacts are mixed together similarly to stopped-flow, but the reaction is stopped by a quencher from a third syringe Q. The reactions are performed with different aging times and the reaction components can be analysed with a suitable method, e.g. by HPLC. D) Photolysis set-up. In photolysis, the start of the reaction can be controlled tightly by use of a caged compound that is released by a pulse of light. The same optical set-up is used in stopped-flow and photolysis set-ups to observe the reaction.

1.6.1. Stopped-flow spectrometry

Current stopped-flow methods were developed from continuous flow methods by Gibson *et al.* 1952 [129] and are often the preferred choice for measurement of reactions where tightly controlled rapid mixing is required [124, 130]. In the preceding continuous flow techniques the reaction was studied under constant flow by measuring an optical signal at different locations along the flow path. These data reference different time points along the reaction trajectory. One of the main disadvantages of constant flow methods is the requirement of large volumes of the reactants. In a single-mixing experiment on stopped-flow the total volumes required are small and for one reaction ~20 µl can be enough [124, 130]. In single-mixing experiments a pneumatic pump is used to mix and rapidly push two reactants from the syringes into the mixing tube and from there directly into an observation chamber (Figure 14A and Figure 20 in Methods). The reaction mix flow is stopped by the “stop” syringe. The need to achieve complete mixing before the reaction is pushed into the observation chamber causes a dead time of typically 1-2 milliseconds. The optical signal can be achieved by using fluorophores, whose difference in excitation and emission wavelengths offers a useful way to limit the noise from excitation light through the use of cut off filters [128]. The excitation is achieved using a lamp, for example xenon-mercury lamp, and the photons of the emission signal are collected through photo-multiplying tubes at a 90° angle to the path of the exciting light.

Stopped-flow can also be used for double-mixing experiments (Figure 14B), where the two reactants are mixed in an aging loop and then a third reactant is mixed after a delayed time with the already initiated reaction before being pushed into the observation chamber. This can be used to follow the formation of short-lived intermediates followed by their degradation. The mixing of the first reactants is not observable in the typical stopped-flow set-up. Other possible measurements on the stopped-flow are fluorescence anisotropy measurements using polarised light. The stopped-flow is set to ‘T-format’ that allows the detection of both the parallel and

perpendicular polarised light emitted. The values from the detectors can be analysed using Equation 2 (Section 1.5.2) to determine the anisotropy change in the reaction.

In this thesis, the ensemble methods performed on the stopped-flow are single-mixing experiments with use of fluorescently labelled substrates. Ensemble methods rely on synchronisation. In these experiments, the synchronisation of PcrA helicase in the ensemble measurements is mostly achieved by controlled mixing with ATP. In this way the signal observed can be explained and understood, as long as or while the synchronisation is maintained in the majority of the population.

1.7. Rapid reaction kinetics with fluorophore labelled enzyme

A change in fluorescence when a labelled molecule binds to another molecule, such as a labelled protein binding to its ligand, can be used to determine the equilibrium constant as well as the association and dissociation rate constants of the ligand and the protein in question [124]. Here, the equations used are for fluorescently-labelled enzyme and they are used to demonstrate how the equations can be used to analyse the rapid reaction kinetics data. If the fluorescence signal is large enough, a simple titration experiment on a spectrofluorometer can be carried out to determine the protein's affinity to its ligand. This is expressed as equilibrium dissociation constant (K_d). If the signal is too small for titrations, it is often large enough to measure binding and dissociation kinetics using a stopped-flow instrument. In these experiments the association rate constant (k_{on}) and dissociation rate constant (k_{off}) are obtained and from the ratio of k_{off}/k_{on} the equilibrium dissociation constant can be calculated (Equation 4).

In a typical association experiment the fluorescently labelled binding partner is mixed with a large (> 10-fold) excess of the unlabelled species, providing pseudo-first-order conditions. In this case the kinetics can be described by a single exponential function with apparent first order rate

constant, k_{obs}. When the signal is due to protein binding to the ligand, the observed rate constant (k_{obs}) increases linearly with increasing ligand concentration (Scheme 1, Equation 3).

See Figure 15A for an example of a hypothetical ligand binding measurements with a fluorophore-labelled protein. As shown in Equation 3 the association rate constant (k_{on}) can be determined from the slope and the dissociation rate constant (k_{off}) from the y-intercept value of a linear fit to k_{obs} versus ligand concentration. In some cases the k_{off} is too close to zero. For these reasons the estimation of k_{off} from the y-intercept of binding measurements is often not accurate.

A displacement assay is more accurate way to determine k_{off}, if the binding is fast and high concentration of the unlabelled protein is available. This can be done by loading the labelled protein with ligand and then rapidly mixing with a large excess of unlabelled protein (Scheme 2). If dissociation is a single step process (first order reaction) and the unlabelled protein is in large enough excess, the observed rate constant does not vary with the unlabelled protein concentration represents the dissociation rate constant. The dissociation constant K_d can be calculated using Equation 4 if the values for k_{on} and k_{off} are known.

Some binding measurements show hyperbolic dependence of the observed rate constant with increasing concentration of the ligand. This indicates a two-step binding process, where one of the steps is the binding and the other is a conformational change associated with the change in fluorescence (Scheme 3). See Figure 15B for an example of hypothetic labelled protein binding measurements to ligand indicating a two-step binding process. In this situation the observed rate constant can be calculated by Equation 5, K_{d1} is the dissociation constant of the first step, k_{+2} is the association rate constant and k_{-2} the dissociation rate constants of the second step. The y-intercept corresponds to k_{-2}. At very high [D] the value of k_{obs} is $k_{+2} + k_{-2}$. The dissociation constant for the overall reaction, $K_{d\,(overall)}$, can be calculated using Equation 6.

Scheme 1:

$$P + D \underset{k_{off}}{\overset{k_{on}}{\rightleftharpoons}} P^*.D$$

P is the labelled protein. *P** is the labelled protein with a fluorescent signal change. *D* is the ligand.

Equation 3:

$$k_{obs} = k_{on}[D] + k_{off}$$

Scheme 2:

$$P^*.D \xrightarrow{k_{off}} P^* \qquad D \xrightarrow[k_{on}]{P} P.D$$

$$k_{off} << k_{on}$$

Equation 4:

$$K_d = \frac{k_{off}}{k_{on}}$$

Scheme 3:

$$P + D \underset{K_{d1}}{\rightleftharpoons} P.D \underset{k_{-2}}{\overset{k_{+2}}{\rightleftharpoons}} P^*.D$$

Equation 5:

$$k_{obs(slow)} = \frac{k_{+2}[D]}{K_{d1} + [D]} + k_{-2}$$

Equation 6:

$$K_{d(overall)} = K_{d1} \times \frac{k_{-2}}{k_{+2}}$$

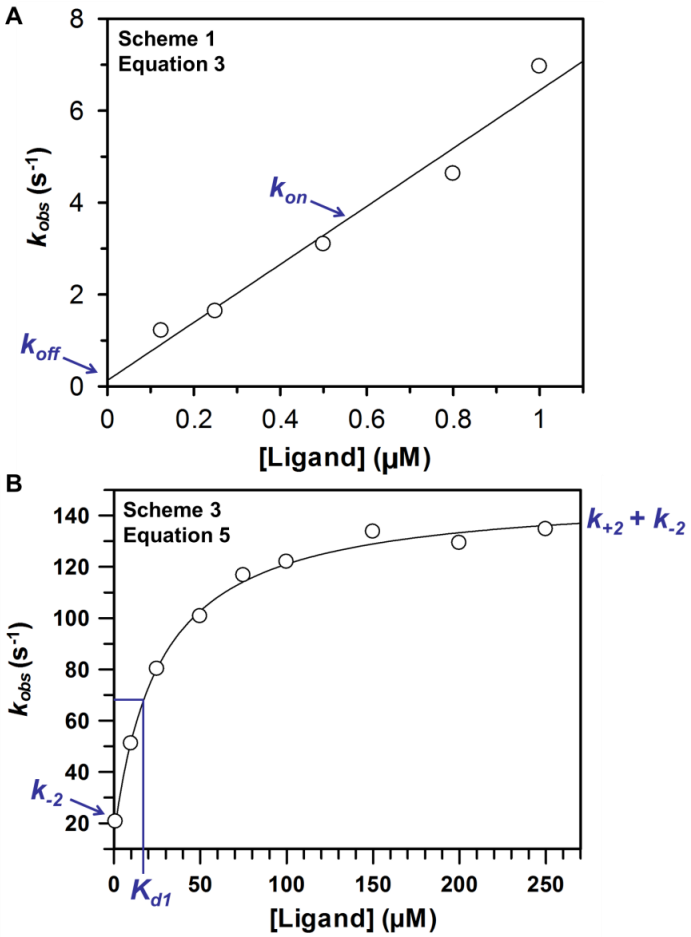

Figure 15. Protein binding kinetics measured using different concentration of the ligand.

A) k_{obs} follows the ligand concentration dependence according to Scheme 1 and Equation 3. B) k_{obs} follows the ligand concentration dependence according to Scheme 3 and Equation 5.

1.8. Single molecule assays

Single molecule assays are biophysical techniques that allow investigation of properties of individual molecules. This is very different to ensemble methods that look at how vast number of molecules function at the same time, where the signal observed is an average of those multiple processes taking place simultaneously. Since the first single molecule experiment was performed in the 1970s on ion channels, the number of studies and their importance in answering biological questions has increased. Often they are used to complement and offer an alternative perspective to the ensemble experiments. The most obvious benefit of single

molecules assays is their ability to measure individual molecules. This removes the effect of averaging applied to ensemble assays and enables the measurement of possible multiple chemical states, macromolecular conformations or kinetics steps present in a reaction. Observation of individual molecules may also show different populations of biomolecules. These properties of single molecule experiments are represented in Figure 16, which shows a diagram of the “single molecule paradigm”. The diagram depicts three types of traffic, where the cars represent individual biomolecules such as motor proteins. All the traffic in all three scenarios has the same average speed, which represents the signal observed in ensemble experiments. In scenario 1 all cars are moving in a uniform manner at the same speed. In setting 2 the cars are moving at different speeds, but in a uniform manner in the separate lanes, with some of the cars stalling. The third case shows cars moving in a random manner, changing lanes, stalling and re-starting. Single molecule assays can overcome the drawbacks of averaging the speed of the cars, in other words the behaviour of biomolecules in large populations. They also enable measurements of the dynamics of enzymes at equilibrium conditions and other conditions that cannot be easily synchronised. Ensemble methods rely on synchronisation, which may not always be achievable.

Single molecule measurements, such as those using magnetic tweezers, enable the measurement of direct molecular forces and as single molecules are observed the variation between the molecules and possible populations within the sample can be determined. In some systems, single molecule assays may enable the observation of only active enzymes as inactive enzymes do not show a signal and are excluded from the analysis. Co-operative activity of enzymes is often not detectable at single molecule level, but specific assays have been developed at single molecule level, which in fact look at the co-operativity of an enzyme. An example of this are the ATP binding and hydrolysis studies of 16 subunit chaperonin TriC [131], where Cy3-labelled ADP photobleaching was measured on TIRFM. This showed distinct steps of individual Cy3-ADP/ATPs photobleaching, which gave clues as to the number of ATPs bound to chaperonin.

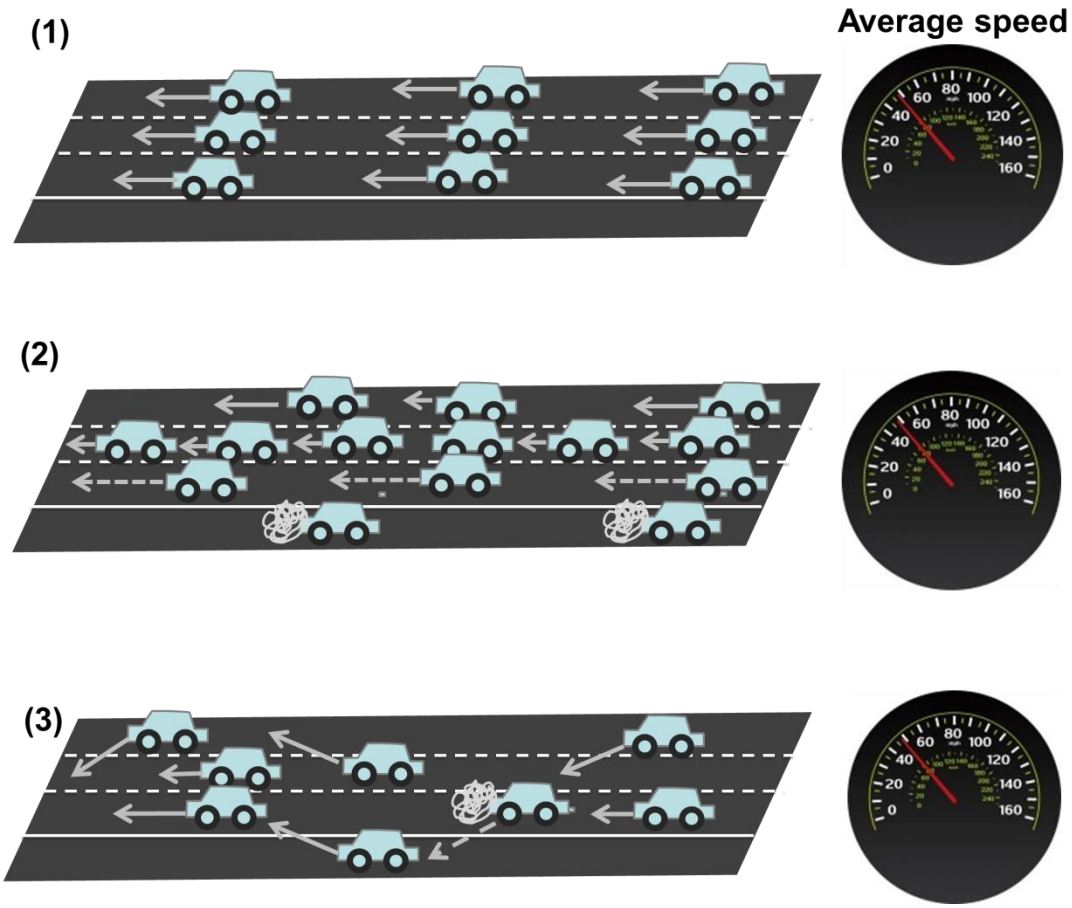

Figure 16. Single molecule paradigm.

The image shows a cartoon representation of three different ensemble assays using traffic flow as an analogy. All three scenarios have the same average speed, which represents the signal observed in ensemble experiments, which is an average of all events in a reaction. In single molecule assays one can observe individual molecules, here represented by cars, and possibly determine different behaviours, conformations and kinetics of the individual macromolecules. For example, in scenario 1 all the cars are moving at a uniform speed and manner. In scenario 2, some of the cars are stalled and others are travelling at various speeds, but moving in a uniform manner. The cars in scenario 3 are moving at various speeds and manners, with some of them stalling and re-initiating.

Single molecule work can be divided into structure-, force- and fluorescence-based techniques. Examples of the structure-based methods include single particle tomography using electron microscopy (EM) and atomic force microscopy (AFM). Both of these methods look at “snap shot” images of molecules once the reaction has been stopped and can be used to visualise protein-protein/protein-DNA interactions and different conformational states of biomolecule of interest. Figure 17A, shows an image captured using the AFM set-up. The biomolecules of interest are attached to a mica surface and a cantilever is dragged along the surface producing a surface height map using laser and diode detector. Both, AFM and EM tomography have been successfully used to determine characteristics and functions of helicases. Cryo-EM, for example, has been used to show the hexameric ring structure of the Rho helicase [132] and the ring structure of the homohexameric archaeal MCM helicase. Analysis of the latter showed a channel large enough to accommodate dsDNA, indicating MCMs ability to translocate on dsDNA [30]. AFM has been used to take “snap shots” of a helicase in action by starting the reaction and stopping at a desired time point. With PcrA, the plasmid unwinding states of unwound, partially unwound and fully unwound plasmid can be observed when different time points are used for stopping the reaction [133] (Arbore C. *et al.* and Lynch G. *et al.* personal communications). Similarly, AFM has been used to study DNA unwinding by the DEAD box helicase [134].

Studying a biological process in an aqueous environment at single molecule level enables the measurement of reactions in real time. This is especially beneficial and important for molecular motors, such as DNA translocases and helicases. The most common of these types of techniques are the magnetic tweezers, optical tweezers and fluorescence-based methods on a total internal reflection microscope. These set-ups are shown in Figure 17B to D.

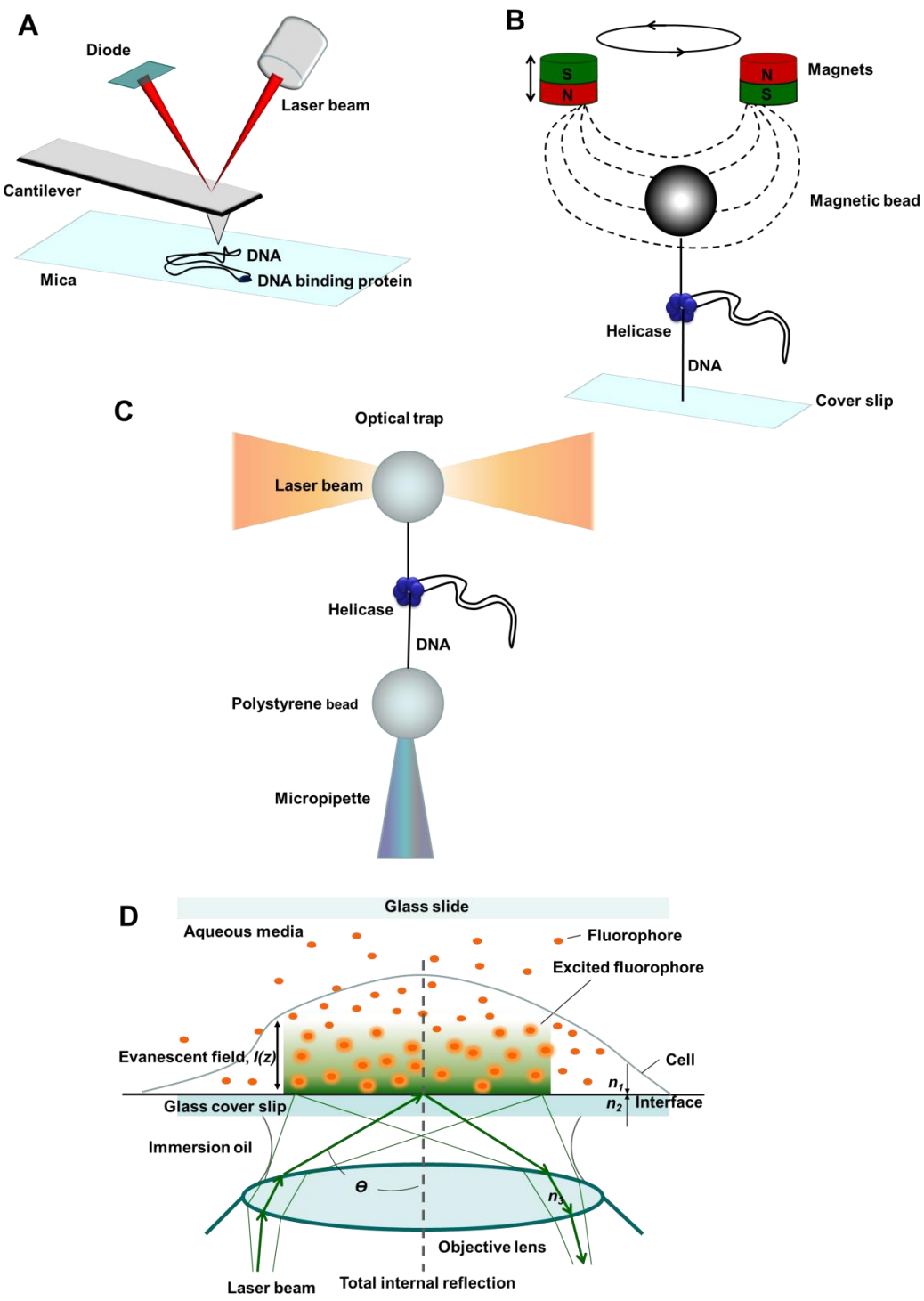

Figure 17. Single molecule assay methods.

A) Atomic force microscopy used to observe DNA structure and interaction with DNA binding proteins. B) Magnetic or optical tweezers C) set up to study helicase unwinding. D) Model of TIRF assay set up for the observation of molecules in the cell or on the cell surface. n_1 and n_2 are the refractive indexes for the different media in the TIRF assay, Θ is the incident angle for the light, which has to be larger than Θ_C for TIR to take place. The Θ_C is calculated by $\Theta_C = \arcsin^{-1}(n_2/n_1)$ [135]. n_1 = 1.51 for glass and n_2 = 1.33 for water.

1.8.1. Total internal reflection microscopy

Total internal reflection describes the physical property of light when it travels from a high- to a low-refractive index medium and hits the interface of two media at an angle called the critical angle (Θ_c). If the angle is equal to or higher than the Θ_c, the light will be reflected from the interface and won't pass through the first to the second medium. For example, in the case of water and glass, which have the refractive indexes of n_1 = 1.33 and n_2 = 1.51, respectively, the critical angle is 62°. The critical angle for two media can be calculated using the equation $\Theta_c = \arcsin(n_2/n_1)$. The region where the light is reflected produces an evanescent field at the optical frequency above the cover slide. This evanescent field can be used to excite fluorophores at a specific wavelength and it decays exponentially in space. TIRFM takes advantage of this property of light and the evanescent field in typical TIRFM set-up is ~100 nm [136]. The restricted excitation area and depth provides a low background for TIRFM measurements, hence enabling measurements of individual fluorophores when they are present at very low concentration. TIR illumination can be achieved using two different methods, prism-coupled and optical lens-coupled. In the prism-coupled method TIR is produced by use of a prism. Figure 17D shows an experimental set-up for TIRFM experiments and Figure 21 in Methods shows a more detailed image of the optical lens-coupled TIRFM method used in the single molecule measurements in this thesis. The images are captured using an electron multiplying charge-coupled device camera (EMCCD).

TIRFM single molecule measurements in cell cultures have been used to determine the behaviours of receptor proteins on the cell surface, such as the dimerisation and dissociation of muscarin receptors [137]. Single molecule FRET (smFRET) has been used to look at several functions of helicases on TIRFM. One of the first smFRET experiments with helicases was an unwinding measurements with Rep helicase [138].This assay used Cy3-Cy5-labelled DNA constructs immobilised to a glass surface with a ssDNA overhang for Rep binding. Unwinding was initiated by addition of

ATP and visualised as a decrease in FRET as the Cy3-Cy5 got separated from one another, showing stalling and re-initiation of unwinding. Several other assays have been developed since to investigate helicase and other DNA binding protein functions, many using fluorescent labelling of the helicase or SSB [94, 138-144]. The single molecule FRET measurements may enable observation of properties undetectable by other methods. This was the case with the SSB sliding movement on ssDNA, which was demonstrated using single molecule FRET measurements [145]. Fili N. *et al.* 2009 developed a fluorescence based helicase assay using Cy3B-SSB and biotinylated linear DNA attached to a glass surface [146]. This enabled the determination of the AddAB helicase rate of unwinding at the single molecule level. A range of unwinding rates showed AddAB pausing and re-starting and also allowed for the determination of the maximum length of DNA that can be visualised for unwinding in the TIRFM set-up (~1.5 kb). This assay has been further developed as part of this thesis to investigate PcrA unwinding of full length plasmids.

1.8.2. Optical and magnetic trapping of molecules

Optical and magnetic trapping techniques enable the trapping of individual molecules and observation of single reactions in real time. They use two very distinct mechanisms for the immobilisation of molecules in place. Figure 17 shows examples of magnetic tweezers and optical tweezers set-ups.

The optical tweezers apparatus uses a focused laser beam to “trap” a bead covered with a suitable coating. A biomolecule such as DNA can be attached to this coating [147, 148], while the other end of the DNA is attached to another bead held in place either by another laser beam or attachment to a micropipette. The trapping by light enables measurements of force changes in the system, for example dsDNA being unwound to ssDNA. This method has been used successfully to look at DNA unwinding by NS3

helicase [149] and DNA packing by the viral packing motor φ29 [150-152]. The measurements using optical tweezers with NS3 helicase showed an interesting property of uneven step size (~1.5 nt, ~2.5 nt and ~3.5 nt) [149]. This indicates possible uneven release of the two component strands produced from unwinding that could only be seen at the single molecule level.

Magnetic tweezers are made up of a minimum of two permanent magnets that are held above the sample. The magnets create a magnetic field that exerts torques on the magnetic particles, such as supermagnetic beads, and can be used to hold them in place. The beads are coated to enable attachment of a biomolecule on to the bead. For example, avidin coating can be used to attach biotin modified DNA on to the bead. The microscope-based tracking system is formed of an inverted microscope and the EMCCD camera used for capturing the image.

The initial experiment using magnetic tweezers included elasticity measurements of DNA. These were measured by determining the tensile strength of the DNA before it breaks [153, 154]. For this, DNA was stretched between the magnetic bead and a glass slide and measurements were taken at known magnetic and hydrodynamic forces. The function of the ring shaped helicase T7 has been studied by Johnson *et al*. 2007 using a magnetic tweezers set-up, where the DNA substrate is stretched between the bead and the coverslide [141]. The single tethered DNA hairpin structure has a dsDNA section, which the T7 helicase unwinds. The unwinding results were compared to nonring-shaped helicases and this showed a significant difference between the unwinding mechanisms of the two types of helicases. The bacteriophage T4 helicase gp41 function has been studied in a similar assay using magnetic tweezers [155]. These results show that the gp42 helicase translocates at the speed of 400 bp s^{-1} on ssDNA, but unwinds at the speed of 30 bp s^{-1}, indicating it to be a passive helicase when unwinding DNA on its own.

The use of single molecule assays, mainly optical and magnetic tweezers and TIRFM, has provided scientist with invaluable information that cannot be determined solely from ensemble measurements. Together, with the ensemble methods they have become a standard for studying the function of molecular motors. In future, these three main single molecule assays may be combined to provide even more sensitive ways to measure helicase function [156].

1.9. Purpose of the investigation

This project aimed to further our understanding of PcrA helicase unwinding activity in plasmid replication. This process is driven by PcrA translocation on ssDNA and its interaction with other components of the DNA unwinding complex such as RepD, the initiator protein, and by the hydrolysis of ATP.

New ensemble assays were developed to study PcrA function in ssDNA translocation and dsDNA unwinding. These assays were based on labelling of PcrA helicase with environment sensitive fluorophores. Previous fluorescence–based work has included the investigation of PcrA ssDNA binding and translocation, the ATP hydrolysis cycle and linear dsDNA unwinding using fluorescently labelled substrates [51, 54, 87, 157, 158]. The labelling of PcrA has not been done before and so provides an alternative method for previous fluorescence based assays, but ultimately this should provide us with more detailed information of how PcrA functions and interacts with the plasmid unwinding complex that has not been observed in previous experiments. For example, these will include the studies of PcrA translocation rate on different ssDNA substrates and its dependence on the DNA sequence.

The interaction between PcrA and RepD is vital for processive plasmid and linear DNA unwinding [87]. The location and nature of the interaction of these two proteins remains unsolved. One of the main aims is to label PcrA at multiple locations to find a signal that indicates the interaction site on PcrA and enables the investigation of the interaction between the two proteins and how this interaction may change during plasmid unwinding. PcrA plasmid unwinding has been shown to be processive only in presence of RepD. The loading of PcrA is the initial step of unwinding. This will be looked at using the fluorophore-labelled PcrAs in terms of the biochemistry of PcrA binding to ssDNA, but more importantly the binding of PcrA to RepD-DNA/plasmid complex. ATP binding has been

shown to affect PcrA structure [21] and the impact of ATP presence on PcrA binding kinetics will also be tested, as ATP is present under *in vivo* conditions.

PcrA plasmid unwinding was also the aim of investigation at single molecule level. Single molecule measurements remove the averaging of the signal observed in ensemble assays and can provide more detailed information of the biological process in question and highlight possible intermediate states and different populations of the molecules that are lost by averaging. Single molecule plasmid unwinding measurements can be used, not only to determine the speed and processivity of PcrA on individual DNA molecules, but to determine possible stalling and re-initiation properties of PcrA while unwinding plasmid DNA. These are the first measurements where complete plasmids are unwound and investigated at the single molecule level. PcrA has been applied in a similar single molecule assay using linear DNA substrate [146]. Using full length plasmid provides a more natural substrate for PcrA. Also, the circular nature of the plasmid may cause force changes within the PcrA-RepD-plasmid complex not present with linear DNA.

The ensemble plasmid unwinding assays also used in this thesis will provide a comparison to the newly developed single molecule plasmid unwinding assay. The determination of the rate of translocation on ssDNA and the rate of dsDNA unwinding at the same conditions by PcrA enable the comparison of these rates, which in turn can be used to determine whether the PcrA unwinds DNA actively or passively [61]. This function of PcrA has not been determined before and may be an important characteristic to be discovered to unravel the function of PcrA.

2. Materials and Methods

2.1. Chemicals and reagents

The chemicals and reagents were primarily purchased from Sigma-Aldrich Ltd with exceptions stated in the protocols.

2.2. Buffers and media

PcrA assay buffer: 50 mM Tris·HCl pH 7.5, 150 mM NaCl and 3 mM $MgCl_2$.
K100 buffer: 50 mM Tris·HCl pH 7.5, 100 mM KCl, 1 mM EDTA, 10 mM $MgCl_2$ and 10%(v/v) ethanediol.
K200 buffer: 50 mM Tris·HCl pH 7.5, 200 mM KCl, 1 mM EDTA, 10 mM $MgCl_2$ and 10% (v/v) ethanediol.
TIRF buffer: of 50 mM Tris·HCl pH 7.5, 100 mM KCl, 1 mM EDTA and 10 mM $MgCl_2$.
2YT broth: 1.6% Tryptone, 1% Yeast extract, 0.5% NaCl, pH 7.5.
Luria-Bertani media/broth: 1.0% (w/v) Tryptone, 0.5% (w/v) Yeast Extract, 1.0% (w/v) NaCl, pH 7.0.
NZY+ media: 1% (w/v) NZ amine (casein hydrosylate), 0.5% (w/v) NaCl, 0.5% (w/v) Yeast Extract, 0.2% (w/v) $MgSO_4 \cdot 7H_2O$, pH 7.5.
SOC media: 2% (w/v) Tryptone, 0.5% (w/v) Yeast Extract, 0.05% (w/v) NaCl, 1mM $MgCl_2$,1 mM $MgSO_4$ and 0.2% (w/v) glucose.

2.3. Transformation of *Escherichia coli*

Plasmids containing the gene of interest were transformed to *E. coli* XL-1 Blue cells (Stratagene) for amplification and B834 (DE3), B834 (DE3) pLysS or BL21 (DE3) pLysS cells for expression. This was done by addition of 10-20 ng of plasmid to 50 µl of cells in 1.5 ml Eppendorf tubes and incubating for 30 min on ice. After incubation, cells were heat shocked at 42 ºC for 45 s and incubated 2 min on ice, followed by addition of 800 µl of pre-warmed NZY^+ or SOC media. Cells were then incubated for 1 h at 37 ºC on rotary shaker at 225 rpm. 200 µl of culture was plated on LB agar plates containing ampicillin (100 µg ml^{-1}) when no pLysS was present and when

pLysS or pBirAmc was present plated on LB plates containing ampicillin (50 µg ml^{-1}) and chloramphenicol (10 µg ml^{-1}).

2.3.1. Expression cell lines

Strain	*Genotype*	*Protein*
B834(DE3)	F^- *ompT hsdS*$_B$(r_B^- m_B^-) *gal dcm met* (DE3)	PcrA
B834(DE3) pLysS	F^- *ompT hsdS*$_B$(r_B^- m_B^-) *gal dcm met* (DE3) pLysS (Cam^R)	RepD
BL21(DE3)	F^- *ompT hsdS*$_B$(r_B^- m_B^-) *gal dcm met* (DE3)	bioPcrA

2.3.2. Small, medium and large scale plasmid purification

Small scale plasmid preparations were done using QIAGEN quick mini preparation kit and protocol (maximum yield 20 µg), whereas medium and large scale preparations were done using QIAGEN maxi (maximum yield 500 µg) and giga (maximum yield 10 mg) preparation kits, respectively. The main difference between the kits is the starting volume of bacterial cultured used resulting in larger yield of purified plasmid. The QIAGEN plasmid purification kits are based on Birnboim and Doly alkaline lysis method developed to extract high purity plasmid DNA from *E. coli* [159]. By this method, the *E. coli* cells, containing the wanted plasmid, were grown in LB media overnight. The cells were then centrifuged into a pellet and resuspended P1 buffer (50 mM Tris·HCl pH 8.0, 10 mM EDTA and 100 µg ml^{-1} RNase A). The cells were lysed by alkaline solution, P2 solution (200 mM NaOH and 1% SDS). The lysis reaction was neutralised by addition of N3 buffer (4.2 M guanidinium hydrochloride, 0.9M potassium acetate, pH 4.8) in case of mini preparation kit and by P3 buffer (3M acetic acid, pH 5.5) in case of maxi and giga preparation kits. The neutralised mixture was spun using centrifuge to separate the crude cell debris from DNA. The plasmid DNA was further purified from RNA and other cellular components by optimised buffers and QIAGEN columns provided as a part of the kits. These columns contain a silica membrane, which is selective in adsorption of plasmid in high-salt conditions and elution in low-salt conditions. The supernatant containing the extracted plasmid was applied to the QIAGEN column equilibrated with QBT buffer (750 mM NaCl, 50 mM MOPS, pH 7.0,

15% (v/v) isopropanol, 0.15% Triton X-100). The plasmid DNA was washed on the column membrane using PB buffer (5 M Guanidine-HCl and 30% (v/v) isopropanol) and PE buffer (10 mM Tris-HCl pH 7.5 and 80% ethanol) in case of mini preparation kit and with QC buffer (1.0M NaCl, 50 mM MOPS pH 7.0 and 15% isopropanol) in case of maxi and giga preparation kits. The plasmid DNA was eluted with EB buffer (10 mM Tris·HCl, pH 8.5) (mini preparation kit) or with QF buffer (25 M NaCl, 50 mM Tris·HCl pH 8.5 and 15% isopropanol) (maxi and giga preparation kits). The plasmid DNA purified using maxi and giga kits were also washed with 70% ethanol after elution and resuspended in EB buffer. The plasmid DNA was stored at -20 °C.

2.4. Site-directed mutagenesis

Site-directed mutagenesis of PcrA and RepD were done using QuikChange II site-directed mutagenesis kit and protocol from Stratagene. The protocol is based on the use of primers with mismatch sequence, which enables the introduction of an amino acid change site-specifically using the polymerase chain reaction (PCR). The primers were designed to have single stranded DNA overhangs and the primer sequences used are stated in Sections 2.4.1 and 2.4.2 and were obtained from Sigma-Aldrich Ltd. The PCR reactions had 50 ng template plasmid, 125 ng of forward and reverse primers, 1 µl dNTP mix, and 2.5 U *PfuTurbo* DNA polymerase with 5 µl of 10 x reaction buffer that was provided with the enzyme. The reactions were made to 50 µl with distilled H_2O. The PCR was done using programme of preheating the reactions for 30 seconds at 95 °C, followed by 16 cycles of denaturing at 95 °C for 30 seconds, primer annealing at 55 °C for 1 minute and DNA synthesis for 6 minutes (1 minute/1 kb of template DNA) at 68 °C, which was followed by final 5 minute extension at 68 °C to ensure completion of DNA synthesis. The PCR reactions were then digested with *Dpn* I restriction endonuclease for 1 hour at 37 °C to remove the template plasmid DNA (10 U of enzyme per 50 µl of reaction). The plasmids created by PCR were then transformed into XL-1 Blue *E. coli* cells using protocol stated in

Section 2.3. The mutated gene sequences were checked by sequencing (Cogenics Ltd or GATC Ltd).

2.4.1. Primers used for site-directed mutagenesis of RepD

Mutation	Primer sequence
RepD(C225A)	5'-TAC TGG AAT GAT GCC TTT GAT GAT TTA CAC ATT T-3'
	5'-ATC ATC AAA GGC ATC ATT CCA GTA ATC AAC CAT A-3'
RepD(W310C)	5'-CGT GAA TTT AGA TTT TGT AAG TAG AAT TCA AGC TTG GCT G-3'
	5'-GAA TTC TAC TTA CAA AAT CTA AAT TCA CGT TGC CAA AA-3'
RepD(S2C)	5'-GGA GAT ATA CAT ATG TGT ACA GAA AAT CAT TCA AAT T-3'
	5'-GAT TTT CTG TAC ACA TAT GTA TAT CTC CTT CTT AAA GTT-3'

RepD(W310C) and RepD(S2C) were done on a RepD construct to which the C225A mutation was introduced before.

2.4.2. Primers used for site-directed mutagenesis of PcrA

Mutation	Primer sequence
PcrA(H53C)	5'-TGG CGG AAA AGT GTG TGG CGC CGT GGA ACA TTT-3'
	5'-ACG GCG CCA CAC ACT TTT CCG CCA TCA AAT A-3'
PcrA(K138C)	5'-ATA GAC CCG AAA TGT TTT GAG CCG CGG ACG ATT TTA-3'
	5'-TCC GCG GCT CAA AAC ATT TCG GGT CTA TGT TTT TTT-3'
PcrA(T167C)	5'-CGC CAA GCG GGC CTC GTG CTA TTA CGA AAA AGT CGT CAG CG-3'
	5'-CTG AAA AAG CAT TAT CGT GCT CCG GGC GTT CCG CTT AAC GAG G-3'
PcrA(E314)	5'-GCT TTG GAC GTG CAA CCC GGA AGG AAA GCC GAT TC-3'
	5'-CCT TCC GGG TTG CAC GTC CAA AGC CGT TTC GGC TTC CG-3'
PcrA(E347C)	5'-GCG GTG GAG CGC TGC GAA CGC CGC TAC CGT GAT TTT GC-3'

	5’-GGT AGC GGC GTT CGC AGC GCT CCA CCG CCT CGC GGA TGC-3’
PcrA(E447C)	5’-GCG CTC GGC TGC CTA GAG ATG ATC GGG CTT GGC G-3’
	5’-CGA TCA TCT CTA GGC AGC CGA GCG CCT CAA ACA AGG-3’
PcrA(E449C)	5’-TCG GCG AGC TAT GTA TGA TCG GGC TTG GCG CCA-3’
	5’-AGC CCG ATC ATA CAT AGC TCG CCG AGC GCC TCA AA-3’
PcrA(M450C)	5’-GCG AGC TAG AGT GCA TCG GGC TTG GCG CCA AAG CGG-3’
	5’-GCC AAG CCC GAT GCA CTC TAG CTC GCC GAG CGC CTC-3’
PcrA(L453C)	5’-GAG ATG ATC GGG TGT GGC GCC AAA GCG GCC GGG-3’
	5’-CTT TCG CGC CAC ACC CGA TCA TCT CTA GCT CGC CG-3’
PcrA(Y477C)	5’-AGC TGC AAG AAT GCG TCT CCG TCA CCG AAC TCG T-3’
	5’-TGA CGG AGA CGC ATT CTT GCA GCT CAC AGG TAA-3’
PcrA(R501C)	5’-AAG GCG GAG TGT ACG ATT GAA GCA CAA AGC CGC CT-3’
	5’-TGC TTC AAT CGT ACA CTC CGC CTT GAG CAT CT-3’

2.5. Agarose gel electrophoresis

Mini-prep plasmids and plasmids used in site-directed mutagenesis were run on 1% (w/v) agarose gels prepared using 0.5 g of agarose (Bio-Rad) to 50 ml of TAE (40 mM Tris-acetate and 1 mM EDTA). 1 µg/ml ethidium bromide was added to melted agarose. This was then poured to cast and allowed to set. DNA samples were run with 1 x loading buffer (made of 30% (v/v) glycerol, 0.25% (w/v) bromophenol blue) with TAE at 100 volts for 45 min.

2.6. DNA structures and sequences

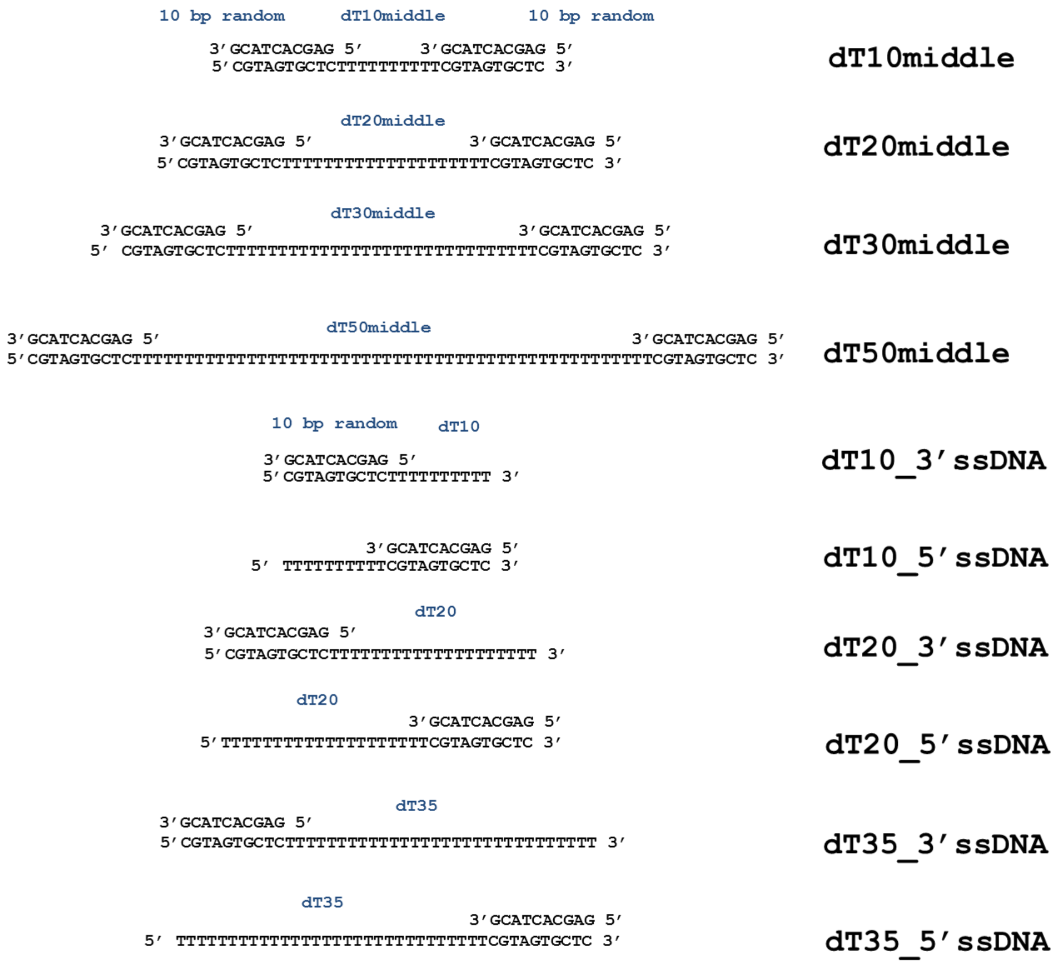

Figure 18. DNA structures for MDCC-PcrA(K138C) ssDNA binding studies.

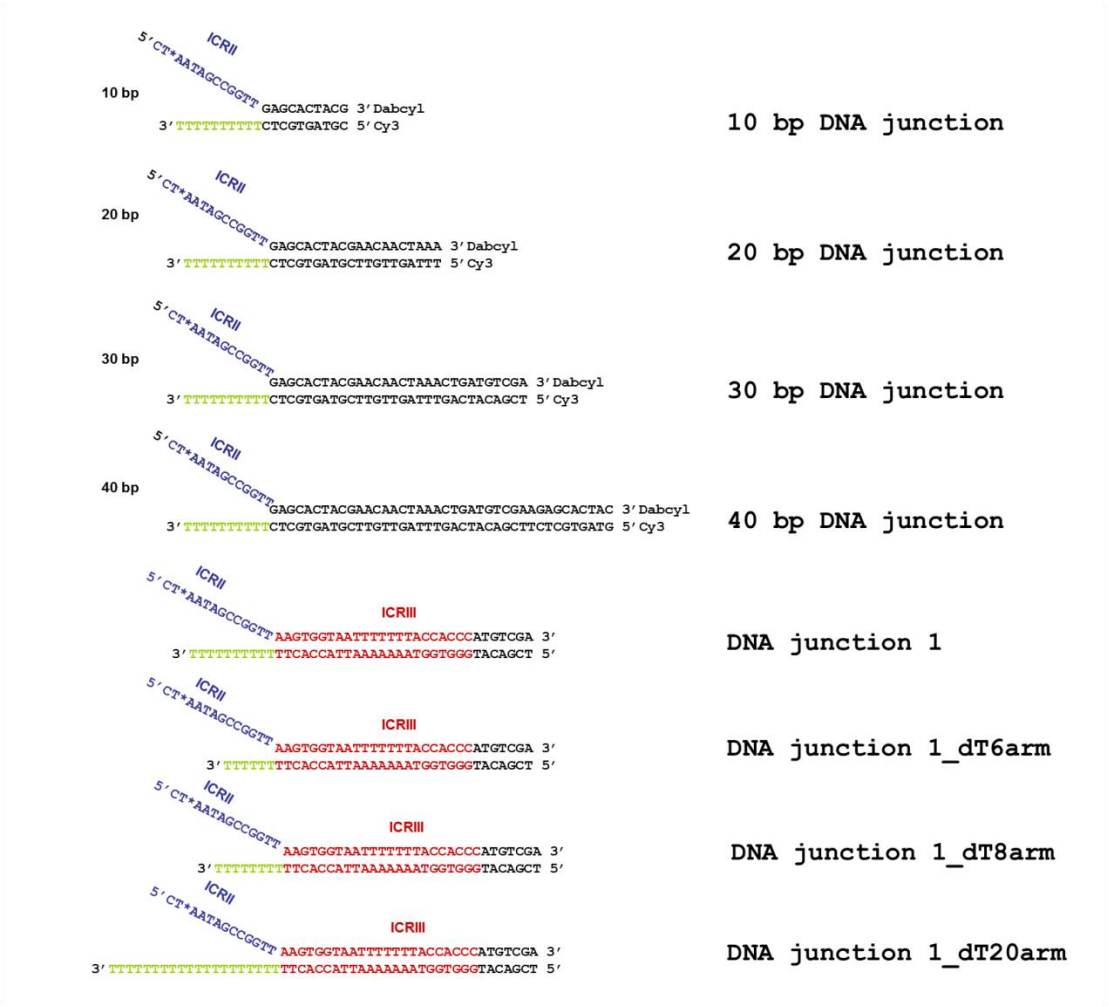

Figure 19. DNA junction structures and sequences for dsDNA unwinding and PcrA-RepD interaction studies.

DNA junctions for unwinding assay have dabcyl-Cy3 or dabcyl-AlexaFluor350 pair depending on the fluorophore on the PcrA or RepD to prevent overlap of excitation and emission spectra of the DNA junctions and labelled protein. The unmodified DNA junctions for MDCC-PcrA(E449C) binding and unwinding assays without ICRIII sequence had the identical sequences to 20 to 40 bp DNA junctions. *, designates the site of RepD nicking.

2.7. Protein expression and purification

2.7.1 SDS-PAGE analysis of expressed proteins

SDS-PAGE was done to analyse and check for presence of PcrA, RepD and bioPcrA. 12% SDS-PAGE running gels were prepared using 7.5 ml of 30% (w/v) acrylamide and bis-acrylamide min (37.5:1), 3.8 ml of 1.5 M

Tris pH 8.8, 3.4 ml of distilled di-ionised water with the conductivity of 5.4 (SEM 1.3) µS/cm, 150 µl 10% SDS (w/v) and setting with 100 µl of ammonium persulfate and 5 µl of TEMED (makes total of 4 gels). 5% stacking gels were prepared using 1.7 ml of 30% (w/v) acrylamide and bis-acrylamide (37.5:1), 1.25 ml of 1 M Tris pH 6.8, 6.8 ml of distilled di-ionised water. Distilled di-ionised water had a conductivity of 5.4 (SEM 1.3) µS/cm, 150 µl 10% SDS (w/v) and set using 100 µl of 10% (w/v) ammonium persulfate and 5 µl of TEMED (BioRad #161-0801).

15 µl of samples were mixed with 15 µl of 2 x sample buffer (125 mM Tris·HCl pH 6.8, 4% SDS, 20% (v/v) glycerol, 10% (v/v) 2-mercaptoethanol and 0.25 mg/ml bromophenol blue) and boiled 5 min at 95 ºC. Gels were run with buffer made of 25 mM Tris, 1.44% (w/v) glycine and 0.1% SDS at 200 volts for 60 min. Gels were stained with coomassie brilliant blue R-250 (BioRad) for approximately 15 min at room temperature and destained with mix of 10% (v/v) acetic acid and 50% (v/v) methanol for 2-3 h.

2.7.2. *Bacillus Stearothermophilus* PcrA wild type and mutant preparations

100 ml of LB broth with ampicillin (100 µg/ml) was inoculated with *E. coli* strain B834 (DE3) that carries plasmid pET22-*Bst*PcrA (a gift from Dale Wigley, CR UK) and grown overnight at 37 ºC on shaker at 225 rpm. 4 x 5 ml of this was used to inoculate 4 x 500 ml of LB with ampicillin in 2 litre flasks and grown to OD_{595} 0.5. PcrA expression was induced with 1 mM IPTG (CALBIOCHEM # 420322) and grown 3 h at 37 ºC on rotary shaker at 225 rpm. After incubation cells were centrifuged at 4 ºC at 4000 rpm in JS 4.2 swing bucket rotor (Beckman Coulter) for 30 min. 2 x 500 ml culture pellets were resuspended into 20 ml of buffer containing 50 mM Tris·HCl pH 7.5, 2 mM, EDTA, 1 mM DTT, 200 mM NaCl and 10% (w/v) sucrose. Cells were then stored at -80 ºC until PcrA extraction and purification.

To extract PcrA from *E. coli*, the cells were thawed and PMSF was added to final concentration of 0.1 mM. Cells were lysed using probe sonicator at bursts of 4 x 30 s on ice (nominally 360 W Vibra-Cell from Sonics

& Materials Inc.) and spun at 13200 rpm at 4 ºC for 20 min using 45 Ti rotor (Beckman Coulter). Supernatant containing proteins was removed and measured. To this volume 0.7 times of saturated $(NH_4)_2SO_4$ was added gradually over 5 min period, whilst stirring at room temperature. Mix was then centrifuged at 13 200 rpm at 4 ºC for 20 min using 45 Ti rotor (Beckman Coulter). Supernatant was thrown away and the pellet was resuspended into 20 ml of buffer (50 mM Tris·HCl pH 7.5, 2 mM EDTA, 1 mM DTT and 100 mM NaCl).

Fast protein liquid chromatography (FPLC) purification of PcrA was done on an AKTA FPLC (GE Healthcare) using a 20 ml heparin Sepharose column (GE Healthcare). First, the conductivity of the protein mixture was matched to the conductivity of re-suspension buffer used in FPLC by adding buffer containing 50 mM Tris·HCl pH 7.5, 2 mM EDTA and 1 mM DTT. The sample was then loaded on to the column and equilibrated using 50 mM Tris·HCl pH 7.5, 2 mM, EDTA, 1 mM DTT and 100mM NaCl at 1 ml/min flow rate at 4 ºC. PcrA was eluted on linear gradient of NaCl starting from 100 mM NaCl and finishing at 700 mM NaCl over a volume of 150 ml. Normally, PcrA elutes at ~350-400 mM NaCl and was confirmed using SDS-PAGE.

The fractions from FPLC were pooled and concentrated using 20 ml 10 000 MWCO Vivaspin concentrator (Millipore) by spinning at 4000 rpm at 4 ºC in JS 4.2 swing bucket rotor. Quantification of PcrA was done using the molar extinction coefficient of 75 875 M^{-1} cm^{-1} at 280 nm (calculated from the amino acid sequence). PcrA was stored in aliquots with 10% glycerol (v/v) at -80 ºC. Figure 18A shows a wild type PcrA preparation on a 12% SDS-PAGE gel.

2.7.3. *Staphylococcus aureus* RepD preparations

RepD wild type was expressed from pET11a vector (given as a gift to the lab by Christopher D. Thomas, University of Leeds) transformed into *E. coli* strain B834 (DE3) pLysS. 100 ml of 2YT broth with 1% glucose (w/v), 50 µg/ml ampicillin and 10 µg/ml chloramphenicol were inoculated with the *E.*

coli and grown overnight at 30 ºC in orbital shaker at 225 rpm. 5 ml of the overnight cultures was used to inoculate each 500 ml of 2YT media (typically total of 2 l) with 50 µg/ml ampicillin and 10 µg/ml chloramphenicol and grown at 30 ºC in orbital shaker at 225 rpm until the cell density reached 0.5 at OD_{595}. RepD expression was induced with 0.1 mM IPTG and cells were grown for a further 6 h. Cells were centrifuged at 4 ºC, at 4000 rpm in a JS 4.2 swing bucket rotor for 30 min. The pellets were resuspended to 40 ml of 50 mM Tris·HCl pH 7.5, 1 mM EDTA, 10% (v/v) ethanediol, 500 mM KCl, 1mM DTT and 10% sucrose and stored at -20 ºC until purification.

Resuspended cells were thawed and to each 50 ml of cells, 1 tablet of protease inhibitor (Complete, Santa Cruz biotechnology) was added. Cells were sonicated 2 x 15 s on ice using probe sonicator (nominally 360 W, Vibra-Cell from Sonics & Materials Inc.). The lysate was then centrifuged at 15 ºC, at 12 000 rpm for 30 min using 45 Ti rotor (Beckman Coulter). Supernatant containing the protein was removed and measured. To this two times the volume of a buffer containing 50 mM Tris·HCl pH 7.5, 1 mM EDTA, 10% (v/v) ethanediol and 3 M $(NH_4)_2SO_4$ was added. Cell debris was precipitated by incubating on ice for 30 min and centrifuged at 4 ºC, at 12 000 rpm for 30 min using 45 Ti rotor (Beckman Coulter). Pellets were then resuspended into of 50 mM Tris·HCl pH 7.5, 1 mM EDTA, 10% (v/v) ethanediol and 500 mM KCl, and pooled. Conductivity of the lysate was matched to buffer containing 50 mM Tris·HCl pH 7.5, 1 mM EDTA, 10% (v/v) ethanediol and 200 mM KCl, using buffer 50 mM Tris·HCl pH 7.5, 1 mM EDTA and 10% (v/v) ethanediol. The sample was then further centrifuged at 15 ˚C, at 12 000 rpm for 30 min using 45 Ti rotor (Beckman Coulter).The supernatant was purified using two columns. First, on 6 ml Q-Sepharose column (GE healthcare), and second on 20 ml heparin Sepharose column (GE healthcare), that had been equilibrated in 50 mM Tris·HCl pH 7.5, 1 mM EDTA, 10% (v/v) ethanediol and 200 mM KCl at 1 ml/min using AKTA FPLC (GE healthcare). After application of sample, a gradient of KCl was run from 200 mM to 700 mM over 200 ml to elute RepD. Elution fractions were analysed by SDS-PAGE and the absorbance at 260 and 280 nm was monitored. Fractions with A280/A260 ratio higher than 1.5 were pooled and

concentrated using 20 ml 10 000 MWCO Vivaspin concentrator (Millipore) in centrifuge at 3000 rpm at 4˚C in a JS 4.2 swing bucket rotor. RepD was quantified using absorbance at 280 nm and an extinction coefficient of 119 514 M^{-1} cm^{-1} for the dimer.

2.7.4. Biotinylated *Bacillus Stearothermophilus* PcrA expression and purifications

The pET22b-bioPcrA construct (a gift from Mark Dillingham, University of Bristol) was transformed into BL21 (DE3) *E. coli* (Novagen) together with pBirAMc vector expressing the biotin ligase (Avidity) and plated on LB agar plates with 10 µg/ml of chloramphenicol and 50 µg/ml of ampicillin and incubated overnight at 37 ºC. This was used to inoculate 100 ml overnight culture of liquid LB containing 10 µg/ml of chloramphenicol and 50 µg/ml of ampicillin. The overnight liquid media (1/100 dilution) was used inoculate 2 L of LB with above antibiotics and concentrations. Cells were grown to OD_{595} 1 at 37˚C with shaking 225 rpm and the expression was induced with 1 mM IPTG. Also, biotin (Sigma) was added to final concentration of 100 µM. The cells were grown 3 h after which they were harvested by spinning at 4000 rpm in JS 4.2 swing bucket rotor at 4 ˚C. The pellets were resuspended into 40 ml of buffer 50 mM Tris·HCl pH 7.5, 100 mM NaCl, 1 mM EDTA, 1 mM DTT, 10% (w/v) sucrose and protease inhibitor tablet (Complete, Santa Cruz biotechnology).

The bioPcrA was purified by lysing the cell by sonication of four times for 30 s as for PcrA. The lysate was spun at 13 200 rpm in Beckman Coulter 45 Ti rotor for 20 min. The protein was precipitated using solid ammonium sulphate to 50% saturation stirring at room temperature. The precipitated bioPcrA was spun at 13 200 rpm using Sorvall 45 Ti rotor for 20 min and pellet was resuspended in buffer A (50 mM Tris·HCl pH 7.5, 100 mM NaCl, 1 mM EDTA and 1 mM DTT). The protein was then loaded onto Softlink Avidin column (Promega) equilibrated in buffer A. The column was then washed 10 column volumes. The bioPcrA was eluted with same buffer containing 5 mM biotin. The flow was stopped after one column volume and incubated for 30

minutes to allow biotin to exchange with biotinylated protein. After this the protein was eluted and highest absorbing fractions were pooled and loaded onto 5 ml HiTrap heparin column (GE healthcare #17-0407-01) equilibrated with buffer A. The column was washed overnight with 300-400 ml of buffer A. The bioPcrA was eluted with a gradient of NaCl (100 mM to 1 M). The bioPcrA was concentrated using Vivaspin 10 000 MW CO column and buffer exchanged to buffer Tris·HCl pH 7.5, 200 mM NaCl, 1 mM EDTA , 1 mM DTT and 10% glycerol by overnight dialysis. The bioPcrA was then aliquoted and stored at -80˚C.

2.8. Labelling of PcrA and Rep with maleimide-fluorophores

The purified protein was stored in elution buffer (from FPLC purification) containing DTT and this was separated from protein by loading onto PD-10 gel filtration column (GE healthcare). First, the column was equilibrated using buffer K200 (50 mM Tris·HCl pH 7.5, 200 mM KCl, 1 mM EDTA, 10 mM $MgCl_2$ and 10% (v/v) ethanediol) for RepD labelling and with PcrA labelling buffer (50 mM Tris·HCl pH 7.5, 300 mM NaCl and 3 mM $MgCl_2$) for PcrA. The protein was applied to column and eluted using equilibration buffer in order to remove DTT. Fractions were collected, and analysed using absorbance at 280 nm for the presence of the protein. The fractions with the protein were then pooled and suitable labelling reagent was added at two times the protein concentration. All fluorophores were used as solutions in dimethylformamide and Cy-derivative maleimides were from GE Healthcare; IDCC (N-[2-(iodoacetamido)ethyl] -7-diethylaminocoumarin -3-carboxamide) and MDCC (N-[2-(1-maleimidyl)ethyl]-7-diethylaminocoumarin-3-carboxamide) were synthesized by J. E. T. Corrie (MRC NIMR, UK). The microcentrifuge tubes containing the protein and fluorophore were protected from light and incubated for 45 minutes on a rotary mixer. Unbound fluorophore was removed using a PD-10 column and eluted using K200 buffer (RepD) or PcrA labelling buffer (PcrA).

The fractions were analysed for the level of labelling by measuring an absorbance spectrum between 240-600 nm. The fluorophore concentration was determined first using its molar extinction coefficient at the absorbance maximum (MDCC ε_{430} - 44800 M^{-1} cm^{-1}, IDCC ε_{430} - 44800 M^{-1} cm^{-1}, Cy3 ε_{547} - 150000 M^{-1} cm^{-1}, Cy3B ε_{559} -130000 M^{1} cm^{-1} and Cy5 ε_{649} -250000 M^{-1} $cm^{-}1$). This was used to determine the fluorophore absorbance at 280 nm (MDCC and IDCC ε_{280} - 7470 M^{-1} cm^{-1}, Cy3 ε_{280} – 11730 M^{-1} cm^{-1}, Cy3B ε_{280} – 9450 M^{-1} cm^{-1} and ε_{280} - 7270 M^{-1} cm^{-1}). The fluorophore absorbance at 280 nm was then deducted from the protein absorbance to enable accurate determination of protein concentration. The molar extinction coefficient used for PcrA was 75 875 M^{-1} cm^{-1} and 119 514 M^{-1} cm^{-1} for RepD. The labelling efficiency could then be expressed as a percentage. The labelling and quality of the new modified protein was also determined using electrospray mass spectrometry provided as a service by MRC NIMR, UK and done by S. Howell. The labelled protein was stored in 300 mM NaCl PcrA labelling buffer at -80 °C (PcrA) and in K200 buffer at -20 °C (RepD).

2.9. PcrA and PcrA mutant steady-state ATPase hydrolysis assay using fluorescent spectrophotometer

Wild type PcrA and mutant PcrA ATPase activities were determined using inorganic phosphate (P_i) biosensor, 6ATR-PBP which detects inorganic (P_i) production from hydrolysis of ATP by PcrA. This was measured using CARY Eclipse spectrofluorometer at 20ºC. 5 nm slits were used for excitation and 5 nm slit for emission and measurements were averaged over 1 s. The excitation wavelength for 6ATR-PBP was 553 nm and emission wavelength of 577 nm.

Each reaction had 10 nM of PcrA, 500 nM of $dT_{30/50}$ (ssDNA) (Eurogentec Ltd), 10 µM of MDCC-PBP made in assay buffer containing 50 mM Tris·HCl pH 7.5, 3 mM $MgCl_2$ and 150 mM NaCl. The total of reaction volume in the cuvette was 60 µl. ATP was added to solution at different concentrations and the fluorescence change was followed over time. The same reaction mix was used to calibrate the fluorescence intensity using a P_i

titration. This enables the determination of the PcrA affinity to ATP measured as K_m (μM) and the maximum velocity of the reaction catalysed by PcrA expressed as V_{max} (M s^{-1}) by fitting the results to the Michaelis-Menten equation shown below (Equation 7) on GraFit 7 software (Erithacus software Ltd). The enzyme turnover number by PcrA expressed as k_{cat} (s^{-1}) was calculated by dividing the V_{max} by the PcrA concentration. *S* is the substrate concentration, which is the ATP concentration in these experiments.

Equation 7:

$$v = \frac{V_{max}[S]}{(K_m + [S])}$$

2.10. DNA junction unwinding assay using stopped-flow apparatus

Wild type and mutant/labelled PcrA helicases were tested with wild type RepD for their ability to unwind dsDNA junctions. A HI-TECH scientific SF61MX stopped-flow (TgK Scientific Ltd) with xenon-mercury lamp was used. See Figure 20 for the stopped-flow set-up. Each reaction had 100 nM PcrA, 2.5 μM RepD (wild type), 200 μM ATP, 500 nM DNA substrate (10 bp, 20 bp, 30 bp or 40 bp junctions labelled with Cy3 and dabcyl or with AlexaFluor350 and Dabcyl were from Eurogentec Ltd, Eurofins MGW Operon or Sigma-Aldrich Ltd) mixed in assay buffer K200. First, the RepD was mixed with DNA junction and incubated 5 min at 30 °C to allow the RepD loading and nicking of the DNA junctions. To this PcrA was added and the solution was incubated again for 5 min at 30 °C, after which the unwinding reaction was initiated by mixing with ATP in the stopped-flow apparatus. The reactions were measured at 30 °C. In each reaction, the PcrA and RepD are mixed together with ATP and excited at 548 nm and emission recorded through a 570 nm cut-off filter for Cy3-Dabcyl paired junctions. For AlexaFluor350-Dabcyl DNA junctions the excitation was at 346 nm and 400 nm cut-off filter was used. Data from the stopped-flow experiments were

recorded using Kinetic Studio software (TgK Scientific Ltd). The fitting and analysis of traces was done using GraFit 7 software (Erithacus software Ltd).

2.11. Plasmid unwinding assay on stopped-flow apparatus

Plasmid unwinding was measured on a stopped flow apparatus at 30 °C. A HI-TECH scientific SF61MX stopped-flow (TgK Scientific Ltd) with xenon-mercury lamp was used. At typical reaction contained 0.5 nM pCER*oriD* plasmid, 190 nM PcrA, 2 nM RepD, 200 nM DCC-SSB(G26C) and 1 mM ATP. In syringe A, plasmid was mixed with DCC-SSB and to this RepD was added and reaction was incubated for 30 seconds to allow RepD nicking. Then PcrA was added to syringe A and reaction was incubated further 30 s. Then the reaction was mixed with ATP in syringe B, which also contained 200 nM DCC-SSB. The excitation is done at 436 nm and emission is measured using 455 nm cut-off-filter.

pCER*oriD* plasmids other than 3094 bp plasmid were constructed by Andy Slatter, MRC NIMR, UK [87]. The original pCER*oriD* plasmid 3094 bp was initially constructed to study PcrA-RepD plasmid unwinding from pUC19 plasmid with insertion of *oriD* and hence most of the experiment here were performed with this plasmid [85, 88].

2.12. RepD nicking assay

Each nicking reaction contained 1 µM RepD (10 µl of 2 uM RepD stock) and 10 µM of ICRII oligo (5'-CT*AATAGCCGGTT-3', containing the RepD nicking sequence) made to total reaction volume of 20 µl using K200 buffer. The reaction was incubated 5 min at 30 °C. One of the monomers of an active RepD dimer will nick and covalently bind the ICRII oligo. This runs slower on SDS-PAGE gel than the monomer unbound by ICRII oligo. The reactions were stopped by adding 20 µl of 2 x sample buffer (125 mM Tris·HCl pH 6.8, 4% SDS, 20% (v/v) glycerol, 10% (v/v) 2-mercaptoethanol and 0.25 mg/ml bromophenol blue) and boiled 5 min at 95 ºC. 10 µl of the reaction mix with the sample buffer were loaded onto 12% SDS-PAGE gels.

Gels were run with buffer made of 25 mM Tris, 1.44% (w/v) glycine and 0.1% SDS at 200 volts for 60 min. Gels were stained with coomassie brilliant blue R-250 (BioRad) for approximately 15 min at room temperature and destained with mix of 10% (v/v) acetic acid and 50% (v/v) methanol for 2-3 hours. The band sizes were quantified using UVIpro software.

2.13. Tests for fluorescent signals of labelled PcrAs

The labelled PcrA were tested for signal change on Cary spectrofluorometer by measuring excitation and emission spectrum and titrating in the substrate. For example, 200 nM MDCC-PcrA(E449C) was titrated with 1 µM RepD-DNA junction 1 complex with 2-fold excess of RepD. The emission maximum was determined by measuring the fluorescence spectrum (varying the excitation from 350 to 450 nm) with and without substrate. Similarly, the excitation maximum was determined by measuring the fluorescence spectrum (varying the emission from 450 to 550 nm).

The newly labelled PcrA/RepD species were tested for fluorescent signals on a stopped-flow apparatus by mixing the labelled PcrA/RepD with high excess of PcrA/RepD ligand/substrate. For coumarin (MDCC/IDCC) labelled species a 436 nm wavelength excitation was used with a 455 nm cut-off filter. The signals were fitted using Kinetic Studio programme (TgK Scientific Ltd) and further analysed using GraFit 7 (Erithacus software Ltd). The fitting equations were chosen according to the mechanistic model best represented by the equation. The equations used were single, double exponential or single/double exponential with straight line and are stated with the results for individual measurements.

2.14. DTNB assay

The DTNB (Dithionitrobenzoic acid, Ellman's reagent) assay was done to determine the accessibility/reactivity of the thiols on cysteine residues. This was done by dissolving 10 mM DTNB (# D8451 Invitrogen) into K200 buffer. RepD was added to this at 5 or 10 µM final concentration. The absorbance change was measured on spectrophotometer at 412 nm

wavelength at room temperature. DTNB reacts with the thiol(s) in proteins cleaving the disulfide bond in DTNB resulting in an absorbance change.

2.15. Size exclusion chromatography – multi angle light scattering (SEC-MALS)

The oligomeric states of wild type PcrA and bioPcrA were determined on JASCO PU-1580 HPLC connected to Optilab rex (Wyatt) light scattering detector and a differential refractometer (dRI) (dn/dc = 0.186) (Dawn Helios, Wyatt). Possible different oligomer states were separated using a Superdex 200 HR 10/30 column in 50 mM Tris·HCl pH 7.5, 100 mM KCl, 1 mM EDTA and 10 mM $MgCl_2$ at a flow rate of 0.5 ml/min. 100 µl of samples were injected at the concentration of 0.5 mg/ml. The data were recorded using JASCO Chrompass Chromatography data system and ASTRA software.

2.16. Stopped-flow apparatus set-up for fluorescence measurements

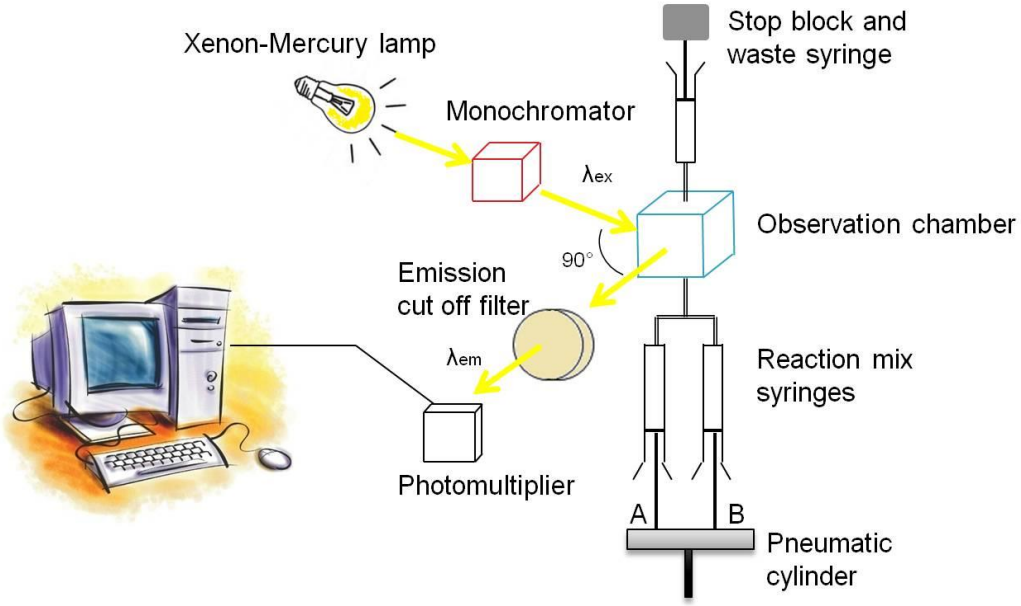

Figure 20. Stopped-flow set-up.

Reactants in the syringe A and B are mixed by pneumatic pump and obeserved in the observation chamber. The reaction flow is stopped by stopper block. Xenon-mercury lamp is the source for the white light that is passed through a monochromator enabling the excitation at specific wavelength. The emiting light is observed at 90° angle and passed through a cut-off filter at chosen wavelength. The intensity is measured using photomultiplier tube and converted to fluorescence units using Kinetic Studio software.

2.17. Single molecule experiments

2.17.1. Flow-cell preparation for TIRFM assays

The quartz slides were plasma cleaned and treated with Vectabond to obtain aminosilanisation of surfaces that were then PEGylated with a mixture of N-hydroxysuccinimide (NHS) ester- modified PEG with and without biotin. The flow cells were constructed by gluing three glass cover slips of 3 x 40 mm on to a coverslip using UV glue. The PEGylated coverslip was glued on the three slips on the cover slip forming a chamber of volume of 15 µl with two open ends.

2.17.2. Total internal reflection microscope set-up

Total internal reflection fluorescence microscopy (TIRFM) was used to visualise the fluorescent objects (Figure 21). Excitation was via a totally internally reflected (TIR) green laser (λ = 532 nm). A shutter was used to control the laser exposure time and enable time lapse imaging that allowed increased the overall observation time of the sample before photobleaching. Initially, the laser beam travels through set of lenses and mirrors, which expand the laser beam and then focus it at the back aperture of the objective lens; by moving one of the lenses (lense III) the incident TIR angle could be adjusted. Before hitting the glass-water interface, the laser travels through a high-numerical aperture objective lens (Fluar, 100x, 1.45 NA), which focuses the light beam. TIR light is used to excite the fluorophores at the evanescent field (~100 nm depth from glass cover slip). After passing through an emission filter (560 nm-590 nm), the emitted light is captured using a high sensitivity Andor digital, electron multiplying, charge-coupled device, camera (EMCCD camera) at 20 frames per second.

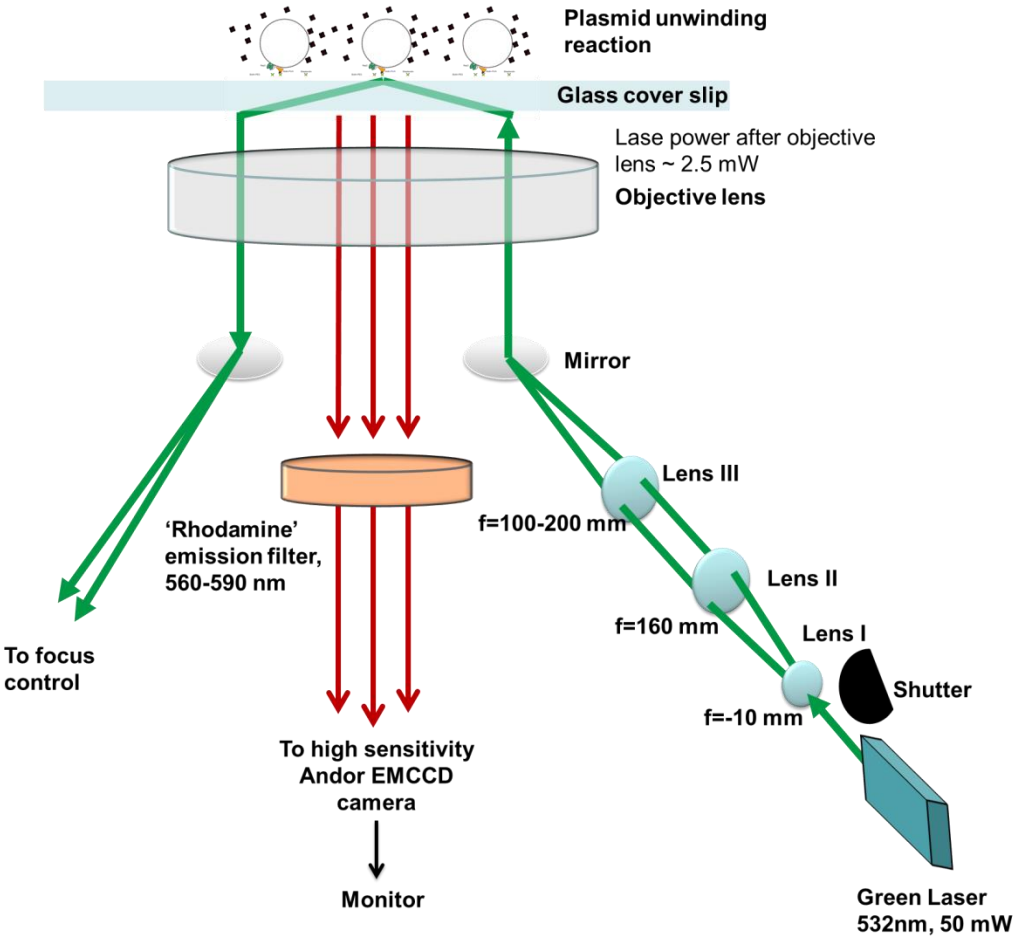

Figure 21. Set-up of objective type lens TIRFM.

2.17.3. Photobleaching and PcrA density measurements on the glass surface using TIRFM

The rate of photobleaching and measurement of the Cy3B-bioPcrA(E449C) density on the flow-cell surface was measured under identical conditions used in the experiments using the same TIRF microscope. Flow-cells constructed with the PEGylated coverslips (as described earlier) were incubated with 20 µg ml^{-1} of streptavidin for 15 minutes and washed 5 times to remove excess streptavidin with buffer K100. The required concentration of Cy3B-bioPcrA(E449C) was added into the flow-cells and incubated at room temperature, in the dark, for 30 minutes after which they were washed 5 times with K100 buffer. PEGylated surfaces were "blocked" with biotin by incubation of Cy3B-bioPcrA(E449C) together with 9 µM of free biotin.

The flow-cells were then visualised using TIRFM with the laser power adjusted to 2.5 mW, measured at the sample plane (i.e. after passing through the objective lens). This laser power causes the sample to photobleach fairly rapidly so that step-wise photobleaching events could be measured. The video records were analysed using the "Single Fluorophore Detection Algorithm" (SFDA) within the GMimPro software (GMimPro, freely available at http://www.nimr.mrc.ac.uk/gmimpro/). The computer algorithm searches the video data for sudden decreases in intensity at each pixel position over time, corresponding to Cy3B photobleaching events [160]. When the loading concentration of Cy3B-bioPcrA(E449C) was too high (0.5 nM and above) to visualise individual spots at the beginning of record, the number of objects on the first frame was determined by extrapolation. The extrapolation was done by averaging 5 frames and counting the objects at each time point using the "Automatic Single Particle Tracking" (ASPT) algorithm within the GMimPro programme [160] and by plotting the number of objects against time and fitting a single exponential with the rate constant determined from the exponential fitting of the photobleaching decay (measured from the change in integrated intensity across the entire field-of-view over time). The y-intercept (i.e. the amplitude) of the fit gives the total number of objects at the start of the records (See Figure 99 in the Appendix for the fits).

Analysis of experimental measurements made using protein concentrations below 0.5 nM was done by averaging the first three video frames and performing ASPT detection followed by SFDA detection on the entire record. For spot density and photobleaching measurements the SFDA and ASPT analysis were done with the default settings (see GMimPRO helpfile for details): The ASPT default settings are Max.(R)adius of 5 pixels, Track(L)en of 20 steps, Q-threshold of 10, (C)last Thr of 300 counts/pixel and FWHM of 250 nm. Max.(R)adius is a parameter that determines the maximum radius used to link objects between frames. In another words, this is the maximum movement allowed between two frames for individual spot detected. Q-threshold is the estimate of how well the shape of the detected objects matches the ideal shape of a single fluorophore (Ideal shape of the single fluorophore is the 2D Gaussian distribution of fluorescence).

(C)lastThr, the clustering threshold, is the maximum intensity limit for the tracked object. This was selected as very high to include all the fluorescent objects with multiple fluorophores clustered together. Track(L)en selects for objects that last for certain number of frames. If the tracked object is terminated before a minimal number of data points then the track is discarded. FWHM is the full width at half maximum, which determines the size of single particle in nanometres. This is selected to the point spread function of the image system, which is close to the diffraction limit (For example for 500 nm light the FWHM is ~250 nm.)

2.17.4. Single molecule plasmid unwinding assay

The flow-cells constructed using the PEGylated coverslip (see above) were incubated with 20 µg/ml of streptavidin for 15 minutes and washed 5 times to remove excess streptavidin with K100 buffer. The required concentration, typically 0.2 or 0.5 nM, of Cy3B-bioPcrA(E449C) or unlabelled bioPcrA was added into the flow-cell and incubated at room temperature in the dark for 30 minutes before washing 5 times with K100 buffer. The RepD-plasmid complex of 8 nM pCER*oriD* plasmid and 250 nM RepD was prepared on a heat block by incubation at 30 °C for 10 minutes. The RepD-plasmid complex was then incubated in the flow-cell for 10 minutes to allow bioPcrA binding to the RepD-plasmid. The reaction was started after the flow-cell has been mounted onto the TIRF microscope using 1 mM ATP and 25 nM Cy3B-SSB in buffer containing the oxygen scavenger and ATP regenerator system consisting of 10 mg ml^{-1} glucose, 50 µg ml^{-1} glucose oxidase, 400 µg ml^{-1}, catalase, 500 µg ml^{-1} BSA, 1 mM DTT, 1 mM ascorbic acid and 1 mM methyl viologen. 15 µl of the ATP mix was flowed into cell by placing the pipette at one end of the flow cell and pipetting in the mix and simultaneously, drawing out the buffer already present in the flow-cell from the other end using a small piece of blotting paper. The experiments were done at room temperature (22 °C).

Data analysis for single molecule plasmid unwinding was performed using GMimPro computer software, which is freely available at

http://www.nimr.mrc.ac.uk/gmimpro/ [160]. Intensity changes due to accumulation or loss of fluorescent material at different positions on the coverslip surface ("spots" or "events") were measured using the ASPT algorithm within GMimPro software with setting Max.(R)adius – 2 pixels , Q-threshold - 10, (C)lastThr -30 000 counts/pixel, Track(L)en>100 steps and FWHM-250 nm. The ASPT parameters are explained above in Section 2.17.3.

The tracked events were then analysed using another piece of custom-software called "Motility", which can be considered as a satellite programme of GMimPro that allows one to remove erroneous events such as "spot landings" (where an aggregate of material suddenly arrives at the surface) or duplicate events and events with intensity change over 500 (often due to overlap when two neighbouring events are closer than the diffraction limit). The plasmid unwinding events were then fitted to a single exponential process using Igor Pro 6.0.1.0 (Wave Metrics, Inc.). The fitting of the plasmid unwinding traces to a single exponential ($N(t) = N_o\ e^{-t/tau}$) gives a value for tau, which was multiplied by four to give the best estimate of Δt (See Figure 100 in the Appendix for example fits). This method was used as a semi-automated analysis method to allow objective analysis of a large number of data traces. The single exponential fit was found to match the form of the data obtained from a large number of individual plasmid unwinding events. The fluorescence amplitude of the events, ΔI, is given by the amplitude of the single exponential fit. The onset of plasmid unwinding varied between individual events within a field of view and it was determined independently for each event by fitting a straight line to the intensity data around the time at which the first sudden increase in fluorescence intensity occurred and then finding the time at which that line cut the zero axis (the fluorescence background level before the start of the unwinding event). This fitted line also gave an estimate of the initial rate of unwinding. To test whether the maximum intensity was a function of unwinding rate ΔI was plotted against Δt. Also to investigate the dispersion in unwinding rates and final signal amplitudes the Δt and ΔI distributions were plotted in histograms and fitted to Gaussian distribution on GraFit 7 (Erithacus software Ltd).

3. Results-Fluorescent species of PcrA and RepD

3.1. Introduction

PcrA is a relatively well characterised helicase and many of its enzymatic processes have been determined in ensemble assays using fluorescently labelled substrates. For example, mantATP has been used to study ATP cycle of PcrA and 2-aminopurine/fluorescein labelled DNA structures have been used to investigate the ssDNA translocation and PcrA binding to DNA [51, 54, 87, 157, 158]. Fluorescent labelling of PcrA itself has not been used in the previously published work to study PcrA function in ensemble. The labelling of PcrA with environmentally sensitive fluorophores opens up another way to look at the known PcrA functions, but also may enable investigation of traits that cannot be determined solely by fluorescent labelling of its substrates and interactors. Previous work has included the fluorescent labelling of PcrA with fluorophores suitable for single molecule assays, mainly for FRET pairing with either DNA or by doubly labelling the PcrA (typically with Cy3 and Cy5 fluorophores) [94].

Here, PcrA has been site-specifically labelled with the environmentally sensitive fluorophores using cysteine-maleimide chemistry together with fluorophores suitable for single molecule assays using TIRFM and FRET pairs. The method of designing the positions for labelling and their effect on PcrA and RepD are discussed in this Chapter. PcrA cysteine mutants were produced using site-directed mutagenesis and expressed and purified using the same method as wild type PcrA (Methods, Sections 2.4 and 2.7.2.). The aim was to develop probes for several processes such as the ss/dsDNA binding with and without RepD, the PcrA interaction with replication/unwinding complex, PcrA translocation on ssDNA and while unwinding linear and plasmid DNA, which are both coupled to ATP hydrolysis. Similarly, RepD has been a target of site-specific labelling and together, the labelled PcrA and RepD with the use of suitable fluorophores

enabled the development of a FRET signal between PcrA and RepD and also the labelling of RepD with environmentally sensitive fluorophores.

Site-specific labelling of PcrA has been achieved by the use of site-directed mutagenesis, whereby 1 to 3 nucleotides are changed to code for cysteine residue at the desired location (see Methods for more detailed protocol for mutagenesis). Cysteine residues are required as they contain thiol groups (-SH), which are reactive and form covalent non-reversible bonds with maleimide or iodoacetamide groups [120, 161, 162]. The fluorophores attached through the maleimide or iodoacetamide group in them. Each site of labelling was chosen close to the interaction site of the process in question, as determined from the PcrA crystal structures at apo and substrate bound form. Since RepD does not have a crystal structure or a highly compatible homology model, the selection of RepD labelling sites has been more complicated, but the labelling was achieved by same method as PcrA labelling. The process of site selection is discussed in Section 3.3.

An important consideration of site selection is the accessibility of the label to the site of modification. This means that all the sites chosen for labelling are on the PcrA surface and the amino acid residues orientated out from the core of PcrA. The sites are chosen so that they should not disrupt the native interaction and function of PcrA and its substrate, but close enough to cause an environmental or distance change on the fluorophore(s) when the two interact. To ensure a minimal effect on the enzymatic function of the PcrA, the labelled mutants have been tested using several assays, which measure the ATP hydrolysis rate during ssDNA translocation, the rate of linear dsDNA unwinding and the rate of full length plasmid unwinding [87, 93, 157].

The PcrA and RepD mutations done as a part of previously published work were also taken into account to ensure a minimal disruption of the wild type enzyme activity. Another factor to be considered is the

presence of wild type cysteines. These either need to be mutated out or should not be accessible to labelling.

The 2B subdomain of PcrA has been postulated as the RepD interaction site, as this domain is the closest to ICRIII sequence at the initiation complex and has no other indicated functions [21]. Seven mutations were introduced on the 2B domain; E447C, E449C, M450C, L453C, R501C and Y477C, of which four are on the top of 2B domain (Figure 22 and Table 1). All four mutations on the top of 2B domain E447C, E449C, M450C and L435C showed a RepD-specific signal. The results with these mutants are discussed in Chapter 5. Most of the work done here is with the labelled PcrA(E449C) as it showed the largest and the most RepD-specific signal when tested with the RepD-DNA.

The other sites chosen for cysteine mutation locations were sites for possible interaction signals with ss/dsDNA (H53C, K138C and also includes the Y477C and R501C) and ATP (E314C and G347C). The T167C is on 1B domain and together with other labelled PcrA mutants serves as a control for signals showing specificity to certain ligand binding, especially for possible RepD interaction site.

PcrA(E449C) mutation was also successfully used for the development of FRET pair labelled PcrA and RepD (with fluorophore pairs MDCC-Cy3 and Cy3-Cy5) and so the E449C mutation was introduced to bioPcrA to be used in the single molecule assays and for the possible development of the single molecule FRET assays on TIRFM.

3.2. Fluorescent labelling of PcrA

3.2.1. Fluorophore-labelled PcrA

Eleven single cysteine mutations were designed on PcrA surface covering all four subdomains (Figure 22). All the purified PcrA cysteine mutants have been labelled with several fluorophores, but the first choice for environmentally sensitive fluorophores were the coumarin derivatives, MDCC and IDCC. These fluorophores have been successfully used in the past for development of highly specific and stable fluorescent biosensors with large signal changes [89, 118, 120, 121]. Several other environmentally sensitive fluorophores (CPM and MIANS) were also tested but none showed improvement to signals observed with MDCC. The other fluorophores included Cy3-derivatives suitable for FRET pairing and single molecule assays. Table 1 lists the location of mutation and the target of interaction and signals observed. The actual results with labelled PcrAs are discussed on in the following Chapters. Figure 23 shows the SDS-PAGE gel of the most significant labelled PcrA mutants. The expression, purification and labelling method clearly produce stable and pure labelled PcrA species.

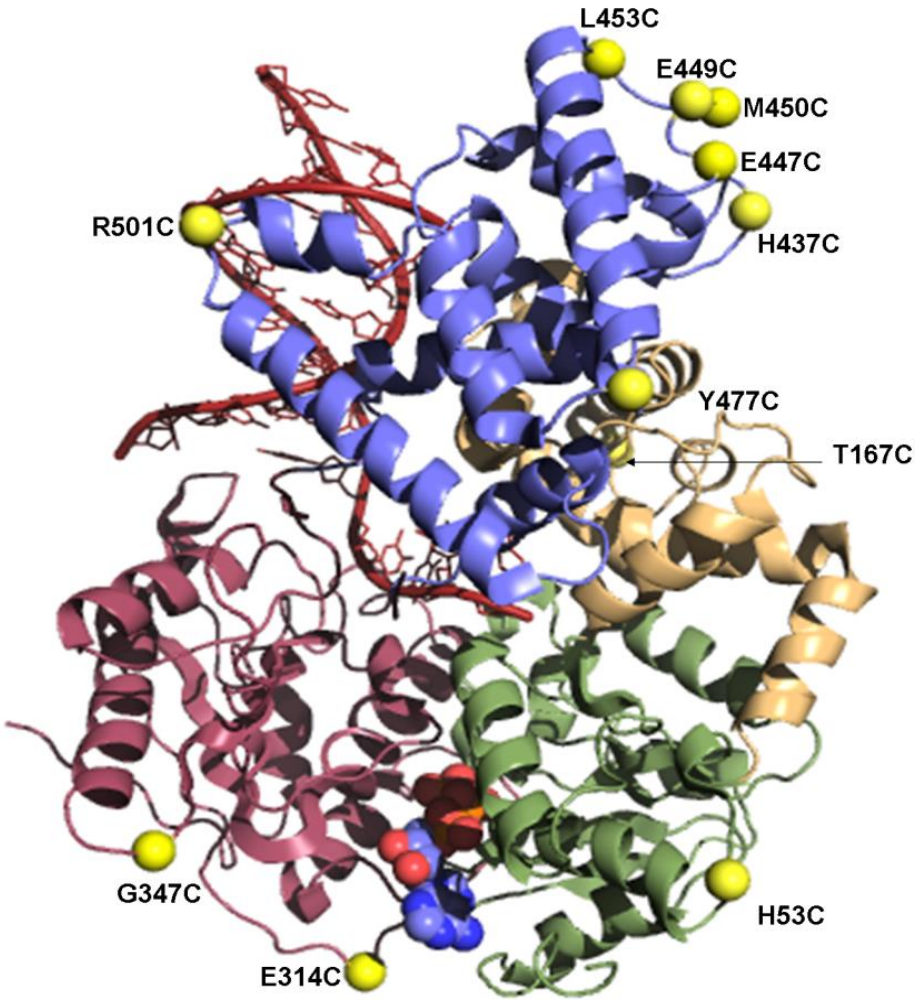

Figure 22. PcrA cysteine mutations on substrate bound PcrA structure.

PcrA(K138C) mutation is at the back of PcrA on the 1B domain loop and not visible in this figure. Yellow spheres indicate the mutation sites. Blue, 2B domain. Yellow, 1B domain. Red, 2A domain. Green, 1A domain.

PcrA mutation	Domain	Closest interaction site	Signal observed with
H53C	1A	ATP, ssDNA	ATP, ssDNA
K138C	1B	ss/dsDNA	ss/dsDNA, ATP
T167C	1B	dsDNA	No signal
E314C	2A	ATP, ssDNA	ATP, ssDNA
G347C	2A	ATP, ssDNA	ATP, ssDNA
E447C	2B	ss/dsDNA	dsDNA, RepD
E449C	2B	ss/dsDNA	dsDNA, RepD
M450C	2B	ss/dsDNA	ss/dsDNA, RepD
L453C	2B	ss/dsDNA	dsDNA, RepD
Y477C	2B	ssDNA	ssDNA
R501C	2B	ss/dsDNA	ss/dsDNA

Table 1. PcrA cysteine mutations and their closest interactors according to substrate bound PcrA crystal structure.

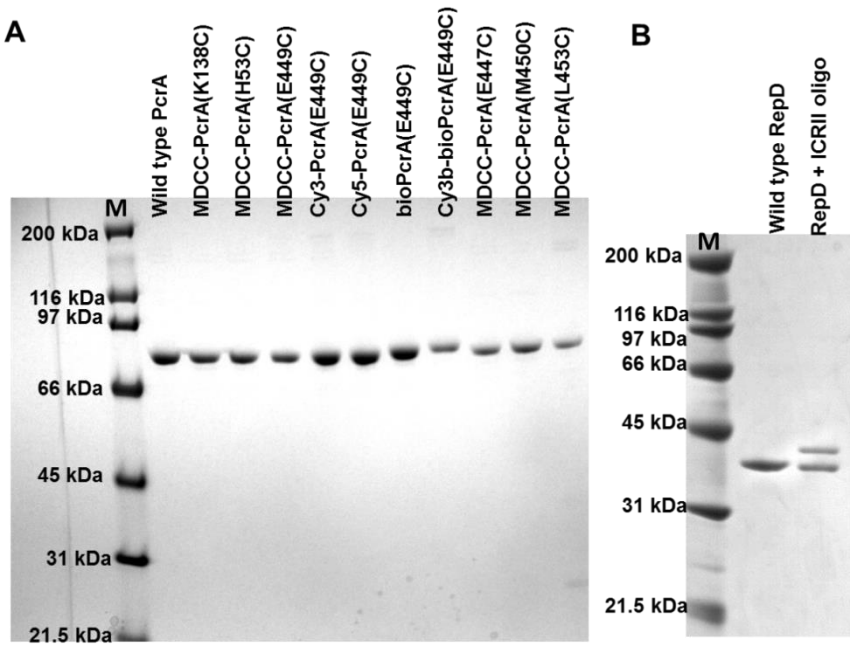

Figure 23. 12% SDS-PAGE gel analysis of the fluorophore-labelled PcrA and RepD wild type.

A) 12% SDS-PAGE gel of wild type PcrA, labelled PcrA, bioPcrA(E449C) and labelled bioPcrA(E449C). The gel shows that new mutant PcrA are similar in size and contain no degradation of the protein. B) 12% SDS-PAGE gel of wild type RepD. The prepared wild type RepD has the ability to nick DNA with ICRIII sequence.

The efficiency of PcrA labelling was determined by calculating the protein and fluorophore concentrations using absorbance measurements. These were obtained by measuring the absorbance at 280 nm (mainly protein, but partly also fluorophore) and at the maximum absorbance of the fluorophore (MDCC/IDCC – 430 nm, Cy3 – 550 nm, Cy3B – 559 nm and Cy5 – 649 nm). The protein and fluorophore concentrations could then be expressed as a ratio of fluorophore per protein or as labelling percentage, where 100% labelling means one to one ratio of fluorophore to protein. This is a quantitative way to determine labelling efficiency, but does not enable distinction between free and bound fluorophore and can falsely indicate higher levels of labelling or multiple labelling of the protein. For this reason and to determine the correct expression and purification of the mutant, all labelled samples were also tested using electron-spray mass spectrometry. Mass spectrometry is not quantitative method to determine the ratio of the unlabelled versus labelled species, but can clearly indicate if some unlabelled protein is present. Mass spectrometry shows the molecular weights present to accuracy of +/- 2 Da.

An important point before labelling any protein is the determination whether wild type cysteines exist in the protein and can these be labelled at conditions used for site-specific labelling. PcrA wild type has two cysteines, C247 and C96, which are buried in the PcrA and so are expected to be poorly reactive. This was tested by using same labelling protocol and conditions used for PcrA cysteine mutants labelling. The electron-spray mass spectrometry of labelled wild type PcrA showed a single macromolecule of molecular weight of 82,470.6 +/-2 Da. This corresponds well with the expected molecular weight of unlabelled wild type PcrA, 82,472 Da. This indicated that the labelling conditions for PcrA modification do not cause significant labelling of the native cysteines and the labelling percentage determined are for site-specific labelling of PcrA.

The labelling of cysteine mutants was highly specific. Table 2 summarises the molecular weight of the fluorophore labelled PcrA mutant,

the labelling percentage and the protein yield per 0.5 L of bacterial culture. All the mutants expressed indicated similar levels of expression, apart from PcrA(T167C), which had half of the expression levels compared to other mutants. No clear reason has been found for this as on crystal structures the mutation of T167 doesn't indicate an obstruction to the PcrA activity. Also, once the PcrA(T167C) mutant was labelled and tested for helicase activity, it was shown to have wild type-like activity. PcrA(R501C) is the only mutant that showed high precipitation during labelling with MDCC (not quantified). This is most likely due to the close proximity of the cysteine to the dsDNA interaction site on 2B domains (Figure 22). Even this mutant was shown to have wild type-like helicase activity (Table 3).

Labelled PcrA mutant	Molecular weight (Da)	Labelling percentage	Protein yield (mg/0.5 L)
MDCC-PcrA(E449C)	82 828.5	100.2%	15.7
Cy3-PcrA(E449C)	83 200.3	101.2%	15.7
Cy5-PcrA(E449C)	83 226.2	106.2%	15.7
MDCC-PcrA(H53C)	82 820.8	99.4%	10.5
MDCC-PcrA(K138C)	82 830.0	99.6%	11.9
MDCC-PcrA(T167C)	82 894.3	102.6%	7.1
MDCC-PcrA(E447C)	82 829.6	96.4%	15.6
MDCC-PcrA(M450C)	82 824.8	103.0%	17.9
MDCC-PcrA(L453C)	n/a	101.7%	14.8
MDCC-PcrA(Y477C)	82 791.1	106.1%	13.6
MDCC-PcrA(R501C)	82 908.2	97.8%	13.4
bioPcrA	84 767.1	n/a	2.6
Cy3B-bioPcrA(E449C)	85 425.0	91.0%	2.2

Table 2. The analysis of the quality of new fluorophore labelled PcrA mutants.

As a standard the final product, PcrA with fluorophore, was analysed using absorbance and mass spectrometry measurements. The labelling percentage was determined from the absorbance spectra. The protein yield was measured to confirm similar levels of expression and purification expressed here as total protein per 0.5 L of bacterial culture used.

3.2.2. The effect of mutations and labelling on PcrA activity

A dsDNA junction unwinding assay was used to test the modified PcrA. This assay was developed to study the rate of DNA unwinding using DNA junctions modified with a quencher-fluorophore pair (at the distal end) on the stopped-flow [163]. Processive unwinding of DNA junctions by PcrA requires the presence of RepD [87] (Figure 24). In the assay PcrA was loaded on to the RepD-DNA before the unwinding was initiated by mixing with ATP. Once the helicase reached the end of the DNA junction, separation of the quencher from the fluorophore was detected as a fluorescence increase. The time that the helicase took to reach quencher-fluorophore pair was observed as a lag, which is dependent on the number of base pairs unwound (Figure 24). The lag phase duration for each junction was then plotted against the number of base pairs unwound to obtain the value for rate of unwinding. This assay is an efficient way to look at the effect of the modification on PcrA, as it tests all the functions required for PcrA to be a processive helicase such as interaction with RepD, ssDNA translocation, dsDNA unwinding and ATP hydrolysis.

When the DNA unwinding assay was done with coumarin-derivative labelled PcrA, Cy3-Dabcyl fluorophore-quencher pair labelled DNA junctions were used as the excitation and emission spectrum of Cy3 do not overlap with the coumarin excitation and emission spectrum. However, when Cy-dye labelled PcrA/RepD was tested, DNA junctions with an AlexaFluor350-Dabcyl pair were used to avoid the overlap of excitation and emission of the Cy-dyes.

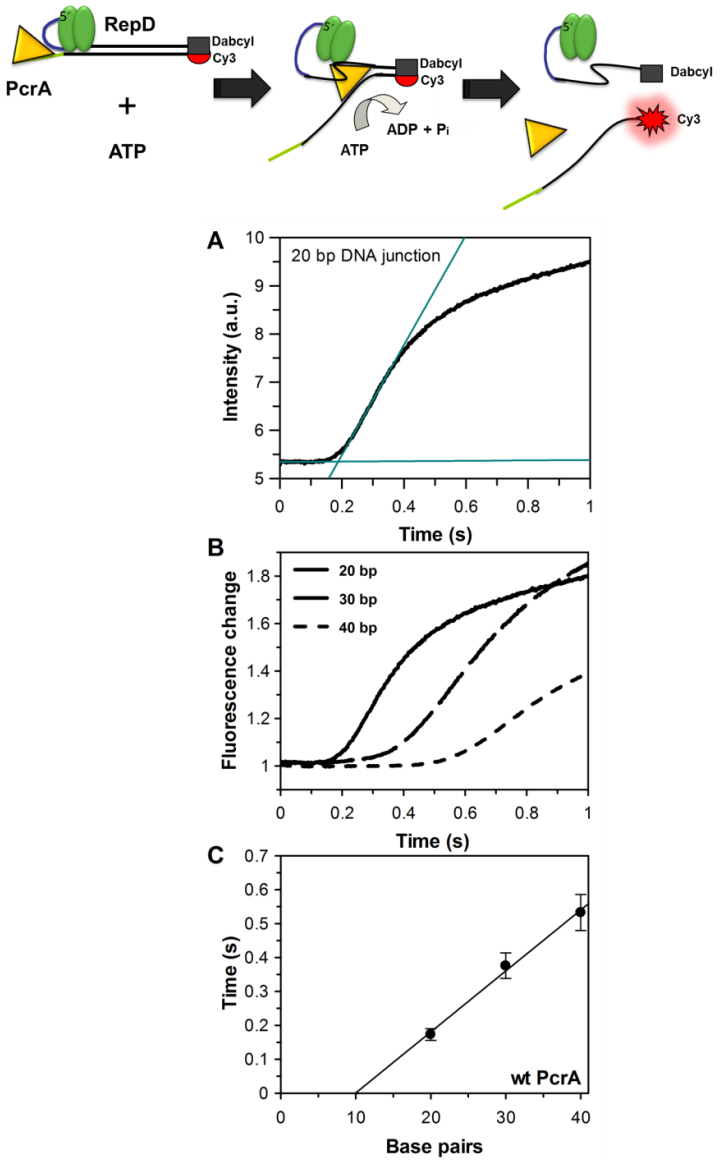

Figure 24. DNA junction unwinding assay.

Top image is a cartoon representation of DNA junction unwinding assay showing the structure of the DNA junctions. A) An example trace for 20 bp DNA junction with linear fits to the lag phase and the increasing phase. The intercept of two linear fit is used as the time point for end of unwinding, which is 0.2 s for the example. B) Normalised traces for three lengths of DNA junctions. C) The linear fit of lag phase durations against number of base pairs for four DNA junctions. The gradient is 0.018 (SEM 0.0013) and gives rate of unwinding of 56.6 bp s^{-1} (+/- 4.0). The experiments were done with 100 nM PcrA, 500 nM DNA, 2.5 µM RepD and 200 µM ATP in K200 buffer at 30 °C. See Figure 18 for the DNA junction sequences. Typically, three DNA junction lengths were used in the assay. This has been shown to measure PcrA unwinding accurately as the same assay was carried out using four lengths of DNA junctions (10, 20, 30 and 40 bp) with wild type PcrA and this had unwinding rate of 48 bp s^{-1}.

The rate of unwinding on DNA junctions was measured for all PcrA mutants labelled with MDCC and for many labelled with other fluorophores and modification with biotin. They all showed similar unwinding rates to wild type PcrA with the rate varying between ~46-57 bp s^{-1}. The average of all experiments was 51.5 bp s^{-1} (Table 3). The published rate for unwinding of DNA junctions is ~50 bp s^{-1} [87]. This shows that PcrA can be successfully mutated and labelled without affecting its helicase activity and the sites chosen here have no significant effect on PcrA helicase function. The unwinding rate of Cy3B-bioPcrA(E449C) was 52 bp s^{-1} showing that the biotinylation peptide on the N-terminal end, the biotin and the Cy3B do not disrupt its ability to interact with RepD and unwind DNA.

PcrA helicase	Unwinding rate (bp s^{-1})
DCC-PcrA(E449C)	57
MDCC-PcrA(E449C)	57
Cy3-PcrA(E449C)	52
Cy5-PcrA(E449C)	49
MDCC-PcrA(Y477C)	53
MDCC-PcrA(K138C)	50
MDCC-PcrA(H53C)	46
MDCC-PcrA(E314C)	50
MIANS-PcrA(H53C)	48
CPM-PcrA(H53C)	51
MDCC-PcrA(T167C)	49
MIANS-PcrA(R501C)	50
MDCC-PcrA(E447C)	51
MDCC-PcrA(M450C)	54
MDCC-PcrA(L453C)	55
CPM-PcrA(R501C)	50
bioPcrA	50
Cy3b-bioPcrA(E449C)	52
PcrA wt	54

Table 3. DNA unwinding rates of labelled PcrA cysteine mutants and bioPcrA.

The assay was repeated for three times for MDCC-PcrA(E449C) and MDCC-PcrA(K138C). Between the different mutants and labels, the ~20% variation in rate of unwinding is generally observed.

The ATPase activity of the PcrA labelled mutants was surveyed to show any effect of cysteine mutation and the label. This was done by a steady-state, ssDNA-dependent ATP hydrolysis assay. Measurements were done using the P_i biosensor, 6ATR-PBP, as a fluorescent signal increase caused by the production of P_i from ATP hydrolysis by PcrA translocating on ssDNA ($dT_{30/35}$) [120, 164]. The assay was repeated at various ATP concentrations and Figure 25 shows the P_i production rates against ATP concentration for MDCC-PcrA(E449C) on dT_{30} oligo and MDCC-PcrA(K138C) on dT_{35}. These rates were then compared to wild type PcrA ATP hydrolysis rate. Table 4 shows the values for K_m and k_{cat} for the reactions determined by Michaelis-Menten equation (Equation 7, Methods) for a variety of labelled PcrA. K_m for the MDCC-PcrA(K138C) dT_{30} translocation varies between 2.2 and 4 μM and is just over 4 μM for the dT_{35} translocation. This further demonstrates that the mutations and the labelling do not change the PcrA activity.

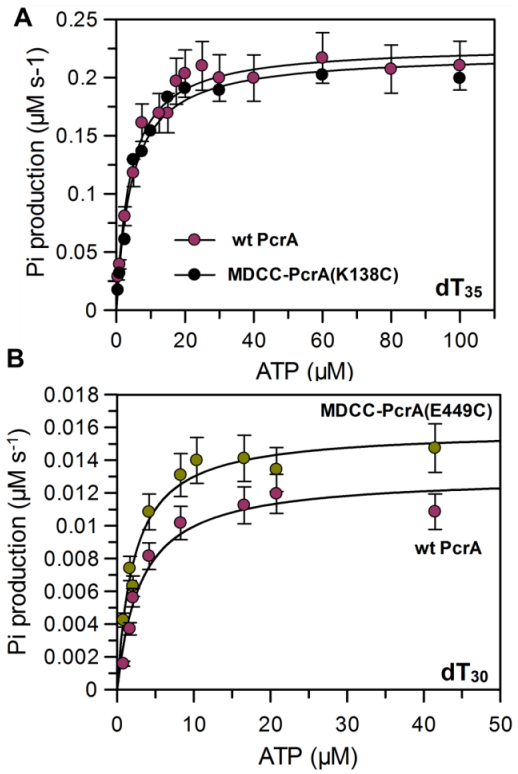

Figure 25. PcrA steady-state ATP hydrolysis on ssDNA translocation measured using Pi biosensor.

Measurements done at 20 °C in buffer 50 mM Tris·HCl pH 7.5, 3 mM $MgCl_2$ and 150 mM NaCl with 10 nM of PcrA, 500 nM of dT_{35} (A) or dT_{30} (B) and 10 μM of 6ATR-PBP in Cary spectrofluorometer (Varian). ATP concentration was varied in each reaction. P_i biosensor was calibrated in same reaction mix using known concentration of P_i. The K_m and k_{cat} were determined by fitting the data to the Michaelis-Menten equation (Equation 7, Methods).

PcrA	K_M (μM)	k_{cat} (ATP s^{-1})	ssDNA
PcrA wt	3.1 (SEM 0.7)	6.5 (+/-0.4)	dT_{30}
MDCC-PcrA(E449C)	2.2 (SEM 0.3)	7.9 (+/-0.3)	dT_{30}
DCC- PcrA(E449C)	4.0 (SEM 0.7)	8.8 (+/-0.4)	dT_{30}
Cy3B- PcrA(E449C)	3.1 (SEM 0.4)	7.9 (+/-0.3)	dT_{30}
MDCC-PcrA(T167C)	3.1 (SEM 0.8)	10.5 (+/-0.7)	dT_{30}
PcrA wt	4.0 (SEM 0.4)	22.8 (+/-0.5)	dT_{35}
MDCC-PcrA(K138C)	4.5 (SEM 0.6)	22.1 (+/-0.8)	dT_{35}

Table 4. Reaction rates of fluorophore labelled PcrAE449C, PcrAK138C and wild type PcrA.

3.2.3. MDCC-PcrA(K138C) activity in plasmid unwinding

The MDCC-PcrA(K138C) helicase unwinding activity was further tested by measuring plasmid unwinding on the stopped-flow apparatus. The cartoon representation of the assay is shown in Figure 26. The assay uses the ssDNA biosensor DCC-SSB(G26C), which has high affinity and high fluorescence change when binding to ssDNA [89]. Once PcrA-RepD-plasmid complex is mixed with ATP, PcrA starts to unwind the plasmid releasing increased amounts of ssDNA to which DCC-SSB binds. DCC-SSB has high affinity to ssDNA (K_d = 28 nM for dT_{35}) and at concentrations the free ssDNA will be bound by DCC-SSBs [121]. The traces observed are biphasic with a ~25 s lag phase (Figure 27A). The first increasing phase is faster and is the actual plasmid unwinding and its duration varies with the length of the plasmid. The second slower increasing phase is most likely to be caused by the RepD nicking and re-ligation activity, which leads to some of the plasmids being relaxed but closed. Relaxed plasmids are poor substrates for RepD. This means that some of the plasmid unwinding is initiated later and observed as the second slower increasing phase. The breakpoint of the fast and slow phase is the end of single turn over unwinding, which is determined as the intercept of two linear fits, one to each phase. The assay was done with several lengths of plasmids and the plasmid unwinding durations were plotted against the number of base pairs of the plasmid to determine the rate of unwinding.

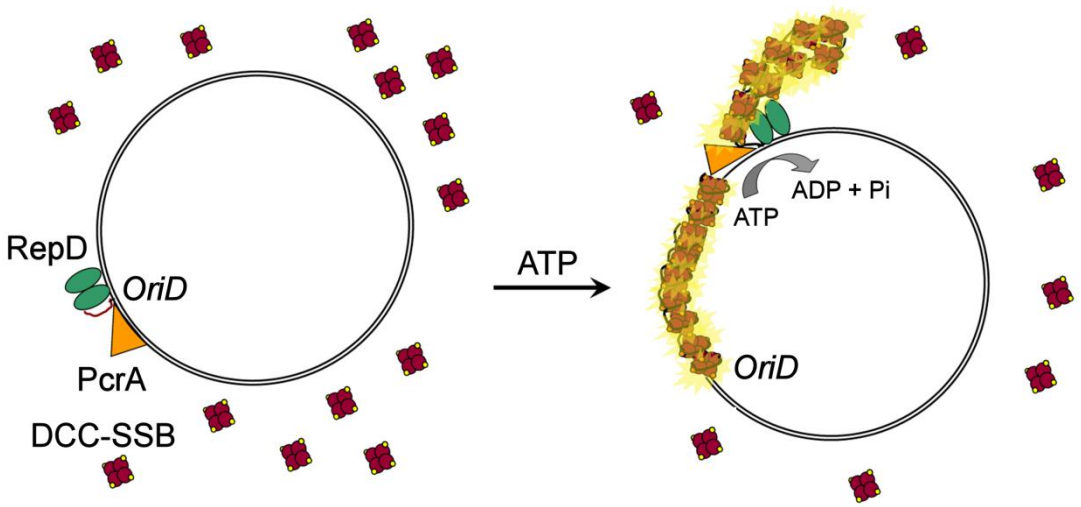

Figure 26. DCC-SSB plasmid unwinding assay.

The assay was done on the stopped-flow apparatus by mixing the pre-incubated PcrA-RepD-plasmid complex with ATP in presence of ssDNA biosensor DCC-SSB.

The plasmid unwinding rate by wild type PcrA and MDCC-PcrA(K138C) are very similar, both ~30 bp s^{-1}, showing that the plasmid unwinding is not affected by the MDCC-labelling or the K138C mutation of PcrA (Figures 27 and 28).

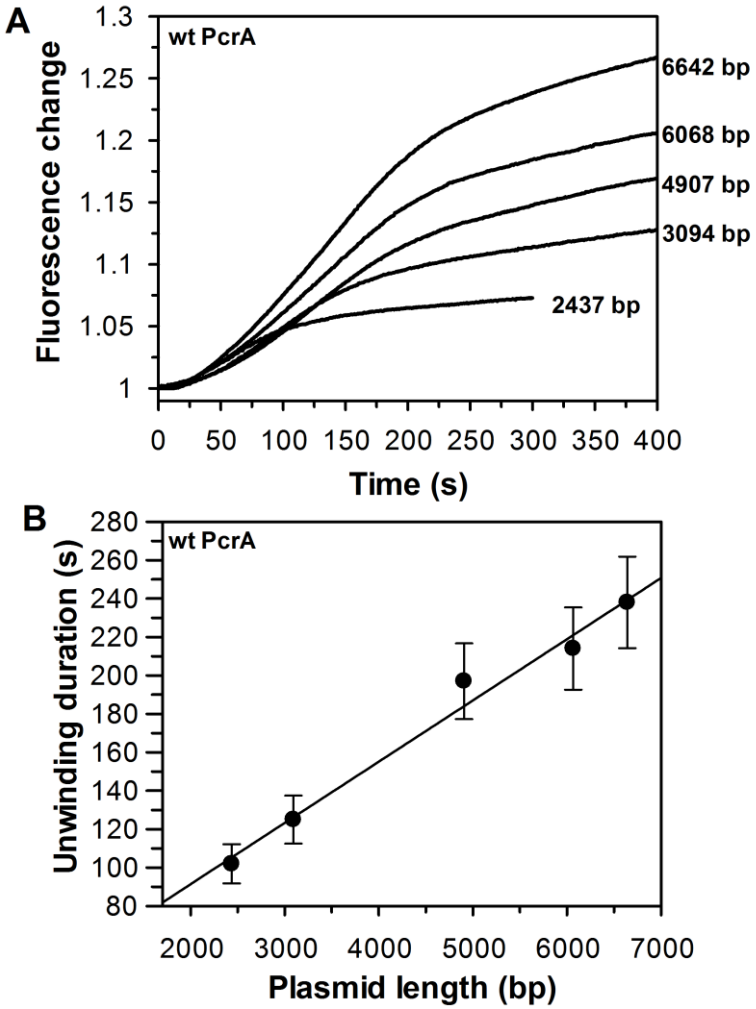

Figure 27. PcrA wild type DCC-SSB plasmid unwinding assay.

A) Individual traces for five lengths of plasmid. The two phases were fitted with linear fits and the intercept of the fits was used as the end point of unwinding. B) Plasmid unwinding duration is dependent on the length of the plasmid. The linear fit of unwinding duration as a function of length of the plasmid has a gradient of 0.0323 (SEM 0.0022).The reciprocal of this gives an unwinding rate of 30.95 +/- 2.1 bp s^{-1}. The experimental conditions were 100 nM PcrA, 0.5 nM pCER*oriD* plasmid, 2 nM RepD, 200 nM DCC-SSB and 1 mM ATP in K200 buffer at 30 °C.

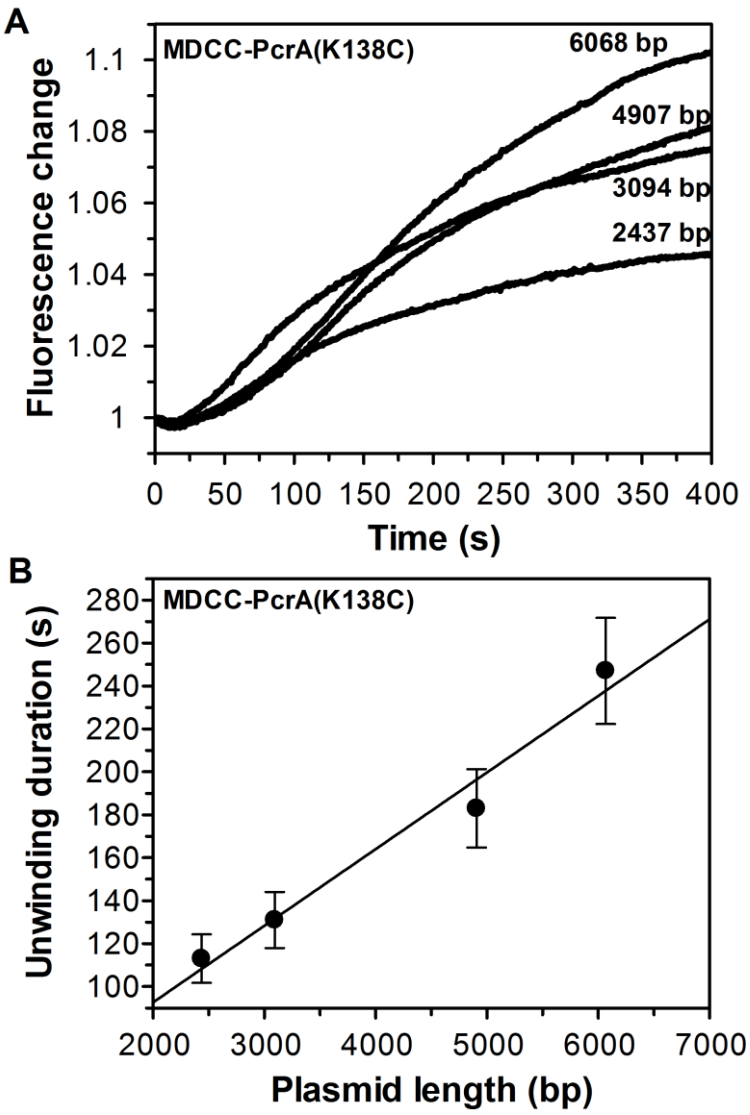

Figure 28. MDCC-PcrA(K138C) DCC-SSB plasmid unwinding.

A) Individual traces of four lengths of plasmid. B) Plasmid unwinding duration dependence on length of the plasmid. The linear fit of unwinding duration against the length of the plasmid has a gradient of 0.0357 (SEM 0.0042). This gives an unwinding rate of 28.0 +/- 3.3 bp s^{-1}. Experimental conditions were same as Figure 27. MDCC-PcrA(K138C) traces show higher noise due to high background fluorescence from the coumarin label on the protein. This is also the most likely reason for the overlapping or crossing of traces shown in graph in Figure 28A and the small difference in total fluorescence change between the plasmids.

3.3. Fluorescent labelling of RepD

3.3.1. Fluorophore-labelled RepD wild type

RepD wild-type and cysteine mutants were labelled to enable development of a FRET assay with labelled PcrA. The FRET paired PcrA and RepD might be used in measurements in ensemble and at single molecule level. The same cysteine mutant locations were also used for labelling with environment sensitive fluorophores and tested for a fluorescent signal when RepD interacts with ss/dsDNA and PcrA. RepD wild type and RepD cysteine mutants were expressed and purified according to protocol stated in the Methods, Section 2.7.3.

RepD is a 311 amino acid protein without a known crystal structure or a close homology based structural model. RepD wild type has one cysteine residue (residue 225). To test the thiol accessibility on RepD wild type, DTNB (Ellman's reagent) assay was used. Figure 29 shows a measurement of DTNB reaction with the RepD. The traces have two phases, a faster phase and slower phase. The faster phase can be calculated to correspond to 10.8 µM TNB by converting the absorbance at 412 nm to TNB concentration (The molar extinction coefficient of 14 150 M^{-1} cm^{-1}). In the reaction there are 20 µM of monomers (10 µM of RepD dimers) and each monomer has single thiol (equals to 20 µM of thiols). The assay indicates that both the thiols on RepD dimer are accessible and slowly reactive. There may be a difference between the two thiols as two phases are observed. Possibly once one of the monomers (thiols) has reacted, the second thiol on the other monomer is poorly accessible or reactive. This may be due to physical change in the RepD dimer structure or the first fluorophore blocking the accessibility to the second thiol.

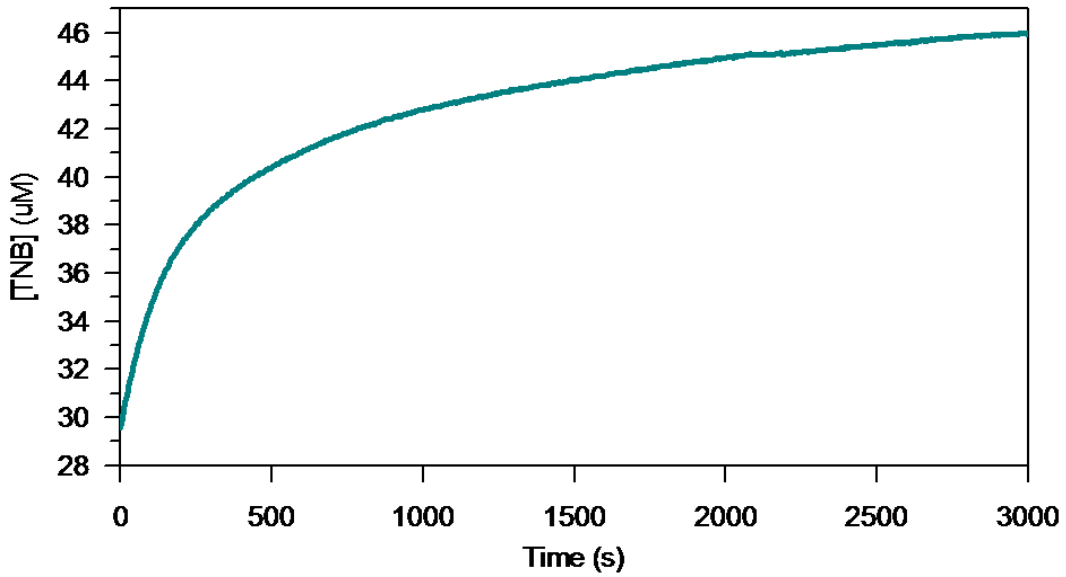

Figure 29. Thiol reactivity on wild type RepD dimer.

RepD shows two phases of increased absorbance at 412 nm. Here, the absorbance has been converted to concentration of TNB. First phase has been fitted to a single exponential fit and the second to linear fit. First phase has a rate constant of 8.1 x 10^{-3} is equivalent of 10.8 µM TNB. The gradient of the linear phase is 2.8 x 10^{-6} µM s^{-1}.

As the C225 on RepD was shown to be reactive, the aim was to use it for labelling. The RepD labelling was carried out with MDCC, Cy3-, Cy3B- and Cy5-maleimide. The labelling of wild type RepD varied between ~30 to 50% with two occasions reaching to ~70% of labelling but never achieving 100% labelling. To simplify and provide comparison between different labelling attempts Cy3-maleimide was used for multiple testes of RepD labelling. These showed varying labelling percentages that rarely resulted over 50% labelling of monomers. This suggests only one of the RepD subunits is labelled. This kind of labelling is not common but could take place for example if the cysteines are located in the cleft of the dimerisation surface proving very limited space for fluorophore entry. In another words, if one monomer has covalently bound fluorophore on, there would be no more room for second one to react with the thiol of the second monomer. Due to large variation between labelling efficiency and not clear labelling of single RepD subunit, the wild type RepD proved not to be a good candidate for labelled RepD.

3.3.2. RepD N- and C-terminal cysteine mutants

Another approach to label RepD was also used, in which the N- and C- terminal ends of the RepD were target for site-directed mutagenesis to produce cysteine residues. The N- and C- terminal ends of proteins are often on the surface of the proteins and as the structure of RepD is not known and no high sequence similarity homologue model exist/have been able to produce, the N- and C- terminals ends were the most preferable target for cysteine mutations. Wild type RepD has a single cysteine on its sequence and as shown here, this can be labelled to certain extent. For this reason it was necessary to mutate C225 to alanine. This mutation was confirmed by sequencing. RepD(C225A) was expressed and tested for activity (Figure 30).

The construct containing the RepD(C225A) was then mutated using site-directed mutagenesis to have a cysteine mutation at N- or C- terminal ends (S2C and W310C). The RepD cysteine mutants were expressed and purified. Both RepD mutants, S2C and W310C, were labelled with Cy3-maleimide. The absorbance spectrum of RepD(C225A, S2C) showed no maximum at 550 nm indicating that the S2C cysteine is not labelled with Cy3 and is inaccessible for the maleimide reaction. RepD(C225A, W310C) in contrast showed high labelling percentage (>80%) and electron-spray mass spectrometry showed only labelled species of the RepD mutant with molecular weight of 37 985.4 +/- 2 Da as expected. RepD mutants and the final labelled RepD were tested for wild type-like activity by RepD nicking assay on SDS-PAGE and by DNA junction unwinding assay (Figure 30 and Table 5). The RepD nicking assay is based on RepD function of only nicking and binding to DNA (here an ICRII oligo) using one of its subunits (often expressed as RepD/D*) [84]. On SDS-PAGE the monomer with DNA (RepD*) will run differently to the monomer without DNA (RepD) as was seen in on the gel in Figure 30. All the RepD mutants and Cy3-RepD(C225A,W310C) were able to nick DNA as shown by SDS-PAGE. Cy3-RepD(C225A,W310C) was also shown to initiate the dsDNA unwinding and make PcrA processive helicase similarly to wild type RepD

by DNA junction unwinding assay on the stopped-flow apparatus (Table 5). The nicking assay on SDS-PAGE shows an extra band on lane 9 in Figure 30. This is possibly unlabelled RepD(C225A,W310C), but mass spectrometry analysis of the sample showed only labelled RepD species. Together the experiments provided enough evidence to say that the unlabelled species were in very low concentration compared to labelled species and they should have little effect on the overall results in the further experiments.

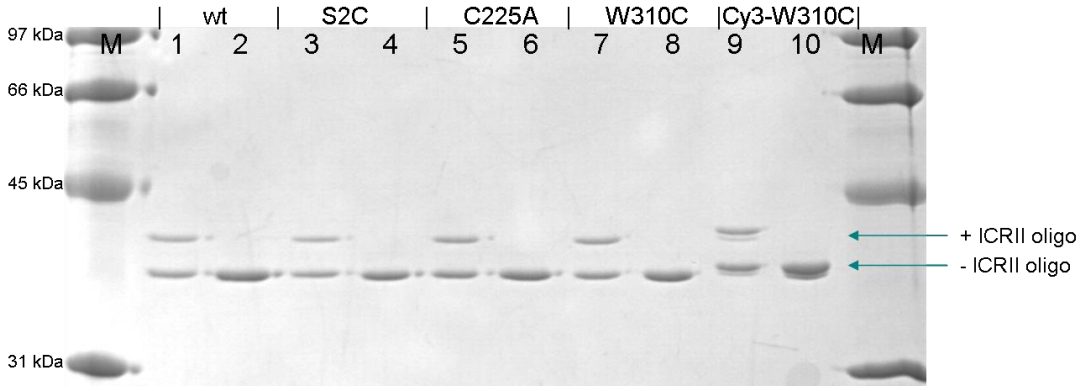

Figure 30. SDS-PAGE gel of RepD nicking assay.

M, protein standard marker. Wild type RepD with ICII oligo (1) and without oligo (2). Unlabelled RepD(C225A, S2C) with ICRII oligo (3) and without oligo (4). RepD(C225A) with ICRII oligo (5) and without oligo (6). Unlabelled RepD(C225A, W310C) with ICRII oligo (7) and without oligo (8). Cy3-RepD(C225A, W310C) with ICRII oligo (9) and without oligo (10). The nicking assay was done by 5 minute incubation of 1 µM RepD with 5 µM DNA in K200 buffer at 30 °C. The monomers of RepD/D* dimer run differently on SDS-PAGE.

RepD (wt PcrA)	Unwinding rate (bp s^{-1})
RepD(C225A,W310C)	51
Cy3-RepD(C225A, W310C)	50
wt RepD	54

Table 5. DNA junction unwinding is not affected by labelling and mutations on RepD.

Wild type PcrA was used in all unwinding experiments. Experimental conditions were same as in Figure 24.

3.4. Discussion

3.4.1. Fluorophore-PcrA adducts

The labelling of PcrA was achieved to high level of specificity using thiol-maleimide chemistry. This has proven to be relatively simple and fast methods to produce fluorescently labelled PcrA. For example, once the wanted cysteine mutant has been purified, preparation of 100% labelled PcrA can be achieved in less than three hours and several labelling preparations can be done simultaneously (Table 2). The selection method of residues for site-directed mutagenesis by estimation of possible signal and accessibility has been successful for all expressed and purified proteins.

The activity of labelled PcrA has been tested mainly by the DNA junction unwinding assay, which measures PcrA unwinding rate. For PcrA to unwind DNA junctions successfully it must interact with RepD, bind and translocate on ssDNA, unwind DNA and turn over ATP [87]. By itself the assay provides a good indication of the activity of PcrA and the effect the mutations and labelling have had on it. All labelled PcrAs unwind DNA similarly to wild type at approximately 50 bp s^{-1}. Steady-state ATP hydrolysis assay was carried to test the PcrA ssDNA translocation coupled ATP hydrolysis. This demonstrated that the labelled PcrA mutants have no significant change in K_m or k_{cat} of ATP turn over while it translocates on ssDNA. The assay was done to labelled PcrAs with most significant results which are used for results in Chapters 4 and 5 (MDCC-PcrA(K138C) and MDCC-PcrA(E449C)).

MDCC-PcrA(K138C) was further tested in plasmid unwinding assay that uses full length plasmids. This was done as previous mutational work on PcrA has indicated in different helicase assay without RepD that mutating K138 to alanine, reduces PcrAs ability to unwind dsDNA without significant effect on ssDNA translocation activity [165]. The assay was done

in comparison to wild type PcrA and both showed a similar unwinding rate confirming that the RepD dependent unwinding is not affect by the mutation of K138 to cysteine and labelling this with MDCC.

3.4.2. Fluorescently labelled RepD

RepD labelling was attempted using two methods. The first approach was to label the cysteine in RepD wild type (C225), and the second, was to introduce cysteine to N- or C-terminal ends of RepD. The labelling of wild type is beneficial for the obvious reason of not having to change the wild type RepD as introduction of mutations is more time consuming and may affect the actual function of the protein. The C225 did react with maleimide linked fluorophores but not to 100% labelling. The accessibility of the C225 was tested using DTNB that indicated slow reactivity and possibly to mainly one of the subunits on the RepD dimer. This could indicate that the dimers bind in orientation that positions the thiols close together and once one thiol is labelled, the other is poorly reactive. Having a single fluorophore on RepD dimer would have been advantageous for future experiments. It could have caused less disruption the wild type activity of RepD but also simplified the interpretation of the results.

As the full labelling of the C225 RepD was not achieved, the C225 was mutated into alanine and site-directed mutagenesis was used to introduce cysteines to the N- and C- terminus of RepD. The C- and N-terminal ends of proteins are often located on the protein surface and may be accessible for labelling. This method was successful as highly labelled RepD(C225A, W310C) was achieved with Cy3 and MDCC. RepD(C225A, S2C) showed no labelling implying that the orientation or the C-terminal end is buried in the RepD. MDCC-labelled RepD did not show a signal indicating that it is located or orientated far from interaction sites. Other possible explanation could that the RepD structural changes are too minor to cause environmental change in the MDCC fluorescent properties. The successful labelling of RepD enabled the development of FRET pair with labelled PcrA.

4. Results- PcrA binding and translocation on ssDNA

4.1. Introduction

PcrA has an important function in replication of certain plasmids by separating the dsDNA into ssDNA, which is then replicated by DNA polymerase III [79]. The single stranded DNA that PcrA requires for loading onto DNA is opened by RepD nicking the dsDNA [85, 88]. PcrA translocates on ssDNA destabilising actively or passively the DNA base pairing. Therefore, the PcrA plasmid unwinding function is dependent on the ability of PcrA to bind and translocate on ssDNA, which is driven by the energy derived from ATP hydrolysis. Hence, understanding the PcrA characteristics of binding and translocating on ssDNA is vital for fully understanding how PcrA functions during plasmid unwinding. PcrA may also have other endogenous function(s) in bacteria that do not require PcrA helicase activity but rely on its ability to translocate ssDNA. This function could be in DNA repair. For these reasons developing assays to investigate the interaction of PcrA with ssDNA and translocation on ssDNA are beneficial for understanding the function of PcrA.

PcrA K138 was chosen for site-directed mutagenesis and fluorophore labelling as it is located close to the ssDNA interaction site on PcrA (Figure 31). The PcrA(K138C) mutant has been labelled with several fluorophores, but a signal specific for ssDNA binding and translocation was observed with MDCC-maleimide labelling. This signal has been characterised and MDCC-PcrA(K138C) has been used to study PcrA binding and dissociation from ssDNA, PcrA translocation on ssDNA and how the DNA sequence affects the rate of translocation.

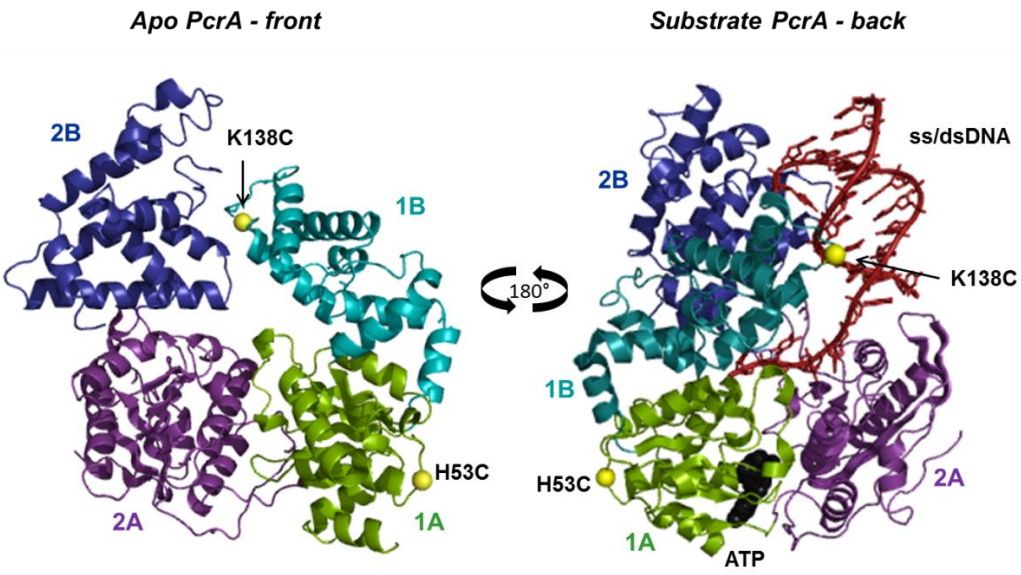

Figure 31. Cartoon representation of PcrA structures showing the K138C location.

The yellow spheres indicate the location of cysteine residues introduced site-specifically on the surface of PcrA. The coordinates for the images were taken from PDB files 1PJR (open, apo) and 3PJR (closed, substrate bound) and visualised using PyMol (http://www.pymol.org/).

4.2. MDCC-PcrA(K138C) binding to ssDNA

4.2.1. MDCC-PcrA(K138C) has different affinities and fluorescent states when binding to the middle or to the ends of ssDNA

When MDCC-PcrA(K138C) was mixed with ssDNA on the stopped-flow instrument a fluorescent signal was observed. This signal was further characterised by mixing the MDCC-PcrA(K138C) with the varying length of the ssDNA, as the number of binding sites changes with the length of ssDNA (Figure 32). The signal varied according to the length of ssDNA. A very short oligo dT_{10} showed a decreasing signal, whereas the oligos longer than 35 bases had an increasing signal. Interestingly, the dT_{20} had two phases, which were a decreasing phase followed by an increasing phase. These results can be explained by MDCC-PcrA(K138C) having two different fluorescent states and affinities when binding to different parts of the ssDNA. The simplest explanation would that PcrA binds to the middle of ssDNA

differently than to the ends of ssDNA. As the short ssDNA dT_{10} with the largest end to middle ratio, has only a decreasing signal, PcrA bound to ssDNA ends must have lower fluorescence than free MDCC-PcrA(K138C) in solution. dT_{50} and poly dT with small end to middle ratios, showed only increasing signals. The primary form of binding is to the middle of ssDNA, which has higher fluorescence than MDCC-PcrA(K138C) free in solution. Together, the experiments with the different lengths of ssDNA confirm the end to middle binding-hypothesis suggested before [51], where the binding to the ends of ssDNA is faster than to the middle, but the middle state is thermodynamically more stable. The strongest evidence for this is the dT_{20} ssDNA signal, which shows signals for both forms of binding. Initially the fluorescence decreases due to fast binding to the ends followed by an increase due to slow equilibration towards the more stable, middle-bound state.

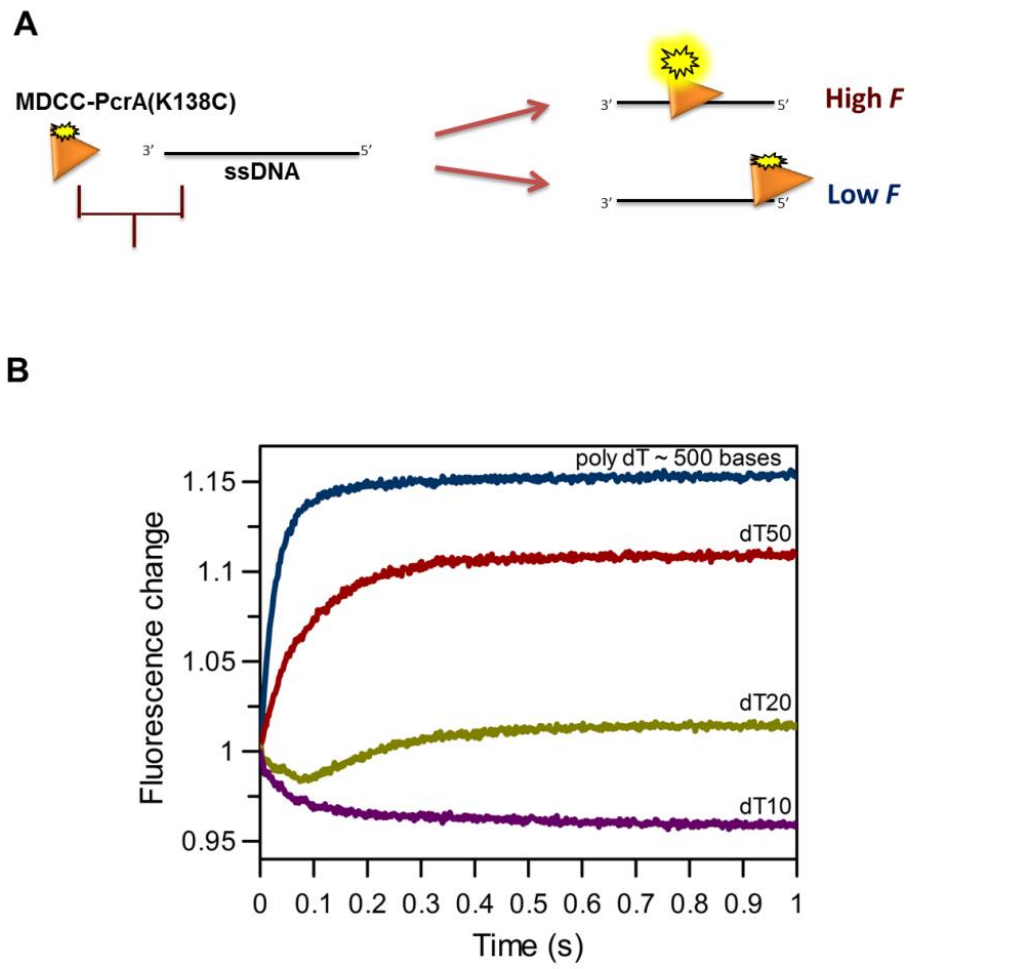

Figure 32. MDCC-PcrA(K138C) binding to ssDNA has different fluorescent states whether binding to the middle or the end of ssDNA.

A) Cartoon representation of the reaction on the stopped-flow apparatus. B) PcrA binding to four lengths (dT_{10}, dT_{20}, dT_{50} and poly dT ~500 bases) of ssDNA. The experimental conditions were 100 nM MDCC-PcrA(K138C) mixed with 1 µM of ssDNA at 30 °C in K200 buffer. The excitation was done at 436 nm and the emission was measured using a cut-off filter at 455 nm.

To test the model further, the measurements were repeated with DNA structures lacking the ssDNA ends (Figure 33). These structures had a defined number of ssDNA (dT 10, 20, 30 or 50) between 10 bp double stranded structures at the 5'-and-3' ends. They were called dT_{middle} with a number indicating the length of the ssDNA middle. The different lengths of "no ends"-ssDNA structures were tested by mixing with MDCC-PcrA(K138C) on the stopped-flow apparatus. Regardless of the length of the ssDNA, all the DNA structures showed only an increasing phase. The signals obtained from ssDNA with and without ends were qualitatively and quantitatively more alike when longer ssDNA was used as they have the largest middle to end ratio. These measurements confirmed that the MDCC-PcrA(K138C) binding to the middle of ssDNA adopts a higher fluorescent state than when it binds to the ends of ssDNA.

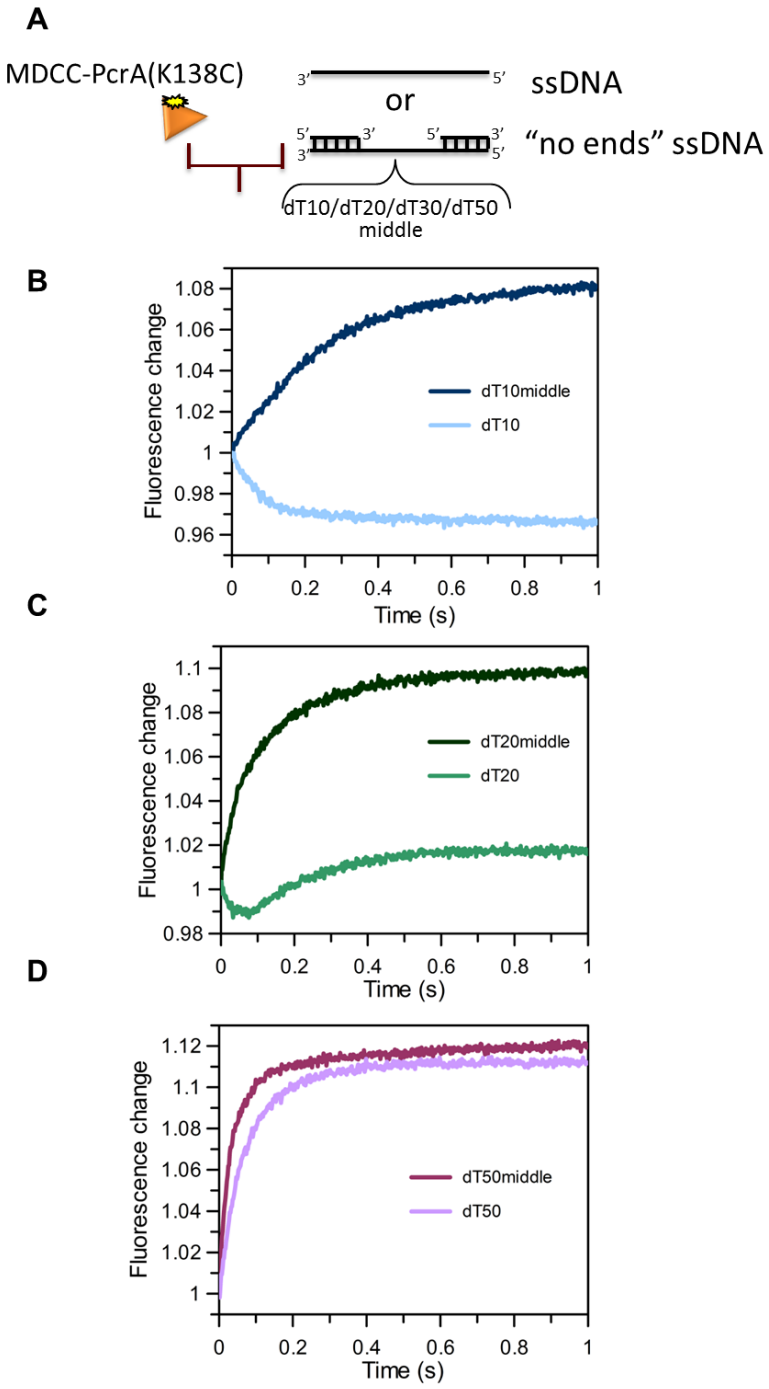

Figure 33. MDCC-PcrA(K138C) end binding signal is removed when ssDNA has no single stranded ends.

A) Cartoon representation of the reaction and the DNA structures used for measurements. B) Normalised traces for dT_{10} and dT_{10}middle. C) Normalised traces for dT_{20} and dT_{20}middle. D) Normalised traces for dT_{50} and dT_{50}middle. The experimental conditions were the same as in Figure 32. Figure 18 in the Methods shows the DNA oligonucleotides used.

MDCC-PcrA(K138C) binding to no ends-ssDNA traces were fitted with double exponentials. The first phase had an increase in the rate constant and the signal amplitude with increasing length of the middle ssDNA (Figure 34), while the rate constant and amplitude of the second phase were independent of ssDNA length. The biphasic nature of the signal indicates that two different processes are observed. These could be two binding modes even though ssDNA has “no ends”. PcrA may have a different conformation and affinity when it binds to a ssDNA/dsDNA junction than when it binds to the middle of ssDNA. However, the second phase does not show concentration dependence, which is normally observed with binding measurements (Scheme 1, Equation 3). This indicates the second phase to be something else than binding. It could be the conformational change in PcrA or the PcrA-DNA complex after binding to ss/dsDNA junction, which may be specifically induced by the DNA junction; hence it is not observed when binding to ssDNA with ssDNA ends.

The rate constant k_{obs1} and the fluorescence change of the first phase have been plotted against the number of ssDNA bases and the data were analysed by a linear fit. The gradient of the fit is 0.46 s^{-1} nt^{-1} (SEM 0.06). Increasing the length of the ssDNA increases the number of PcrA binding sites (Figure 34).

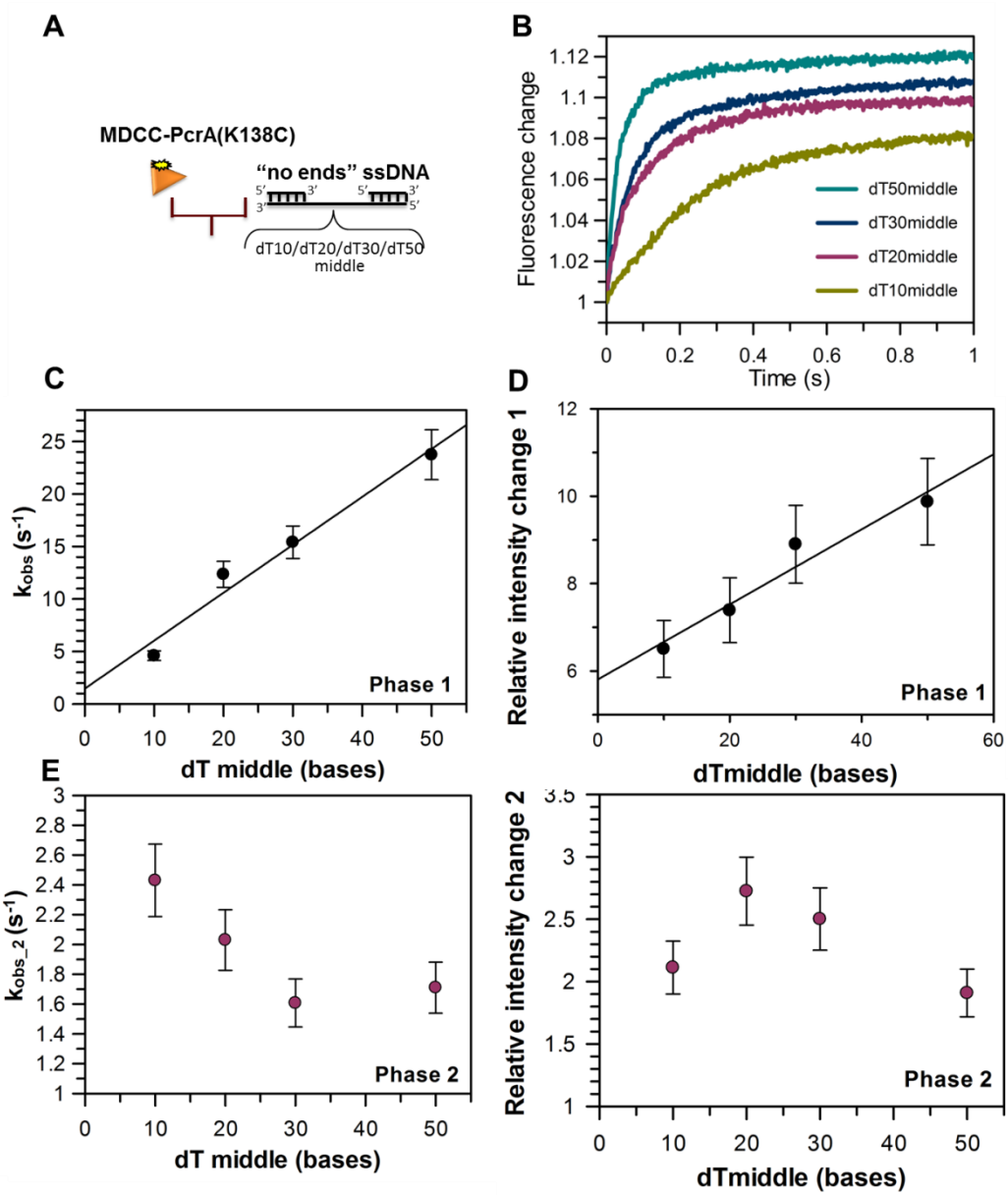

Figure 34. Binding kinetics of MDCC-PcrA(K138C) to dT_{middle} DNA structures are dependent on the ssDNA length.

A) Cartoon representation of the reaction. B) Normalised traces for each length of dT_{middle} ssDNA, which were analysed using a double exponential curve fit. C) The observed rate constant of the first phase (kobs1) from the double exponential fit plotted against the number of dT_{middle} bases together with the linear fit. D) Relative intensities of the first phase (A1) plotted against the number of dT_{middle} bases. Data were analysed by linear regression. The calculation for relative A1 was done by (absolute A1/(absolute A1+ absolute A2))*(C/A_{start}), where A2 is the phase 2 relative intensity and C the end fluorescence. The observed rate constant of the second phase (E) and relative intensity (F) plotted against the number of dT_{middle} bases. The normalisation of amplitude was done analogous to phase1.

4.2.2. PcrA binding kinetics to ssDNA (k_{on})

Rapid mixing of MDCC-PcrA(K138C) with a dT_{20} oligonucleotide in the stopped-flow apparatus showed two phases with different fluorescence properties and rate constants. The two phases observed included a fast decreasing phase (binding to the ends of ssDNA called the end phase) with ~2% signal change, followed by a slower increasing phase with ~4% signal change (binding to the middle of ssDNA called the middle phase). The second phase is a mixture of binding processes to ends and to the middle of ssDNA (Figure 35).

Varying the dT_{20} concentration showed that both phases have observed rate constants that are dependent on the concentration of dT_{20} (Figure 35C and E). Figure 82 in the Appendix shows examples of the fits. The data for k_{obs} at different dT_{20} concentrations were analysed by linear regression. The average of two measurements had a second order binding rate constant, k_{on}, of 29.9 $\mu M^{-1} s^{-1}$ for the end binding mode and 1.1 $\mu M^{-1} s^{-1}$ for the second phase corresponding mainly to the middle binding mode.

The two phases of dT_{20} binding indicate two different processes or two forms of the same process that are the binding to the end and to the middle of ssDNA, as discussed and shown before. The end and middle phase amplitudes do not increase with dT_{20} concentration, but this is not surprising as the concentration of dT_{20} in the experiments is above the K_d value for the dT_{20} binding, which means that the fluorescence signal is saturated at concentrations used (Table 6). Analysis of dT_{20} oligo results was complicated due to nature of processes and the signal observed, hence more emphasis were placed on the results with dT_{10} (shorter) and dT_{50} (longer) binding measurements.

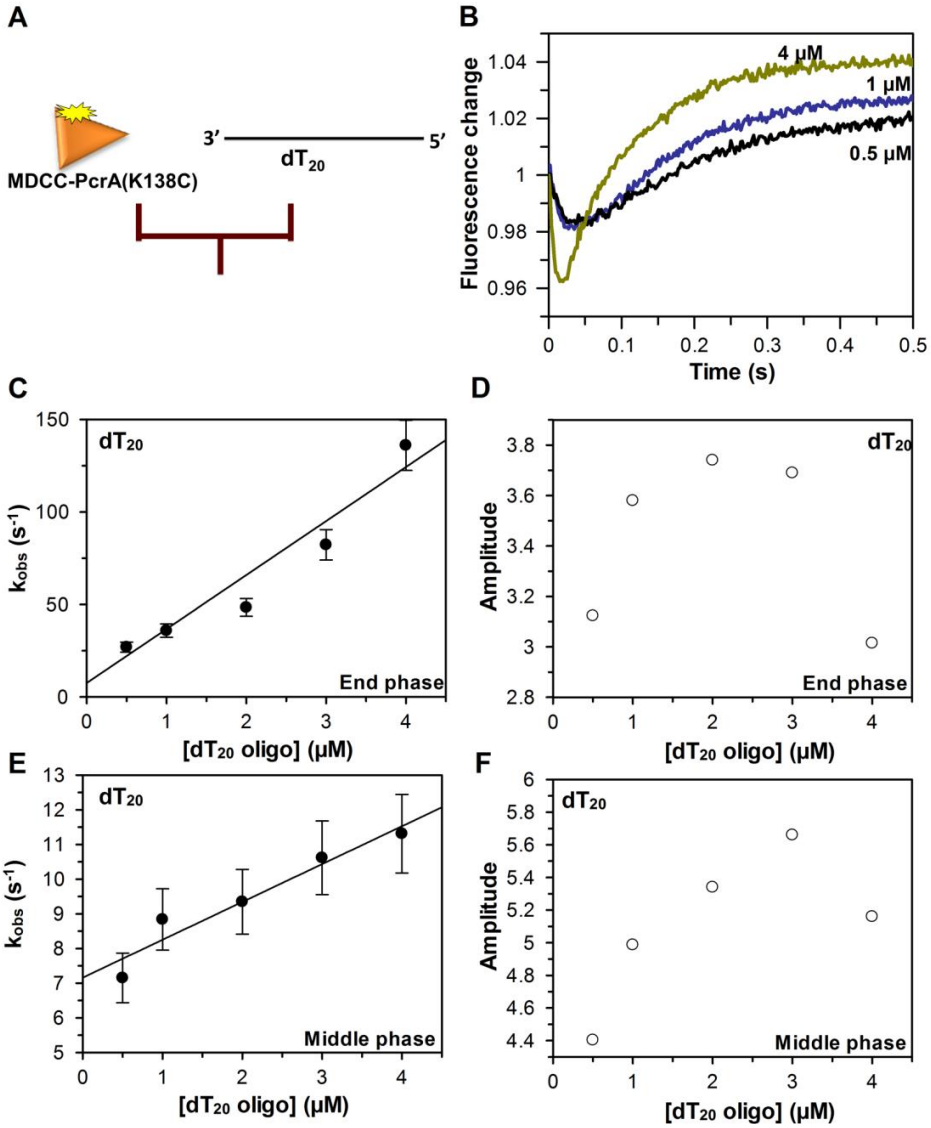

Figure 35. MDCC-PcrA(K138C) binding to dT_{20} ssDNA.

A) Schematic illustration of MDCC-PcrA(K138C) binding to ssDNA measured using a stopped-flow apparatus. B) Normalised traces of MDCC-PcrA(K138C) binding to different concentrations of dT20 ssDNA. The traces were analysed using double exponential curve fitting. As described in Section 4.2.1. the fast fluorescence decrease likely corresponds to binding of PcrA to the ssDNA ends, while the following increase reflects equilibration towards the more stable middle position. C) The observed rate constant of PcrA binding to the ends of ssDNA (1^{st} phase) show concentration dependence. Fitting the k_{obs} versus [dT_{20}] data with a linear function gives the k_{+1} as the slope, which is 29.9 μM^{-1} s^{-1} (SEM 4.9) (Equation 3, Scheme 1). D) Plot of the amplitude of the first phase against the concentration of dT20. E) The observed rate constant of the second phase (final binding to the middle) is concentration dependent. Fitting the k_{obs} to linear fit gives the k_{+1} as the slope, which is 1.1 μM^{-1} s^{-1}(SEM 0.2). The measurements were done on the stopped-flow apparatus with 100 nM MDCC-PcrA(K138C) and varying concentrations (0.5 to 4 µM) of dT_{20} oligo (only containing thymidines) in K200 buffer at 30 °C. The excitation was done at 436 nm and emission measured using a cut-off filter at 455 nm.

The binding kinetics of PcrA to other lengths of ssDNA were also measured using MDCC-PcrA(K138C). Figure 36 shows the individual traces and the fitting of the results for the binding of PcrA to varying concentrations of dT_6 oligonucleotide. The dT_6 binding traces were fitted to single exponentials. The amplitude and the k_{obs} was dependent on the dT_6 concentration. Observation of a single phase indicated that the signal represents a single biochemical process. This could be expected as the dT_6 is approximately the minimum binding length of PcrA binding "footprint" on ssDNA (estimated to be ~7 bases) [21, 51]. This means that dT_6 oligo has room to bind only a single PcrA molecule as when ssDNA is longer multiple binding sites may exist. MDCC-PcrA(K138C) binding to a dT_6 oligonucleotide is the only one tested not having two phases for binding, which can also be explained by its short length. Binding to dT_6 most likely reflects only the end binding mode for PcrA.

The kinetics of binding of PcrA to dT_6 showed hyperbolic dependence on dT_6 concentration. Hyperbolic concentration dependence indicates two step binding, where the first phase is the actual binding and the second is a conformational change that causes the fluorescence signal (Scheme 3). The results from the fit are K_{d1} of 4.96 µM (SEM 0.55) with k_{-2} of 0.66 s^{-1} and k_{+2} of 3.72 μM^{-1} s^{-1} (k_{+2} + k_{-2} of 4. 38, SEM 0.15). These were then used to calculate the $K_{d(overall)}$ using Equation 6. The $K_{d(overall)}$ was determined to be 880 nM.

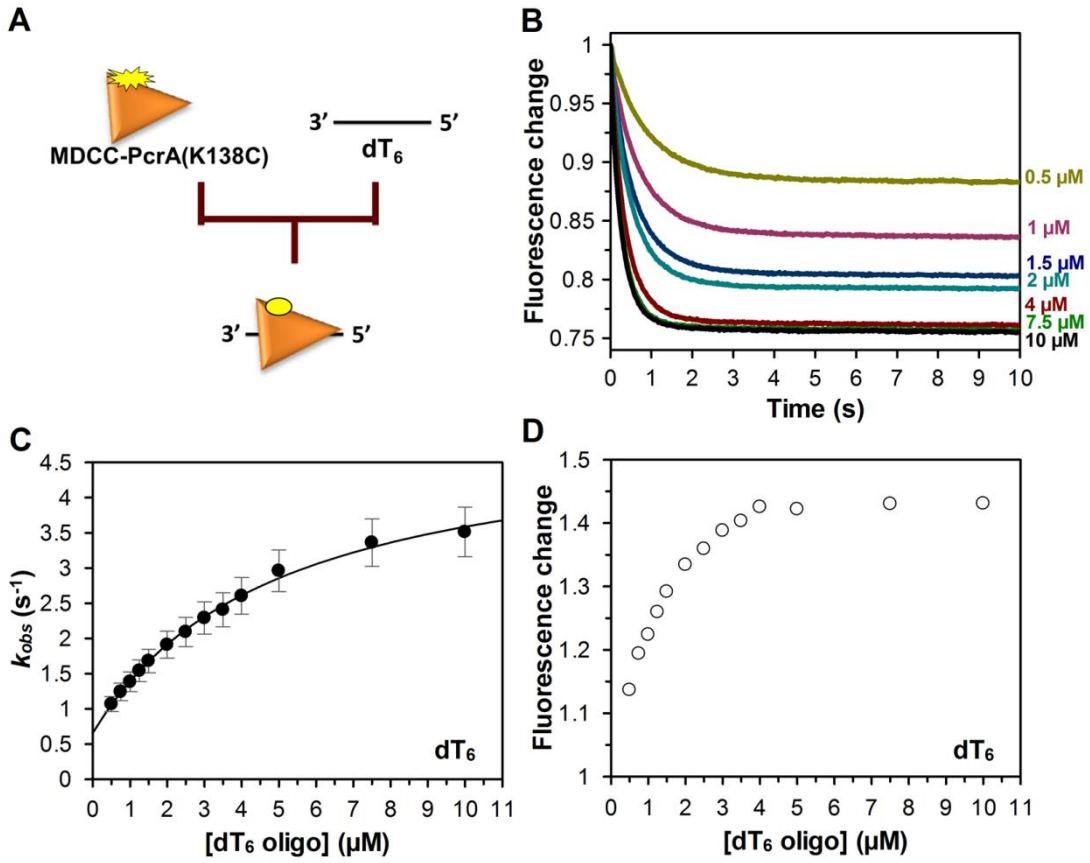

Figure 36. MDCC-PcrA(K138C) binding to dT_6 ssDNA.

A) Cartoon representation of the reaction. B) Normalised traces for varying concentration of dT_6. The traces were fitted to single exponential curves. C) Plot of the observed rate constant versus dT6 concentration. Data are well described by a hyperbolic fit. Results are average of a minimum of three traces. D) The fluorescence change plotted against the concentration of dT_6. The experimental conditions were the same as in Figure 35 except the dT_6 concentration was varied from 0.5 to 10 µM. Example fits are shown in the Appendix, Figure 83.

The concentration dependence of the observed rate constants was also measured with dT_{10} and dT_{50} oligonucleotides (Figure 37 and for the example fits, see Appendix, Figures 84 and 85). The signal of MDCC-PcrA(K138C) binding to dT_{10} was decreasing. The second order rate constant for the first phase was 4.65 μM^{-1} s^{-1} (SEM 0.47).

Mixing MDCC-PcrA(K138C) with dT_{50} showed an increasing fluorescence signal from which the binding rate constant of 10.8 μM^{-1} s^{-1} was obtained (an average of two measurements). This was determined by

fitting the traces to a single exponential. This phase corresponds primarily to binding to the middle of ssDNA due to the large ratio of binding sites in the middle to binding sites at the end of longer ssDNA oligos. The signal had a slower second phase with small amplitude that did not show concentration dependence and hence has not been used for the analysis of the data. The amplitude of the first phase did not increase with the concentration of dT_{50}. This is due to the high affinity of PcrA to dT_{50} (low K_d), which means that measurements were done in conditions where the PcrA binding was saturated at all dT_{50} concentrations used.

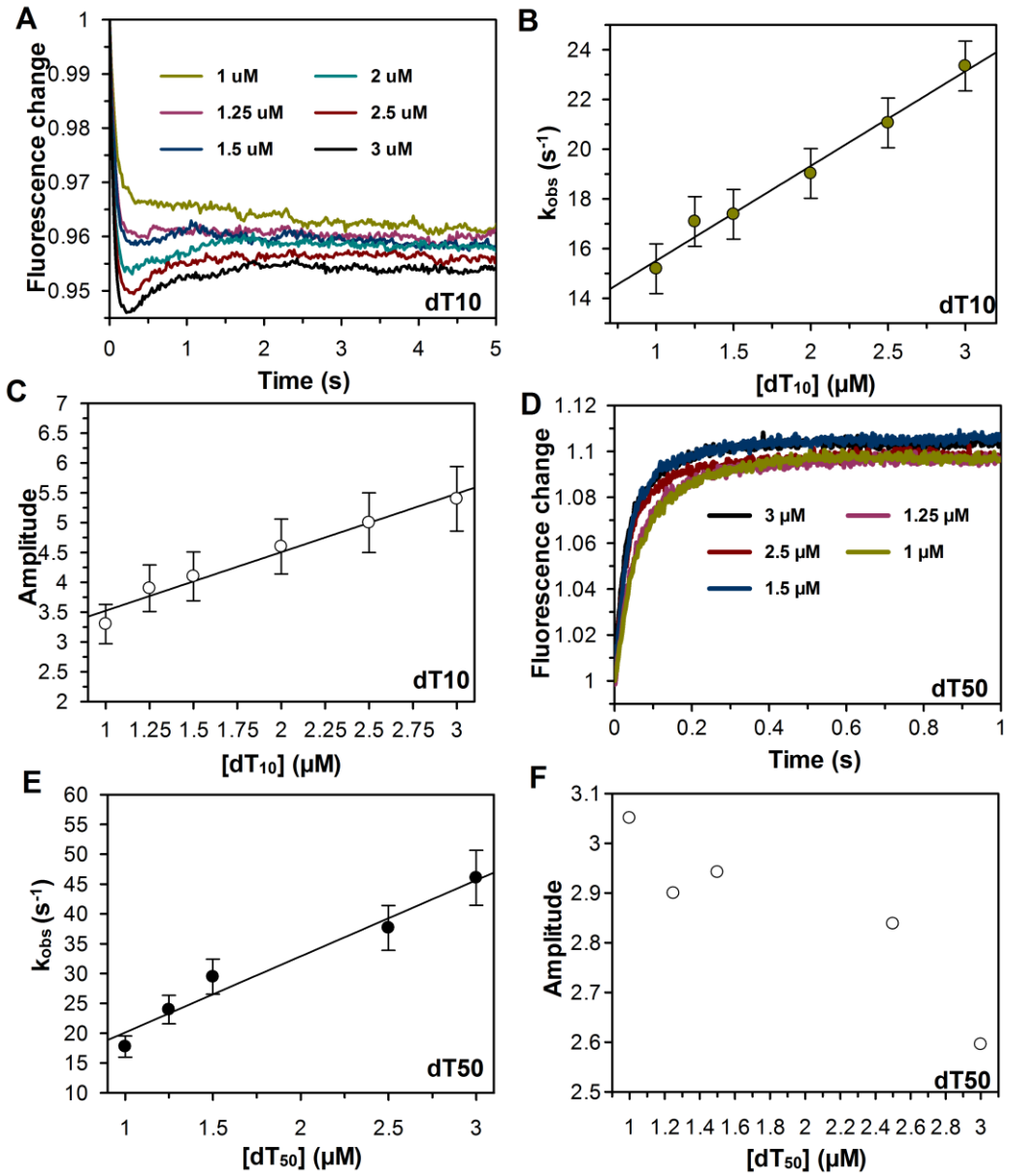

Figure 37. MDCC-PcrA(K138C) binding to dT_{10} and dT_{50} ssDNA.

A) Normalised data traces for MDCC-PcrA(K138C) binding to varying dT_{10} concentrations. The traces showed a second increasing phase after 2 µM of dT_{10}.The signal was too low for accurate fitting to determine the k_{obs} for the phase. B) The observed rate constants and C) the amplitudes from fitting of the decreasing phase (end binding) to single exponentials. k_{obs} and amplitude were plotted against the dT_{10} concentration and fitted to a linear function. The results are averages of three traces. The gradient of the linear fit of k_{obs} is 3.81 $\mu M^{-1} s^{-1}$ (SEM 0.24) The gradient of the linear fit of the amplitude is 0.98 per intensity μM^{-1} (SEM 0.09) D) Normalised data traces for MDCC-PcrA(K138C) binding to varying dT_{50} concentrations. These were fitted to double exponentials for the analysis. E) The observed rate constants and F) the amplitudes for the first phase (end binding) plotted against the dT_{50} concentration. Fitting the k_{obs} values to a linear function yields the second order rate constant 9.73 $\mu M^{-1} s^{-1}$ (SEM 1.21). The results are averages of three traces. The experimental conditions were the same as in Figure 35 except the dT_{10} and dT_{50} concentrations were varied from 1 to 3 µM.

4.2.3. PcrA dissociation kinetics from ssDNA

To determine the dissociation rate constant, k_{off}, for PcrA dissociation from ssDNA, a displacement assay was carried out on the stopped-flow apparatus. This was done by pre-loading the MDCC-PcrA(K138C) with ssDNA and mixing the complex with high concentration of unlabelled wild type PcrA (Scheme 2, Section 1.7).

The displacement assay with dT_6 had only a single phase with increasing fluorescence, understandably as it can be bound only by one PcrA. Data were well described by a single exponential. Having a single the dissociation rate constant was determined to be 0.71 s^{-1} (SEM 0.1 x 10^{-2}) for primary dissociation from ssDNA ends (average of three traces at two different concentration of wild type PcrA). The rate of dissociation did not vary significantly between the two concentrations of wild type PcrA (12.5 and 25 µM). An example trace is shown in Figure 38A.

The displacement assay of MDCC-PcrA(K138C) from dT_{10} with wild type PcrA showed two phases (Figure 38B). The first phase was a fast fluorescence increase corresponding to wild type PcrA binding, and the second phase had a rate constant that was independent of wild type PcrA

concentration indicating displacement (Figure 87, Appendix). The second phase (dissociation phase) also had an increase in fluorescence. From these measurements a k_{off} of 0.6 s^{-1} (SEM 0.01) was obtained. The main form of PcrA dissociation from dT_{10} was expected to be from the ssDNA ends. The k_{off} value of dT_{10} dissociation indicates this to be so as it is similar to the dT_6 dissociation rate constant. With longer ssDNA oligos the dissociation was more complicated to interpret due to possibility of several PcrAs binding along one ssDNA oligo.

The displacement reaction with dT_{20} had three phases (Figure 38C and D). As with dT_{10}, the first phase was a fast increase in fluorescence with a rate constant, which was dependent on the concentration of wild type PcrA. This indicated it to be informative of wild type PcrA binding in close proximity of MDCC-PcrA(K138C) on dT_{20} (Figure 87, Appendix) and not actual displacement. The two other phases were a fast increasing phase with a rate constant, k_{off} of 11.98 s^{-1} (SEM 0.44) corresponding to dissociation from the ends of ssDNA and a slower decreasing phase with k_{off} of 0.14 s^{-1} (SEM 0.7 x 10^{-3}) corresponding to dissociation from the middle of ssDNA.

The displacement assay to measure MDCC-PcrA(K138C) dissociation from dT_{50} had two primary phases, one for PcrA wild type binding (fast, increasing in fluorescence) and another for displacement from the middle of dT_{50} (slower decreasing phase) (Figure 38E). The fitting of the decreasing phase had a k_{off} of 0.14 s^{-1} (SEM 0.002). This is similar to the k_{off} value observed for the second phase of dT_{20} dissociation which indicates the same process being observed, most likely dissociation from the middle of ssDNA.

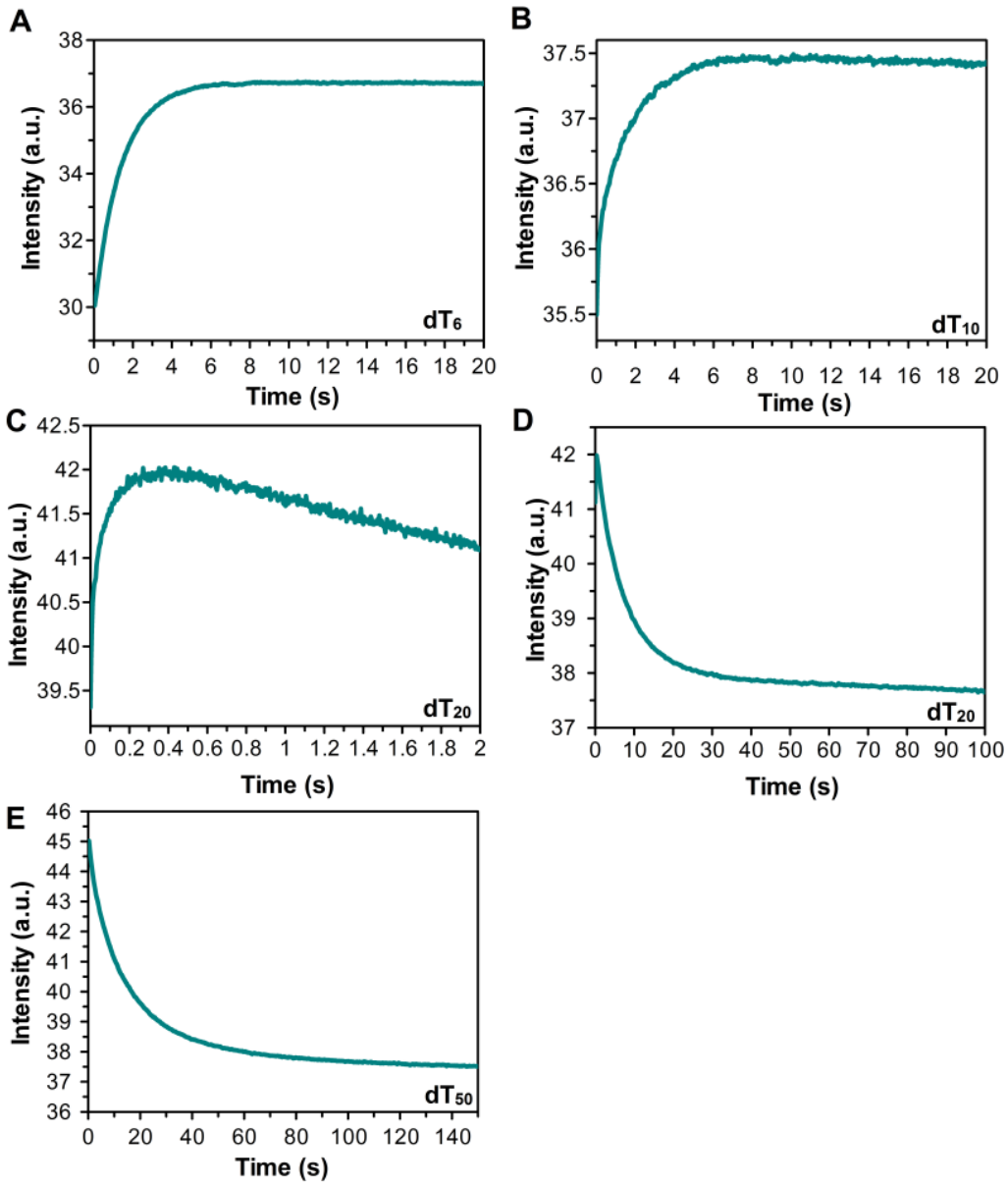

Figure 38. PcrA dissociation kinetics from ssDNA.

The dissociation was measured using a displacement assay where the MDCC-PcrA(K138C) is first bound to ssDNA and mixed with high excess of wild type PcrA. A) Displacement trace of MDCC-PcrA(K138C) from dT_6 oligonucleotide. This was fitted to a single exponential. B) Displacement trace of MDCC-PcrA(K138C) from dT_{10}, which was fitted to a single exponential. C) Displacement trace of MDCC-PcrA(K138C) from dT_{20} on a short time scale. Data in this range were fitted to a double exponential. This trace shows the fast phase of wild type PcrA binding and the dissociation phase from ends of ssDNA. Displacement trace of MDCC-PcrA(K138C) from dT_{20} (D) and from dT_{50} oligonucleotide (E) on a longer time scale (100 seconds) representing dissociation from the middle of the DNA. This was fitted to a single exponential plus a slope. The experiment was done by mixing 100 nM MDCC-PcrA(K138C) and 0.3 µM of dT_{50} or 0.5 µM $dT_{6/10/20}$ with 6 and 12.5 µM of wild type PcrA for dT_6 and dT_{10}, 12.5 and 25 µM for dT_{20} and 25 and 50 µM of wild type PcrA for dT_{50} at 30 °C.

4.2.4. PcrA dissociation constant (K_d) for ssDNA

The comparison and understanding of these rate constants and values for the affinities are complicated by the fact that when the length of the ssDNA is increased, the number of PcrA binding sites increases. The size of the PcrA binding site has been estimated to be approximately 7 bases [21]. This makes the exact determination of binding site concentration complicated. The above experiments indicate that the signals are from the MDCC-PcrA(K138C) binding to different lengths of the ssDNA (Section 4.2.2.) and from the dissociation of MDCC-PcrA(K138C) by displacement with wild type PcrA (Section 4.2.3.). The dT_6 oligo is the only one to show binding kinetics that fit well to a single exponential and the only one to show one phase in dissociation measurements without a second phase for PcrA binding. This is expected as dT_6 should be too short to bind two PcrA helicases and these results indicate it to be so. In displacement assays using other tested oligos, dT_{10}, dT_{20} and dT_{50}, a fast phase for binding of a second (or more?) wild type PcrA close to MDCC-PcrA(K138C) proceeds the dissociation phase. This does not necessarily mean that two or more PcrAs are directly interacting forming an oligomeric helicase as the fluorophores are relatively large and have long linkers, so their environment might change when two or more proteins bind close to each other on the same ssDNA. The increasing phase is fast followed by the displacement signal, which should be little affected by the binding signal. The measurements of k_{on} and k_{off} for different lengths of ssDNA are summarised in Table 6. The dissociation constants K_d were calculated according to Equation 6 (Section 1.7) and are also shown in Table 6.

PcrA dissociation constant to dT_{10} was calculated as 130 nM using Equation 4 and the measured k_{on} and k_{off} values. The MDCC-PcrA(K138C) affinity to dT_{50} had a K_d of 13.9 nM. These two results are the most accurate measurement of PcrA affinity to ends of ssDNA (dT_{10} K_d) and to the middle of ssDNA (dT_{50} K_d). PcrA binding to the middle of ssDNA, has a tighter affinity than PcrA binding to the end of ssDNA as expected, as most of the

PcrA finally ends up there in binding measurements after an initial fast binding-dissociation from the ends of ssDNA.

For dT_{20}, determining accurately the K_d is complicated. Even it can be expected that the two phases of binding and dissociation were corresponding primarily to one of the process, binding to the ends or to the middle of the ssDNA. The second phase of binding and the first phase of dissociation are unlikely to be reporting of a single process due to very probable re-arrangement caused PcrA binding and dissociation from all the parts of ssDNA. For dT_6, the binding measurements showed a two step process and enabled determination of $K_{d\ (overall)}$ from a hyperbolic fit to the binding data and yielding an affinity of 880 nM. The k_{off} was measured in a displacement assay and was 0.71 s^{-1} for dT_6. This is very similar to k_{off} observed for dT_{10} and for k_{-2} calculated from the hyperbolic dependence of the MDCC-PcrA(K138C) binding to dT_6 (Table 6).

Binding with linear dependence						
dT (bases)	$k_{on\ end}$ ($\mu M^{-1}s^{-1}$)	$k_{on\ middle}$ ($\mu M^{-1}s^{-1}$)	$k_{off\ end}$ (s^{-1})	$k_{off\ middle}$ (s^{-1})	K_{d_end} (nM)	K_{d_middle} (nM)
6	n/a*	n/a	0.71	n/a	n/a*	n/a
10	4.65	n/a	0.61	n/a	130.1	n/a
50	n/a	9.73	n/a	0.14	n/a	13.9

Binding with hyperbolic dependence				
dT (bases)	K_{d1} (μM)	$k_{+2\ end}$ ($\mu M^{-1}s^{-1}$)	$k_{-2\ end}$ (s^{-1})	$K_{d\ (overall)\ end}$ (nM)
6	4.96	3.72	0.66	880.0

Table 6. Rate constants and equilibrium binding constants for the interaction of PcrA with different lengths of ssDNA.

The k_{on} and k_{off} values for dT oligonucleotides were obtained from binding and dissociation measurements using MDCC-PcrA(K138C). Binding kinetics of dT_{10} and dT_{50} showed a linear dependence of k_{obs} on ssDNA concentration, whereas the dT_6 results are from PcrA binding to dT_6 measurements, where hyperbolic dependence of rate constant was observed with increasing dT_6 concentration. The $K_{d(overall)}$ for dT_6 is significantly higher than what was measured for dT_{10}. This most probably caused by its short length, which makes it poorer binding substrate for PcrA than longer oligo nucleotides.

4.3. PcrA translocation on ssDNA using MDCC-PcrA(K138C)

4.3.1. MDCC-PcrA(K138C) signal when translocating on ssDNA

Making the use of the different signals of MDCC-PcrA(K138C) binding to ssDNA, a ssDNA translocation assay was developed on the stopped-flow apparatus. When MDCC-PcrA(K138C) was pre-bound to ssDNA and then mixed with ATP, a signal was observed for rapid MDCC-PcrA(K138C) translocation to the 5' end of the ssDNA that enabled the measurement of the duration of translocation on the ssDNA (reaction 1, Figure 39A). PcrA, ssDNA and ATP are all that is required for translocation and fast ATP hydrolysis by PcrA.

The reactions in Figure 39A vary in what component is premixed with PcrA. When MDCC-PcrA(K138C) is pre-bound to ssDNA (reaction 1) it starts from a higher fluorescence state than ATP bound PcrA (reaction 3). In reaction 2, where MDCC-PcrA(K138C) is mixed with ATP and ssDNA at the same time, a fast decreasing phase is observed corresponding to ATP binding shown in graph B as reaction 4 (Figure 39B). The reactions with PcrA, ssDNA and ATP all end in the same steady-state, where PcrA repeatedly binds, translocates and dissociates from ssDNA (Figure 39A).

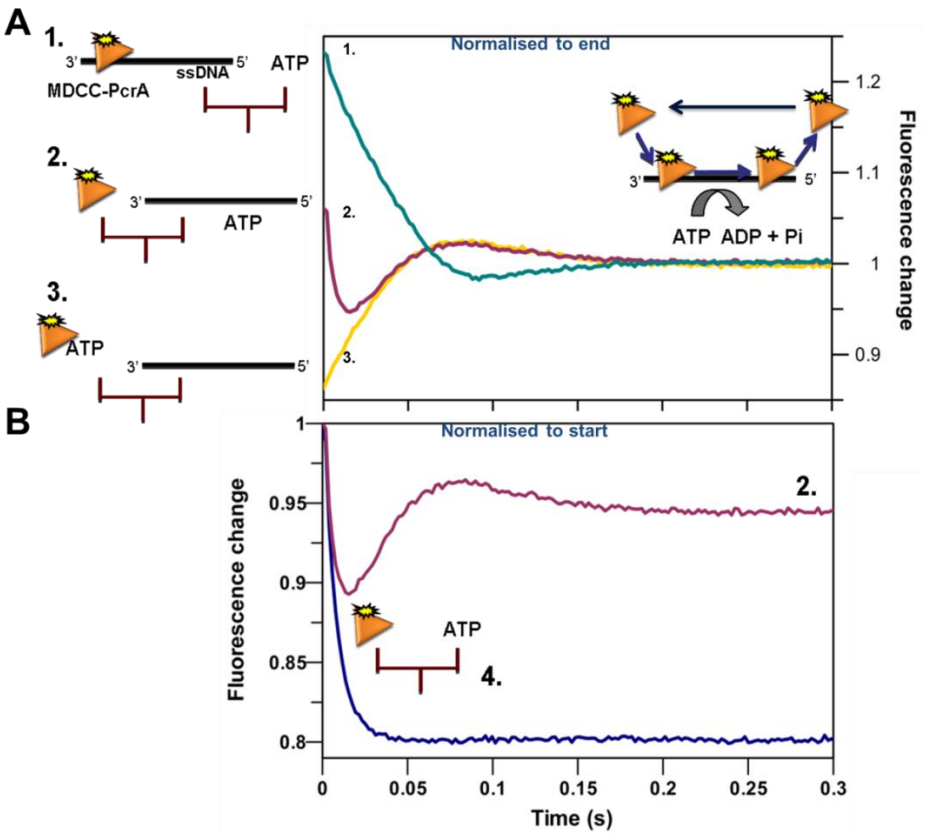

Figure 39. MDCC-PcrA(K138C) signal in ssDNA translocation.

Reactions 1 - 4. 1. Green trace, MDCC-PcrA(K138C) was pre-bound to ssDNA and then mixed with ATP. 2. MDCC-PcrA(K138C) was mixed with ATP and ssDNA. 3. MDCC-PcrA(K138C) was pre-bound to ATP and then mixed with ssDNA. 4. MDCC-PcrA(K138C) was mixed with ATP only. In graph A, in all experiments the same steady-state of PcrA binding, translocating and dissociating from ssDNA should be reached. Therefore, the traces were normalised to the fluorescence value at the end of the trace. In Graph B, the traces were normalised to the beginning of the trace, since they should start from the same fluorescence level (only MDCC-PcrA). Graph B shows that the initial phase in reaction 2 is the ATP binding. The experimental conditions for the reactions were 100 nM MDCC-PcrA(K138C), 1 µM dT_{20}, 200 µM ATP in K200 buffer at 30 °C, except reaction 4 did not include dT_{20}.

The signal observed when MDCC-PcrA(K138C) was pre-bound to ssDNA and then mixed with ATP (Figure 39, reaction 1) was further analysed and used to develop an assay for determination of the translocation rate of PcrA on ssDNA. Out of the three reactions this reaction represents the simplest system for observation of PcrA ssDNA translocation. Figure 40A shows the three different phases of the signal. This is observed as a constant decrease in fluorescence. The duration of the decreasing

phase is dependent on the length of the ssDNA. Using various lengths of ssDNA has enabled the determination of the translocation rate of PcrA on ssDNA under different conditions. The reciprocal of the gradient of a linear fit to the translocation end points against the number of bases gave a translocation rate of 99 +/- 2.0 bases s^{-1} at 20 °C (Figure 40). These measurements were done in the same conditions as previously published for PcrA translocation on ssDNA to validate the assay [51]. The previously published assay used 2-aminopurine labelled oligos and the rate observed here (99 bases s^{-1}) is similar to what had been observed previously (>80 bases s^{-1}) taking into account the possible difference between preparations of PcrA, and oligonucleotides and fluorophores used. The comparison of the two assays confirms the functionality of the MDCC-PcrA(K138C) based assay to study the PcrA translocation rate on ssDNA.

Often in translocation and unwinding assays several lengths of DNA are used. This is important to dissect the translocation from other processes such as binding, conformational changes and dissociation, which are not linearly dependent on DNA length. For example, if a conformational change of PcrA and/or DNA is required at the beginning, this should be the same for all the DNA lengths tested. This would be removed by measuring the translocation on several lengths of DNA as the rate is determined from the reciprocal of the gradient of a linear fit to translocation/unwinding durations against the number of bases for each DNA length.

The assay was repeated in K200 buffer at 30 °C to provide a rate of translocation at the same conditions as in the DNA junction unwinding and plasmid unwinding assays (Figure 40). The rate of translocation was 240 +/- 4.1 bases s^{-1}. Similarly, the assay was repeated at single molecule assay conditions at 22 °C in TIRF buffer and with dT oligos varying from 10 to 70 bases (Figure 88, Appendix). This had a translocation rate of 133.3 +/- 5.3 bases s^{-1}. This will be used in Chapter 6 to compare the ssDNA translocation rate to the plasmid unwinding rate measured at single molecule level using TIRFM.

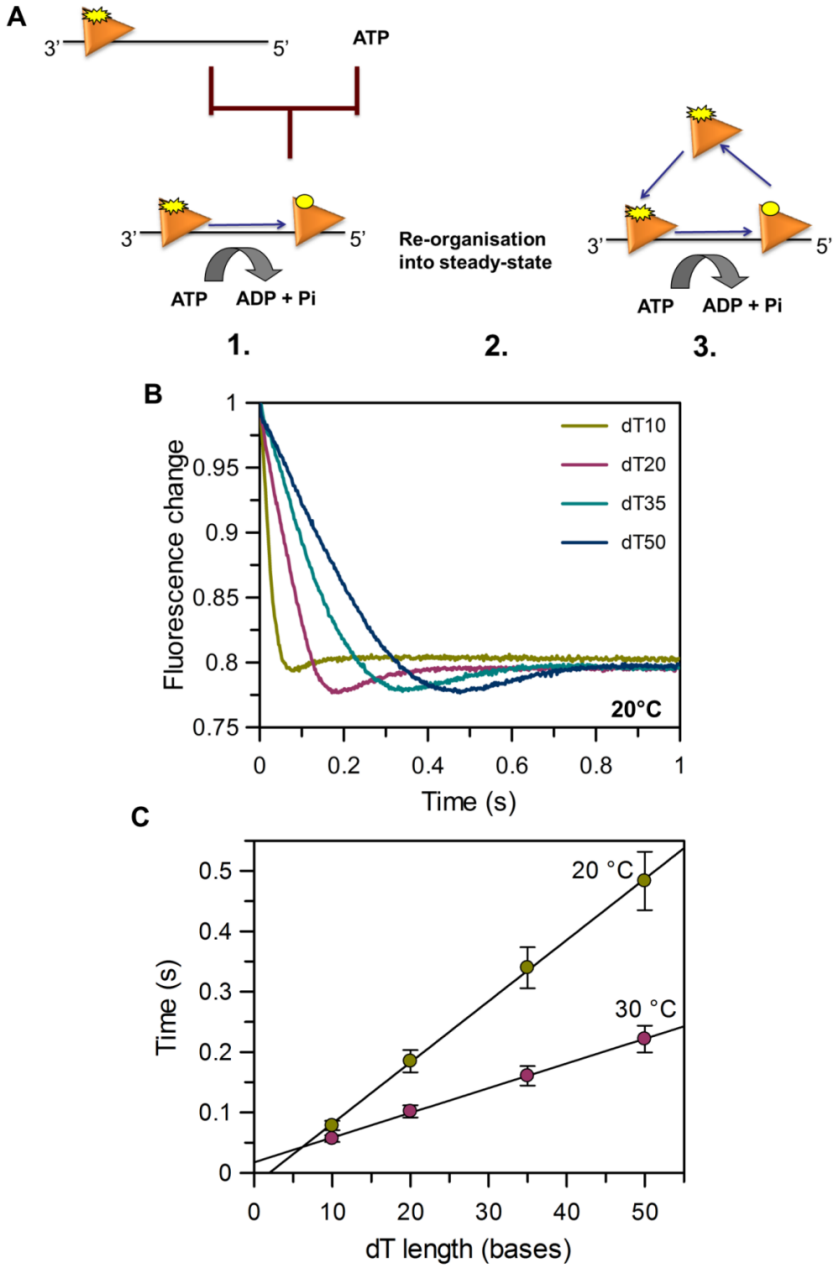

Figure 40. PcrA translocation rate on ssDNA.

A) Schematic illustration of MDCC-PcrA(K138C) translocating on dT_{20}. The three phases of each trace are 1. PcrA translocation to the 5' end of ssDNA, 2. re-organisation of steady-state and 3. steady-state of PcrA binding, translocation and dissociation. B) Normalised traces for K138C translocation on four lengths of ssDNA (dT_{10}, dT_{20}, dT_{35} and dT_{50}) at 20 °C. The time point with the lowest fluorescence, which is the same as the end of the first phase indicates the end of the first round of ssDNA translocation. C) Linear fits to ssDNA translocation durations for four lengths of ssDNA. The gradient at 20 °C is 0.0101 (SEM 0.0002) and at 30 °C the gradient is 0.0041(SEM 6.0 x 10^{-5}). The experiments at 20 °C were done in PcrA assay buffer and at 30 °C in K200 buffer and had 100 nM MDCC-PcrA(K138C), 1 µM dT oligo and 200 µM ATP.

The translocation signal was tested for the possible effects of varying the ATP concentration. In these measurements, the ATP was in high excess to prevent it from being the limiting factor for the rate of translocation. The translocation assay was done as before on the stopped-flow instrument with dT_{35} ssDNA at varying ATP concentrations (50 to 300 µM) (Figure 41). As the end point of translocation varied minimally between the measurements, it could be concluded that the ATP at concentrations used in the assay (200 µM) does not affect the rate of translocation or the fluorescent signal. This is expected as the ATP is well above the known K_m for PcrA ATP binding [157].

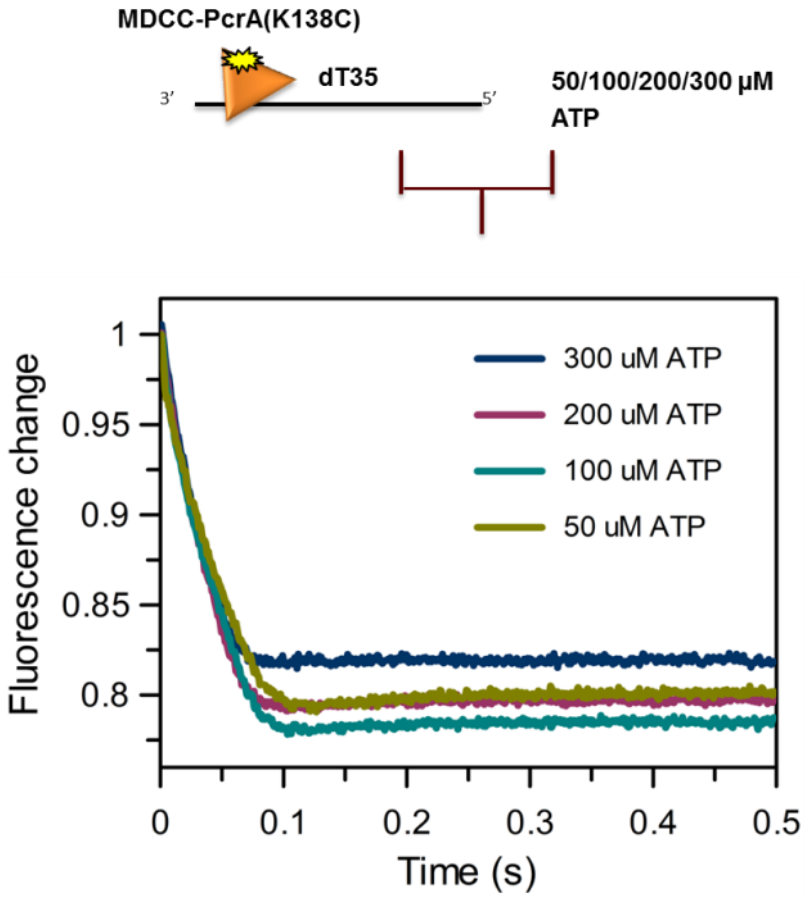

Figure 41. MDCC-PcrA(K138C) translocation reaction is not affected by the ATP concentration in the range used.

The experimental conditions were as in the Figure 40 at 30 °C except that the ATP concentration was varied from 50 to 300 µM.

4.3.2. PcrA translocates at different speeds on different deoxynucleotide sequences

The development of a simple assay to monitor PcrA translocation on ssDNA enabled the investigation of PcrA translocation rates on different types of DNA sequences. Interestingly, when the oligonucleotide sequence was changed the signal varied and showed that PcrA translocates at different rates on different deoxynucleotides. The translocation on dC oligos was measured to be 526 bases s^{-1} +/- 26.5 at 30 °C (Figure 42). This is double the translocation rate on dT oligos. The difference between translocation rates on dCs and dTs could also be observed with oligos made of differing proportions of dT and dC repeats. By changing the dC proportion from 42% to 57% in a 35 base oligonucleotide showed a faster translocation. With four repeats for dCs (5'-CCCCC TTTTT CCCCC TTTTT CCCCC TTTTT CCCCC-3') the end of translocation was 0.097 s and with three repeats of dCs (5'-TTTTT CCCCC TTTTT CCCCC TTTTT CCCCC TTTTT-3') it was 0.102 s.

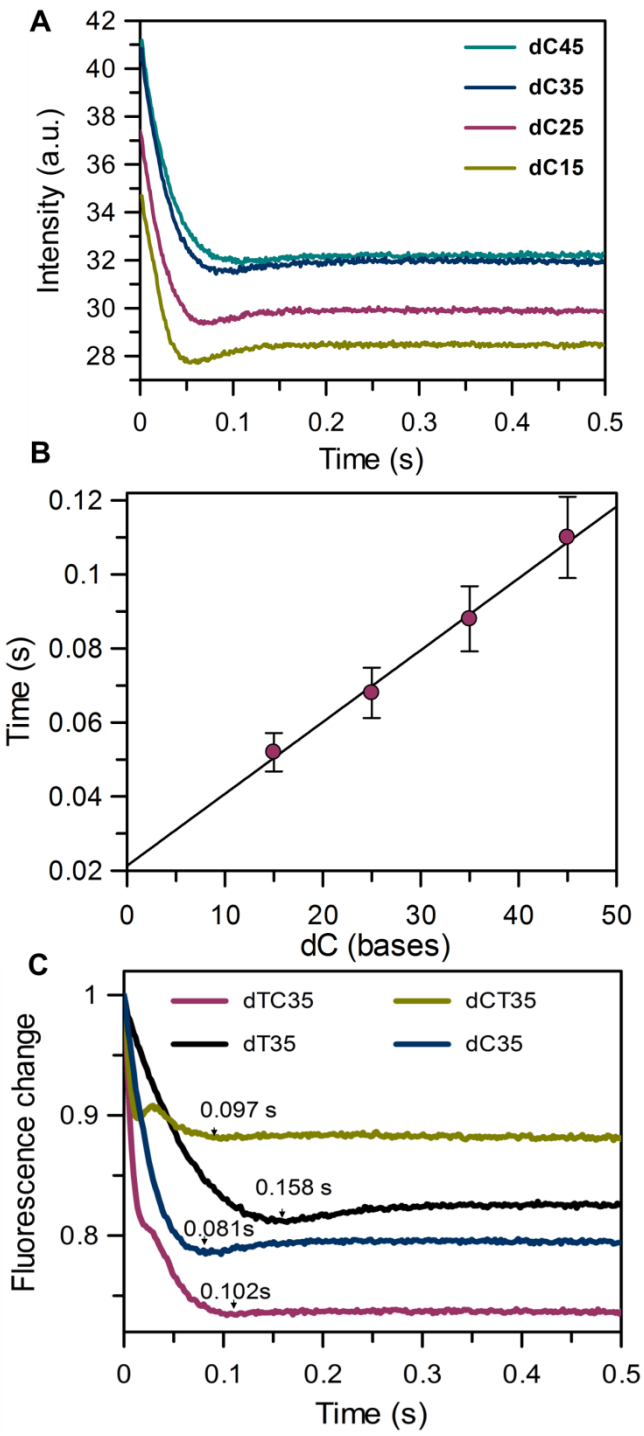

Figure 42. PcrA translocates faster on dC oligos than on dT oligos.

A) Raw data traces for MDCC-PcrA(K138C) translocation on dC oligonucleotides. B) Plot of translocation durations against the number of bases on the dC oligonucleotide. C) The PcrA translocation duration varies according to the composition of the ssDNA sequence. The dTC35 has 35 bases of which 20 are dTs and 15 are dCs. dCT has 35 bases of which 15 are dTs and 20 are dCs. Experimental conditions are the same as in the Figure 40 at 30 °C.

The ssDNA translocation experiment was repeated with oligonucleotides made of dA bases. The traces were qualitatively and quantitatively dependent on the length of ssDNA (Figure 43). The shorter lengths (dA10 and dA20) did not show obvious end points of translocation when reaching the 5'-end, but clearly were indicating shorter translocation duration. This was also seen with dT_{10} oligo at 30 °C in the same assay. With longer dA oligos the end point of translocation is more defined and using several longer dA oligo lengths (up to 70 bases), the translocation rate has been determined as 260.9 +/- 16.6 bases s^{-1} (average of two measurements).The dA_{35} and dA_{50} oligos have signals with more defined end points of translocation that are 0.14 s for dA_{35} and 0.20 s for dA_{50}. Compared to dC and dT ssDNA translocation, these values are very similar to what has been observed for dT oligonucleotides (dT_{35} -0.15 s and dT_{50} – 0.21 s). The rate of translocation on dA was shown to be similar to what was measured for dT (Table 7). The dA_{35} signal showed an unexpected shoulder before the decrease in signal, which could not be explained, but was reproducible. It could be a result of the dA_{35} preparation and its quality as a single preparation was used in all the measurements.

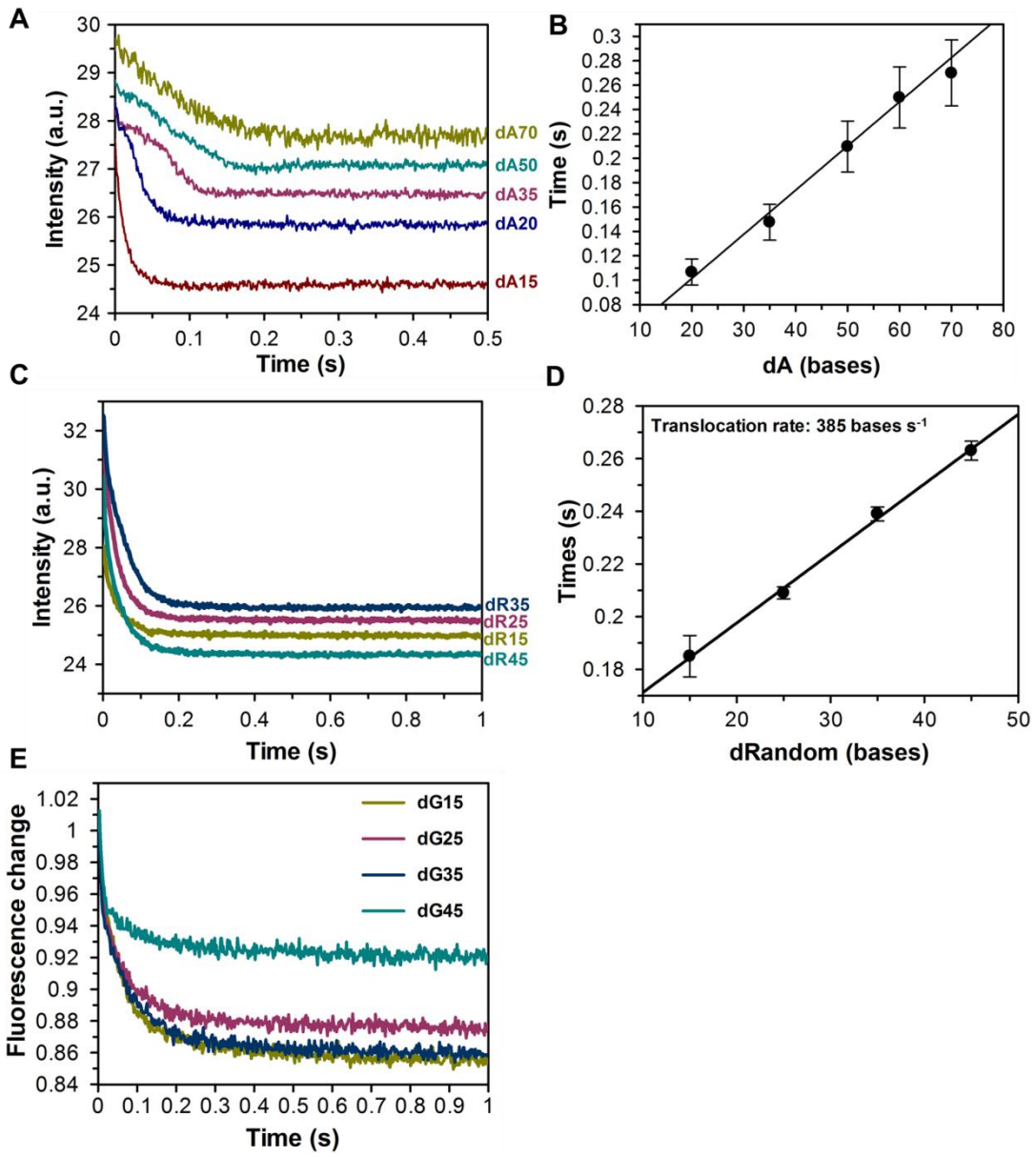

Figure 43. MDCC-PcrA(K138C) translocation on oligonucleotides with different base composition.

A) Normalised data traces for translocation on dA oligonucleotides. B) The end points of translocation plotted against the number of bases on dA oligos. The linear fit has a gradient of 0.0036 (SEM 0.0002). C) Raw data traces for MDCC-PcrA(K138C) translocation on oligonucleotides with a random sequence. D) The translocation durations plotted against the length of the oligonucleotide. The gradient of the linear fit is 0.0026 (SEM 8.5 x 10^{-5}). The end point of translocation was determined as the intercept of two linear fits, the first fitted to the fast decreasing phase and the second to the constant or slowly decreasing phase. See Figure 89 in Appendix for the fitting to determine the duration of translocation. E) Normalised trace translocation on dG oligonucleotides without clear signal for end of ssDNA translocation. All the experiments were done as stated in Figure 40.

The random sequence oligonucleotides containing all four bases (C, T, A and G) showed traces similar to that of the dT oligonucleotides, but without a clear second phase, which would corresponds to re-organisation to steady-state (Figure 43C and D). This made the time point for the end of translocation more complicated to determine. However, the first phase corresponding to ssDNA translocation varied in steepness and in the time taken to reach the steady-state with the length of the oligo. The time points were plotted against the number of bases of each oligonucleotide. The reciprocal of the plot gave a translocation rate of 385 +/- 12.6 bases s^{-1}. The method used to analyse the individual random sequence traces was significantly different to the way traces with the re-organisation phase were analysed. This cause some error in the actual rate of translocation, but as the parameter used for fitting was directly dependent on the length of oligo, this should be equally accurate method as used for dT, dC and dA oligos. The rates for PcrA translocation on different oligo sequences have been summarised in Table 7.

Different lengths of dG oligonucleotides were obtained and tested (Figure 43E). These were complicated to produce and especially dG45 was reported to be impure (HPLC analysis done by the manufacturer). No difference was observed between the different lengths of oligonucleotides. The deoxyguanosine repeats are known to form G-quadruplexes and certain helicases have been shown to remove these structures [166, 167]. The ability of dG repeats to form secondary structures may be the reason for the more complicated purification and production, but also for the signals observed with PcrA. This could indicate that PcrA is not able to remove secondary structures from ssDNA. The possible secondary structure of dG oligos could be tested further using circular dichroism.

ssDNA	Rate ($bases\ s^{-1}$)	Temperature (°C)	Buffer
dA	260.9 (+/- 16.6)	30	K200
dT	238.3 (+/- 15.5)	30	K200
dC	526.3 (+/- 26.5)	30	K200
dG	n/a	30	K200
dRandom	384.6 (+/- 12.5)	30	K200
dT	99.0 (+/- 2.0)	20	PcrA
dT	133.3 (+/- 5.3)	22	TIRF

Table 7. Summary of PcrA translocation rate on different oligonucleotide sequences.

4.4. Discussion

4.4.1. PcrA has different modes of binding to different parts of ssDNA

The labelling of the PcrA cysteine mutant K138C with a coumarin fluorophore (MDCC) enabled the investigation of PcrA binding to ssDNA. The comparison of signals with different lengths of ssDNA indicated that MDCC-PcrA(K138C) has different fluorescent states and affinities when binding to the end or to the middle of ssDNA. The crucial evidence was the MDCC-PcrA(K138C) signal with dT_{20}, showing a decreasing signal for binding the ssDNA ends followed by an increasing signal for binding to the middle. Oligonucleotides shorter than dT_{20} had only a decreasing phase. The longer oligonucleotides had only an increasing fluorescent phase. This was further tested by removal of ssDNA ends by introducing double stranded DNA sequences at the 3' and 5' ends. The traces obtained with these "end-less" DNA structures did not show a decreasing fluorescent phase, regardless of the length of ssDNA in the middle, When one ssDNA end (3' or 5') was present, the traces showed a phase for end binding with a decrease in fluorescence, indicating that both 3' and 5' –ends are bound by PcrA and induce a low fluorescence state. After the decreasing phase, the traces varied in size and shape, but no distinction could be made between binding to the two ends of ssDNA (3' or 5').

The difference in affinity for ssDNA ends versus the middle of ssDNA may serve a purpose *in vivo* in DNA reeling used for removing RecA off from DNA in DNA repair (without RepD) [94], as the end parts of ssDNA may be faster to "find" but for PcrA to perform its helicase/translocase activity it is better located at the middle of ssDNA for movement. In addition, the conformation of PcrA when bound to ssDNA ends might be different from the PcrA-ssDNA complex bound in the middle. The actual *in vivo* substrate for PcrA is a plasmid, which doesn't have free ends and is a substrate with ssDNA/dsDNA junctions opened up by RepD, hence preferred binding to the

middle of ssDNA is likely to be required for the actual plasmid unwinding function of PcrA (Process 2 in Figure 9).

Previous experiments measuring ATP hydrolysis during ssDNA translocation have indicated a possible difference in PcrA association and dissociation from the end versus the middle of ssDNA [54]. MDCC-PcrA(K138C) has provided the first direct evidence for this process. Another advantage of using labelled PcrA over assays using 2-aminopurine labelled oligonucleotides is the lack of DNA length limitations. 2-aminopurine labelled oligonucleotides show no fluorescent signal when the oligonucleotide is 30 bases or above as in longer ssDNA PcrA binds too far from the fluorophore [51]. This is not a limitation with the labelled PcrA, hence MDCC-PcrA(K138C) showed a signal for binding to long ssDNA such as poly dT (~500 bases) (Figure 32).

4.4.2. PcrA affinity to ssDNA using MDCC-PcrA(K138C)

The MDCC-PcrA(K138C) enabled us to determine the affinity of PcrA to different lengths of ssDNA. These varied from 14 nM to 880 nM in K_d for oligonucleotides from dT_6 to dT_{50} bases. The variation of the K_d values is relatively large, but not surprising as the experiments showed that PcrA has different affinity to the ends and the middle of ssDNA. In other words, with the different lengths of ssDNA one form of binding is preferred or dominating over other(s) leading to different affinities.

The dT_{20} oligonucleotide is the only one of the tested ssDNA lengths to show clearly two phases for two modes of binding in both association and dissociation measurements. The determination of K_d values for the end and middle phases from the results is complicated as there is likely to exist some form of rearrangement during the phases observed. The K_d for the end binding can most confidently be determined from dT_{10} measurements, which had a K_d of 130 nM. Similarly, the PcrA affinity to the middle of DNA can be most confidently be determined from dT_{50}

measurements. This had a K_d of 14 nM. The K_d values indicate that the binding to the middle is 9 times tighter than to the ends of ssDNA and support the hypothesis of a more thermodynamically stable binding to middle of ssDNA than to the ends of ssDNA. This tighter binding to the middle of ssDNA is likely to be a requirement for a more processive and efficient helicase activity in the plasmid unwinding *in vivo*.

With short lengths of ssDNA, such as dT_6, PcrA is binding only in the "end binding mode", hence PcrA has the lowest observed affinity to dT_6 ($K_{d\ (overall)}$ = 880 nM). The K_d is higher than what was observed for all other lengths of ssDNA. The dT_{50} is the opposite of dT_6 in terms of having PcrA bound mainly to the middle of ssDNA and therefore has the lowest K_d of 14 nM and so the tightest PcrA binding.

The MDCC-PcrA(K138C) binding to dT_{10} showed binding with two phases at higher dT_{10} concentrations (from 2 µM onwards), but only the first phase was used for determination of the binding rate constant. The signal of the second phase was too small for accurate fitting but as it is increasing in fluorescence, it can be postulated to be the binding to the middle of dT_{10}. The displacement assay showed only one phase of dissociation. The K_d value for PcrA binding to dT_{10} was calculated as 130 nM and is significantly lower than the K_d for dT_6. This is interesting as dT_{10} is only 4 bases longer than dT_6 and implies that this difference has a large effect on the PcrA affinity and possibly dT_6 is too short for high affinity binding by PcrA.

The dissociation rate constants are summarised in Table 6. With shorter oligonucleotides, dT_6 and $dT_{10,}$ the dissociation rate constants are faster than with the dT_{20} and dT_{50} (signal primarily due to dissociation from the middle). This proves that the PcrA dissociates faster from the ends of ssDNA than from the middle of ssDNA. The dT_6 dissociation has only one phase showing that PcrA is primarily dissociating in one process and confirm that the dissociation rate constant from the intercept of a hyperbolic fit to the binding data (k_{-2} = 0.66 s^{-1}) (Figure 36) is describing the same as process as the k_{off} = 0.71 s^{-1} directly measured in the displacement assay (Figure 38).

4.4.3. PcrA translocation on ssDNA reported by MDCC-PcrA(K138C)

The fluorescence of MDCC-PcrA(K138C) is lower when it is bound signal to the end of ssDNA than at the middle. When MDCC-PcrA(K138C) translocates from the middle to the end, the fluorescence of the signal decreases. This could be exploited to develop a translocation assay on the stopped-flow apparatus where PcrA is premixed with ssDNA to which it binds randomly. The complex is then mixed with ATP. This initiates PcrA translocation to the 5' end of the ssDNA. The end of translocation is observed as the lowest point in fluorescence, which is followed by a phase with a small increase in fluorescence. This second phase represents the re-organisation to the steady-state formed of binding, translocation and dissociation with constant fluorescence. The published translocation rate of PcrA on ssDNA is ~80 bases s^{-1} at 20 °C at different buffer conditions than the DNA junction and plasmid unwinding assays [51]. To validate the MDCC-PcrA(K138C) translocation assay the same conditions were used with MDCC-PcrA(K138C) and the rate of translocation was 99 bases s^{-1} indicating that MDCC-PcrA(K138C) is able to report PcrA translocation accurately. The rate of translocation increases with temperature, which is generally expected for a function of an enzyme (at 20 °C - 99 bases s^{-1} and at 30 °C - 240 bases s^{-1}).

Previous experiments with PcrA have not looked into the dependence of the translocation rate on DNA sequence. This is important as DNA sequences *in vivo* are formed of all four nucleotides and vary in nucleotide content. The PcrA translocation rate was determined on several oligonucleotides with different sequences using the MDCC-PcrA(K138C) translocation assay. The rate of translocation changed with different deoxynucleotide sequences. For dT at 30 °C it was 240 bases s^{-1}. At the same conditions but with dC oligonucleotides the translocation rate was over 500 bases s^{-1}, which is two times faster than on dT oligonucleotides. The difference in the rate for dT and dC ssDNA could also be observed by just varying the proportion of the two bases in the oligonucleotides and the translocation to the 5' end took longer the more dTs the oligonucleotide had.

The translocation on dA oligonucleotides indicated a similar rate of translocation as on dT. This is an interesting point as dA and dT form base pairs with each other and the possible significance could be in the way PcrA interacts with the bases that are able to form different number of hydrogen bonds. dC bases are able to form three hydrogen bonds when base pairing with dG bases, whereas dT and dA only form two. These results indicate that the structure of the base may affect the PcrA affinity to it. For example, if the k_{on} is constant and the k_{off} is faster with dC than with dT oligos then the rate of translocation will be faster on dC oligos. This could be the effect of the structural difference between the two bases. Some indication could be obtained by having crystal structures of PcrA binding to dC, dT, dA and dG oligos, as the binding pocket interactions may show variation according to the bases it is binding. In the structure published by Velanker *et al.* 1999 PcrA is bound to a ss/dsDNA junction with random sequence. From this, it is impossible to determine the PcrA interaction differences between different bases as they may vary according to their location in the pocket and not just by the base PcrA is interacting with.

The PcrA translocation on ssDNA sequences made of all four nucleotides A, T, C and G had no clear translocation end point and lacked the state of slow but short lived increase in fluorescence corresponding to re-organisation of the reaction into steady-state. The end of PcrA translocation on ssDNA was determined from the time point where fluorescence turns constant (reaches the steady-state) by linear fit to the steady-state. A translocation rate of 385 bases s^{-1} was obtained from this analysis. The fitting was done in different ways to the dC and dT oligos, but the time taken to reach steady-state was dependent on the number of bases in the oligonucleotide. The loss of a clear end point of the translocation with the random sequences could be due to PcrA having a different affinity to different sequences or bases that causes the asynchronisation of random PcrA binding or be caused by faster ATP hydrolysis when bound to certain bases or sequences. The translocation rate of random sequence oligonucleotides is faster than on dT oligos and slower than on dC oligos. The DNA sequences used in the assay typically had ~20% of dCs, dGs and

dTs and ~40% of dAs bases. The measurement of the PcrA translocation rate on random sequence oligonucleotides may be the most accurate indication of the actual speed PcrA is moving on ssDNA *in vivo*.

These experiments show for the first time that the PcrA translocation rate is dependent on the ssDNA sequence it moves on. Translocation on deoxycytodine oligonucleotides is faster than on deoxythymidines. As the movement on ssDNA does not require breaking of hydrogen bonds, one cannot expect the translocation to be similarly slowed down on dCs and dGs as with unwinding of dsDNA. The faster movement on dC oligos must be caused by one of the following factors that include PcrA binding, ATP hydrolysis or dissociation from dCs being faster. The ATP hydrolysis rate could possibly be tested with assays measuring the ATP turnover such as the ATP hydrolysis assay using a Pi biosensor [87]. This would be an interesting addition to the results observed here.

MDCC-PcrA(K138C) could provide a tool to study PcrA involvement in removal of secondary structures and proteins from ssDNA. The importance of the PcrA translocation on ssDNA has not been fully unravelled and *in vitro* evidence indicates that PcrA is involved in removal of RecA filaments that is important for genomic stability in response to DNA damage [94]. This function requires PcrA movement or reeling of ssDNA coupled to ATP hydrolysis. Using coumarin labelled PcrA(K138C) one could possibly look at what change is observed in the signal when ssDNA is coated with RecA. Labelling of DNA and/or RecA with fluorophores suitable for FRET pairing could facilitate the development of an assay for PcrA-RecA interaction studies on the stopped-flow instrument and on the TIRFM. This is just one possibility for new assay development with fluorophore-labelled PcrA(K138C) as it could be used for other FRET measurements such as the investigation of a possible interaction of PcrA with SSB protein and other components of the plasmid replication complex.

4.4.4. Summary

MDCC-PcrA(K138C) has a useful signal measuring for ssDNA binding, which shows that PcrA binding to the ends of ssDNA is faster than to the middle. This may be needed in certain *in vivo* processes other than plasmid replication such as PcrA involvement in DNA repair, where PcrA may be required to bind very short DNA overhangs, in other words, bind in the end binding mode. PcrA is known to unwind DNA junctions with dT-arms of only 4 bases (C. Toseland and M. Webb, personal communication), which means that PcrA is able to bind ssDNA of 4 bases and start to translocate or unwind from it.

These experiments show for the first time that the PcrA translocation rate is dependent on the ssDNA sequence it moves on. The faster movement on dC oligos than on dT oligos must be caused by one of the following factors that include PcrA binding, ATP hydrolysis or dissociation from dCs being faster. As the DNA in nature is formed of all the four nucleotides (dA, dC, dT and dG), the measurements in random sequence oligos may be the most accurate measurement *in vitro* to estimate the ssDNA translocation rate of PcrA *in vivo*, which was ~380 bases s^{-1}.

5. Results- PcrA interaction with the initiator protein RepD during plasmid unwinding

5.1. Introduction

RepD-PcrA interaction is a vital component for a successful plasmid unwinding. PcrA is not able to unwind even short DNA junctions without RepD and presence of RepD increases PcrA unwinding processivity [87, 88]. The interaction seems to exist either directly or through DNA. The top of the PcrA 2B domain, which is the 2B site furthest of the ATP binding site, was chosen for fluorescent labelling to enable the development of a signal and assays, which observe the PcrA interaction with the RepD (Figure 44). The 2B domain was selected as the target as it has not been shown to be involved in other process such ATP hydrolysis or DNA binding. The E447, E449, M450 and L453 residues are at the top of 2B domain pointing outwards from PcrA core. Therefore, they are likely to be near the suggested PcrA-RepD interaction site. Single cysteine residues were introduced using site-directed mutagenesis at these sites and labelled with environmentally sensitive fluorophores.

There are several main aims for obtaining a RepD-specific signal. These include evidence for the RepD interaction site on PcrA, investigation of PcrA affinity to RepD or RepD-DNA complex and determination of how their interaction changes during plasmid unwinding. The sites mutated on the top of the 2B domain have also been used for labelling with suitable fluorophores, which can be used for FRET pairing with labelled RepD.

The E449C and other cysteine mutants were labelled with fluorophores of coumarin-maleimide and Cy-dye derivatives (as stated in Methods and described in Chapter 3). The fluorescently-labelled PcrA(E449C) has shown a signal with RepD specificity and enabled the investigation of PcrA-RepD interaction. This was observed on *oriD*-mimic

DNA junction structures similar to that used in DNA junction unwinding assays (Figure 19, Methods). The junctions were used to provide a simple model system that can be used as a comparison to RepD-plasmid complex. RepD-plasmid complex was also used in these experiments to look for signal to investigate PcrA binding to the complex, interaction with RepD and during unwinding DNA.

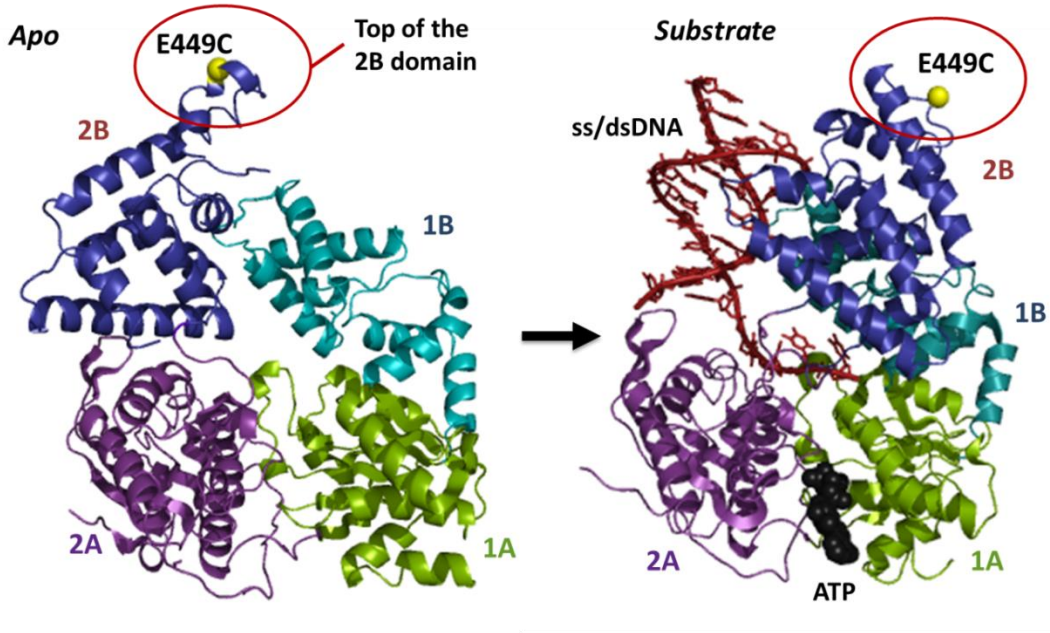

Figure 44. The location of E449C mutation on PcrA.

The coordinates for the image were taken from PDB files 1PJR (open, apo) and 3PJR (closed, substrate bound) and visualised using PyMol (http://www.pymol.org/). The site of E449C mutation is shown as a yellow sphere on “the top of the 2B domain” (circled red).

5.2. MDCC-labelled PcrA(E449C) and signal on interaction with RepD, complexed with DNA

5.2.1. RepD interaction site on PcrA is on the top of the 2B domain

All the MDCC-labelled PcrA cysteine mutants were tested for possible RepD specific signal on the stopped-flow apparatus (Table 1). The RepD specificity was only observed with a PcrA that was labelled at the top of the 2B domain. The highest fluorescent signal change (above 20%) was

observed with PcrA(E449C), labelled with MDCC-maleimide (Figure 45). The other mutations E447C, M450C and L453C on the 2B domain, labelled with the same fluorophore, showed lower fluorescence change or specificity to RepD-DNA than MDCC-PcrA(E449C) (Figure 46). The labelled mutations M450C and E447C showed only ~10% signal change when interacting with RepD-DNA junction complex. The labelled L453C had similar amplitude of signal change to E449C with RepD-DNA junction 1, but it also had a large signal change with DNA junction 1 without RepD. This indicated the signal to be specific to the DNA binding, rather than RepD, and so not useful for investigation of PcrA-RepD interaction. The high specificity to DNA with labelled L453C is understandable as the site of labelling is the closest to the DNA on the substrate bound crystal structure of the other 2B top domain mutations.

All the MDCC-labelled PcrA mutants, whether on 2B, 1B, 1A or 2A domain, have also been tested for signal for PcrA binding to RepD-DNA junction complex and to the RepD by itself. None of the other labelling sites outside of the 2B domain top show RepD specificity. Good examples are the Y477C and R501C mutations, which are located on the 2B domain and the H53C on 1A domain (Figure 22, Chapter 3). The Y477C is at the opposite side of the 2B domain (compared to E449C domain), close to the ssDNA interaction site. R501C is on the 2B domain very close to the dsDNA interaction site, according to the substrate bound crystal structure. Neither Y447C nor R501C showed signals of RepD-specificity. Generally speaking, the mutations have been located on all PcrA domains and should cover most of the possible sites of possible RepD-PcrA interaction. Together, all the labelled PcrA constructs strongly indicate that RepD interacts with PcrA on the 2B domain.

The MDCC-PcrA(E449C) fluorescent signal with RepD-DNA junction 1 had a signal change between 20-30% (Figure 45). DNA junction 1 structure has part of ICRII with the RepD nicking sequence as a single stranded overhang (5'-CT*AATAGCCGGTT-3', where * is the RepD nick site) and the whole ICRIII (23 base pair sequence) for high affinity RepD

binding (Figure 19). When DNA junction 1 was mixed with MDCC-PcrA(E449C) in the absence of RepD the signal increase was ~6%. No signal change was observed on mixing RepD and MDCC-PcrA(E449C) in the absence of DNA. More precisely, none of the labelled PcrA variants in Table 1 showed a signal when mixed with RepD on the stopped-flow instrument. This implies that the PcrA and RepD do not interact strongly in solution and the interaction is facilitated through DNA as the interaction signal has been only observed with RepD-DNA complex. A small (~2%) signal was observed with MDCC-PcrA(E449C) binding to ssDNA and translocating on it. No signal is observed with MDCC-PcrE449C binding to ATP (data not shown here).

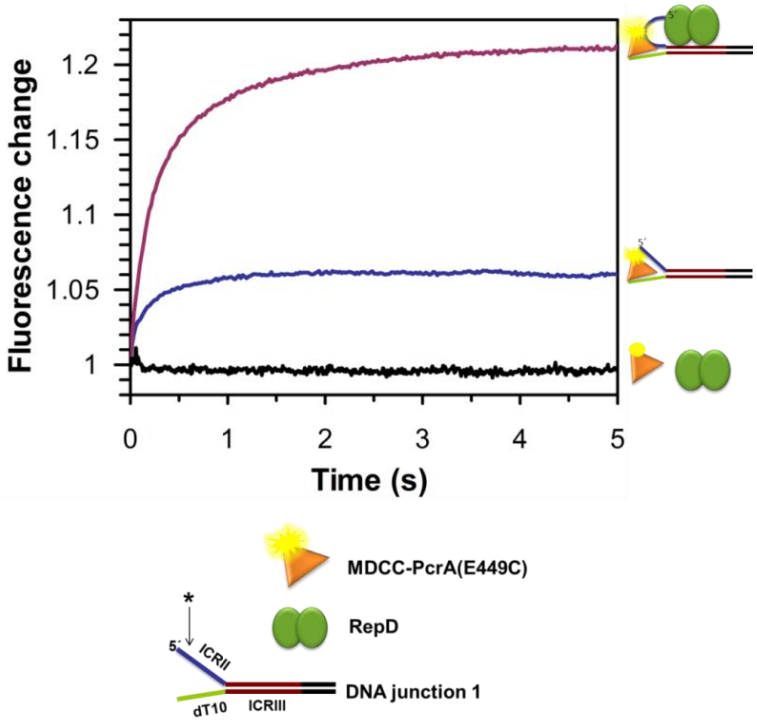

Figure 45. MDCC-PcrA(E449C) signal when binding to RepD-DNA junction 1.

Purple, MDCC-PcrA(E449C) binding to the RepD-DNA junction 1 complex. Blue, MDCC-PcrA(E449C) binding to the DNA junction 1. Black, MDCC-PcrA(E449C) and RepD in solution. Experiments were done using the stopped-flow instrument at 30 °C. The final concentrations were 100 nM MDCC-PcrA(E449C), 1 µM RepD and 0.5 µM DNA junction 1 in K200 buffer. The DNA junction and RepD were incubated 5 minutes at 30 °C to allow RepD-DNA complex formation. The cartoons next to the graph represent the end point of reaction shown. See Figure 19 in Methods for the sequence structure of the DNA junction 1. * is the RepD nick site on the ICRII-arm of DNA junction 1.

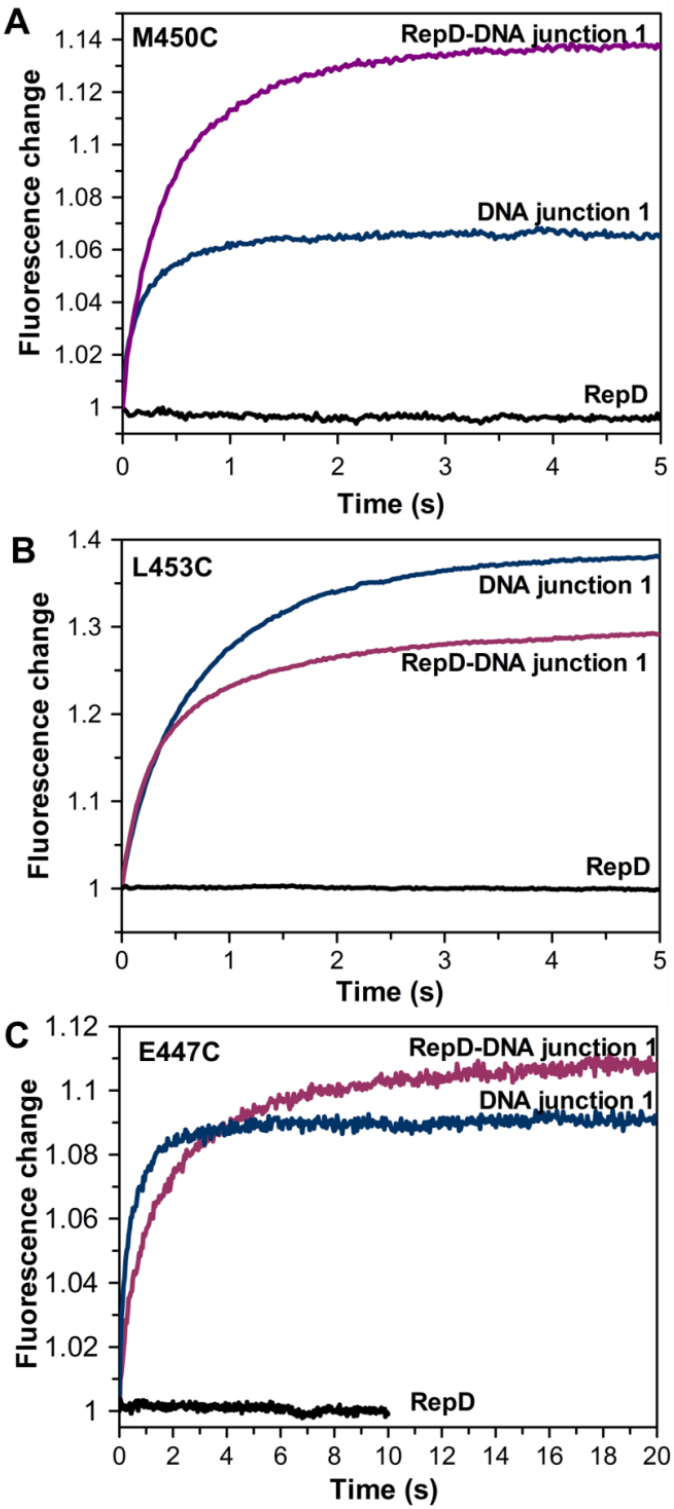

Figure 46. MDCC-PcrA(E449C) binding to RepD-DNA junction/RepD/DNA junction.

A) MDCC-PcrA(M450C) binding to the DNA junction 1 and the RepD-DNA junction 1. B) MDCC-PcrA(L453C) binding to the DNA junction 1 and the RepD-DNA junction 1. C) MDCC-PcrA(E447C) signals binding to the DNA junction 1 and the RepD-DNA junction 1. The experimental conditions were same as in the Figure 45.

The results for the fitting of the MDCC-PcrA(E449C) binding signals to DNA junction 1 and RepD-DNA junction 1 are summarised in the Table 8. The k_{obs} for PcrA binding to DNA junction 1 was 3.5 to 4 -folds faster than binding to the RepD-DNA junction 1 complex. This is most likely to be caused by the higher number of possible binding sites, i.e. bare ssDNA, on DNA junction 1 than when RepD is bound to it.

Reaction	k_{obs1} (s^{-1})	k_{obs2} (s^{-1})	Amplitude 1	Amplitude 2	End *F*	Signal change
DNA junction 1	21.71	2.59	0.91	0.95	30.51	6.5%
RepD-DNAj1	4.89	0.70	4.21	2.30	37.18	21.2%

Table 8. MDCC-PcrA(E449C) binding to DNA junction 1 and RepD.

The fitting was done using a double exponential fit. The reaction conditions were same as in Figure 45.

The fluorescence time courses on PcrA binding to DNA junction 1 and to the RepD-DNA junction 1 complex were biphasic. This indicated two different processes occurring. The second order rate constant (k_{on}) for MDCC-PcrA(E449C) binding to RepD-DNA junction 1 was determined. This was done by repeating the above assay with varying RepD-DNA junction 1 concentrations. The measurements were done similarly to previous binding measurements with MDCC-PcrA(K138C) (Chapter 4) where the concentration of the ligand was varied and its effect on k_{obs} was investigated. This is based on the Scheme 1 (Section 1.7, Introduction) and the results were fitted using Equation 3 (Section 1.7, Introduction). Example fits are shown in Figure 92, Appendix). Figure 47 shows the k_{obs} dependence on the RepD-DNA junction 1 concentration. The k_{on} for the fast phase is 6.1 μM^{-1} s^{-1} and for the slow phase it is 0.6 μM^{-1} s^{-1}(average of three experiments). As both phases show concentration dependence it can be concluded that both phases are processes of binding.

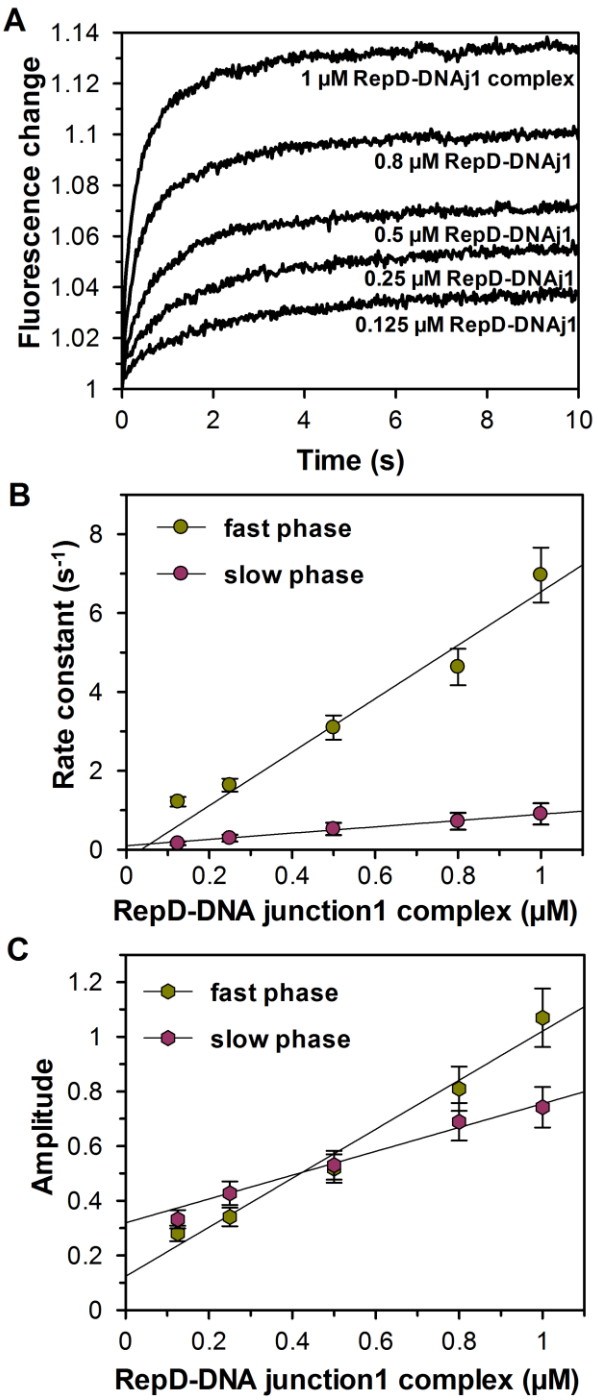

Figure 47. MDCC-PcrA(E449C) signal with RepD-DNA junction 1 complex is observing its binding to the complex.

A) Normalised MDCC-PcrA(E449C) binding signals with varying concentration of RepD-DNA junction 1 complex. The traces were fit to double exponential fit and each data point is an average of three traces. B) The k_{obs} and C) amplitude values plotted against the concentration of RepD-DNA complex and fitted using linear regression (fast and slow phase of binding). The fast phase has k_{on} of 6.8 μM^{-1} s^{-1} and the slow phase 0.8 μM^{-1} s^{-1}. Experiments were done as in the Figure 45 expect the RepD-DNA junction 1 complex concentration were varied from 0.125 – 1 μM and the MDCC-PcrA(E449C) concentration was 50 nM.

This could be explained by PcrA binding to the DNA junction 1 at two different sites, namely the two different ssDNA arms as shown in Figure 45. PcrA may have different affinities to these arms or to other parts of the ssDNA (ssDNA end) and to the ds/dsDNA junction.

The biphasic signal of PcrA binding to the RepD-DNA junction 1 might have a different origin as there is only one ssDNA overhang (dT_{10}-arm) free for PcrA binding. The other ssDNA overhang (ICRII-arm) is covalently bound to RepD, if nicking has been efficient. Alternative possibilities for the biphasic signal include two different conformations of PcrA, different binding sites on dT10-arm or two different RepD-DNA junction 1 complexes.

Several assays were carried out to determine what caused the biphasic signal when MDCC-PcrA(E449C) bound to RepD-DNA junction. dT_{10} is long enough to more than one PcrA to bind to it and this was shown by the displacement assay with MDCC-PcrA(K138C) (Figure 38B, Chapter 4 and Figure 87, Appendix).To test this DNA junctions with varying lengths of polyT arm were used (dT_6, dT_8, dT_{10} and dT_{20}) (Figure 48A). The DNA junctions with dT_6 and dT_8 showed reduced amplitude, but still had the two phases. This indicated that the biphasic signal is not due to two PcrAs binding on same dT_{10}-arm, but to do with the structure and form of the interaction between PcrA and RepD-DNA junction complex. MDCC-PcrA(E449C) binding to dT_{20}-arm DNA junction also showed a biphasic signal. The rate constants for the first phase of binding for the dT_6, dT_8 and dT_{20}-arm DNA junctions are similar, but they have double the rate constant of the dT_{10}-arm DNA junction binding (Table 9, No ATP). This anomalous and cannot fully be explained.

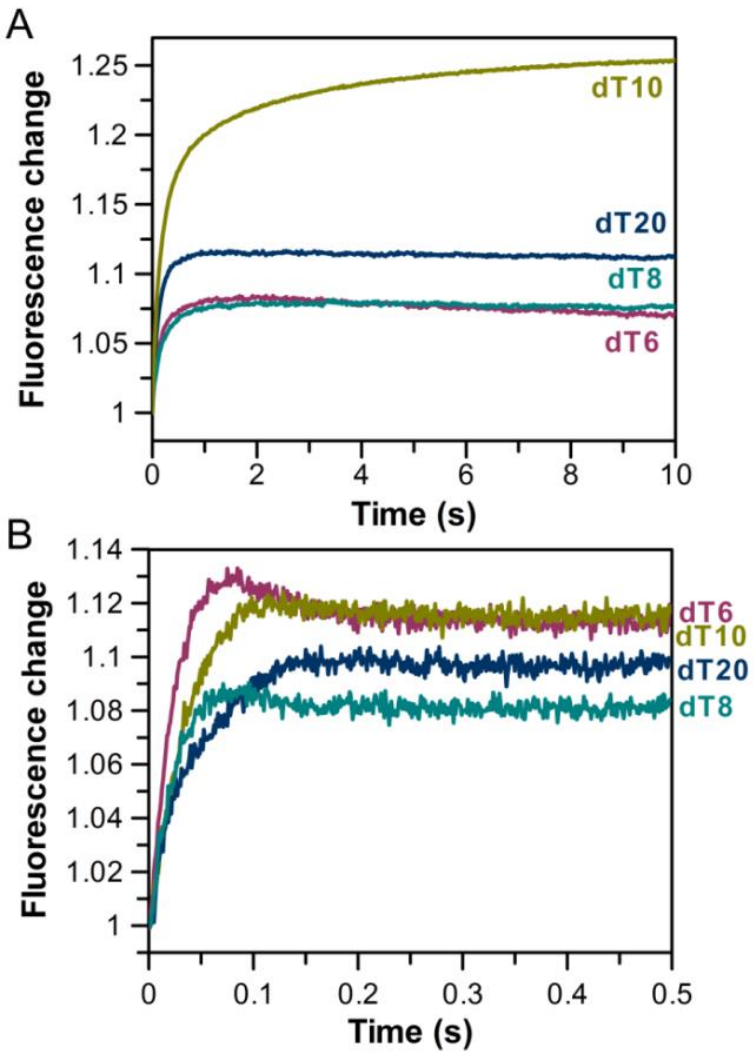

Figure 48. MDCC-PcrA(E449C) binding signal to varying lengths of dT-arm on DNA junction 1.

A) MDCC-PcrA(E449C) biding to the DNA junctions with varying dT-arm length without ATP. All the increasing phases were fitted using double exponential fit. B) MDCC-PcrA(E449C) biding to the DNA junctions with varying dT-arm length with ATP. The DNA junctions have the same sequence structure as DNA junction 1 except for the number of dT's on PcrA binding arm. The traces without ATP were fitted to single exponential. Experimental conditions were same as in the Figure 45.

	No ATP				With ATP	
dT-arm	$k_{obs\ fast}$ (s^{-1})	$k_{obs\ slow}$ (s^{-1})	Signal change, fast phase	Signal change, slow phase	k_{obs} (s^{-1})	Signal change
6	11.29	2.59	5.0%	3.5%	45.8	13.8%
8	9.33	1.92	4.9%	2.8%	44.5	9.3%
10	4.89	0.7	14.7%	7.6%	31.3	13.1%
20	11.16	3.54	7.7%	3.7%	22.9	9.6%

Table 9. MDCC-PcrA(E449C) binding to DNA junction 1 with varying dT-arm lengths.

Another possibility for the biphasic signal at binding by MDCC-PcrA(E449C) is the presence of two different RepD-DNA complexes. One possible reason for this would be to have only partial nicking. It has been shown that PcrA to unwind DNA junctions processively, the RepD does not have to be covalently bound to DNA [93]. First, this was confirmed here by using the DNA junction unwinding assay (Figure 24) with DNA unwinding junction lacking the known RepD nicking sequence, CT*A (5'-**CT*A**ATAGCCGGTT-3', the CT*A-sequence removed is highlighted and * is where RepD nicks) (Figure 49). In the assay, the lag phases that correspond to the actual dsDNA unwinding were almost identical for the two DNA junctions used (with and without CT*A-sequence). This meant that the CT*A-sequence and the covalent bond formation between RepD and DNA are not required for vital RepD-PcrA interaction. The RepD is still required to enhance the PcrA unwinding function [87]. The intensity change with the DNA junctions (with or without CT*A) vary by two fold and this is may be due to the level of purity and labelling of the DNA junctions or complications of concentrations determination of fluorescently-modified DNA.

The MDCC-PcrA(E449C) binding signal with DNA junction lacking the RepD nick sequence, CT*A, was still biphasic (Figure 49B). The traces were fitted to a double exponential and the k_{obs} values were similar to PcrA binding to DNA junction with CT*A (Table 10). To determine whether the two phases were actual binding, the experiments were repeated with varying

concentrations of RepD·DNA junction (no CT*A) (Figure 94, Appendix) (Scheme 1 and Equation 3 shown in Section 1.7). These measurements determined the binding rate constant, $k_{on,}$ for PcrA binding. The $k_{on\ fast}$ for RepD-DNA junction (with ICRIII, no CT*A) was 6.7 $\mu M^{-1} s^{-1}$. The slow phase k_{obs} did not follow concentration dependence. This indicated that the slow phase signal is not actual binding.

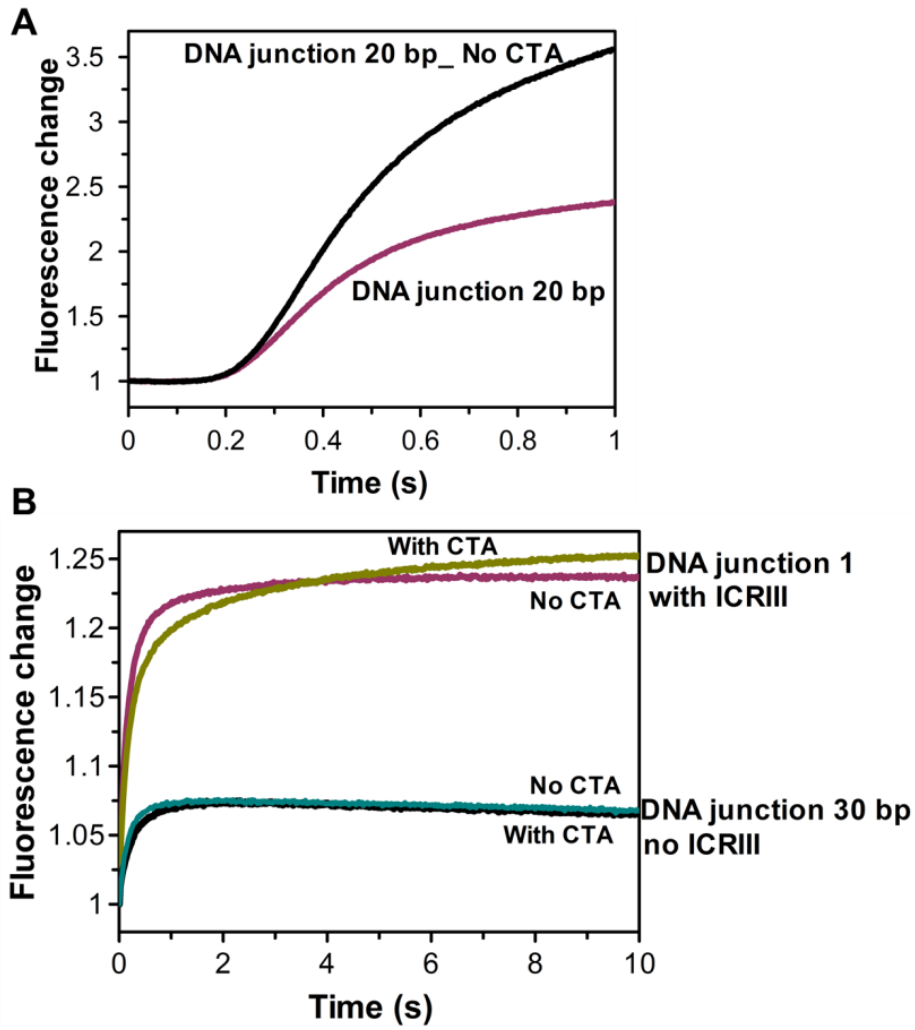

Figure 49. MDCC-PcrA(E449C) binding and unwinding a DNA junction lacking RepD nick sequence.

A) DNA junction unwinding assay with 20 bp DNA junction with and without CT*A-sequence of the ICRII (RepD nick site). The DNA junction unwinding was done with the same conditions and as shown in the Figure 24. B) MDCC-PcrA(E449C) binding to DNA junctions with and without CT*A-sequence. The binding measurements to these junctions were done at same conditions as in Figure 45.

DNA junction	$k_{obs\ fast}$ (s^{-1})	$k_{obs\ slow}$ (s^{-1})	Signal change, fast phase	Signal change, slow phase	Total signal change
DNAj1_with CT*A	4.86	0.7	16.1%	6.6%	23.8%
DNAj1_no CT*A	6.41	0.77	17.8%	3.4%	21.8%
DNAj30bp_ with CT*A	10.70	2.43	2.6%	5.0%	7.7%
DNAj30bp_ no CT*A	7.43	2.52	4.9%	2.2%	7.2%

Table 10. MDCC-PcrA(E449C) binding signal to DNA junction +/- ICRIII and +/- CT*A.

To test the effect of ICRIII on PcrA binding, the high affinity site for RepD, k_{on} was measured for PcrA binding to a RepD-DNA junction without ICRIII (Figure 93, Appendix). The MDCC-PcrA(E449C) binding traces were also biphasic and the k_{on} was 15.1 μM^{-1} s^{-1} for the fast phase and 1.9 μM^{-1} s^{-1} for the slow phase. This was 2.5 times faster than the binding to DNA junction 1 with ICRIII (Table 11). This could be due to the change in the RepD-DNA complex structure caused the lack of ICRIII, but could also imply that less nicking of the DNA junctions has taken place when the DNA junction does not have the ICRIII sequence.

The same measurements were also repeated with DNA junctions lacking the CT*A and the ICRIII sequence. The k_{on} for PcrA binding to the RepD-DNA junction (no ICRIII, no CT*A) is 22.4 μM^{-1} s^{-1} for the fast phase and 3.4 μM^{-1} s^{-1} for the slow phase. These binding rate constants were similar to k_{on} values for PcrA binding to DNA junctions without RepD (Table 11). This may be an indication that the PcrA binding to the RepD-DNA complex without ICRIII or nicking is similar in some way to PcrA binding to the DNA junction only and this also indicates that covalent binding of RepD doesn't increase the k_{on} of PcrA binding.

To distinguish between binding to RepD-DNA junction complex and to the DNA junction only, the k_{on} was determined for two DNA junctions, the

DNA junction 1_dT_{6}-arm and the DNA junction_dT_{10}-arm (Figure 90, Appendix). The k_{on} for the fast phase was 34.3 μM^{-1} s^{-1} (dT_{10}-arm) and 35.2 μM^{-1} s^{-1} (dT_{6}-arm) for the two DNA junctions. For the slow phase they were 2.9 μM^{-1} s^{-1} (dT_{10}-arm) and 0.9 μM^{-1} s^{-1} (dT_{6}-arm). The fast phase binding rate constants were very similar regardless the difference in the length of the polyT-arm. This indicated that the binding process to these junctions are same or similar, which is most probably the binding to the fork junction. The k_{on} for the fast phase of the PcrA binding to DNA junction without RepD is six times faster than to RepD-DNA junction 1 (Table 11). This may imply that RepD may restrict the binding of PcrA, for example sterically.

Reaction	$k_{on\ fast}$ (μM^{-1} s^{-1})	$k_{on\ slow}$ (μM^{-1} s^{-1})
DNA junction 1_dT_{10}arm	**34.3 (SEM 6.7)**	**2.9 (SEM 0.4)**
DNA junction 1_dT_{6}arm	**35.2 (SEM 4.0)**	**0.9 (SEM 1.3)**
RepD-DNA junction 1	**6.1 (SEM 0.8)**	**0.6 (SEM 0.3)**
RepD-DNA junction (No ICRIII)	**14.9 (SEM 0.7)**	**1.9 (SEM 0.5)**
RepD-DNAj1_no CT*A	**6.7 (SEM 0.9)**	**n/a**
RepD-DNA junction (No ICRIII)_no CT*A	**22.4 (SEM 5.0)**	**3.4 (SEM 0.9)**

Table 11. PcrA binding rate constants (k_{on}) for different DNA junctions and Rep-DNA junctions complexes, determined using MDCC-PcrA(E449C).

5.3. The effect of ATP on PcrA binding to RepD-DNA complex

5.3.1. MDCC-PcrA(E449C)·ATP binding signal with RepD-DNA junction complexes

The effect of ATP on PcrA binding to RepD-DNA junction 1 (with the high affinity RepD binding sequence, ICRIII) was investigated using MDCC-PcrA(E449C) on the stopped-flow apparatus (Figure 50). However, in measurements including ATP, unwinding of the DNA junctions can be

expected to take place subsequent to the PcrA binding. When MDCC-PcrA(E449C) was ATP bound, the maximum signal change was less than 15%. This is approximately half of the signal change when MDCC-PcrA(E449C) is not ATP bound. The signal had three phases. Phase 1 was increasing in fluorescence and is likely to be the MDCC-PcrA(E449C) binding to the RepD-DNA junction 1 complex. Phase 2 was a decrease and possibly corresponded to re-organisation to steady-state. The phase 3 was the steady-state signal of MDCC-PcrA(E449C) binding, translocating and dissociating from DNA junction dT_{10}-arm or from unwound DNA junction sequences. The phase 1 corresponding to the PcrA·ATP binding to RepD-DNA complex was fitted using single exponential. The k_{obs} was 31.3 s^{-1} for PcrA·ATP binding to the RepD-DNA complex. This is 6 times larger than the k_{obs1} without ATP (Table 12 and Figure 47).

The PcrA·ATP binding kinetics to the RepD-DNA was determined according to Scheme 1 by varying the RepD-DNA junction complex concentration in presence of ATP and fitting the results using Equation 3, Introduction, Section 1.7.(Figure 50). The k_{on} for PcrA binding to RepD-DNA junction 1 complex with ATP was 24.9 μM^{-1} s^{-1} for average of two experiments. This is over four times faster than when ATP is not present (Table 11). This implies that the binding is faster and more uniform (as only single phase is observed) when PcrA is bound to ATP. Both can be a result of conformational change on PcrA when bound to nucleotide or the actual translocation on ssDNA to the dsDNA junction.

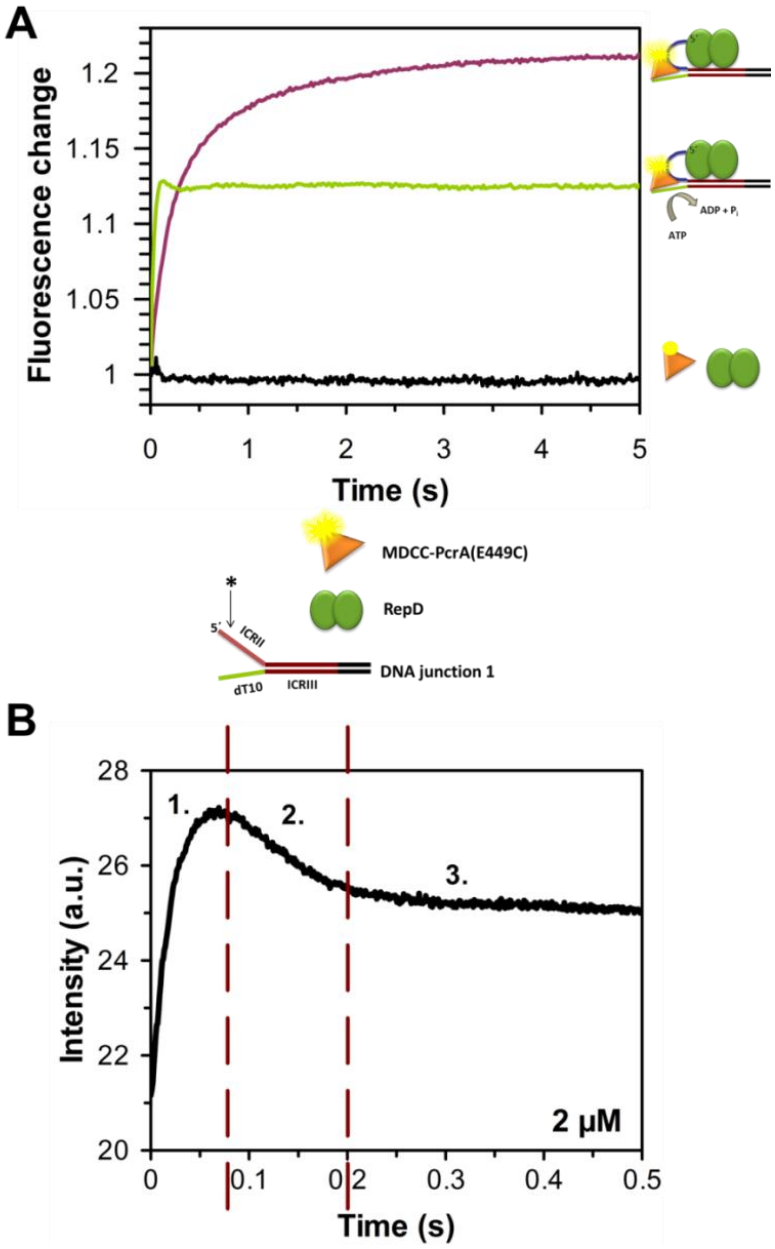

Figure 50. MDCC-PcrA(E449C) binding to RepD-DNA junction 1 with ATP.

A) Purple, MDCC-PcrA(E449C) binding to the RepD-DNA junction 1 complex. Green, MDCC-PcrA(E449C)·ATP binding to the RepD-DNA junction 1 complex. Black, MDCC-PcrA(E449C) and RepD in solution. Experiments were done on the stopped-flow instrument at 30 °C. The final concentrations were 100 nM MDCC-PcrA(E449C), 200 µM ATP, 1 µM RepD and 0.5 µM DNA junction 1 in K200 buffer. The cartoons represent the end point of reaction shown. See Figure 19 in Methods for sequence structure of DNA junction 1. * indicates the RepD nick site on the ICRII-arm of DNA junction 1 (13 bases). B) The breakdown of the signal of MDCC-PcrA(E449C) binding to the 2 µM RepD-DNA junction complex. Other reactions components were same as in (A).

Reaction	Fit	k_{obs1} (s^{-1})	k_{obs2} (s^{-1})	Signal change
RepD-DNAj1	Dbl	4.89	0.70	23.8%
RepD-DNAj1 + ATP	Sgl	31.28	n/a	14.9%
RepD-DNA j. 30 bp (No ICRIII)	Dbl	23.61	3.60	5.5%
RepD-DNA j. 30 bp (No ICRIII) + ATP	Sgl	58.19	n/a	3.5%

Table 12. MDCC-PcrA(E449C) binding to RepD-DNA junction complex with ATP.

Sgl, the trace has been fitted to single exponential, and Dbl, means fitting done using double exponential fit.

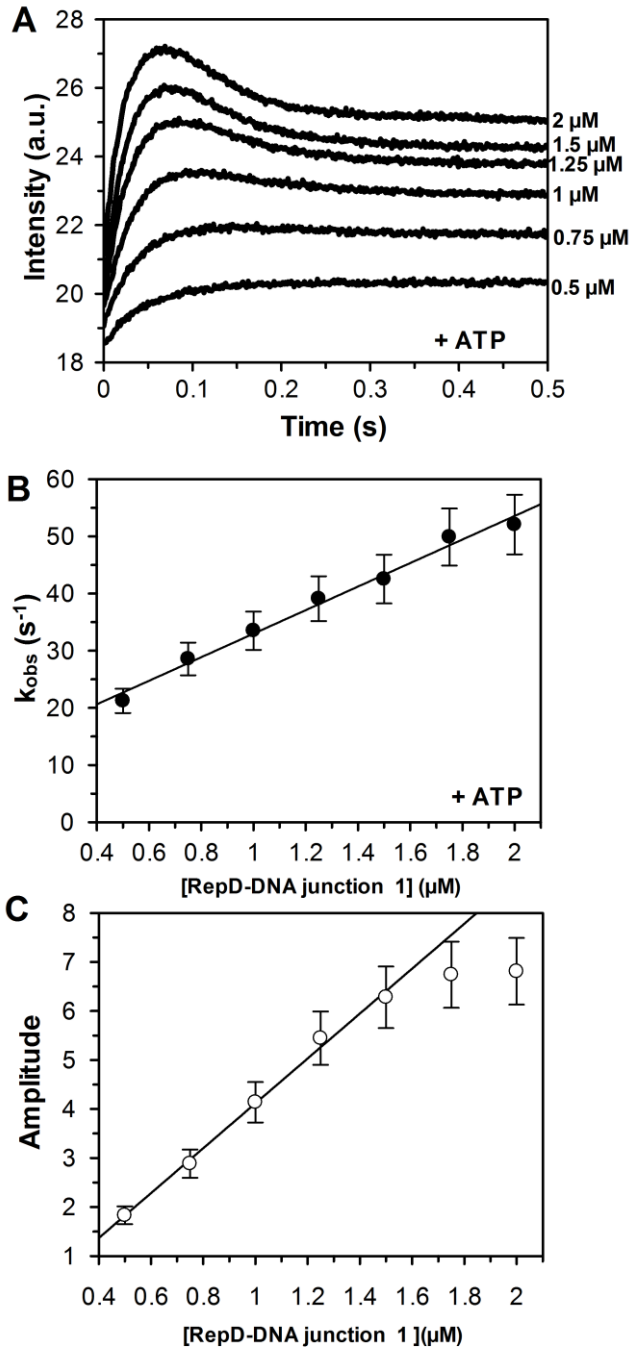

Figure 51. MDCC-PcrA(E449C)·ATP binding to RepD-DNA junction.

A) The raw data traces of MDCC-PcrA(E449C)·ATP binding to varying concentrations of RepD-DNA junction 1 complex. B) The three phases observed at higher RepD-DNA junction 1 complex concentration. 1. Binding. 2. Re-organisation to steady-state. 3. Steady-state of translocation on ssDNA. C) The linear fit of k_{obs} at different RepD-DNA junction 1 complex concentrations. The gradient of fit gives k_{on} of 20. 6 $\mu M^{-1}s^{-1}$ (SEM 1.0). D) The signal amplitude change with the concentration of RepD-DNA junction 1 complex. The linear fit was fitted up to 1.5 µM and has a gradient of 4.6 (SEM 0.2) of intensity per µM of complex. Experiments were done as in Figure 45 in presence of 200 µM ATP with 100 nM MDCC-PcrA(E449C). The RepD-DNA junction 1 complex concentration was varied from 0.5-2 µM.

MDCC-PcrA(E449C) binding signal has also been tested with *oriD*-mimic DNA junction that lacks the ICRIII sequence (Table 12). This has the same sequence and structure as the DNA junctions used for DNA junction unwinding assays (Figure 24) and hence should be readily unwound by PcrA when RepD is present. Similarly, to DNA junction 1 (with ICRIII) the binding without ATP is biphasic, but with lower signal change than with DNA junction 1 complex (~6%) (Table 12). The k_{obs} is increased by 4-fold when ATP present for the fast and slow phase. This may indicate that when PcrA is ATP bound, it is in different conformation compared to when it is ATP-free. The ATP bound PcrA conformation may have higher affinity to the RepD-DNA. Hence, the PcrA binding is faster when ATP is present in the reaction.

5.3.2. MDCC-PcrA(E449C) binding signal to RepD-DNA junction complex when bound to non-hydrolysable ATP analogues

The MDCC-PcrA(E449C)·ATP binding signal with RepD-DNA complex was further investigated using non-hydrolysable ATP analogue, ATPγS (Figure 52). PcrA has been shown to have similar affinity to as ATPγS as ATP [157].This can give information how the ATP changes the signal without the effect of actual ATP turnover. In the measurements, the ATPγS was pre-mixed with MDCC-PcrA(E449C) in the stopped-flow syringe before mixing with the pre-incubated RepD-DNA junction complexes. With DNA junctions with ICRIII, the amplitude change of the fluorescent signal was similar to the MDCC-PcrA(E449C) binding to RepD-DNA junction when no ATP is present. The results are summarised in the Table 13. The fluorescence time course could be fitted well using single exponential. The k_{obs} of PcrA·ATPγS binding was half of PcrA binding without nucleotide, and 6- to 10-fold slower than PcrA·ATP binding (Table 13). The measurements were repeated with DNA junction lacking the ICRIII sequence and with this junction two non-hydrolysable ATP analogues were tested, ATPγS and AMPPNP. The results showed similar pattern of PcrA·ATP analogue binding, where a single phase was observed that had k_{obs} 6- to 10-fold slower than PcrA·ATP binding.

These results indicate that the increased k_{obs} with PcrA·ATP may be related to the actual ATP hydrolysis taking place. PcrA may hydrolyse 1 ATP before binding and this complex (PcrA·ADP) may have higher affinity to RepD-DNA complex. This is unlikely as PcrA affinity ADP is low [157]. But, of course, the structural differences between ATP and its analogues may affect the PcrA conformation and its affinity to RepD-DNA. Other possibility for increased k_{obs} when ATP is present would be the ssDNA translocation to the DNA junction that directs PcrA to the junction faster than random binding. As single phase was observed with non-hydrolysable ATP analogues, this implied that PcrA·ATP analogue is binding in single conformation to RepD-DNA.

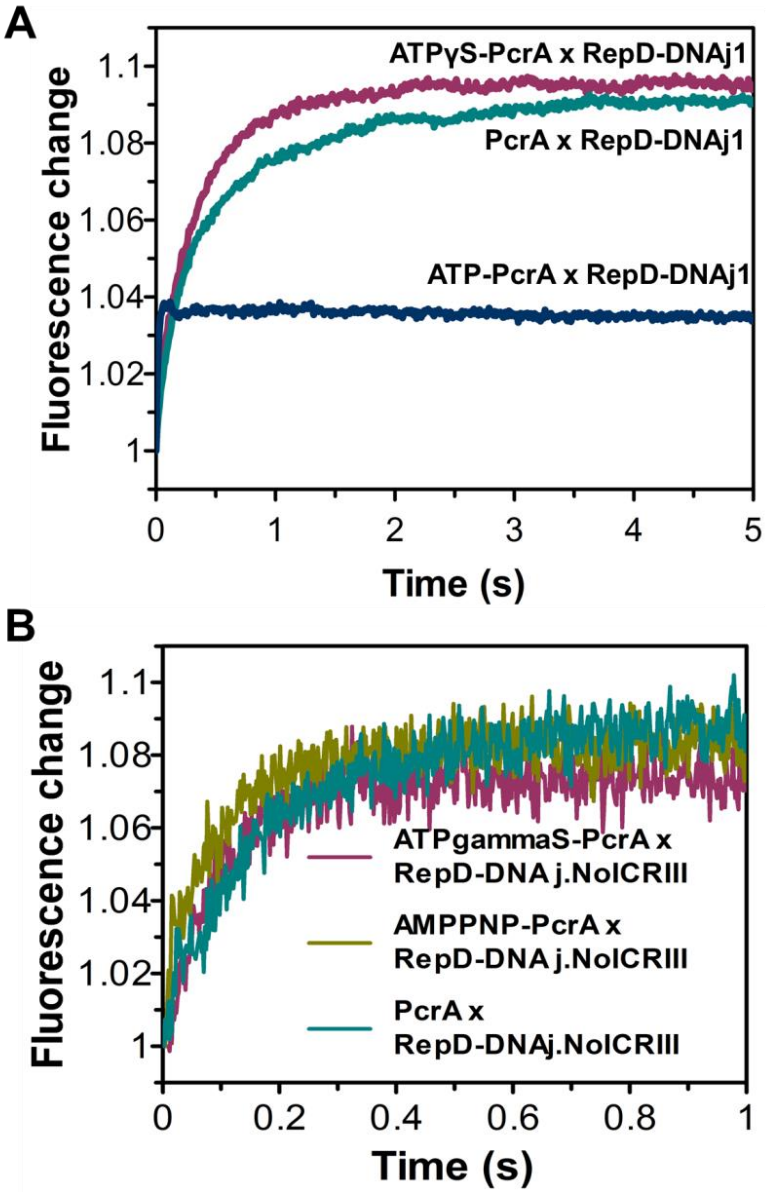

Figure 52. MDCC-PcrA(E449C) binding signal RepD-DNA junctions with non-hydrolysable ATP analogues.

A) ATP/ATPγS-MDCC-PcrA(E449C) binding to RepD-DNA junction 1. B) AMPPNP/ATPγS-MDCC-PcrA(E449C) binding to RepD-DNA junction no ICRIII. (A) The experimental conditions were 70 nM MDCC-PcrA(E449C), 500 nM DNA junction 1, 1 μM RepD and +/- 200 μM ATPγS or ATP and (B) conditions were 100 nM MDCC-PcrA(E449C), 500 nM DNA junction No ICRIII, 1 μM RepD and +/- 200 μM ATPγS or ATP or 600 μM AMPPNP.

Reaction	Fit	$k_{obs\ fast}$ (s^{-1})	$k_{obs\ slow}$ (s^{-1})	Signal change
RepD-DNA junction (No ICRIII)				
No Nucleotide	Dbl	19.84	2.72	7.3%
ATP	Sgl	59.19	n/a	3.5%
ATPγS	Sgl	10.83	n/a	6.2%
AMPPNP	Sgl	9.66	n/a	6.2%
RepD-DNA junction (With ICRIII)				
No Nucleotide	Dbl	5.95	1.07	8.5%
ATP	Sgl	31.28	n/a	14.9%
ATPγS	Sgl	2.48	n/a	7.9%

Table 13. MDCC-PcrA(E449C) binding to RepD-DNA junction complex and ATP and analogues.

The fitting was done either to single or double exponential. The experimental conditions for both sets of experiments are stated in Figure 52.

5.4. PcrA dissociation kinetics from RepD-DNA junction complex

To measure the PcrA dissociation kinetics from the RepD-DNA junction 1 complex, a displacement assay was designed using MDCC-PcrA(E449C) (Figure 53, Scheme 2, Section 1.7). This was done on the stopped-flow apparatus by incubated DNA junction 1 with the RepD and adding MDCC-PcrAE449C to this, to the pre-form the MDCC-PcrA(E449C)-RepD-DNA complex. This was then mixed with a high excess of wild-type PcrA. The time courses showed a decrease in fluorescence and the traces were fitted to single exponential followed by a linear slope (to take account of slow photobleaching) (Figure 95, Appendix). The rate constant for the exponential phase, k_{off}, was 0.16 s^{-1} (average of three traces at three different wild-type PcrA concentrations). Varying the wild type PcrA concentrations had no significant effect on the k_{off} confirming that the displacement assay was indeed measuring the dissociation of MDCC-

PcrA(E449C) from RepD-DNA complex. On very short time courses, an initial, small increase in fluorescence was seen. This could correspond to some wild type PcrA binding to close proximity to the MDCC-PcrA(E449C) before the latter dissociates.

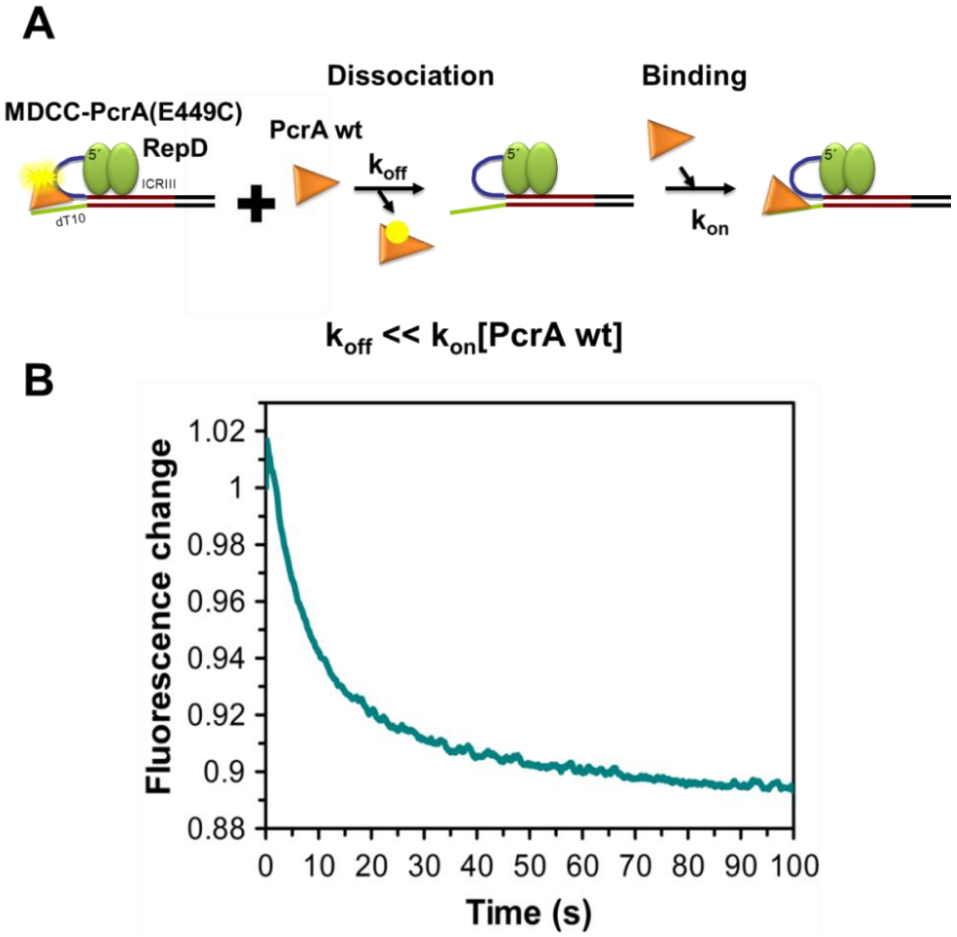

Figure 53. Displacement of MDCC-PcrA(E449C) from RepD-DNA junction 1 to measure dissociation kinetics.

A) Cartoon representation of the reaction of MDCC-PcrA(E449C) displacement assay. B) Normalised data trace of MDCC-PcrA(E449C) displacement by 10 µM wild type PcrA. The trace was fitted to single exponential decay with straight line. This had a k_{off} of 0.14 s^{-1} (SEM 1.2 x 10^{-3}) and the linear regression has a gradient of 7.9 x 10^{-3} (SEM 1.8 x 10^{-4}). The DNA junction 1 was incubated for 5 min with RepD at 30 °C to which MDCC-PcrA was added. The reaction mix was then mixed with different concentrations of wild type PcrA. Excitation was done at 436 nm and emission measured using 455 nm cut-off filter. The final reaction concentrations were 100 nM MDCC-PcrA(E449C), 500 nM DNA junction 1, 1 µM RepD and 5,10 or 15 µM PcrA in buffer K200.

5.5. Association kinetics of PcrA and RepD-plasmid complex

PcrA binding kinetics to RepD-pCER*oriD* complex (full length plasmid) was measured using MDCC-PcrA(E449C) on the stopped-flow apparatus (Figure 54) (Scheme 1 and Equation 3, Section 1.7).The plasmids used for the assay were the same plasmids as used for the plasmid unwinding assay with DCC-SSB (Figure 26). The MDCC-PcrA(E449C) binding signal to RepD-plasmid complex at pseudo-first order conditions of 10-fold excess of RepD-plasmid complex over MDCC-PcrA(E449C) was ~16%. The traces were biphasic and the binding was similar in time scale to the PcrA binding to RepD-DNA junction 1. Measurements with the varying RepD-plasmid complex concentrations showed that the both phases were concentration dependent. The k_{on} has been determined for two different lengths of plasmid, 2437 bp and 3094 bp.

The PcrA binding to the RepD-3094bp plasmid complex had a k_{on} of 46.2 $\mu M^{-1}s^{-1}$ for the fast phase and 4.0 $\mu M^{-1}s^{-1}$ for the slow phase (average of three measurements). This showed that the binding to RepD-pCER*oriD*3094 is almost 10-fold faster than the binding to the RepD-DNA junction 1 complex. This could be indication that the RepD binding and complex formation isn't optimal with DNA junctions compared to plasmid or possible presence of ssDNA contamination in the plasmid preparations, which PcrA would bind, increasing the effective binding site concentration. These ssDNA may be too short to be observed on agarose gel electrophoresis. The biphasic binding signal with the RepD-plasmid complex indicates, similarly to RepD-DNA junction binding signal, that two processes are taking place. These could be due to PcrA having two different binding modes either to possible multiple binding sites on the nicked *oriD*, two different PcrA conformations or different RepD-plasmid complex. Also, the slower phase could be a result of binding to ssDNA contamination from preparation of plasmid.

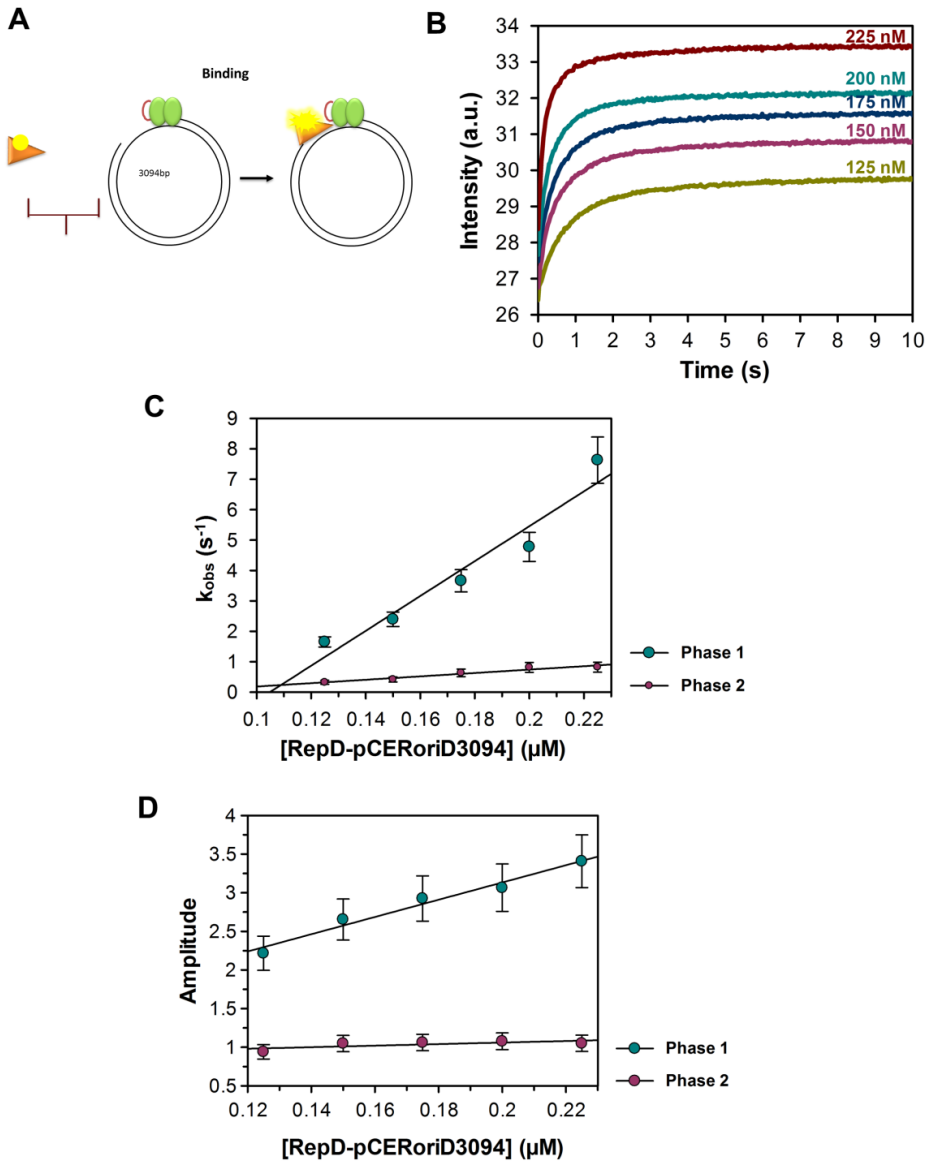

Figure 54. PcrA binding to RepD-pCER*oriD* 3094bp complex.

A) Cartoon representation of the reaction. B) Raw data traces for MDCC-PcrA(E449C) binding varying concentrations of RepD-pCER*oriD* 3094 complex. Traces were fitted to double exponential. C) The observed rate constants for phase 1 and 2 from fitting plotted against the RepD-plasmid concentration. The fits are average of three traces. The linear fit has a gradient of 52.9 $\mu M^{-1}s^{-1}$ (SEM 5.7) for the fast phase 1 and 5.6 $\mu M^{-1}s^{-1}$ (SEM 0.8) for the slow phase 2. D) The amplitudes for phase 1 and 2 from fitting plotted against the RepD-plasmid concentration. The gradient for the phase 1 amplitude is 11.2 per μM and 1.0 per μM for the phase 2. The experimental conditions were 20 nM MDCC-PcrA(E449C) and 125 nM to 225 nM RepD-plasmid complex in K200 buffer. The RepD is in 4-fold excess over the plasmid concentration and the complex was prepared by 5 minute incubation at 30 °C. The reaction mix was then mixed with different concentrations of wild type PcrA. Excitation was done at 436 nm and emission measured using 455 nm cut-off filter.

The PcrA binding kinetics to RepD-pCER*oriD* 2437 bp plasmid was also measured (Figure 55). This had similar biphasic signal with larger signal change (~35%) when RepD-plasmid complex was at 10-fold excess over MDCC-PcrA(E449C) than at low excess. The fast phase for PcrA binding to RepD-pCER*oriD* 2437 bp plasmid had k_{on} of 14.1 $\mu M^{-1}s^{-1}$ and 2.0 $\mu M^{-1}s^{-1}$ for the slow phase (average of three measurements). The amplitude of the first phase followed concentration dependence, but the second phase remained constant with varying the RepD-plasmid concentration.

The k_{on} for PcrA binding to RepD-2437 bp plasmid and for RepD-3094 bp plasmid complex are different (Table 15). This may be an indication that PcrA binds at different rates to different length plasmids, which could be a result of a certain form of secondary structure in the plasmid after the RepD-plasmid complex formation. Also, there may be a different rate of RepD nicking on different lengths of plasmids that has not been investigated before. The PcrA may also be binding to the other parts of plasmid and these may vary between different lengths of plasmids. Other possible reason for the k_{on} variation is the difference between preparations of plasmids that affect the proportion of supercoiled plasmid over the nicked relaxed plasmid. The plasmid preparations were always run on agarose gel, but no accurate quantification of relaxed-nicked versus supercoiled plasmid can be done by gel analysis. Furthermore, RepD is known to nick supercoiled plasmid more efficiently than nicked-relaxed plasmid [93]. Other, likely possibility is the ssDNA contamination in the plasmid preparations. PcrA binds very short nucleotide oligos and these cannot be observed in agarose gel electrophoresis. This has been suggested before for similar plasmid preparations [87]. The amount of ssDNA contamination may vary between different preparations and between different plasmid lengths. Overall, both the 2437 and 3094 bp plasmids show that the k_{on} is several magnitudes faster for PcrA binding to the RepD-plasmid complex than to the RepD-DNA junction complex (Table 15).

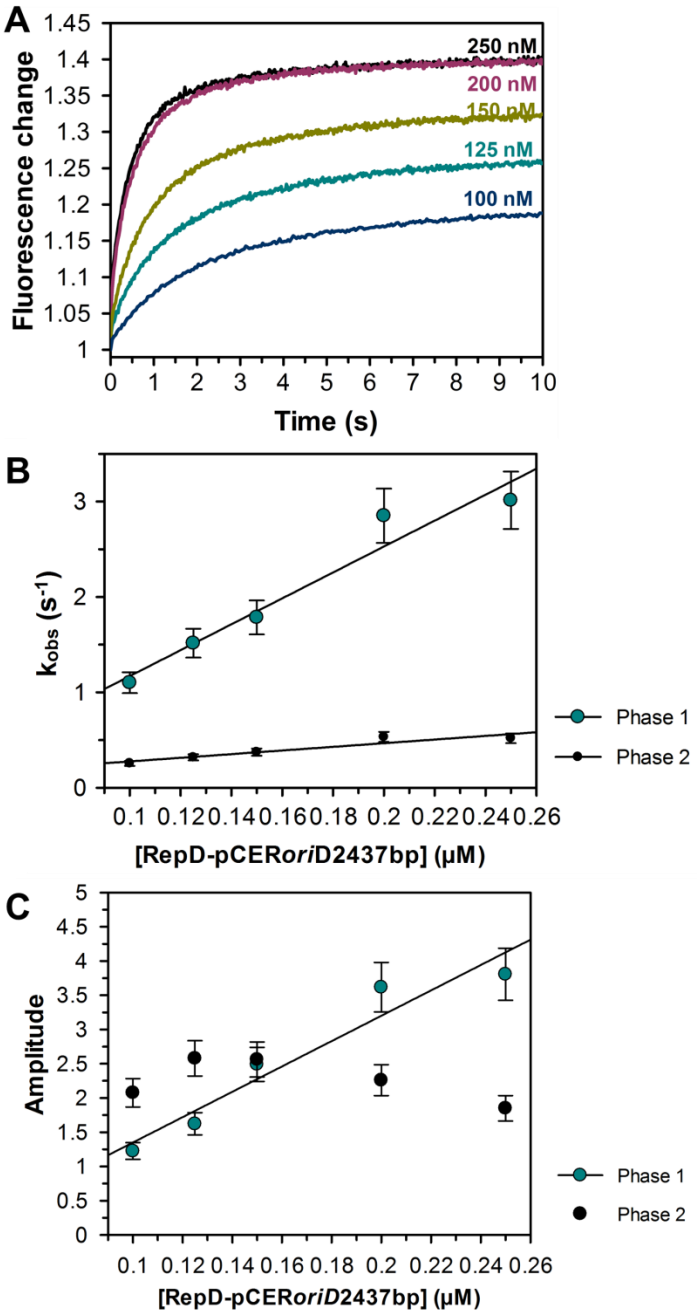

Figure 55. PcrA binding to RepD-pCER*oriD* 2437bp complex.

A) Normalised data traces for MDCC-PcrA(E449C) binding varying concentrations of RepD-pCER*oriD* 3094 complex. Traces were fitted to double exponential. B) The k_{obs} and C) The amplitudes for the phase 1 and 2 from fitting plotted against the RepD-plasmid concentration. The fits are average of three traces. The linear fit has a gradient 13.6 $\mu M^{-1}s^{-1}$ for the fast phase 1 and 1.9 $\mu M^{-1}s^{-1}$ for the slow phase 2. The gradient for the phase 1 amplitude is 18.5 per μM. The second phase of amplitude does not show linear dependence in amplitude with concentration of complex. The experimental conditions were 20 nM MDCC-PcrA(E449C) and 100 nM to 250 nM RepD-plasmid complex.

5.5.1. MDCC-PcrA(E449C)·ATP binding to the RepD-plasmid complex

The effect of ATP and ATP non-hydrolysable analogues on MDCC-PcrA(E449C) binding to the RepD-plasmid complex was investigated using ATP, AMPPNP and ATPγS (Figure 56 and Table 14). These measurements were done with 25% excess of plasmid over MDCC-PcrA(E449C) due to low availability of good quality plasmid and relatively high concentration MDCC-PcrA(E449C) required for observable signal on the stopped-flow measurements. In other words, the conditions used were not in pseudo-first order conditions and the results cannot be directly compared with the PcrA binding measurements to RepD-DNA junction (Figure 45). The measurements with PcrA·ATP analogue binding to RepD-plasmid are purely a comparison between the different PcrA binding measurements with the plasmid. The fitting of traces was not done as a part of the analysis as the reactions were not done in pseudo-first order conditions. This means that many of the RepD-plasmid complexes could have more than one MDCC-PcrA(E449C) binding to them (two processes of binding). The PcrA binding signal with ATP had the lowest fluorescence change of 5.8% and compared to 11.3 to 11.6% with the ATP analogues, ATPγS and AMPPNP, and especially lower than when no nucleotide is present (16.1%). This was also observed with the MDCC-PcrA(E449C) binding to RepD-DNA junction.

The observed binding rate constant of 5.8 s^{-1} is approximately three times faster with ATP present in the reaction than without nucleotide or with the non-hydrolysable ATP analogues, which have k_{obs} of 1.6 to 1.9 s^{-1} for the fast phase of binding. Though, it has to be noted that as the conditions were not pseudo-first order conditions, the observed rate constants cannot be accurately interpreted. The second phase of 10 second traces is slower but has a higher signal change. The k_{obs} of the slow phase varied little between the four experiments and was between 0.2 to 0.3 s^{-1} (with and without nucleotide). The slow phase may be a second MDCC-PcrA(E449C) binding to the complex, rather than being another process of binding, though this may be possible even this was not observed with RepD-DNA junction binding experiments.

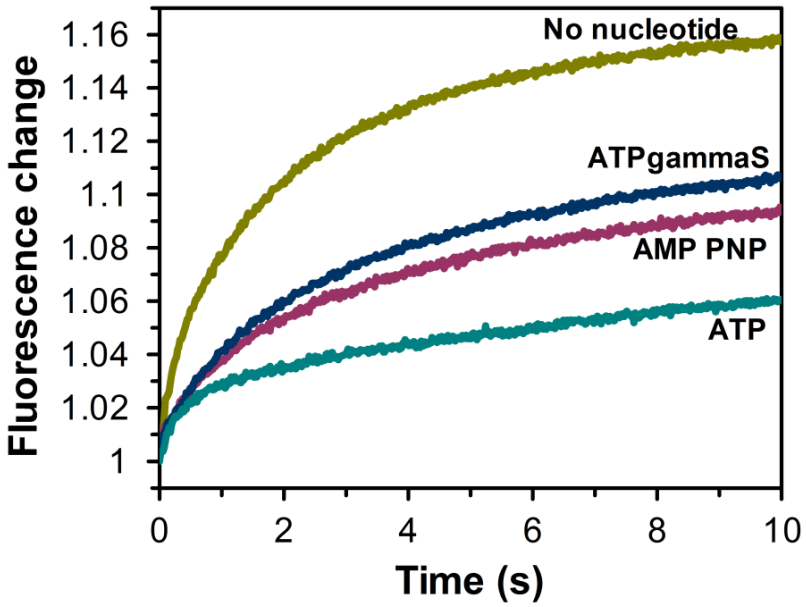

Figure 56. ATP bound MDCC-PcrA(E449C) binding to RepD-plasmid complex.

The experiments were done on the stopped-flow apparatus by pre-incubating the RepD-plasmid complex in syringe at 30 °C and mixing with MDCC-PcrA(E449C) and ATP/ATP analogue in the other syringe. The experiments were not done in pseudo-first order conditions due to low available quantity of plasmid. Each reaction had 30 nM MDCC-PcrA(E449C), 37.5 nM pCER*oriD* 3094bp, 150 nM RepD, 1 mM ATP/ATPγS/AMPPNP. It should be noted that these measurements were not done in pseudo-first order conditions.

Reaction	$k_{obs\ fast}$ (s^{-1})	$k_{obs\ slow}$ (s^{-1})	Fluorescence change total	Fluorescence change, fast phase	Fluorescence change, slow phase
No nucleotide	1.72	0.32	16.1%	4.8%	11.3%
ATP	5.77	0.27	5.8%	1.9%	3.9%
ATPγS	1.55	0.27	11.3%	2.1%	9.2%
AMP PNP	1.91	0.23	11.6%	3.0%	8.6%

Table 14. ATP bound MDCC-PcrA(E449C) binding to RepD-plasmid complex.

The reaction conditions are the same as in the Figure 56. The fitting was done to 10s traces with double exponential fit and results are an average of three traces.

5.6. PcrA dissociation kinetics from RepD-plasmid complex

A displacement assay was carried out to determine the PcrA dissociation rate constant, k_{off}, from the RepD-pCER*oriD* 3094 bp complex (Scheme 2, Introduction, Section 1.7). The MDCC-PcrA(E449C)-RepD-plasmid complex was mixed with 50-fold excess of wild type PcrA, a signal with two phases was observed (Figure 57 and Figure 97, Appendix). The first phase was increasing and the second was decreasing in fluorescence. Varying the wild type PcrA concentration and fitting the increasing phase and part of the decreasing phase to a double exponential showed that the first phase rate constant increased with the increasing wild type PcrA concentration (Figure 57B). This indicated the phase may be due to wild type PcrA binding to RepD-plasmid complex at a close proximity to MDCC-PcrA(E449C) and had a rate constant of 1.3 x 10^{-2} μM^{-1} s^{-1}.

The second phase was fitted by single exponential decay followed by a slope. Increasing the wild type PcrA concentration did not increase the observed rate constant of the phase. This is likely to be PcrA dissociation from the RepD-plasmid complex. The dissociation rate constant, $k_{off,}$ for the dissociation was measured to be 0.019 s^{-1}. This was an average for three traces at three different wild type PcrA concentrations. The slope had a gradient of 0.004 s^{-1} and this is most likely the rate of photobleaching as it is very similar to the rate of photobleaching observed with MDCC-PcrA(E449C) at same conditions (Figure 98, Appendix).

The displacement assay was also repeated for the pCER*oriD* 2437 bp plasmid. The PcrA dissociation rate constant (k_{off}) was 0.017 s^{-1} (average of three traces from measurements with three concentrations of wild type PcrA). This is similar to k_{off} of PcrA dissociation from RepD-3094 bp plasmid complex (Table 15). These measurement were performed with the same plasmid preparations as the binding measurements and showed that the difference observed in PcrA binding to different lengths of plasmid-RepD

complex isn't present in dissociation of MDCC-PcrA(E449C) from the same complexes.

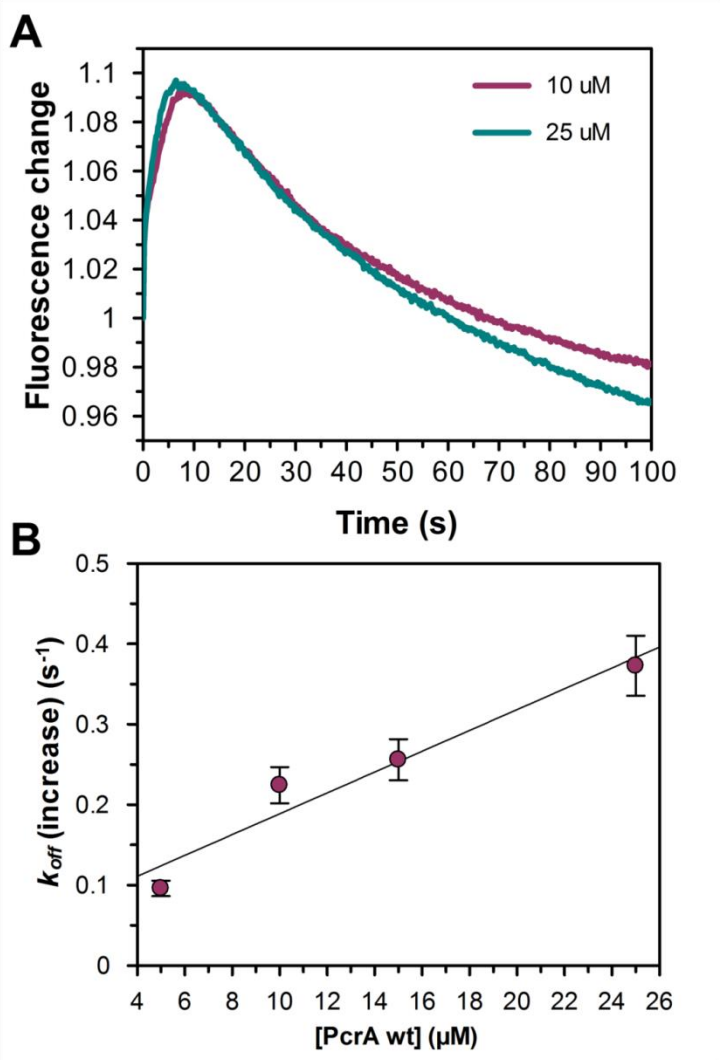

Figure 57. PcrA the dissociation rate constant (k_{off}) from RepD-plasmid complex using MDCC-PcrA(E449C).

A) Normalised traces of MDCC-PcrA(E449C) binding to the RepD-pCER*oriD* 3094bp complex with 10 and 25 μM concentrations of wild type unlabelled PcrA. B) Linear fit of k_{obs} for wild type PcrA binding to complex that gives a second order rate constant of 1.3 x 10^{-2} $\mu M^{-1}s^{-1}$ (SEM 0.01). The assay follows the Scheme 2 shown in Introduction. The experiments were done at 30 °C in K200 buffer with 20 nM MDCC-PcrA(E449C), 100 nM pCER*oriD* 3094/2437bp, 400 nM RepD with varying concentration of wild type PcrA.

5.7. PcrA affinity to RepD-DNA complex

Together, the displacement assays and the binding of MDCC-PcrA(E449C) to RepD-DNA provide the binding rate constants (k_{on}) and the dissociation rate constants (k_{off}). This enables the calculation of K_d values for PcrA affinity to RepD-DNA complex by dividing the k_{off} with the k_{on} (Equation 4, Section 1.7). The measured k_{on} and k_{off} values are summarised in Table 15. The K_d for the RepD-DNA junction 1 (with ICRIII) is 26 nM. The PcrA affinity to RepD-plasmid complex is 0.4 nM for the RepD-plasmid 3094 bp complex and 1.2 nM for the RepD- plasmid 2437 bp complex. This shows that even with the variation in binding rate constants between the two lengths of plasmid, the PcrA affinity to RepD-plasmid complex is at least 20 times tighter than to RepD-DNA junction 1 complex.

Reaction	$k_{on\ fast}$ ($\mu M^{-1}\ s^{-1}$)	$k_{on\ slow}$ ($\mu M^{-1}\ s^{-1}$)	k_{off} (s^{-1})	K_d (nM)
DNA junction 1	34.3	2.9		
DNA junction 1_dT6arm	35.2	0.9		
RepD-DNA junction 1	6.1	0.6	0.16	26.2
RepD-DNA junc. 1_dT6arm	11.2	1.1		
RepD-DNA j.(No ICRIII)	14.9	1.9	0.19	13.0
RepD-DNA j. 1+ ATP	24.9	n/a		
RepD-DNA j.(No ICRIII) + ATP	34.9	n/a		
RepD-DNAj1_noCT*A	6.7	n/a		
RepD-DNAj(NoICRIII) noCT*A	22.4	3.4		
RepD-plasmid 3094 bp§	46.2	4.0	0.019	0.41
RepD-plasmid 2437 bp§	14.1	2.0	0.017	1.21

Table 15. Summary of PcrA binding and dissociation kinetics with RepD-DNA.

§, the actual values for the PcrA association to the RepD-plasmid complex may not be accurate and the reasons for this are discussed in Discussion, Section 5.10.4.

5.8. MDCC-PcrA(E449C) and DNA unwinding

5.8.1. MDCC-PcrA(E449C) and DNA junction unwinding

MDCC-PcrA(E449C) signal interaction with RepD-DNA enabled the development of an assay to investigate the PcrA DNA unwinding on the stopped-flow apparatus. Firstly, an assay was designed where MDCC-PcrA(E449C) unwinds the DNA unwinding junctions without the quencher-fluorophore modifications (Figure 58A). In the assay, the MDCC-PcrA(E449C) was loaded on to the RepD-DNA junction complex and the unwinding was initiated by mixing with ATP on stopped-flow apparatus. As the fluorophore is on PcrA, the other components were in excess over the MDCC-PcrA(E449C) to enable single turnover measurements at pseudo-first order conditions. By having the PcrA at significantly lower concentration than the DNA meant that only single PcrA molecules could be expected to be unwinding individual DNA junctions.

The signal first had a small decreasing phase. This phase probably corresponds for ATP binding to PcrA that is in complex with RepD-DNA or to PcrA in solution that then binds to the RepD-DNA complex. The second phase had an increase in fluorescence. The duration of this phase was dependent on the number of base pairs on the DNA junction. The increase was followed by a decreasing phase. The fluorescent peak (the highest point of fluorescence) formed between the second and third phase was used as the end point of DNA unwinding as it was seen as the end point of DNA unwinding. The fourth phase had a constant fluorescence and corresponded to the steady-state of PcrA binding translocating/unwinding and dissociating from ssDNA. The second phase for the 30 bp DNA junctions had duration of ~0.5 s (Figure 58B). This matched well with the durations of the lag phase in DNA junction unwinding assay where the 30 bp DNA junction has a ~0.4 s lag phase (Figure 27). When the duration of unwinding was measured for the different lengths of DNA junctions and plotted against the number of

base pairs, the gradient gave an unwinding rate of 43 bp s^{-1}. This is very similar to what is observed with DNA junction unwinding assay confirming the signal to be informative of PcrA unwinding linear DNA (Table 3). When the same assay was performed using DNA junction with ICRIII (DNA junction 1) and the number of base pairs is varied (30, 40 and 50 bp), no clear signal or phase corresponding to unwinding was observed (Figure 58D).

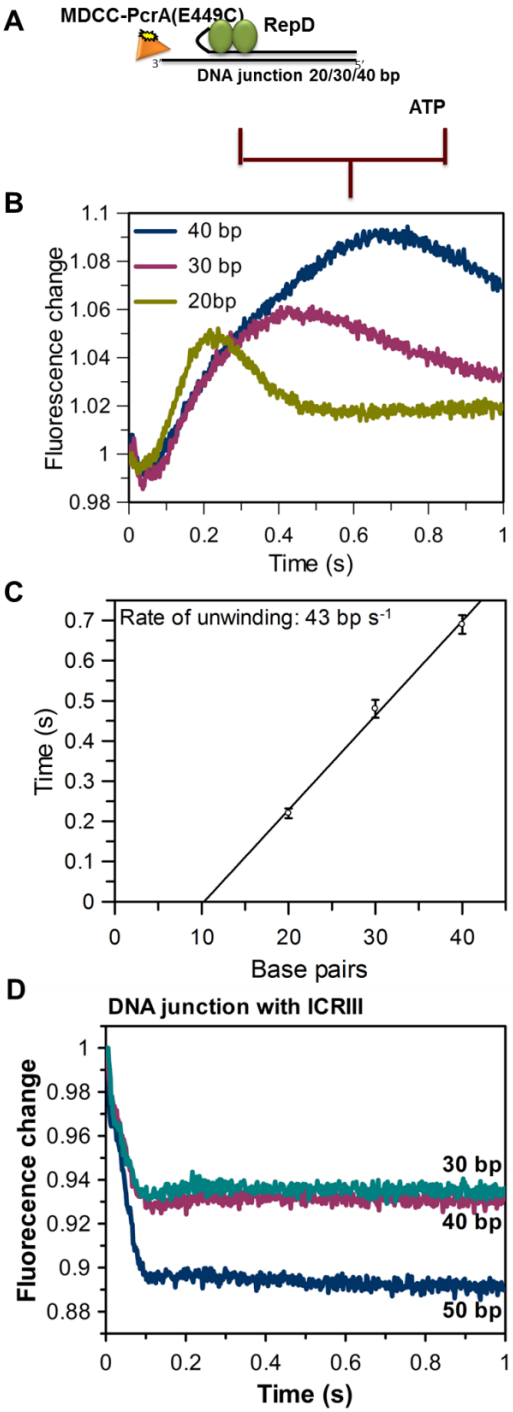

Figure 58. MDCC-PcrA(E449C) and DNA junction unwinding of DNA junctions without ICRIII.

A) Cartoon representation of the reaction. B) Normalised traces for three lengths of DNA junctions. C) Plot of duration of DNA unwinding against the number of bp in the DNA junction. D) DNA junction unwinding assay with DNA junction with ICRIII. The experiments were done at 30 °C in K200 by preforming the replication complex of 100 nM MDCC-PcrA(E449C), 500 nM DNA junction without ICRIII (20/30/40 bp) and 1 µM RepD before mixing with 200 µM ATP. The concentrations are final reaction concentrations. See DNA junction structure sequences in Figure 19. DNA junctions are unmodified and do not have ICRIII.

5.8.2. PcrA DNA junction unwinding is processive

A question often asked with DNA translocating enzymes is how processive they are. This means that how far they move on DNA before they dissociated or falling off. Often this can be followed by binding of another enzyme for example in case DNA unwinding several helicases maybe required for full unwinding of the DNA. The possibility to observe unwinding by labelled-PcrA opened up an opportunity to look into how processive is the DNA unwinding by PcrA. To test this, a competition assay was performed on the stopped-flow instrument. The assay was done by forming the unwinding complex of MDCC-PcrA(E449C)-RepD-DNA before the initiation of unwinding by mixing with ATP. The ATP was added together with high excess of wild type unlabelled PcrA. If the MDCC-PcrA(E449C) dissociates from the complex before end of unwinding, the unwinding signal should have a change in its fluorescence. The results showed that the MDCC-PcrA(E449C) that starts the unwinding is not replaced by wild type PcrA during unwinding and it continues without dissociating until the DNA junction is unwound (Figure 59). This could be concluded from the assay as no significant change was seen in MDCC-PcrA(E449C) DNA junction unwinding signal.

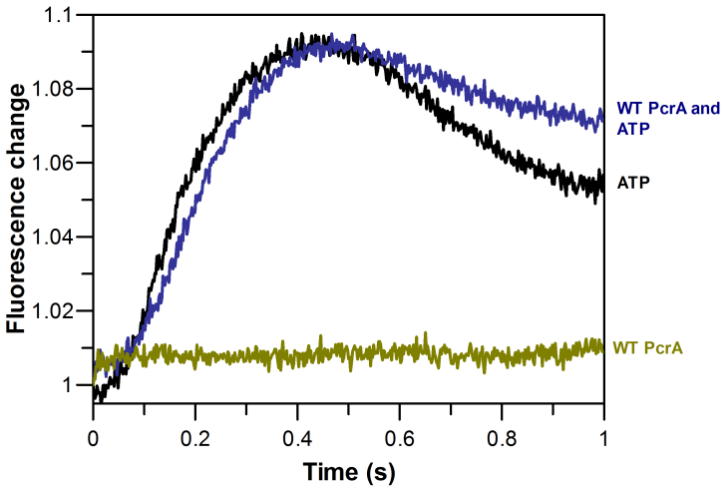

Figure 59. MDCC-PcrA(E449C) does not get displaced by unlabelled PcrA while unwinding DNA junction structures.

MDCC-PcrA(E449C) is pre-bound to RepD-DNA junction (no ICRIII) and then mixed with ATP (black), ATP and wild type PcrA (blue) or wild type PcrA (green). The unwinding of 30 bp DNA junction showed a peak 0.42 s in presence of unlabelled PcrA when it was ~0.4 s just with ATP.

5.8.3. MDCC-PcrA(E449C) and plasmid unwinding

As the MDCC-PcrA(E449C) showed a signal with unwinding linear DNA, the next step was to test whether the MDCC-PcrA(E449C) could be used to observe plasmid unwinding. Indeed, the unwinding of plasmid was observed using MDCC-PcrA(E449C) when it was mixed with RepD-plasmid complex and ATP (Figure 60). The signal had a ~10 s phase of small decreasing fluorescence before a phase with a large fluorescence increase. The cause for the decrease hasn't been determined, but it may be due to the PcrA binding to ATP and then to RepD-plasmid complex. The increasing phase duration varied with the length of the plasmid and presumably corresponded to the plasmid unwinding. This phase was followed by a decreasing phase, which may be dissociation of PcrA from DNA that is then bound by SSB. The end point of unwinding was determined as the time point of end of the second phase. This time point had the highest fluorescence. The time points for unwinding durations for different length plasmids were plotted against the length of the plasmids. The reciprocal of the linear fit gave an unwinding rate of 34.8 bp s^{-1} (average of two measurements). This corresponds well with the plasmid unwinding rate measured using DCC-SSB (Figure 27).

This assay required the presence of SSB. SSB may be preventing the re-annealing or it may be required for possible interaction with PcrA that facilitates processive plasmid unwinding. The peaks used to determine the end point of unwinding were broad and added some uncertainty to the determination of the end of unwinding. The broad peaks are most likely caused by the small proportion of plasmids that are unwound later than majority of plasmids. These plasmids have been nicked and re-ligated by RepD (lost supercoiling). RepD nicks relaxed plasmids at slower rate than supercoiled plasmids.

The fluorescence signal itself for the unwinding is unexpected as during the unwinding t the environment of the MDCC-PcrA(E499C) should

be relatively constant and the major changes in MDCC-PcrA(E449C) environment should be during initiation and termination of plasmid unwinding. One explanation for the unexpected unwinding phase signal would be that the SSB binds to the MDCC-PcrA(E449C) and once the plasmid is unwound SSB starts to bind the available ssDNA, which has higher affinity than to PcrA. This would release MDCC-PcrA(449C) into solution and would be observed as a constant increase in fluorescence until the plasmids are fully unwound. Another possibility would be that the MDCC-PcrA(E449C) is functioning similarly to DCC-SSB by having fluorescent increase when associating with ssDNA. This would require relatively large proportion of plasmid that is not unwound at all during the reaction as otherwise there would not be enough MDCC-PcrA(E449C) to cover the all the ssDNA produced from unwinding. This could be possible and could also explain the broad peaks as MDCC-PcrA(E449C) running out.

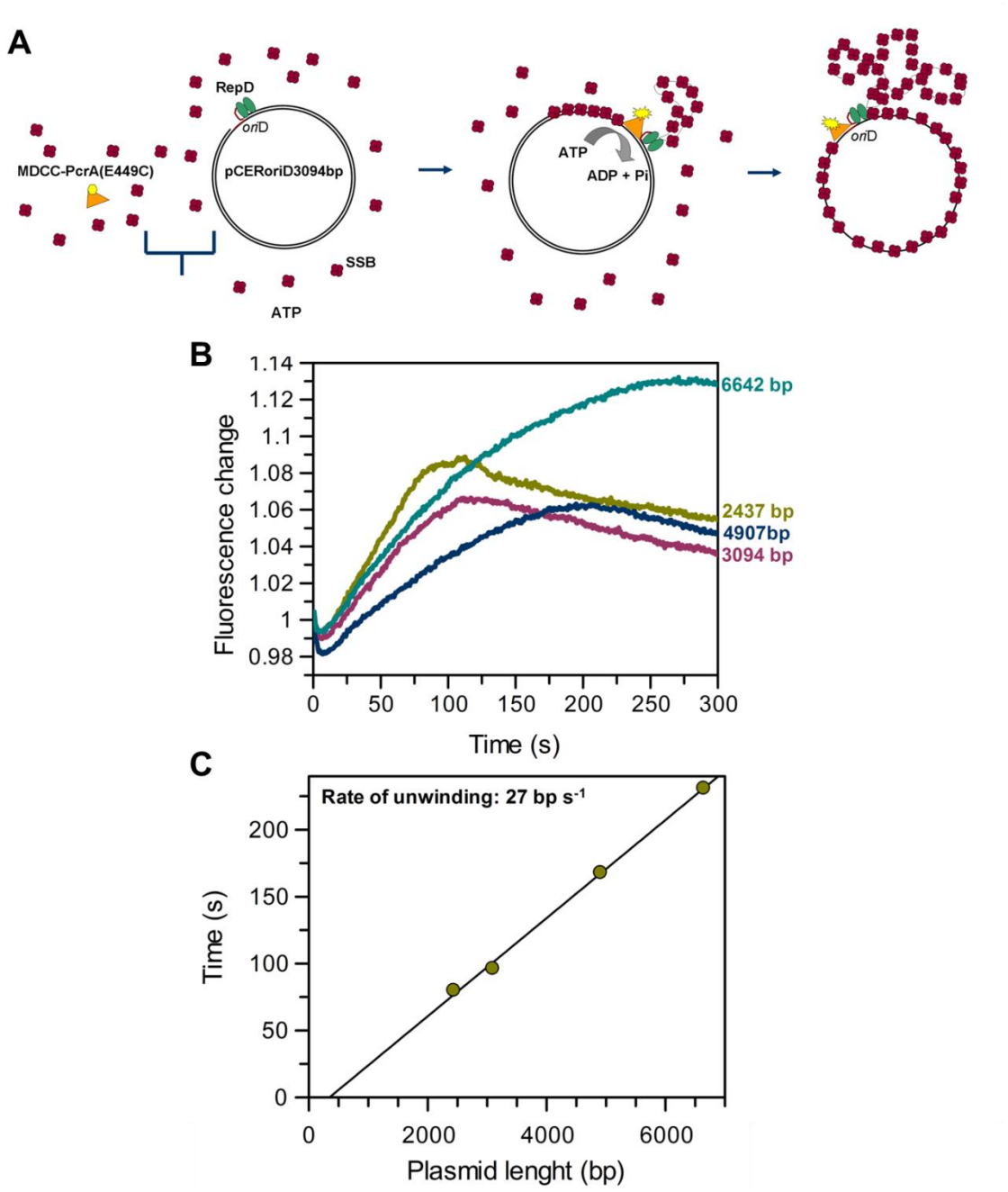

Figure 60. MDCC-PcrA(E449C) enables determination of PcrA unwinding rate on plasmid DNA.

A) Cartoon representation of the reaction. B) Individual normalised unwinding traces for four lengths of pCER*oriD* plasmid. C) The linear fit of time point of the end fluorescence increase against the number of base pairs on the plasmid enable determination of PcrA plasmid unwinding rate. The gradient of the linear fit is 0.00367 s bp^{-1}(SEM 0.0012). The experiments were done at 30 °C in K200 buffer with 30 nM MDCC-PcrA(E449C), 37.5 nM pCER*oriD* plasmid, 150 nM RepD and 1 mM ATP. All measurements had wild type SSB at 2-fold excess over the estimated number of possible SSB binding sites to fully unwound plasmid (SSB binding site ~65 bases and SSB binding to both strands). For example, fully unwound pCER*oriD* 3094bp would have maximum of 95 SSB bound to it (2.9 µM SSB in total reaction).

The MDCC-PcrA(E449C) plasmid unwinding assay was repeated without SSB with different length plasmids (Figure 61A). When SSB is left out of the plasmid unwinding reaction, the signal changes greatly and loses the phase the phase corresponding to plasmid unwinding. The first phase increasing phase is the initial binding of MDCC-PcrA(E449C) to the RepD-plasmid complex. The second increasing phase may be caused by more MDCC-PcrA(E449C) binding to ssDNA freed from plasmid unwinding ("functioning similarly to DCC-SSB"). This would explain why the second phase has same duration for all the plasmid lengths (MDCC-PcrA(E449C) concentration is constant). If signal would be related to the SSB binding, the phase duration should vary with the concentration of SSB, as it is increased with the plasmid length. The third phase is the MDCC-PcrA(E449C) running out seen as constant fluorescence. The fourth phase is likely to correspond to photobleaching of MDCC-PcrA(E449C).

The MDCC-PcrA(E449C) binding to RepD-plasmid complex in presence of wild type SSB showed a 14-fold decrease in amplitude (Figure 61B). This may be an indication that the SSB is blocking PcrA binding to RepD-plasmid complex or interacting with MDCC-PcrA(E449C) preventing it from binding to the RepD-plasmid complex.

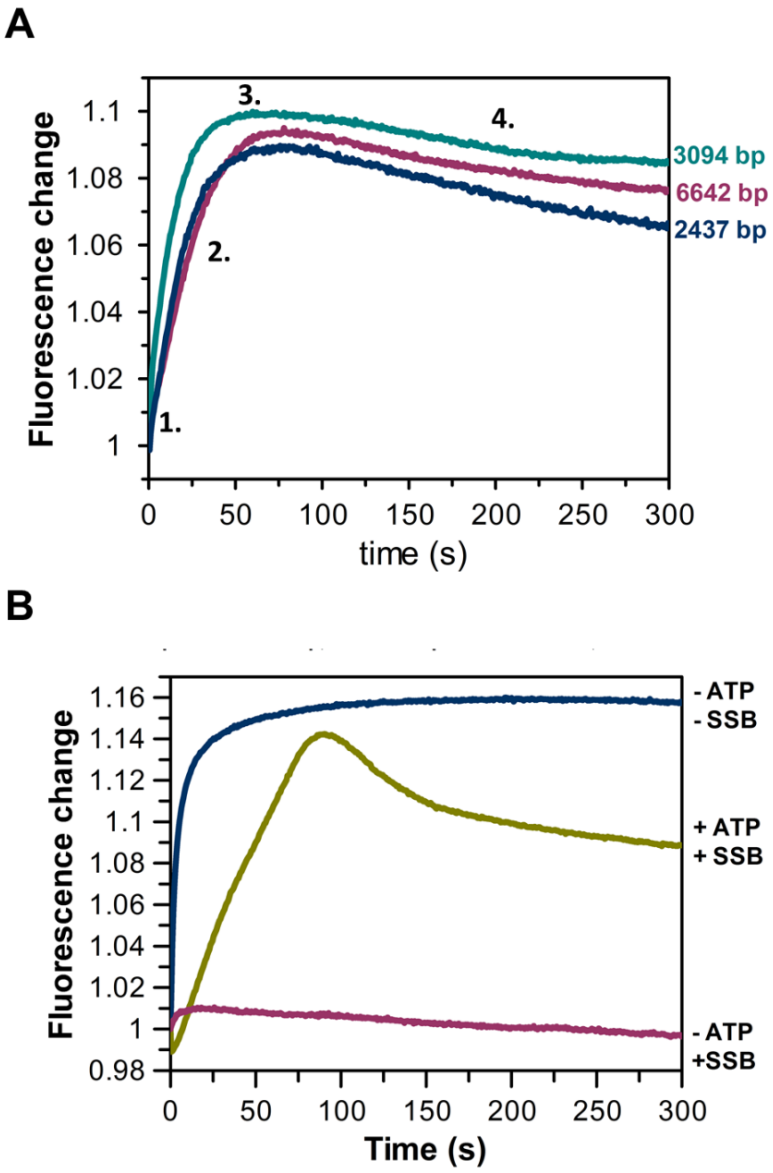

Figure 61. MDCC-PcrA(E449C) and plasmid unwinding signal.

A) When no SSB present in the plasmid unwinding reaction, no signal is observed corresponding to length of plasmid. B) SSB and ATP are required for plasmid unwinding signal with MDCC-PcrA(E449C), SSB seems block E449C binding when no ATP is in the reaction. The experimental conditions for the measurements were 30 nM MDCC-PcrA(E449C), 37.5 nM pCER*oriD* 2437/3094/6642bp, 150 nM RepD, +/- 1 mM ATP, +/- 200 nM SSB.

5.9. FRET signal with fluorophore labelled PcrA(E449C) and RepD(C225A, W310C)

Development of a FRET signal between PcrA and RepD would enable another method to study PcrA-RepD interaction. As FRET is distance and orientation dependent, a FRET signal between the two could provide information on how they interact and how the interaction changes during the plasmid unwinding. Labelling the PcrA(E449C) for FRET purposes was one of the first choices as it had shown the RepD-specific signal and the production of labelled RepD, MDCC-/Cy3-RepD(C225A, W310C) enabled the test for suitable FRET pairs between PcrA and RepD (Chapter 3). PcrA(E449C) and other PcrA mutants and RepD(W310C) have been labelled with several coumarin and Cy-dyes. Signals were observed with Cy3-PcrA(E449C) and Cy5-RepD(C225A, W310C) pair, but the highest signal was observed with MDCC-/Cy3-PcrA(E449C) and Cy3-/MDCC-RepD(C225A, W310C) pair. Figure 62 shows the measurements of emissions spectra of different combinations of labelled and unlabelled PcrA and RepD in complex with DNA junction 1. With unlabelled PcrA and Cy3-RepD exciting at 436 nm, a small Cy3 emission peak was observed at 570 nm. This emission peak from Cy3-RepD was increased almost by double when MDCC-PcrA(E449C) was in the reaction. The control where RepD is unlabelled has no peak at the 570 nm. These measurements indicate FRET transfer of energy from MDCC-PcrA(E449C) to the Cy3-RepD.

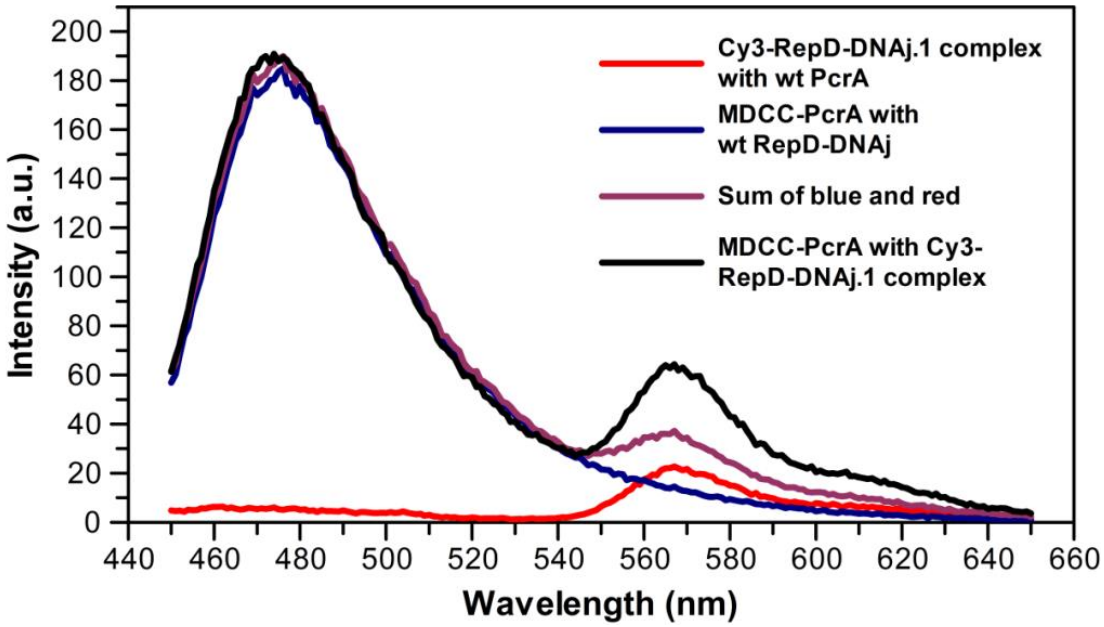

Figure 62. Emission spectra of MDCC-PcrA(E449C) and Cy3-RepD.

Black, emission spectra of MDCC-PcrA(E449C) mixed with Cy3-RepD bound to DNA junction 1 showing increase at 570 nm emission indicating FRET. Controls: Red, unlabelled PcrA and Cy3-RepD-DNA junction 1. Blue, MDCC-PcrA(E449C) and unlabelled RepD-DNA junction1. Conditions were 600 nM PcrA, 0.5 µM DNA junction 1 and 1 µM RepD. The excitation was done at 436 nm and the emission was measured from 450 to 650 nm. Measurements were done at 30°C in K200 buffer.

After identification of FRET signal between fluorophore-labelled PcrA and RepD, stopped-flow experiments were done to test PcrA binding to RepD-DNA junction complex with and without ATP (Figure 63). The fluorescent time courses were biphasic when ATP was not present. When ATP was added to reaction, the fluorescent time courses had a single phase of binding. This resembled the environmentally sensitive signal observed with MDCC-PcrA(E449C) (Sections 5.2. and 5.3.). The observed rate constants with FRET-labelled PcrA and RepD were also almost identical to the MDCC-PcrA(E449C) binding measurements (Figure 63 and Table 12). This indicated that the FRET signal was informative of same process as MDCC-PcrA(E449C) alone. The FRET-labelled PcrA and RepD were also tested on plasmid unwinding assay, but the signal was relatively weak and the measurements with FRET-labelled PcrA and RepD did not provide new evidence of PcrA function compared to environmentally labelled PcrA.

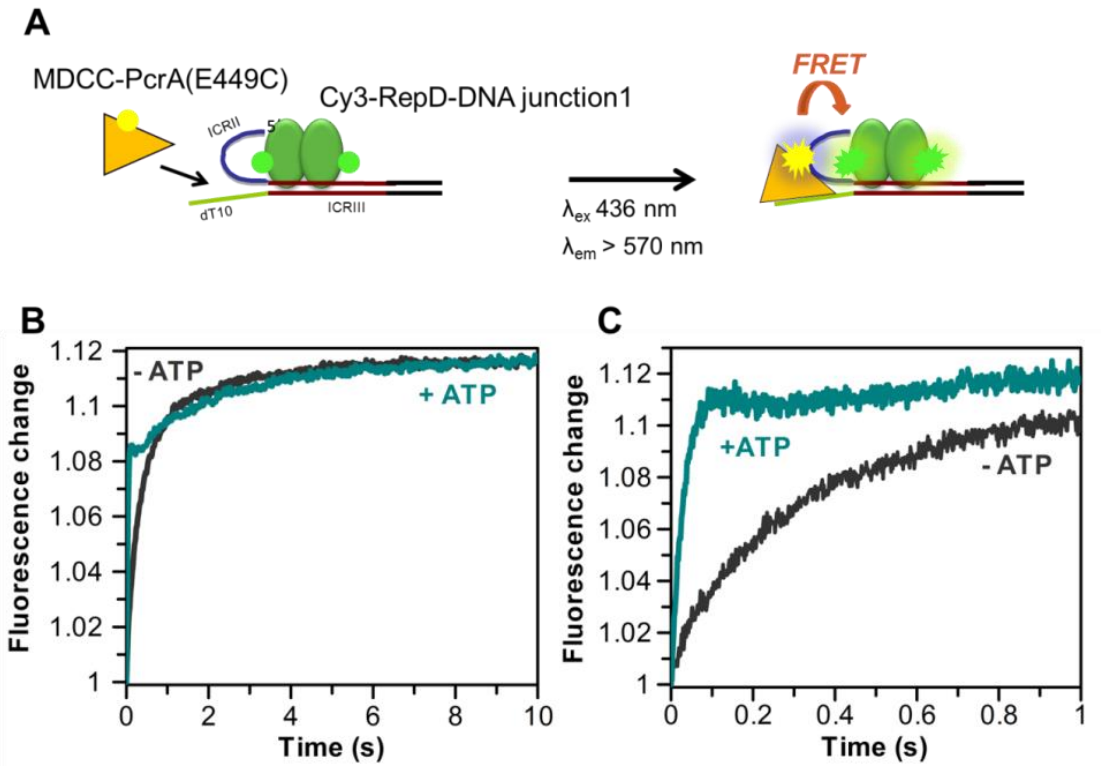

Figure 63. FRET signal on the stopped-flow with MDCC-PcrA(E449C) and Cy3-RepD.

A) Schematic illustration of the experimental set-up with the PcrA-RepD FRET pair. B) Normalised 10 s data traces with and without ATP. C) Normalised 1 s data traces with and without ATP. The traces without ATP were fitted to double exponential decay. The fast phase had observed rate constant (k_{obs}) of 4.2 s^{-1} and the slow phase of 1.3 s^{-1}. The traces with ATP were fitted single exponential and the k_{obs} was 40.2 s^{-1}. The measurements were done with 100 nM MDCC-PcrA(E449C), 0.5 µM DNA junction, 1 µM Cy3-RepD(W310C, C225A) and 200 µM ATP. Measurements were performed at 30 °C in K200 buffer. The excitation was done at 436 nm and the emission was measured using a 570 nm cut-off filter.

5.10. Discussion

RepD interaction with PcrA is a requirement for processive unwinding by PcrA [88]. Details of this interaction are not understood, but PcrA isn't able to unwind even short DNA duplexes by itself [87]. This improved unwinding does not require RepD nicking and covalent binding to DNA when unwinding DNA junctions (Figure 49), but its presence is still required [93]. The plasmid replication always requires the initiator protein RepD to make a single stranded nick on *oriD*, which opens up a single stranded stretch of DNA that PcrA may bind. RepD is thought to be interacting with the PcrA

throughout the plasmid unwinding, but how they interact and how RepD interacts with DNA remains unknown.

5.10.1. RepD interacts with PcrA at the 2B domain

The E447C, E449C, M450C and L453C locations on PcrA were chosen for fluorescent labelling for their location on the top of 2B domain, which is expected to be the closest site to RepD when PcrA binds to *oriD*. As a part of this project, every subdomain of PcrA has been labelled, but the RepD-specific signal has only been observed with the coumarin-labelled PcrA mutants that are labelled at the top of the 2B domain (Figures 45 and 46). This is strong evidence that RepD interaction domain on PcrA is the 2B subdomain. All the labelled mutants have also been tested for RepD-specific signal without DNA and all show no fluorescence change. This implies that the RepD and PcrA only interact when bound to DNA, but the fluorescent signals rely on environment change around the fluorophore. Therefore, the signals may well be dependent on the 2B subdomain rotation, which occurs on binding to DNA.

5.10.2. MDCC-PcrA(E449C) biphasic signal when binding to RepD-DNA

MDCC-PcrA(E449C) binding to RepD-DNA complex caused a 4 to 5-fold increase in fluorescence. The MDCC-PcrA(E449C) binding signal to RepD-DNA junction is biphasic when no ATP is present with both phases have concentration dependent rate constants, indicating two processes of binding. The fast phase had a higher rate constant and amplitude change than the second phase. The first phase was postulated to be the primary binding signal to RepD-DNA junction complex. Several assays were done to test what is causing the biphasic nature of the signal. These included changing the dT-arm length to which PcrA binds to test to see if two PcrA are binding on one arm and to assess the effect of arm length (Figure 48 and Table 9) and removal of RepD nicking site on the DNA junction (Figure 49 and Table 10). None of these assays removed the second phase. In fact,

they indicated that the biphasic signal is not caused by how RepD has formed the complex or that the signal is little affected by whether the RepD is covalently bound to DNA junction or not.

5.10.3. PcrA·ATP binding to RepD-DNA complex in one conformation

PcrA·ATP was shown to bind six-fold faster to RepD-DNA than PcrA without ATP (Table 11). This was shown with DNA junctions and with plasmid experiments using MDCC-PcrA(E449C). When ATP or non-hydrolysable ATP analogues were bound to PcrA to the binding to the RepD-DNA junction (Figures 50 and 52) had only a single phase. This has been the primary condition found where the biphasic signal of MDCC-PcrA(E449C) binding to the RepD-DNA junction complex is lost (Figures 45 and 50). There are two preferred explanations for the effect of ATP on PcrA binding, which are the ATP “locking” the PcrA into single conformation or the fast translocation to fork of RepD-DNA junction. The translocation may be so fast that it causes the loss of second phase. This is unlikely as the measurements with non-hydrolysable ATP analogues showed also a single phase indicating a single process of binding.

This makes the PcrA “locking” by ATP most likely explanation for the single binding mode as the ATP/ATP analogues “lock” PcrA in one conformation and so one form of binding is observed. Whereas when PcrA isn’t bound to nucleotide, it may be in two conformations at equilibrium (open and closed) even when binding to DNA. The locked conformation could be the 2B domain folding over 1B domain (closed conformation) facilitated by ATP. The nucleotide binding (AMPPNP) in crystal structure has been shown to cause a 30° rotational change in 1A and 2A domains, whereby they come closer together. This hypothesis is also supported by the experiments with dT_6-arm of DNA junction 1 that should enable only one PcrA to bind and have only one possible site of binding, still biphasic binding was observed indicating two forms of binding (Figure 48).

The ATP “locked” form of PcrA can also explain the increased binding rate with ATP to the RepD-DNA complex as it may higher affinity to RepD-DNA than the other PcrA conformation(s). Another possibility is the fast translocation to fork of RepD-DNA junction. When the dT-arm length was varied in presence of ATP the observed rate constant reduced with length of dT-arm. This could be because the PcrA that binds at distal end of dT-arm (3’ end) take longer to translocate to the fork junctions and lead to drop in the observed rate constant. Of course, it is possible that the increased k_{obs} of PcrA binding is due to both, as the ATP binding may lock the binding conformation increasing the PcrA affinity to the DNA/RepD-DNA, but at the same time the ATP hydrolysis enables translocation to the DNA fork junction.

A faster rate constant was observed with MDCC-PcrA(E449C) binding to the DNA junction only than when RepD is in complex with DNA junction, possibly indicating that the RepD may have some restrictive effect on the binding (Table 11). Though, the rate constant of PcrA binding to DNA junction can be expected to be higher as they have two ssDNA arms of 10 and 13 bases when no RepD is in the reaction. When DNA junction is covalently bound to RepD only one ssDNA arm is free for PcrA binding. As the binding to DNA junctions have binding rate constant, k_{on}, >30 μM^{-1} s^{-1}, which is five times the k_{on} of PcrA binding to RepD-DNA junction 1, this is unlikely to be the only factor affecting the binding. Hence, the effect must have something to do with the RepD.

5.10.4. PcrA affinity to RepD-DNA

Development of RepD-specific signal enabled the measurement of association and dissociation kinetics, which in turn enabled the determination of PcrA affinity to the RepD-DNA junction and RepD-plasmid complexes. The PcrA binding rate constant, $k_{on,}$ to DNA junction 1 was 6 μM^{1} s^{-1}. When the same assay was done with RepD-plasmid the k_{on} was 52 μM^{-1} s^{-1} for the pCER*oriD* 3094 bp. The k_{on} to pCER*oriD* 2437 bp was

lower at 15 μM^{-1} s^{-1}. This difference in the results could be anomalous even the experiments were repeated with two different plasmid preparations. But there are several possible explanations for the variation. First, the RepD-plasmid complex may be affected by the length of the plasmid and this could affect PcrA binding. Secondly, the different lengths of plasmids vary in sequence and PcrA may be binding these sequences differently. Thirdly, the proportion of the nicked relaxed versus supercoiled plasmid may vary between the plasmid preparations, which is not necessarily obvious on an agarose gel. The relaxed plasmids have been shown to be poor substrates for RepD nicking [93]. Lastly and possibly most likely, a factor that may affect the binding measurements is the proportion of ssDNA contamination in the plasmid preparations. PcrA binds very short ssDNA sequences and if any present, it will bind to it. Determination of ssDNA of less than 100 bases is complicated on an agarose gel, especially when one is determining the quality of plasmid of several thousand base pairs.

The dissociation kinetics of PcrA from RepD-DNA complexes were measured using the wild type PcrA displacement assay. The displacement assay indicated that second PcrA is able to bind to MDCC-PcrA(E449C)-RepD-plasmid complex before the MDCC-PcrA(E449C) dissociated and replaced by the unlabelled PcrA (Figure 57). The second phase of the traces was used to determine the k_{off}. The dissociation rate constant from RepD-plasmid complex for PcrA was 0.019 s^{-1} for the 3094bp plasmid and 0.017 s^{-1} for the 2437 bp plasmid. In other words, there is no significant difference between the dissociation rate constants between the plasmid lengths. This supports the idea that the k_{on} difference between 2437 bp and 3094 bp plasmids is caused by the quantity of RepD-plasmid complexes that is dependent on the quality of the plasmid preparation as the dissociation is independent of the RepD-plasmid complex concentration.

The dissociation rate constant for PcrA from RepD-DNA junction was measured as 0.16 s^{-1} (Table 15). The k_{on} and k_{off} enable the determination of the K_d, which were 0.4 nM for PcrA binding to the RepD-plasmid complex (3094 bp) and 26 nM for the RepD-DNA junction 1 (Table 15). This indicated

that PcrA affinity to RepD-plasmid is over 60 times tighter than to RepD-DNA junctions. This should be taken into consideration when using *oriD*-mimic junctions to study PcrA function, even though the availability of DNA junctions make them ideal substrates for PcrA assays compared to plasmids as they are hard to obtain at high concentrations required for excess over labelled PcrA on the stopped-flow apparatus. Measuring the dissociation of PcrA in presence of ATP was not done as it is complicated by the unwinding/translocation on ssDNA that may prevent the displacement.

5.10.5. Investigation of PcrA unwinding DNA using MDCC-PcrA(E449C)

MDCC-PcrA(E449C) signal with RepD-DNA was used to investigate PcrA unwinding DNA. This was tested on DNA junctions and on plasmid. When MDCC-PcrA(E449C) was loaded onto the RepD-DNA junction 30 bp (no ICRIII) complex and this was mixed ATP, a phase corresponding to DNA unwinding was observed. The rate of unwinding was determined to be ~43 bp s^{-1}, which is similar to what is observed with DNA junctions without ICRIII (Figure 58 and Table 3). Using the same assay with wild type unlabelled PcrA, the processivity of PcrA unwinding on DNA junctions could be tested (Figure 59). This showed that the PcrA that starts to unwind the short linear DNA is not displaced by unlabelled PcrA.

MDCC-PcrA(E449C) was used to develop an assay to look at PcrA unwinding full lengths of plasmid. The length dependent signal was only observed when SSB was in the reaction. The signal was more distinguishable when MDCC-PcrA(E449C) was mixed to complex rather than loaded on to the complex with before addition of ATP. The rate of unwinding was determined as ~30 bp s^{-1}. This is very similar what was observed with plasmid unwinding assay using DCC-SSB (Figure 27).

The requirement of SSB for plasmid unwinding signal with MDCC-PcrA(E449C) may be explained by the separation of component single stranded DNA that can be a requirement for processive unwinding. But other

possibilities exist to explain the signal. The signal may indicate that the SSB is required for activation of PcrA processivity. No evidence exists for this and this would the first indication for it. This is an interesting point for future experiments that could not be assessed here. Other helicases have shown to interact with SSB. For example, the Pri helicase involved in DNA replication restart in *E. coli* has been shown to interact with SSB and require interaction for unwinding activity [168]. Also, the DCC-SSB plasmid unwinding assay developed before to investigate PcrA uses SSB. Only the assays on short linear DNA are done without the presence of SSB and the interaction with SSB may be required for the processivity that is required for unwinding entire plasmid lengths of DNA.

The nature of the fluorescent signal in plasmid unwinding was unexpected as the phase of unwinding was constantly increasing in fluorescence. It can be expected that if the enzyme is preforming a constant function such unwinding a long length of DNA, the enzyme is staying at the same state. This in turn should mean that the environment of the fluorophore is not changing and so the process should be observed as constant fluorescence. This is not the case here. This opens a question of what is actually causing the signal. One possibility would be the MDCC-PcrA(E449C) binding to SSB in solution that would have a lower fluorescence state than when MDCC-PcrA(E449C) is free in solution. Once, the MDCC-PcrA(E449C) starts to unwind plasmid DNA the SSB starts to bind to ssDNA to which it has very high affinity. This would lead to constant increase in fluorescence until plasmid is fully unwound or all MDCC-PcrA(E449C) is free of SSB. The experiments assessing PcrA and SSB interaction using fluorescence such as FRET could possibly answer the questions raised from results observed here and could also involve use of assays such as analytical ultracentrifugation of PcrA and SSB with and without ssDNA.

A second explanation for the unwinding signal observed in MDCC-PcrA(E449C) plasmid unwinding assay is the possibility of MDCC-PcrA(E449C) functioning similarly to ssDNA biosensor (for example the

DCC-SSB). It may that when SSB is present free MDCC-PcrA(E449C) binds to increasing ssDNA together with the SSB. This could lead to constant increase in fluorescence until all the plasmid has been unwound. As the experiments were done with relatively high concentration of MDCC-PcrA(E449C) (30 nM) compared to plasmid (37.5 nM), the reaction could have proportion of free MDCC-PcrA(E449C) in the solution ready to bind ssDNA until the end of plasmid unwinding.

5.10.6. PcrA and RepD FRET pair

The PcrA(E449C) mutant was the first choice used to find a FRET pair between PcrA and RepD. The FRET signal was tested with Cy3 and C5 labels that would be suitable for single molecule FRET on TIRFM, but higher signal was observed with the MDCC and Cy3 labelled PcrA(E449C) and RepD(C225A, W310C). The emission spectra indicated very small drop in the donor fluorophore MDCC on PcrA, but this can expected when taking in account the MDCC-PcrA(E449C) signal when interacting with RepD-DNA. The acceptor (Cy3) emission increased in the presence of MDCC-PcrA(E449C), indicating FRET. MDCC-PcrA and Cy3-RepD were used on the stopped-flow measurements to test PcrA binding to RepD-DNA junction and in plasmid unwinding. The ensemble FRET measurements did not provide new information on PcrA function. Hence, the FRET labelled PcrA and RepD were not used in further experiments, but they do open up a possibility for development of new assays at single molecule level using TIRFM.

5.11. Summary

The signal from MDCC-labelled PcrA cysteine mutants binding to RepD-DNA has provided direct evidence for the location of PcrA and RepD interaction on PcrA surface. The signal was only observed with PcrA mutants that had fluorophores on the top of the 2B domain. The signal was present only when RepD was attached to DNA. The signal from MDCC-

PcrA(E449C) enabled the determination of its affinity to RepD-DNA junctions and RepD-plasmid complex showing that the actual PcrA affinity to RepD-plasmid complex is significantly tighter than to *oriD*-mimic junctions bound with RepD. The ATP makes the binding faster, possibly by “locking” the PcrA into one conformation that has a higher affinity to the DNA/RepD-DNA.

The plasmid and DNA junction unwinding assays have been developed using MDCC-PcrA(E449C) and confirm the previous observed results for rates of unwinding on DNA junctions and plasmids. FRET pair between PcrA and RepD were developed using PcrA E449C and RepD W310C location for labelling. These showed very similar observed rate constants to the MDCC-PcrA(E449C) signal when PcrA was binding to RepD-DNA junction complex, but could prove very useful in the future in single molecule assays.

6. Results – Individual PcrA molecules unwinding plasmid DNA

6.1. Introduction

In Chapters 4 and 5, the PcrA function and interaction with the plasmid unwinding complex was investigated using ensemble based methods. Here, a plasmid unwinding assay has been developed at single molecule on TIRFM to observe individual PcrA helicases unwinding full lengths of circular plasmids. This is important as the investigation of an enzyme such as PcrA at single molecule level may enable the observation of processes that are masked by the averaging in the ensemble assays. These include processes such as stalling, dissociation, re-starting and unwinding processivity. Single molecule assays can also show different populations of the enzyme or intermediate steps it takes not observable using other methods. For example, *in vivo* a helicase can be performing two processes that require two different rates, which are averaged in the ensemble unwinding assays. Also, single molecule assays can give clues to helicase unwinding termination and oligomeric state when unwinding DNA.

The single molecule plasmid unwinding assay on TIRFM was constructed very similarly to the ensemble DCC-SSB plasmid unwinding assay where the RepD-bound pCER*oriD* plasmid is unwound by PcrA hydrolysing ATP and detected by a ssDNA biosensor DCC-SSB [87, 89] (Figure 26). A similar assay has been used to measure helicases unwinding linear DNA [146]. Total internal reflection of light in TIRF microscope produces an evanescent field of ~100 nm in depth above the glass slide it is reflected from [148] The formation of this field is discussed in the Introduction, Section 1.8.1., and the TIRFM set-up used here is shown in Methods, Figure 21. By attaching the unwinding complex either through DNA or PcrA on the surface of a glass slide, the reaction occurs in the evanescent field, which allows the excitation of fluorophores without diffusion. In the single molecule plasmid unwinding assay, DCC-SSB was

replaced by Cy3B-SSB, which was excited with a green laser at 532 nm. Cy3B-SSB does not have large signal change when binding to ssDNA and the single molecule assay relies on the localisation of Cy3B-SSB at the fixed plasmid unwinding site. Synchronisation of the reactions is achieved by addition of ATP at the desired time.

Immobilisation of reactions to PEGylated surfaces can be achieved by use of biotinylated linear DNA, which is available commercially. The biotin can then be used to attach the DNA to avidins such as streptavidin linked to biotinylated polyethylene glycol (bio-PEG). The bio-PEG is added to the surfaces in a mixture with non-biotinylated PEG. The non-biotinylated PEG is used to block the surfaces for non-specific binding of molecules [143]. When large DNA structures are required, shorter oligos/DNA duplexes with biotinylation can be ligated into PCR products/lambda DNA or biotinylated primers can be used to amplify wanted DNA sequences. As plasmids are circular, the attachment of DNA is more complicated to achieve, but can be done by PCR amplification using primers with biotin modification (similarly to site-directed mutagenesis). Attaching circular DNA on a surface was not used here as the attachment may cause restriction to unwinding by pausing the complex at the site of attachment and also possibly only allow unwinding of the partial plasmid. Also, it is likely to prevent the natural termination and release of the plasmid. Hence, another option for attaching the plasmid unwinding reaction to the surface was used. This was done by immobilising the PcrA on the surface of the cover slide by making a biotin-modified PcrA described in Methods, Section 2.7.4. RepD was not used for immobilisation as it is a dimer and so would have two biotins on it, which may complicate the binding to the streptavidin and affect the observed plasmid unwinding. Using this method individual PcrAs were visualised unwinding full lengths of plasmid. This enabled the determination of individual PcrA unwinding rate and reveal new characteristics of PcrA function.

6.2. Immobilisation of biotinylated PcrA for single molecule assays

6.2.1. Biotinylated PcrA and Cy3B-PcrA(E449C)

The biotinylated PcrA was prepared by cloning a biotinylation peptide sequence to N-terminal end of the *pcrA* gene. The PcrA was then expressed together with a biotin ligase in presence of high concentration of free biotin. During expression, the biotin ligase ligates the biotin on to the biotin peptide sequence on PcrA. The expression and purification protocol is described in the Methods, Section 2.7.4., and checked for correct size and level of biotinylation using electro-spray mass spectrometry. The mass spectrometry showed single species at the molecular weight of 84 767.0 +/- 2 Da corresponding to expected molecular weight of bioPcrA. The biotinylation was highly specific as only singly biotinylated PcrA were observed on mass spectrometry without any non-biotinylated PcrA. This indicated that the biotinylation must have been close to 100%.

The E449C mutation was introduced to bioPcrA using site-directed mutagenesis to enable fluorophore labelling of bioPcrA with maleimide/iodoacetamide attached fluorophores. The biotinylated bioPcrA(E449C) was labelled with Cy3B-maleimide and checked for level of labelling and biotinylation by mass spectrometry and absorbance. Cy3B-bioPcrA(E449C) had molecular weight of 85 425.0 +/- 2 Da and a Cy3B-maleimide labelling percentage was measured using absorbance and it was 91%. The labelling of bioPcrA was desirable as this enable the observation of bioPcrA on the surface and possible development of FRET paired bioPcrA for single molecule FRET measurements on TIRFM. The E449 location was chosen as the coumarin-labelled PcrA(E449C) had a RepD-specific signal in the ensemble assays and has been used for development of FRET pair of labelled PcrA and RepD (Chapter 5).

The unwinding activity of the biotinylated PcrA and PcrA(E449C) was checked using an ensemble DNA junction unwinding assay (Table 3,

Chapter 3) and plasmid unwinding assay (Experimental set-up, Figure 26), as previously described. Figure 64 shows the traces for bioPcrA and wild type PcrA unwinding pCER*oriD* 2437 bp. The breakpoint of unwinding was ~110 s for both, the bioPcrA and the wild type PcrA. This confirms that the unwinding function of PcrA is unaffected by the biotinylation.

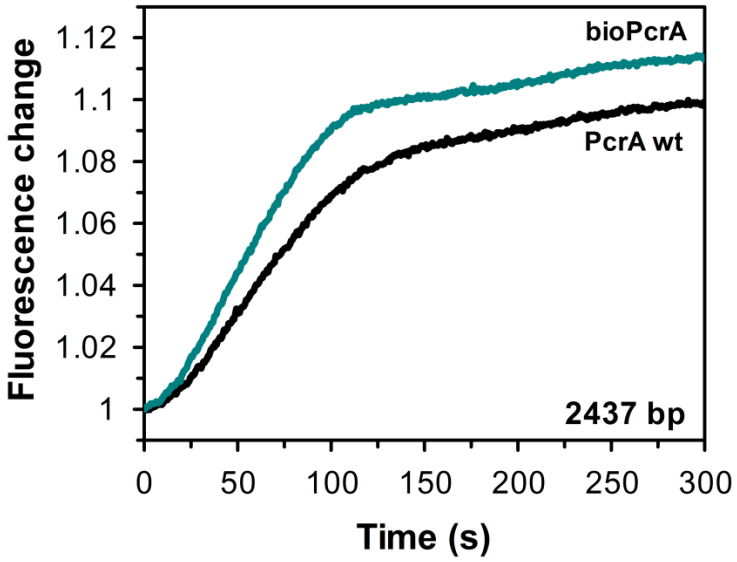

Figure 64. DCC-SSB plasmid unwinding assay of bioPcrA and wt PcrA.
The experimental conditions were same as in Figure 27.

The unwinding activities of Cy3B-bioPcrA(E449C) and bioPcrA were confirmed by the DNA junction unwinding assay at single molecule assay conditions and at ensemble assay conditions (Figure 24, Chapter 3). The normal assay condition for DNA junction unwinding assay is 30 °C in K200 buffer. At these conditions, the rate of unwinding of DNA junctions by bioPcrA and Cy3B-bioPcrA(E449C) was ~50 bp s^{-1}. This is similar to wild type PcrA (Table 3, Chapter 3). Under single molecule assay conditions, the DNA junction unwinding was done at 22 °C in TIRF buffer and the results were compared to wild type PcrA activity at the same conditions. The single molecule conditions were used to ensure that Cy3B-bioPcrA(E449C) was still an active helicase. The unwinding rate at single molecule assay conditions was 23.5 +/-7.5 bp s^{-1} for the wild type PcrA and 24.4 +/-0.5 bp s^{-1} for Cy3B-bioPcrA(E449C). This is half of the rate of unwinding in K200 buffer at 30 °C, but this is not surprising as lower the temperature is

expected to lower the enzyme V_{max}. These assays indicate that the biotinylation peptide, the biotin, the cysteine mutation, and the labelling do not significantly affect the PcrA unwinding activity of Cy3B-bioPcrA(E449C) when compared to the activity of the wild type PcrA. Therefore, it can be used reliably to investigate PcrA function in plasmid unwinding.

6.2.2. PcrA and biotinylated PcrA are monomers in solution when applied to surface of PEGylated TIRFM flow cells

PcrA is thought to function in DNA unwinding as a monomer, but there is no conclusive experimental confirmation for this. PcrA crystallises as a monomer in apo and DNA/substrate-bound forms and most of the biochemical evidence is consistent with the hypothesis that is active as a monomer on ssDNA [21, 22], but some suggestions of PcrA oligomerisation have been made [37]. Closely related helicases, UvrD and Rep from *E. coli*, require oligomerisation for processive unwinding [38, 39]. UvrD can exist as a monomers, dimers or tetramers in solution, but require dimerisation to unwind DNA, even though UvrD crystal structure with DNA junction shows UvrD as a monomer [19, 39]. Rep helicase is monomeric in solution and can bind ssDNA as a monomer, but requires dimerisation for active/processive unwinding [138, 169]. The definite proof of PcrA monomeric activity has been hard to obtain as most assays are only able to indicate dimerisation/oligomerisation. Some assays have been attempted such as the gel filtration where PcrA oligomeric state was tested with DNA and RepD [170]. In the assay PcrA was monomeric, but inability to observe oligomers in solution or without ATP does not exclusively prove that PcrA is not dimeric at certain conditions. For example, PcrA could dimerise when binding to certain length ssDNA or when coming to a fork junction and this could require presence of ATP. The interaction with other proteins or change in conditions such as salt concentration may also facilitate dimerisation.

As the subsequent plasmid unwinding experiments are done with surface immobilised PcrA, it is important to investigate if bioPcrA is bound to surface as a monomer or dimer. This also confirms whether the plasmid

unwinding is performed by monomeric or dimeric PcrA. Also, the correct interpretation of the results is dependent on the knowledge of PcrA oligomeric state.

First, the PcrA oligomeric state in solution was studied using size exclusion chromatography-multiangle light scattering (SEC-MALS). Running a protein on SEC-MALS provides information about the molecule weights of the complexes. Size exclusion chromatography is informative of protein oligomeric or complex state, if run in ideal buffering conditions for the protein or complex in question and provides evidence about the protein oligomeric state and possible aggregation. Figure 65 shows the results for the SEC-MALS carried out for the wild-type PcrA and bioPcrA at the micromolar concentrations used, wild-type and the bioPcrA do not form dimers or oligomers in solution. This provides further evidence to PcrA existence as monomer.

In the subsequent single molecule assays, the bioPcrA is applied to streptavidin in solution at low concentrations without presence of DNA or RepD. According to SEC-MALS results PcrA should bind to streptavidin as a monomer and perform plasmid unwinding in the single molecule assays as a monomer. This in part address the question of PcrA oligomer state being a monomer, as the single molecule assay designed here involves bioPcrA immobilisation to the surface before addition of other plasmid unwinding components, the PcrA should be attached as a monomer on the surface and when unwinding is observed, this can only be by the monomeric PcrA.

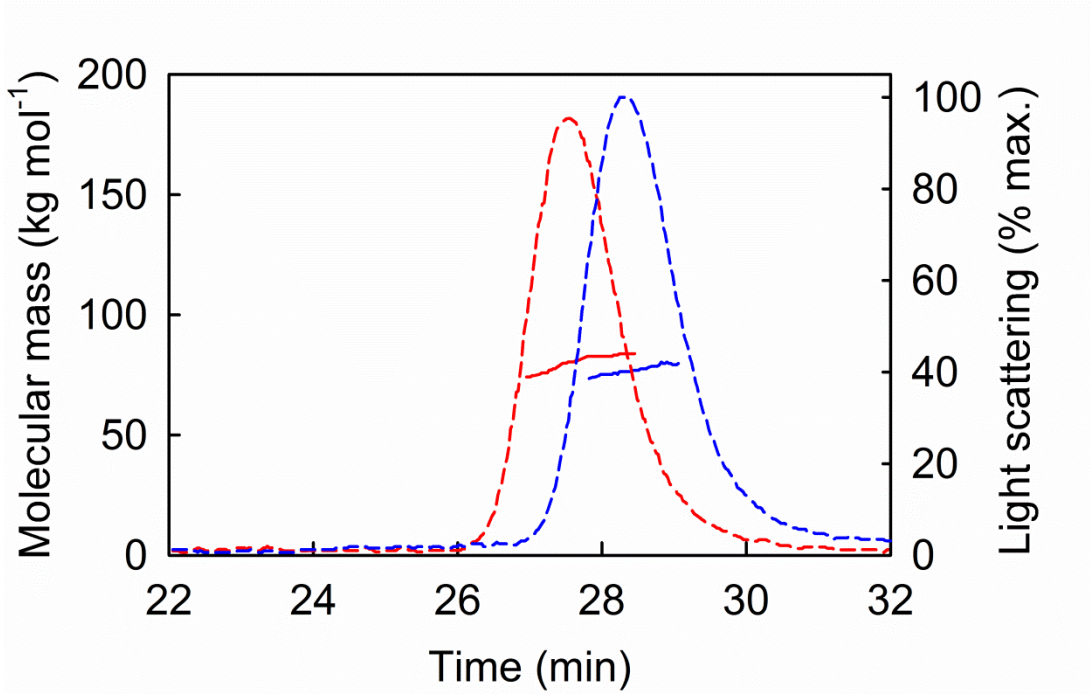

Figure 65. SEC-MALS of bioPcrA and wild type PcrA.

Red. bioPcrA. Blue, wild type PcrA. Solid horizontal lines indicate the molar masses of proteins and the dashed lines are the percentage of light scattering.

6.2.3. Biotinylated PcrA surface density on PEGylated and streptavidin treated surface

Cy3B-bioPcrA(E449C) enabled the observation and quantitation of the helicase on the surface of the flow cell using TIRFM and gave information about the correct working concentration in subsequent unwinding measurements. Density measurements could show the concentration at which the surface is saturated and give indication on the quality of the surfaces. Cy3B-bioPcrA(E449C) was applied to surfaces using standardised method by where aminosilane treated cover slips were PEGylating with NHS ester–PEG to prevent any unwanted surface absorption [111, 143]. The PEGylation was done with mixture of PEG and biotin-PEG to enable attachment of biotinylated PcrA on to the surface using streptavidin, which binds to the biotin on surface and the biotin on PcrA.

The density of Cy3B-bioPcrA(E449C) on the surface was measured as a function of concentration in the applied solution. The Cy3B-bioPcrA(E449C) was exposed to laser light until the fluorophores had

photobleached (the photobleaching assay). The number of spots detected increased with the Cy3B-bioPcrA(E449C) loading concentration (Figure 66 from 0.01 nM to 0.2 nM). The increase was linear (Figure 67). The results were analysed using the GMim Pro programme, Automatic Single Particle Tracking (ASPT), which tracks fluorescent objects in a xy-plane [160]. The analysis of spots is described in detail in Methods Section 2.17.3. When the fluorescent objects are detected using ASPT, they do not need to have a change in fluorescence to be detected. Hence, for analysis of single or complied frames, ASPT was used as it can detect constant still fluorophores and objects on individual frames.

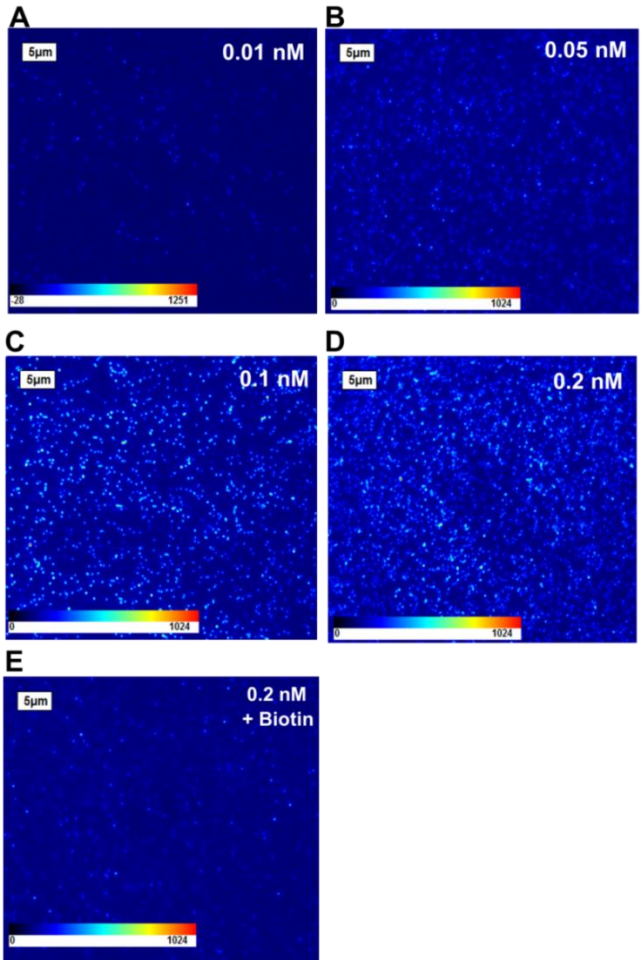

Figure 66. Observation of individual Cy3B-bioPcrA(E449) on TIRFM.

Cy3B-bioPcrA(E449C) was applied to surfaces at 0.01 nM (A), 0.05 nM (B), 0.1 nM (C) and 0.2 nM (D) concentrations. The application of Cy3B-bioPcrA(E449C) at 0.2 nM was also done with 9 µM biotin as control of binding of biotin to streptavidin (E). The surface preparation and Cy3B-bioPcrA(E449C) surface attachment protocols are given in Methods, Section 2.17.3.

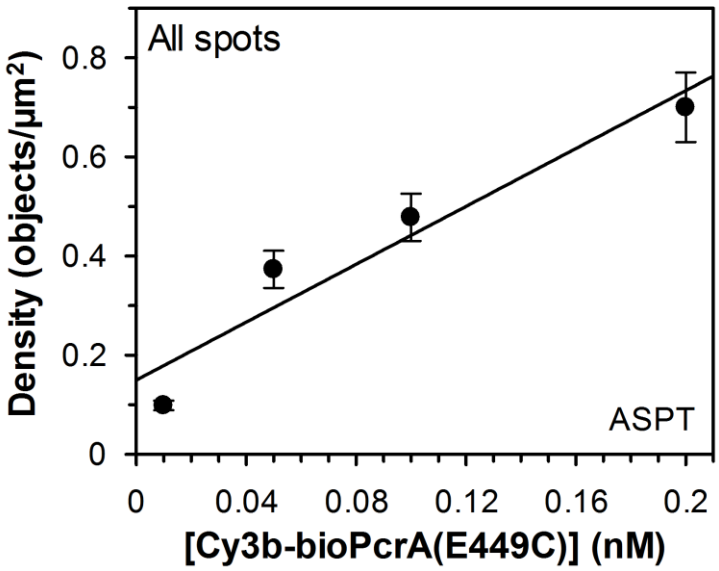

Figure 67. Linear increase of Cy3B-bioPcrA(E449C) object numbers at loading concentration up to 0.2 nM.

Spots tracked by ASPT analysis was done to the sum of 3 first frames of the record. The gradient for ASPT density increase: 2.92 objects per µm^2 per nM of Cy3B-bioPcrA(E449C) (SEM 0.61).

In other set of experiments, the Cy3B-bioPcrA(E449C) was loaded on the PEGylated streptavidin treated surfaces at concentrations from 0.1 nM to 2 nM (Figure 68). The background of the surfaces increased significantly from ~150 at 0.1 nM to ~600 at 2 nM. This indicates saturation of the fluorescence on the surface at higher Cy3B-bioPcrA(E449C) loading concentration.

The method used for the analysis at the higher Cy3B-bioPcrA(E449C) concentrations (>0.5 nM) was unable to detect correctly the number of spots. Figure 69A shows the plot of objects against time for 2 nM Cy3B-bioPcrA(E449C) indicating clear saturation of the surface. At the beginning of the record the number of objects cannot be detected accurately by the ASPT detection. Hence, another method of spot estimation was taken into use, which enabled the calculation of object density at the beginning of the record. On the records where all the fluorophores were photobleached, the number of objects were detected using the ASPT at different time points. These object numbers were plotted against time and fitted with a single

exponential. This enabled the extrapolation of the curve to obtain the number of objects on the first frame at zero time. Figure 99 in Appendix shows and describes the fitting method. Table 16 summaries the number of objects on the surface extrapolated from the fit and Figure 69B shows the linear fit done to the object density versus Cy3B-bioPcrA(E449C) loading concentration plot. The density of objects increases linearly with the Cy3B-bioPcrA(E449C) loading concentration. These results indicate that at least up to 2 nM of Cy3B-bioPcrA(E449C) no significant saturation of streptavidin by the Cy3B-bioPcrA(E449C) is observed by bioPcrA even the fluorescent signal of the field of view has been saturated.

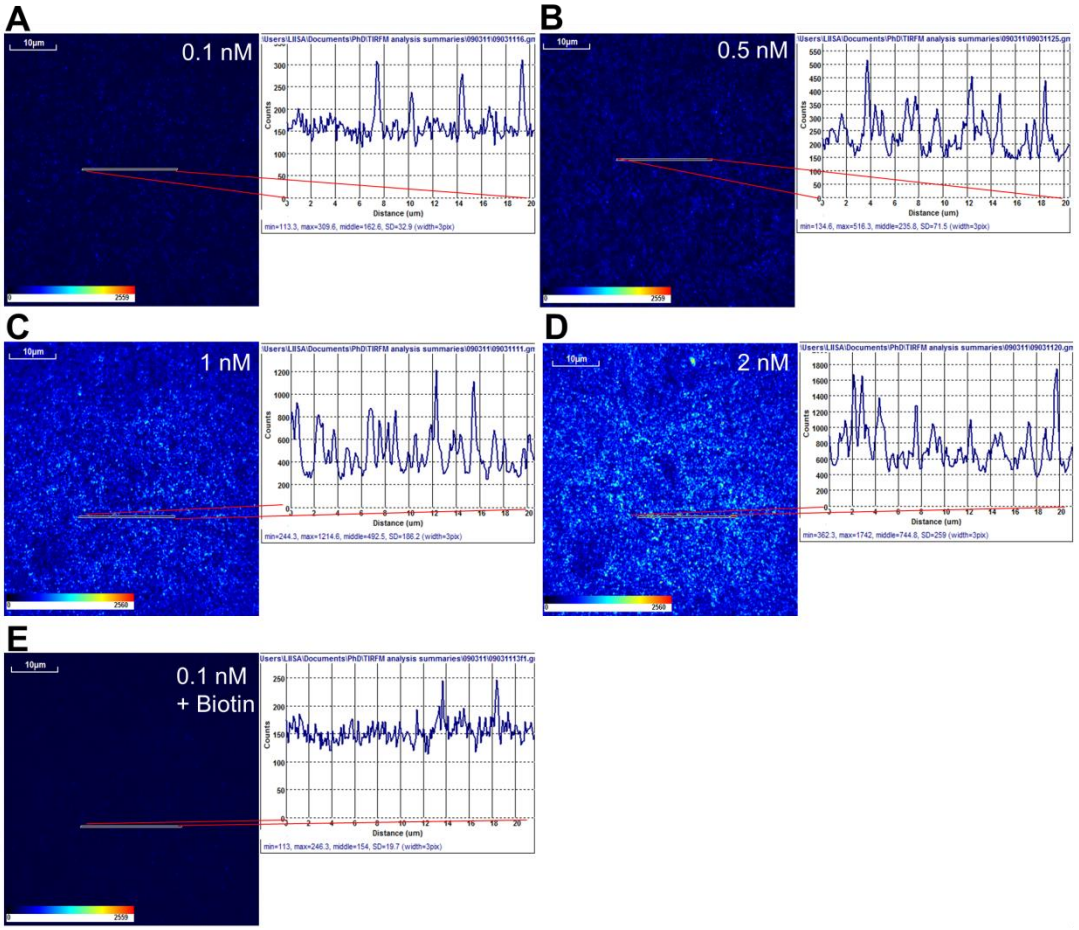

Figure 68. Cy3B-bioPcrA(E449C) on the flow cell surface.

The Cy3B-bioPcrA(E449C) was applied to surfaces at 0.1 nM (A), 0.5 nM (B), 1 nM(C) and 2 nM (D) concentrations. The application of Cy3B-bioPcrA(E449C) at 0.1 nM was also done with biotin block as a control (E). Once, 9 µM biotin was incubated together with 0.1 nM, the ASPT analysis of field of view detected an average of 26 objects. Whereas, without biotin this was 1127 objects at the same Cy3B-bioPcrA(E449C) loading concentration.

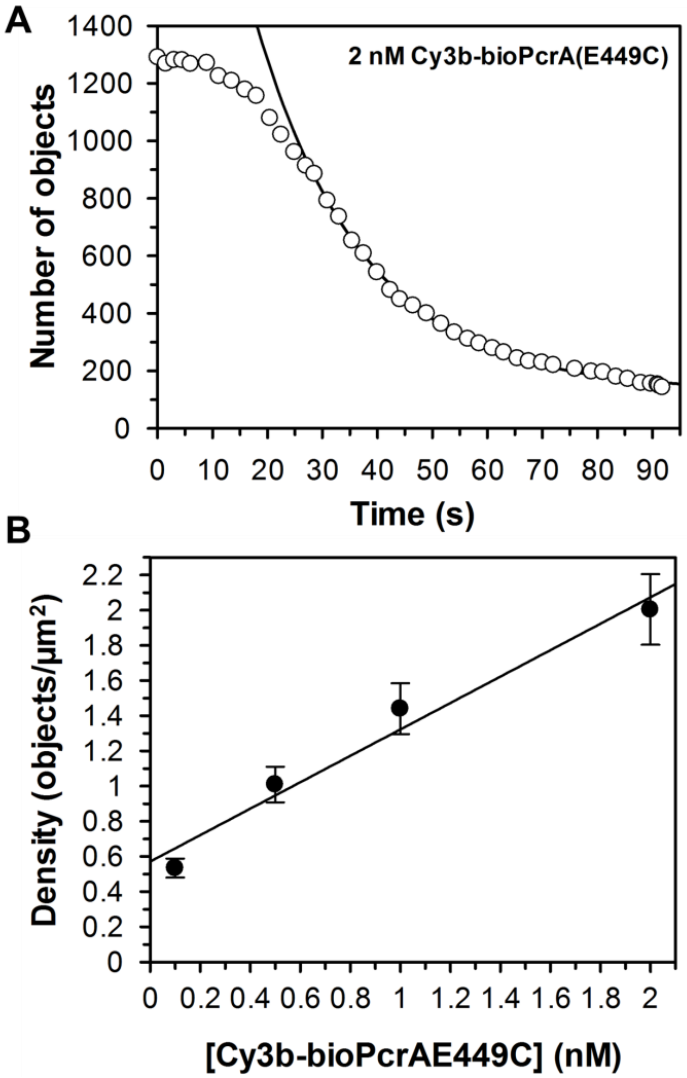

Figure 69. The relationship between ASPT objects count and fluorescence intensity.

A) Spot density of 2 nM Cy3B-bioPcA(E449C) during the photobleaching record. At higher concentrations ASPT was unable to detect individual objects due to their overlap and this was observed as saturation of number of events counted at the beginning of record. The single exponential fit was done from 30 s onwards till end record and shown as black line. The single exponential decay has rate constant of 0.051 s^{-1} for 2 nM Cy3B-bioPcrA(E449C) and the number of objects (y-intercept) is 3180.2 (SEM 138.7) on area of 1394 μm^{-2}. This has a density of 2.23 objects per μm^2. B) Cy3B-bioPcrA(E449C) density relationship with varying loading concentration of Cy3B-bioPcrA(E449C) determined using extrapolation of spots from photobleaching records. The linear fit has a gradient of 0.75 objects μm^{-2} per nM (SEM 0.093).

[Cy3B-bioPcrA(E449C)] (nM)	Number of objects	Density (objects/μm^2)
0.1	962.5	0.53
0.5	1817.1	1.01
1	2592.7	1.44
2	3607.2	2.00

Table 16.Cy3B-bioPcrA(E449C) object density at saturating concentrations.

The fit to determine the y-axis (the number of objects on the surface at frame 1) was done using fixed rate constant (k_c) determined from intensity decay of whole field of view. Data is an average of two records from two experiments. The number of objects was calculated on area of 1800 μm^2. The fitting is shown in Appendix, Figure 99.

6.2.4. Biotinylated PcrA is a monomer on the surface of the glass coverslip

The SEC-MALS experiments showed that PcrA and bioPcrA are monomers in solution and when applied to the flow cell surface, but as streptavidin has four possible binding sites, it could in principle facilitate binding of up to three PcrAs when surface bound. These PcrAs might function together as a dimer or as a monomer on same DNA molecule. Hence, photobleaching experiments were designed using Cy3B-bioPcrA(E449C). For other biological systems, photobleaching experiments at single molecule level on TIRFM have been successfully used to observe the oligomeric state of proteins *in vitro* and in cell cultures [137, 146, 171, 172]. The accuracy of the measurements is dependent on the resolution of TIRFM (~100 nm) and the spread of molecules [173-175].

In photobleaching measurements, the Cy3B-bioPcrA(E449C) or Cy3B-SSB was attached to streptavidin treated surface through biotin in low concentration (below 0.2 nM for Cy3B-bioPcrA(E449C)) to provide individual

spots. These were then viewed under TIRFM and exposed to laser light long enough to photobleach the fluorophores. If the protein was an oligomer, multiple step photobleaching would be observed corresponding to number of fluorophores on the protein. For example, for tetrameric SSB, this was four photobleaching steps [146].

Here, all the photobleaching records at <0.2 nM Cy3B-bioPcrA(E449C) were analysed by SFDA that looks for instant fluorescence decreases, caused by the photobleaching of the fluorophore and called “drops”. The detection of the number of photobleaching steps provides information about the oligomeric state of Cy3B-bioPcrA(E449C). To measure photobleaching steps accurately, the loading of Cy3B-bioPcrA(E449C) had to be at concentrations where only single fluorophores were observed. Figure 70 show an example of spots with multiple photobleaching steps and those with single photobleaching steps. Very few spots with multiple step photobleaching were observed with all concentrations tested from 0.01 nM and 0.2 nM of Cy3B-bioPcrA(E449C). The results for photobleaching Cy3B-bioPcrA(E449C) at various concentrations are given in Table 17 and Figure 71. At all loading concentrations of 0.2 nM and below, over 90% of the spots showed only a single photobleaching step.

When the records with higher loading concentrations of Cy3B-bioPcrA(E449C) were analysed using SFDA tracking, the density at loading concentration of 0.5 nM Cy3B-bioPcrA(E449C) was ~1.8 objects μm^{-2} for single step photobleaching and 0.14 spot μm^{-2} for objects with multiple step photobleaching. This means that at maximum less than 15% of the spots showed multiple step photobleaching. The results clearly indicate that most spots visualised on surfaces are single PcrA molecules and hence PcrA is bound to streptavidin as a monomers. This is important as the loading concentrations used for plasmid unwinding assay were 0.2 and 0.5 nM.

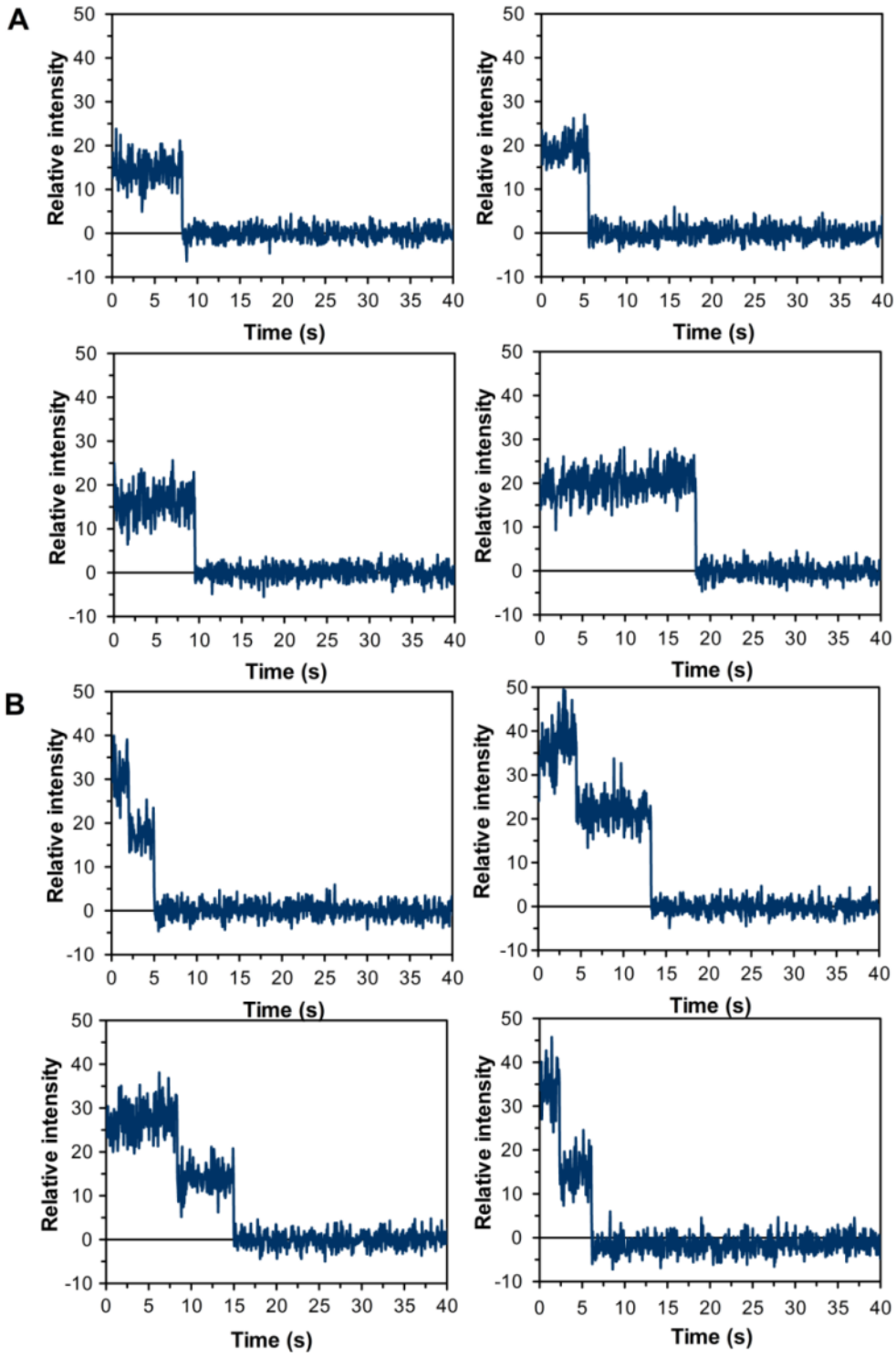

Figure 70. Cy3B-bioPcrA(E449C) photobleaching steps at constant laser power.

A) Examples of spots with single step photobleaching. B) Examples of spots with double step photobleaching. The Cy3B-bioPcrA(E449C) photobleaching examples are from record with 0.1 nM Cy3B-bioPcrA(E449C) in TIRF buffer without oxygen scavenger at laser power ~2.5 mW. The loading of Cy3B-bioPcrA(E449C) was done as described in Methods, Section 2.17.3., and the objects were tracked using SFDA for the entire length of the record.

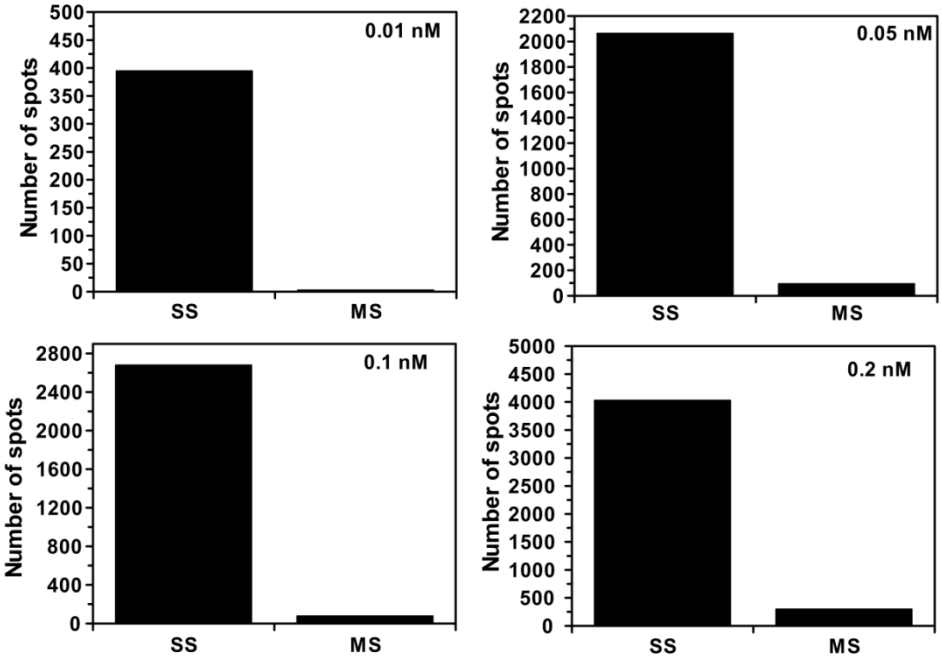

Figure 71. Cy3B-bioPcrA(E449C) is a monomer on the surface of the flow cell.

The loading of Cy3B-bioPcrA(E449C) was done as described in Methods, Section 2.17.3., and the objects were tracked using SFDA for entire record. (SS, single step photobleaching. MS, multiple step photobleaching).

[Cy3B-bioPcrAE449C)] (nM)	Total number of objects	Single step	Multiple step	Objects with steps (average)	Single step (average)	Multiple step (average)	Single step photobleaching (%)	Objects with decrease/μm^2	Current (A)
0.01	253	179	3	338.5	197.5	1.5	99.2	0.19	0.3
0.01	424	216	0						0.6
0.05	985	705	35	971.7	688.3	31.7	95.6	0.54	0.3
0.05	950	796	17						0.3
0.05	980	564	43						0.6
0.1	1675	954	7	1308.3	893.3	26.0	97.2	0.73	0.3
0.1	1085	936	25						0.3
0.1	1165	790	46						0.6
0.2	2121	1713	115	2003.0	1343.7	99.7	93.1	1.11	0.3
0.2	2287	1293	25						0.3
0.2	1601	1025	159						0.6

Table 17. Summary of photobleaching results of Cy3B-bioPcrA(E449C) on TIRFM.

The loading of Cy3B-bioPcrA(E449C) was done as described in Methods, Section 2.17.3., and the objects were tracked using SFDA for entire record. The area used for analysis is 1800 μm^2.

6.3. Individual PcrA helicases unwinding plasmid DNA, detected by TIRFM

6.3.1. Unwinding assay on TIRFM with pCER*oriD* 3094bp plasmid

The surface-bound PcrA enabled the development of single molecule plasmid unwinding assay where individual PcrA helicases, unwinding full lengths of plasmid, could be measured in real time (Figure 72). As the bioPcrA could be visualised using Cy3B-fluorophore, prior to unwinding, a relatively high control over focus could be achieved. This is important as the addition of ATP causes slight movement of the coverslip and could cause loss of information if not corrected accurately. The single molecule plasmid unwinding assay was done by loading bioPcrA at 0.2 or 0.5 nM. To this the RepD-plasmid complex was added. The reaction was initiated using ATP on TIRFM in presence of Cy3B-SSB, oxygen scavenger and ATP regenerator.

The single molecule plasmid unwinding measurements showed a large difference in the number of bioPcrA on the surface compared to how many actual unwinding events were observed. Therefore, most of the measurements have been done with 0.5 nM Cy3B-bioPcrA(E449C).

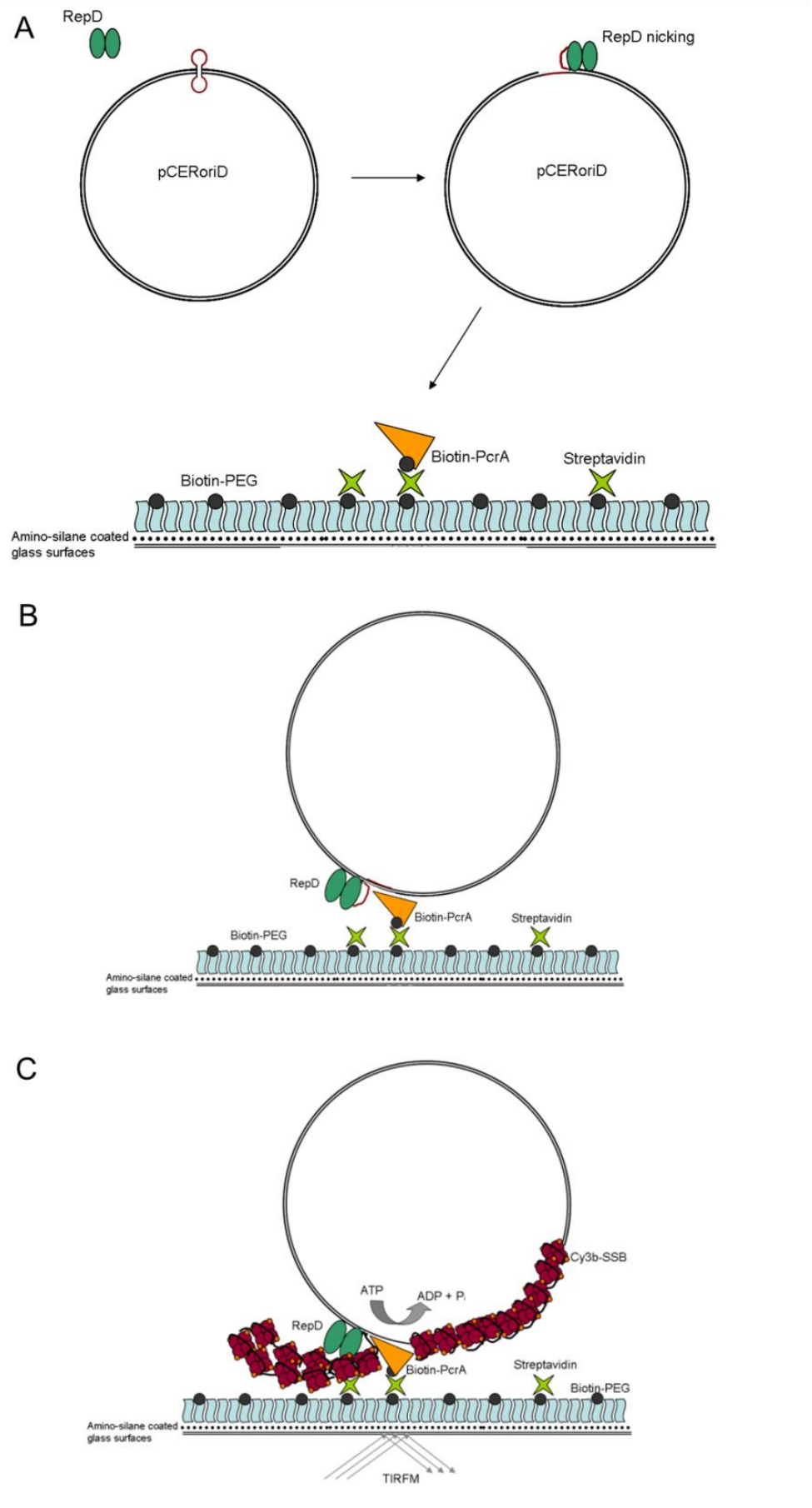
A
RepD
RepD nicking
pCERoriD
pCERoriD
Biotin-PcrA
Streptavidin
Biotin-PEG
Amino-silane coated glass surfaces
B
RepD
Biotin-PcrA
Streptavidin
Biotin-PEG
Amino-silane coated glass surfaces
C
Cy3b-SSB
ATP
ADP + Pi
RepD
Biotin-PcrA
Streptavidin
Biotin-PEG
Amino-silane coated glass surfaces
TIRFM

Figure 72. Plasmid unwinding assay visualised on TIRFM.

A) Biotinylated PcrA is bound to glass surface using streptavidin. The RepD-plasmid complex is formed before applying on the bioPcrA. B) RepD-plasmid complex is then added to surfaces and will bind PcrA. C) The unwinding is initiated by addition of ATP. Once, PcrA unwinds the plasmid the amount of ssDNA increases to which Cy3B-SSB binds. This leads to gradual localisation of SSB on the surface that is observed as a spot with increase in fluorescence.

This assay was done with different length plasmids, but the starting point was the 3094 bp plasmid. Previous helicase unwinding assays on TIRFM using linear DNA had showed that the DNA lengths up to 1.5 kb remained in the evanescent field [146]. Therefore, the 3094 bp plasmid could be expected to remain in evanescent field throughout the unwinding. Figure 73 shows individual Cy3B-bioPcrA unwinding this plasmid over 90 s. The intensity of certain spots increase over time after addition of ATP and Cy3B-SSB, and these events are the actual plasmid unwinding events. Figure 74 shows control experiments without ATP and without RepD.

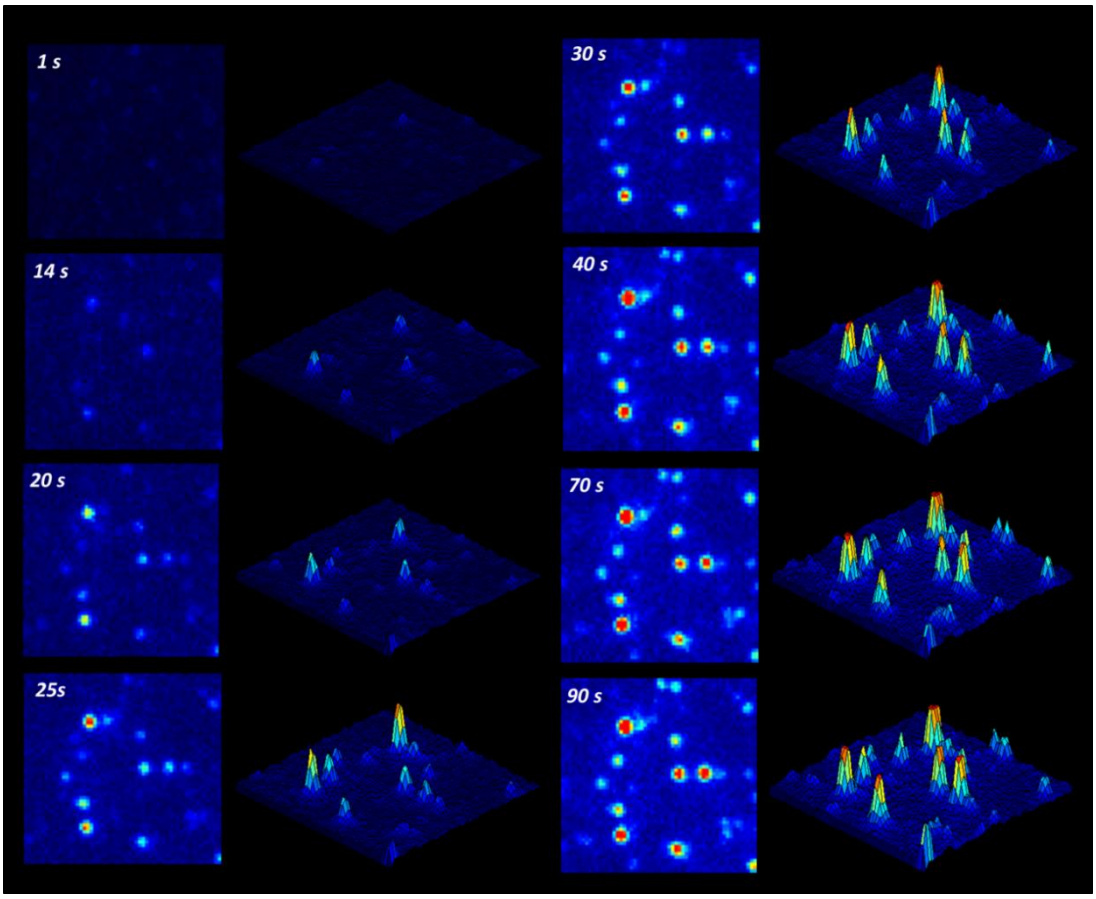

Figure 73. Cy3B-SSB visualised plasmid unwinding of pCER*oriD* 3094bp plasmid under TIRFM.

Left side panel shows 25 μm^2 area of field view at state time points and right panel shows the matching 3D presentation of the intensity landscape of the field of view. The experimental set-up and conditions are described in Methods, Section 2.17.4. Frame 1 s, is the frame 1 s after ATP addition.

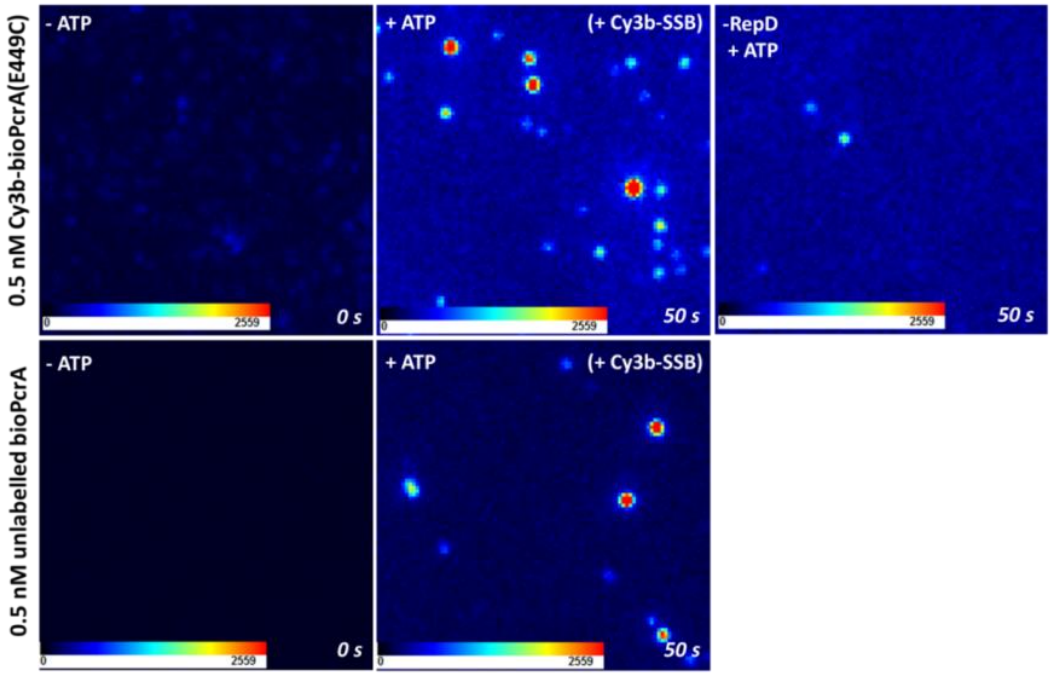

Figure 74. Cy3B-SSB visualised plasmid unwinding of pCER*oriD* 3094bp plasmid using TIRFM.

The 0 s frame is the frame 1 of the records before ATP is added. The 50 s frame is the image taken 50 s after ATP addition. The –RepD image is a control experiment without RepD. The experiment was carried out as described in Methods apart from RepD not being added to the reaction.

The plasmid unwinding event selection and analysis was done using ASPT and Motility (GMimPro) as described in Methods, Section 2.17.4. The event selection excluded those events, which 1) had instant increase as they were likely not be true unwinding events or were landing events of already unwound plasmid-SSB complexes, 2) had no clear end point, as a constant increase in fluorescence is not a property for unwinding of fixed length DNA and 3) had total intensity change above 500, as these are too high in intensity to be result of one plasmid unwinding event. Four main properties of events were analysed, which were the duration (Δt), the total intensity change (ΔI), the start time (t_0) and the density of events. The traces were fitted to single exponential on Igor Pro at two different time scales to enable selection of better fit and determination of Δt and ΔI. Semi-automated analysis method using single exponential fit was chosen after comparison with manual analysis of the data, as no difference was observed between

the results and the semi-automated enabled faster determination of the Δt and ΔI. Therefore, it enabled analysis of relatively large number of events. Examples of the fitting are shown in the Figure 100 in the Appendix.

The density of plasmid unwinding events varied from 0.12 to 0.24 μm^2 and had an average of 0.17 events μm^{-2}. The mean unwinding duration was determined from the unwinding duration (Δt) distribution histogram by fitting to data with Gaussian distribution (Figure 75A). This was 76.3 s (SEM 2.4) for 3094 bp plasmid, which gave the unwinding rate of 40.6 +/-1.3 bp s^{-1} assuming complete unwinding. Averaging four independent measurements with total of 1037 events, the average unwinding rate was 46.3 bp s^{-1} (Table 18).

To test the robustness of the determination of the mean Δt using Gaussian fit, the mean Δt for all events with 3094 bp plasmid was calculated simply by adding the event durations together and dividing by number of events (average, no fitting). This was 92.1 s and the unwinding rate was 33.6 bp s^{-1}. This method gives a lower unwinding rate compared to results from Gaussian fits to Δt distribution. This is most likely caused by the inclusion of unwinding events that are outliers. These events have a very long Δt due, possibly due damaged PcrAs. When these long events are included in the mean Δt calculation, they increase it significantly lowering the mean unwinding rate. When the mean Δt is determined by fitting to Gaussian distribution, the outliers have less of an effect and the emphasis is on the major event population of the unwinding Δt. This may be an indication that the observed rate constant for unwinding at ensemble assays is slower due to averaging of all PcrAs, including those that may be poorly functional helicases, which may result from the protein preparation. Hence, the mean Δt was determined using Gaussian fitting to the distribution histograms.

The ΔI distribution from same record is shown in the Figure 75B. The mean ΔI from Gaussian fit is 203.9 (SEM 11.08). The amplitude of the individual events showed considerable variation. This can be caused by multiple factors such as the variation in the distance of the events from the

surface, movement/fluctuation of the plasmids during unwinding, events going out of evanescent field, presence of partial unwinding events and events taking place close together and observed as a single spot. As the events are highly synchronised at the start of the reaction, one can expect that the observed Δt of events is not affected by detection of two plasmid unwinding events observed as one, but these events would have double the total expected intensity.

Plotting the event Δt against ΔI enables the analysis of how the two correlate with each other (Figure 75C). The plot shows that the overall event intensity increases with the event duration. A significant proportion of events cluster around ΔI ~200 as expected from ΔI histogram. The range of unwinding event durations at ΔI 200 +/-20 give a range of unwinding rates that vary from 15 to 150 bp s^{-1}. The range of unwinding rates is unexpectedly large. This indicates that some PcrA helicases are able to unwind plasmids almost four times faster than the mean population of PcrA helicases. The plot in the Figure 75C has been fitted by linear regression and to straight, horizontal line. The two fits enable the determination of possible dependence of the event duration (Δt) with the event intensity change (ΔI). If linear dependence between intensity change and duration are observed, this implies that the records have significant number of events with partially unwound plasmids. The linear regression fit has ~17% smaller *reduced chi*^{2} than when data is fitted to constant y indicating that the data shows some linear dependence between Δt and ΔI. This is the case with all plasmids tested for *reduced chi*^{2}, which is 10 – 20% smaller for linear regression than for fit to horizontal line. A summary of data is in Table 16. The average of four records for pCER*oriD* 3094 bp unwinding has a gradient of 0.014 s per unit of intensity and reciprocal of this gives the increase of intensity with time which is 6.99 units of intensity s^{-1}. This shows that the records have some partial unwound plasmids but the majority of events are fully unwound plasmids.

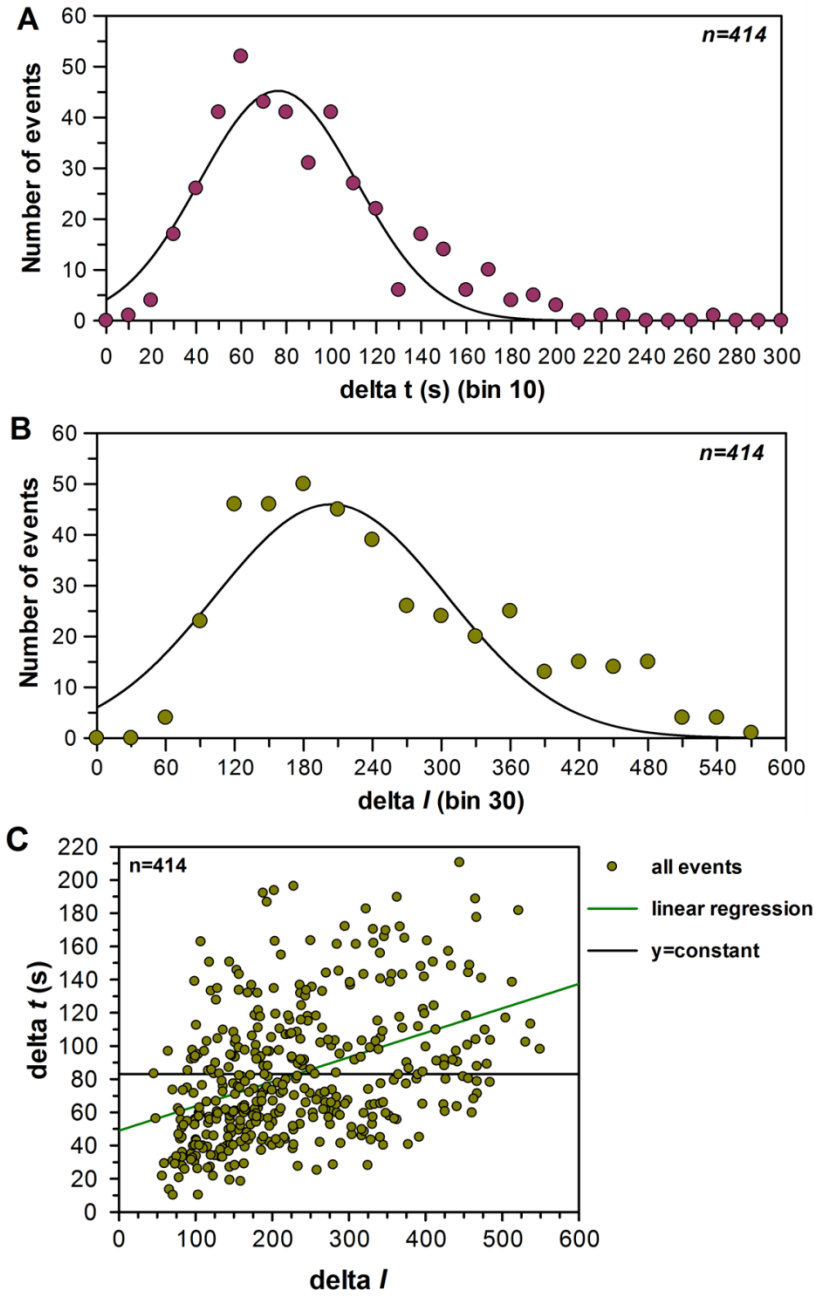

Figure 75. Distribution of pCER*oriD* 3094 bp unwinding events.

A) Unwinding duration (Δt) distribution histogram. The mean Δt from the Gaussian fit is 76.3 s (SEM 2.4). This gives an unwinding rate of 40.6+/-1.3 bp s^{-1}. The variance of the distribution is 34.8 (SEM 2.4). B) Event intensity (ΔI) distribution histogram. The mean ΔI from Gaussian fit is 203.9 (SEM 11.1) and the variance of the fit is 101.0 (SEM 11.3). C) Δt versus ΔI plot of 3094 bp plasmid unwinding events. The gradient for the linear regression is 0.145 s per unit of intensity (SEM 0.016). The *y* is constant is 83.1 s (SEM 2.0). The analysis was using GraFit 7, Erithacus software Ltd. Record: 090212r04.

A 0.5 nM Cy3b-bioPcrA(E449C) + 3094 bp

Record	Number of events	Rate of unwinding (bp/s)	delta *t* (s)	SEM	delta *I*	SEM
090212r04	414	40.6	76.3	2.39	203.92	11.08
130212r01	273	45.7	67.7	2.44	197.8	11.13
050412r05	114	48.8	64.4	5.03	81.88	4.88
130212r05	236	55.6	55.7	2.06	200.6	7.23

B 0.5 nM unlabelled bioPcrA + 3094 bp

Record	Number of events	Rate of unwinding (bp/s)	delta *t* (s)	SEM	delta *I*	SEM
050412r06	211	36.1	85.7	3.59	85.76	3.60
050412r08	130	48.2	64.2	2.55	126.7	9.46

C 0.2 nM Cy3b-bioPcrA(E449C) + 3094 bp

Record	Number of events	Rate of unwinding (bp/s)	delta *t* (s)	SEM	delta *I*	SEM
040412r06	56	43.1	71.78	4.55	116.1	11.7
040412r04	80	41.8	74.01	4.32	124.7	6.2
r04andr06	136	42.4	72.93	3.46		

Table 18. Single molecule plasmid unwinding assay with 3094 bp plasmid.

The plasmid unwinding assays has been measured at two Cy3B-bioPcrA(E449C) loading concentrations A) 0.5 nM and B) 0.2 nM and with labelled and C) unlabelled bioPcrA (the data analysis shown in Appendix, Figures 102).

6.3.2. The plasmid unwinding assay enables observation of unwinding of plasmids short than 3 kb

Other lengths of pCER*oriD* plasmid used in the single molecule measurements were the 2437 bp, 3650 bp and 6642 bp plasmids. pCER*oriD* 2437bp plasmid was made by removing a sequence from the 3094 bp plasmid [87]. The larger plasmids, 3650 and 6642 bp have been made from pCER*oriD* 3094 bp by inserting sequences derived from λDNA.

To test and to validate the plasmid unwinding assay ideally a plasmid of two times larger or smaller would be used in the assay. As the making of 1.5 kb and smaller pCER*oriD* plasmid proved unsuccessful, the pCER*oriD* 2437 bp plasmid was the shortest of plasmid used in single molecule plasmid unwinding assay. The event density for 2437 bp plasmid unwinding was uniform with density ranging from 0.14 to 0.19 μm^{-2} and having an average density of 0.16 events μm^{-2} for the records. Figure 76 shows the ΔI and Δt distributions for the unwinding events. The unwinding rates vary with four measurements from 42 to 56 bp s^{-1} and with an average of 48.2 bp s^{-1} for 1167 events from Gaussian fit. As the plasmid unwinding rate with 2437 bp was similar to that of the 3094 bp plasmid, this showed that the plasmid unwinding is fully observed with the two plasmids and that PcrA has a processivity at least up to ~3kb. The range of unwinding rates between PcrA unwinding 2437 bp plasmid varied between ~18 to 120 bp s^{-1} (Figure 76).

The mean ΔI from a distribution fit for the 2437 bp plasmid was 168.8 (SEM 12.5), 17% less than that for the 3094 bp plasmid unwinding events (ΔI = 203). The expected reduction in mean Δt would be 21% between 3094 and 2437 bp plasmids. This shows that in experiments performed at exactly same optical conditions the amplitude follows the size of the plasmid. This comparison can most correctly be made between experiments done on the same day to minimise day-to-day variation. The fluorescence at the beginning of the record can be used as an indicator of the actual intensity and laser power difference and can be used to validate the comparison. The start fluorescence intensity is not the only aspect affecting the Δt and ΔI as the length of the record and the clustering of type events has an effect on the final analysis and will be discussed further in the Chapter 6 Discussion.

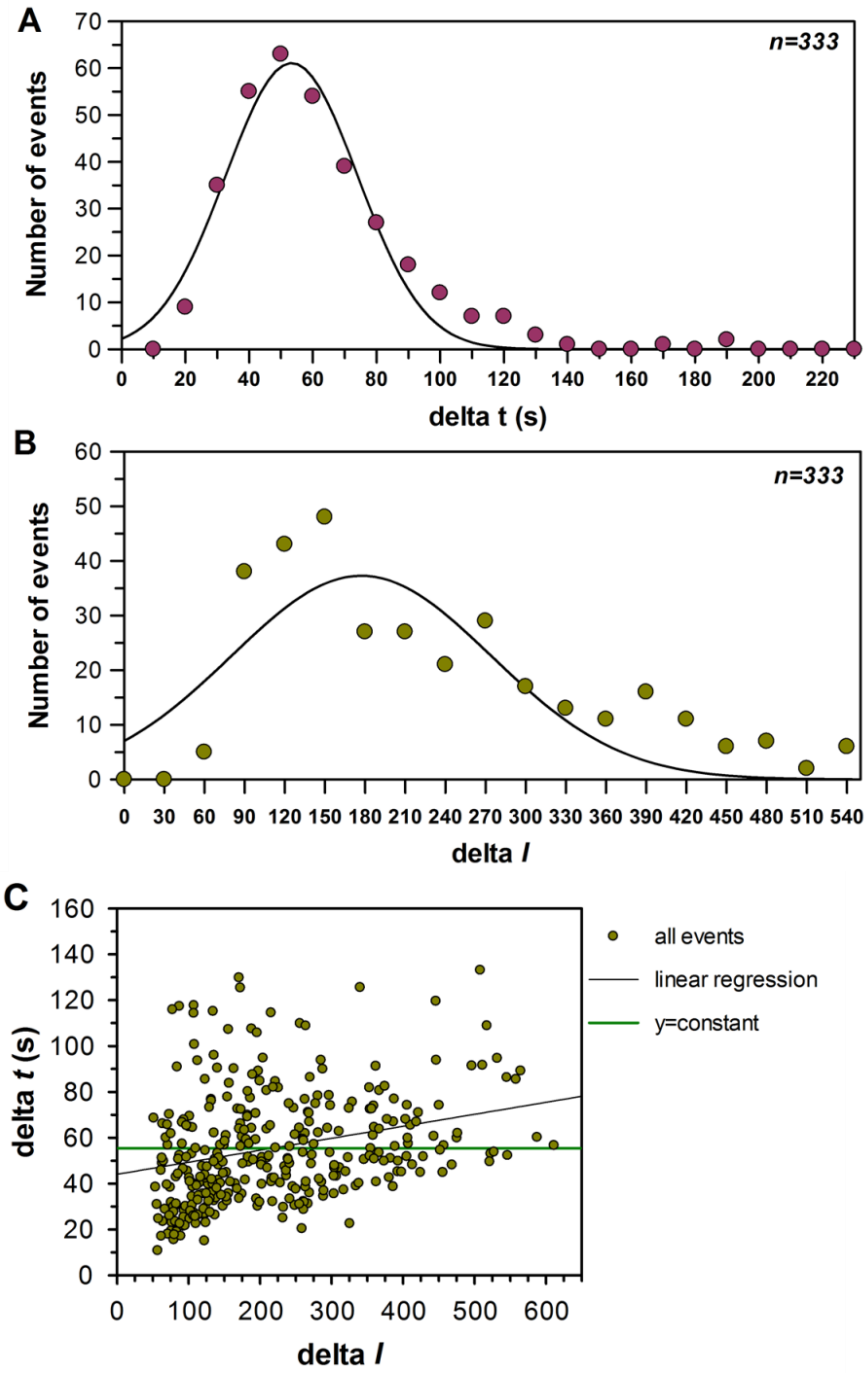

Figure 76. Distribution of pCER*oriD* 2437 bp unwinding events.

A) The histogram of Δt distribution of events. The Gaussian fit has mean value of 43.6 s (SEM 13.8) that would give an unwinding rate of 45.7 +/- 0.9 bp s^{-1}. The variance of the fit is 20.7 (SEM 1.0). B) The histogram of Δl distribution of events. The Gaussian fit has the mean of 177.1 (SEM 14.0). The variance of the fit is 97.0 (SEM 14.6). C) Δt versus Δl plot of 2437 bp plasmid unwinding events. The linear regression has a gradient of 0.05 (SEM 0.01). The y equals constant fit has a value of 55.5 s (SEM 1.5) and rate of unwinding of 43.9 bp s^{-1}. (Record: 090212r09)

The third plasmid length tested was the pCER*oriD* 3650 bp plasmid. The results are summarised in the Table 19 and example of the data is shown in the Figure 77. The average of total of 886 events from two records had a Δt of 68.0 s and the unwinding rate of 53.9 bp s^{-1}. The Gaussian fit to ΔI distribution had a mean of 123.1 +/- 10.2. The distribution showed a large number of events with low ΔI and short Δt. This indicated the presence of a significant number of partial unwinding events.

The distribution and plot of Δt and ΔI indicated broader clustering and many events with lower Δt between 20 to 40 s compared to 3094 and 2437 bp plasmid unwinding (Figure 77). Also, with this graph a second cluster at higher intensity around ~170 to 190 could be seen. These events are the fully unwound 3650 bp plasmid events. The possible reason for increased number of partial unwinding events with the 3650 bp plasmid could be its sequence. The plasmids, which are larger than pCER*oriD* 3094 bp, have extra lambda DNA in them. The increasing length of plasmid and the λDNA may reduce the PcrA processivity. This has not been directly observed with ensemble assays but the effect of partial unwinding events may be hidden if most of the plasmids are unwound fully. Also, the greater length may cause the plasmid partially to go out of the evanescent field.

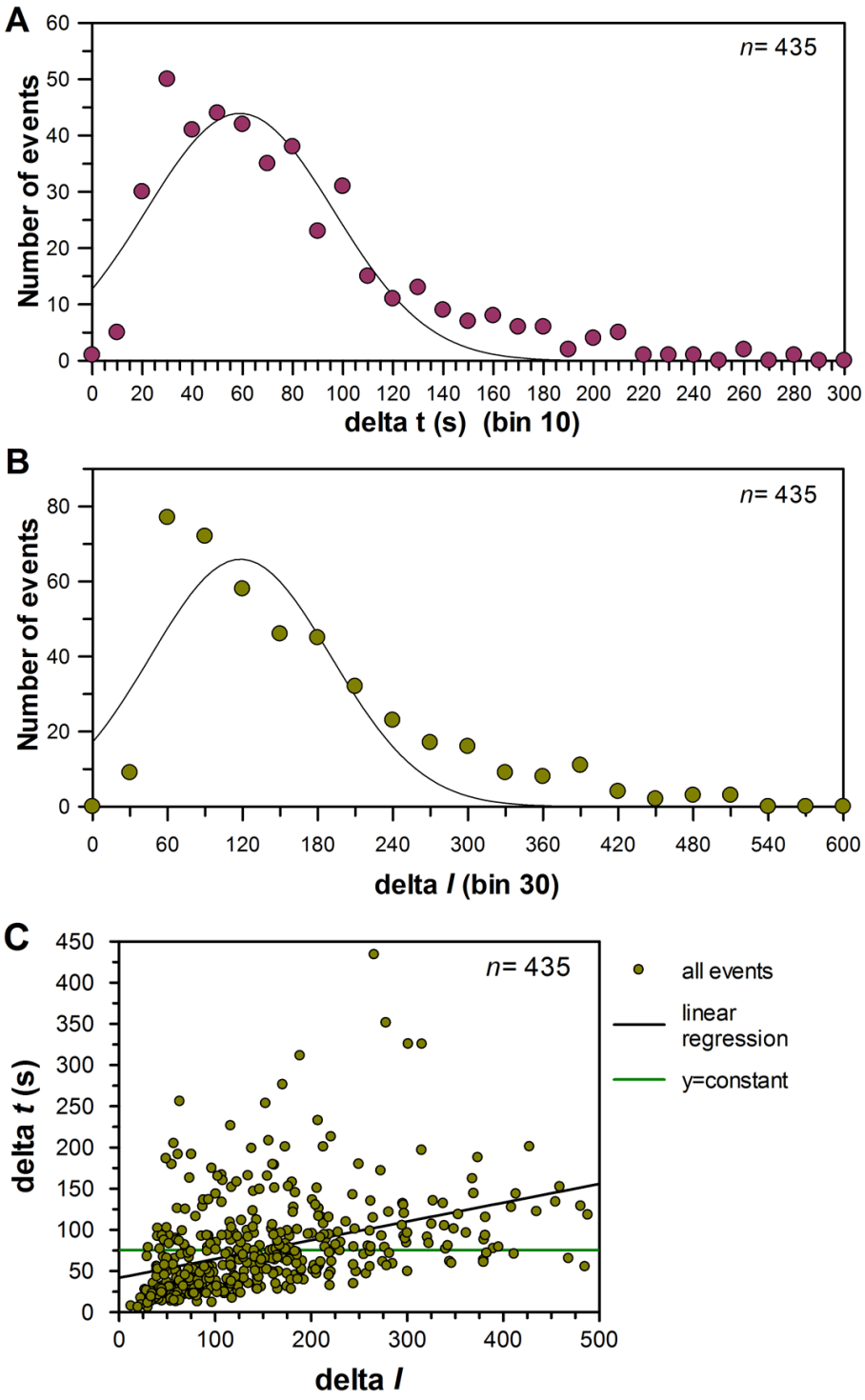

Figure 77. Distribution of pCER*oriD* 3650bp unwinding events.

A) The histogram of Δt distribution of events. The Gaussian fit has a mean of 58.8 s (SEM 2.8) that has an unwinding rate of 62.0+/- 3.0 bp s^{-1}. The variance of the fit is 37.4 (SEM 3.0). B) The histogram of ΔI distribution of events. The Gaussian fit has the mean of 177.1 (SEM 14.0). The variance of the fit is 72.2 (SEM 9.5). C) Δt versus ΔI plot of 3650 bp plasmid unwinding events. The linear regression has a gradient of 0.23 (SEM 0.02). The y equals horizontal line has a value of 75.3 s (SEM 2.7). Record: 220512r09.

A 0.5 nM Cy3b-bioPcrA(E449C) + 2437 bp

Record	Number of events	Rate of unwinding (bp/s)	delta *t* (s)	SEM	delta *I*	SEM
090212r09	333	45.7	53.33	1.02	168.77	12.55
130212r08	294	41.7	58.5	2.15	158.2	6.19
220512r06	428	52.6	46.29	2.43	107.15	4.29
090212r10	112	56.2	43.45	4.07	85.34	6.88

B 0.2 nM Cy3b-bioPcrA(E449C) + 2437 bp

Record	Number of events	Rate of unwinding (bp/s)	delta *t* (s)	SEM	delta *I*	SEM
040412r07, r08 and r09	93	56.5	43.08	1.71	96.68	2.88

C 0.5 nM Cy3b-bioPcrA(E449C) + 3650 bp

Record	Number of events	Rate of unwinding (bp/s)	delta *t* (s)	SEM	delta *I*	SEM
220512r08	443	50.5	72.26	4.29	118.0	8.82
220512r09	442	57.3	63.72	2.82	118.33	9.07
*220512r08**	*443*	*44.0*	*82.86*	*8.91*	*118.0*	*8.82*

D 0.5 nM Cy3b-bioPcrA(E449C) + 6642 bp

Record	Number of events	Rate of unwinding (bp/s)	delta *t* (s)	SEM	delta *I*	SEM
050412r02	163	181.5	36.59	4.48	70.57	2.79
050412r03	118	103.1	64.38	78.33	87.22	7.24
r02 & r03	281	160	41.42	6.96	79.30	4.30

Table 19. Single molecule plasmid unwinding of 2437 bp, 3650 bp and 6642 bp plasmids.

6.3.3. The 6642 bp plasmid unwinding cannot be observed in the plasmid unwinding assay on TIRFM

The assay was repeated with pCER*oriD* 6642bp to test if large size plasmid unwinding could be observed in the assay and this could also provide a comparison for 3094 bp plasmid by being two times larger. The Δt distribution and the ΔI distributions for unwinding of 6642bp plasmid are shown in the Figure 78.The mean Δt from Gaussian fit is 43.8 s (SEM

13.8).The data clearly does not follow Gaussian distribution and shows large number of short events having Δt between 20 to 40 s. The distribution is actually more similar to exponential decay than Gaussian distribution of Δt values.

When the mean Δt for all events was calculated by sum of all events divided by the number of events, the Δt was 77.5 s. The large difference between the two ways of determining the mean Δt values is caused by events that have longer unwinding duration (Δt) than expected. When these are added to mean Δt calculation (no fitting), the average Δt is significantly increased compared to what had been determined using the Gaussian was fitting.

But whichever method was used for determining the mean Δt, the Δt was shorter in duration than expected for 6642 bp plasmid if it is fully unwound or the unwinding is fully observed. This indicated that the pCER*oriD* 6642 bp was primarily not unwound fully and possibly the PcrA stalls/dissociates at quite specific time point/part of pCER*oriD* 6642bp plasmid or the plasmid is moving out of evanescent field due to its size. In both cases the observed event duration/processivity may have sequence and structural dependence and the effect may not only be caused by the length of plasmid. But comparison of the number of events with Δt >200 s between 6642 bp and 3094 bp plasmid showed that there are more Δt >200 s events with the 6642 bp plasmid than with the 3094 bp plasmid.

The Gaussian fit to ΔI distribution had a mean of 79.3 (SEM 4.30) and the plot of Δt versus ΔI, shows a clustering at short events durations (Figure 78C). The ΔI is expected to be over 440 if full unwinding is observed. The lower ΔI with 6642 bp plasmid than with 3094 bp plasmid doesn't support the idea that 6642 bp plasmid moves out of the evanescent field. In another words, if short low intensity unwinding events are likely to be partial unwinding events. These and the 3650 bp plasmid results may indicate that the PcrA processivity is reduced with longer plasmids.

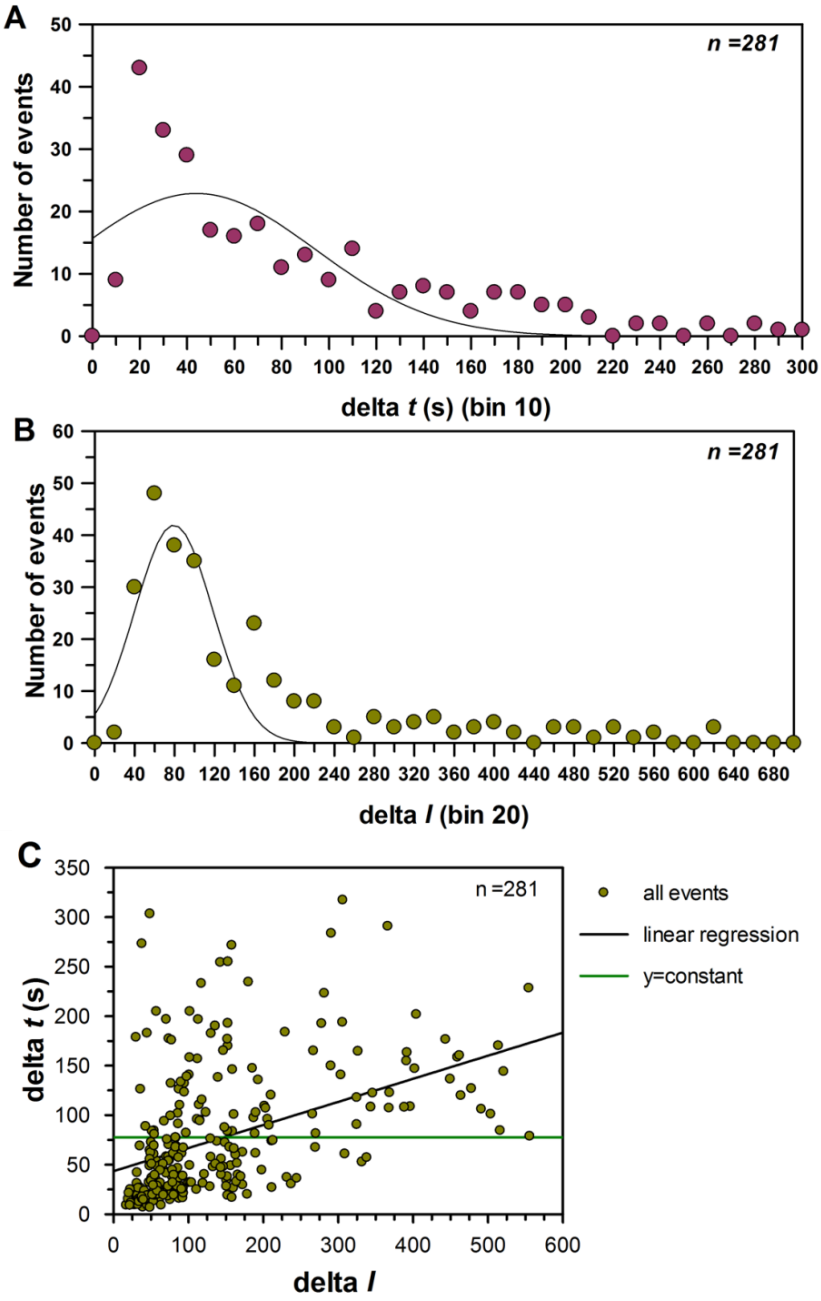

Figure 78. Distribution of pCER*oriD* 6642 bp unwinding events.

A) Histogram of Δt distribution of events. The Gaussian fit has a mean of 43.6 s (SEM 13.8), which gives an unwinding rate of 151.6 +/- 47.7 bp s^{-1}. The variance of the fit is 50.5 (SEM 14.0). B) Histogram of ΔI distribution of events. The Gaussian fit has mean ΔI of 79.3 (SEM 4.3). The variance of the fit is 39.2 (SEM 4.4). C) Δt versus ΔI plot of 6642 bp plasmid unwinding events. The linear regression has a gradient of 0.23 (SEM 0.02). The *y* equals constant fit has a value of 77.5 s (SEM 3.94). Record 050412r02 and r03

6.3.4. Amplitude dispersion of plasmid unwinding events is not affected by the Cy3B-bioPcrA(E449C) concentration

The pCER*oriD* plasmids, which showed primarily full unwinding (2437, 3094 and 3650bp) also showed high variation of events amplitudes (ΔI). One possible reason for this is the observation of two events together. The density measurement using Cy3B-bioPcrA(E449C) indicated that at the 0.5 nM loading concentration two helicases may be observed as one object. This meant that also two plasmid unwinding events could be observed as one event. Therefore, the single molecule plasmid unwinding experiments were repeated with the 2437 bp and 3094 bp plasmids with 0.2 nM Cy3B-bioPcrA(E449C) (Figure 103, 9.3. Appendix). Table 18 and 19 summarise all the results for 3094 bp and 2437 bp plasmid. The results show that decreasing the Cy3B-bioPcrA(E449C) concentrations decreases the number of events observed (81 and 56 events for two individual measurements for 3094 bp plasmid). The mean Δt and so the rate of unwinding is similar to that measured at higher loading concentration (Tables 18 and 19). This indicates that the dispersion of event amplitudes is not caused by two events occurring together. Hence, there must be other reasons for the event ΔI variation, which include differences in the maximum height of the complex above the surface, plasmid fluctuation in and out of evanescent field and variation in the orientation of the event.

The mean of ΔI distribution from fit is 124.7 +/- 6.2. This is lower than mean ΔI for other measurements on other days for 3094 bp plasmid, but the same reduction was observed for the 2437 bp plasmid experiments done on the same day (See Table 18 and 19). The variation in event intensities has been observed on certain days and sets of experiments and as said before, the true comparison of intensities can be only done with the same day experiments. As a control Figure 101 in the Appendix shows the total field of view intensity change for the entire record duration. They show clear difference in total intensity change observed between different days. Other factors may also affect the overall intensity and the intensity may vary

between individual surfaces in one set of experiments as they are all individually made and can have slight tilts in the angle or difference in height of the flow cell. Also, slight movement of TIRF set-up can occur during experiments while addition of ATP causing changes in TIRF angle.

6.3.5. The addition of ATP to PcrA-RepD-plasmid complex initiates the unwinding instantly

The ensemble plasmid unwinding has a ~25 s lag phase at the beginning of the reaction (Figure 27). This lag phase has remained unexplained, but suggestions have been made as to what may be causing it. These include the rearrangement of PcrA-RepD-plasmid complex after ATP addition, PcrA passing through the ICRIII sequence or impaired binding of DCC-SSB to the newly formed ssDNA at early stages.

In these single molecule assays, the majority of events started instantly after ATP addition and the initiation was highly synchronised. Figure 79 shows the distribution of the observed time points (t_0) for start of unwinding after addition of ATP for one of the pCER*oriD* 3094bp unwinding records. The mean t_0 was 3.9 s (SEM 0.01) and the variance of distribution (σ) was 1.3. The time of ATP addition could be determine to less than 0.5 s accuracy as the added Cy3B-SSB could be observed as an increase in the background intensity. This was used as frame 0. The results show that most events start in less than 3 s of the mean t_0 (3.9 s). Table 20 shows the start time analysis for three 3094 bp plasmid experiments. The average mean t_0 for all three experiments was 2.92 s (756 events). The plasmid unwinding is highly synchronised and only 6.3 to 7% of events starting after 15 s of the ATP addition.

The ensemble plasmid unwinding assay on the stopped-flow apparatus uses same principle as the single molecule plasmid unwinding assay developed here [87] (Figures 26 and 72). There are four main differences between the two assays, which are the ssDNA biosensor (DCC- SSB(G26C) in the ensemble assay and Cy3B-SSB(W88C) in the single molecule assay),

concentration of the ssDNA biosensors are different between the assays, PcrA attachment in single molecule assays and use of a high excess of PcrA over the RepD-plasmid complex in the ensemble assay.

The experiments show that the plasmid unwinding starts either over 8 times faster on single molecule assays than on ensemble plasmid unwinding assay or the lag phase in ensemble assay is not actual result of plasmid unwinding but caused by the biosensor DCC-SSB [176]. The latter seems more likely explanation when taking into account the ensemble plasmid unwinding assays with MDCC-PcrA(E449C), which also lacked the ~25 s lag phase (Figure 60, Section 5.8.3.). DCC-SSB is known to bind ssDNA in two modes, the ~35 and ~65 base binding mode [89, 121]. These modes have two different fluorescent states and affinities to ssDNA and it may be that at the beginning of plasmid unwinding the 35 base binding mode is preferred. As the 35 base binding has a lower fluorescence change, a lag phase is observed in ensemble plasmid unwinding assay. The single molecule plasmid unwinding signal is not dependent on the environmental change and no fluorescence difference is observed whether SSB is binding in ~35 or ~65 base mode. Hence, no lag phase is observed with Cy3B-SSB.

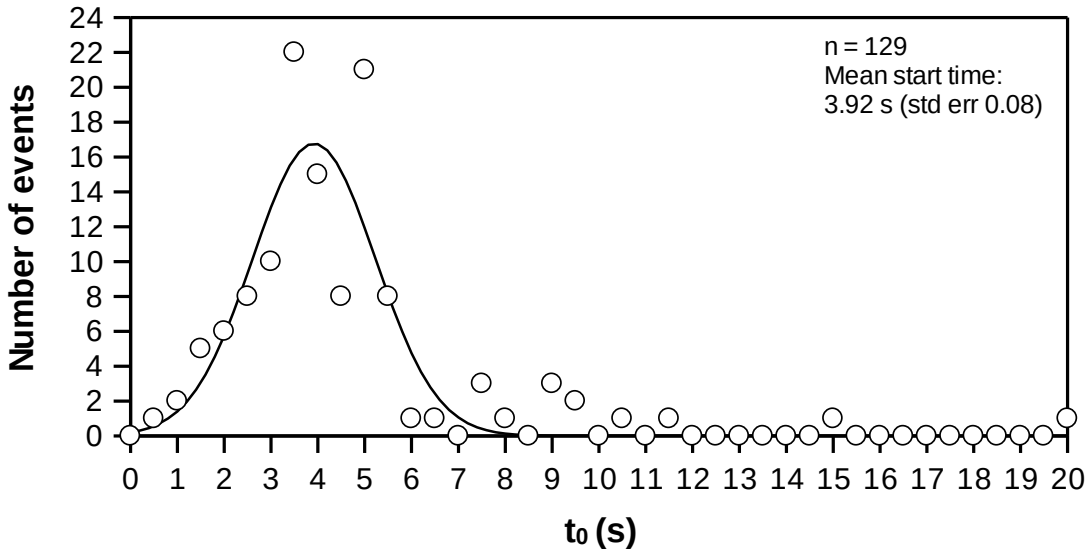

Figure 79. Distribution of plasmid unwinding start times (t_0) with pCER*oriD* 3094 with complete *oriD* sequence.

The mean t_0 from Gaussian fit is 3.94 s (SEM 0.08). The variance of the data (σ) is 1.31 (SEM 0.08).

Record	Number of events	t_0	SEM	σ	SEM
130212r01	334	2.62	0.22	3.11	0.23
090212r04	293	2.81	0.13	2.34	0.15
050412r05	129	3.92	0.08	1.31	0.08

Table 20. The mean t_0 for different pCER*oriD* plasmids.

t_0 (s), the start of observable unwinding. σ, the variance of the Gaussian fit.

6.3.6. Fate of plasmid complexes after completion of unwinding

After the fluorescence increase during the unwinding, the fluorescence traces showed a variety of fluorescent behaviours that correspond to the fate of plasmid unwinding complex once the plasmid unwinding was completed or had stalled. The fate of the plasmid unwinding complex was quantified and investigated by clustering. This may provide information about the fate of plasmid unwinding/replication complex after or at the termination, even though at physiological conditions DNA polymerase III would be included in the reaction and strand exchange could take place. The plasmid unwinding events were grouped by their fluorescence behaviour following the end of plasmid unwinding. This is likely to depend on what happens to the DNA-protein complex at this stage. The clustering was done manually using data from the 3094 bp plasmid. The four major groups selected were full drop, half a drop, no drop and partial unwinding (Figure 80). The full drop events have been further divided into two further groups, depending on whether the fluorescence decrease was instant or slow. The full drop corresponds to complete release of plasmid DNA out of the evanescent field. The half a drop in intensity most represents release of one DNA strand while other remains bound to bioPcrA, itself surface-bound, or possibly directly to the surface. No drop in fluorescence, although there may be fluctuations in intensity, represents complexes that do not dissociate from the surface. The fluctuation is probably caused by the plasmid moving in and out of the evanescent field. The partial unwinding events are defined as those that do

not reach high enough intensity to be full unwinding events (typically events with ΔI<100).

Table 21 summarises the results for the clustering analysis. The most common type of “ending” to plasmid unwinding is the half drop and no drop at all, combined representing more than 50% of events. This indicates either that once PcrA reaches the *oriD* again, it stalls and remains bound to plasmid or that after unwinding the RepD-plasmid-SSB complex does not dissociates from bioPcrA but gets stuck to surface. As no DNA polymerase is in the reaction the plasmid cannot be synthesised into dsDNA and the correct termination reaction cannot occur. This can lead to tangled up plasmid-RepD-SSB complex that PcrA cannot dissociate from. Also the SSB binding to the plasmid may increase its affinity to the surface and so remain in the evanescent field. As the plasmid would have to move a significant distance to be seen as a separate spot, one cannot distinguish between surface binding and binding to PcrA.

The clustering results are dependent on the length of the record after ATP addition. This means that some full drops may not be distinguished from partial and no drop events, if the records are not long enough (>150 s after ATP addition). Therefore, the longer records have larger percentage of events showing full drops, which count for ~25% of all events.

The proportion of partial unwinding events with 3094 bp plasmid seems relatively constant between different records and represent <20% of events. This proportion is higher for longer plasmids as shown by distribution histograms of 3650 (Figure 77) and 6642 bp (Figure 78) plasmids.

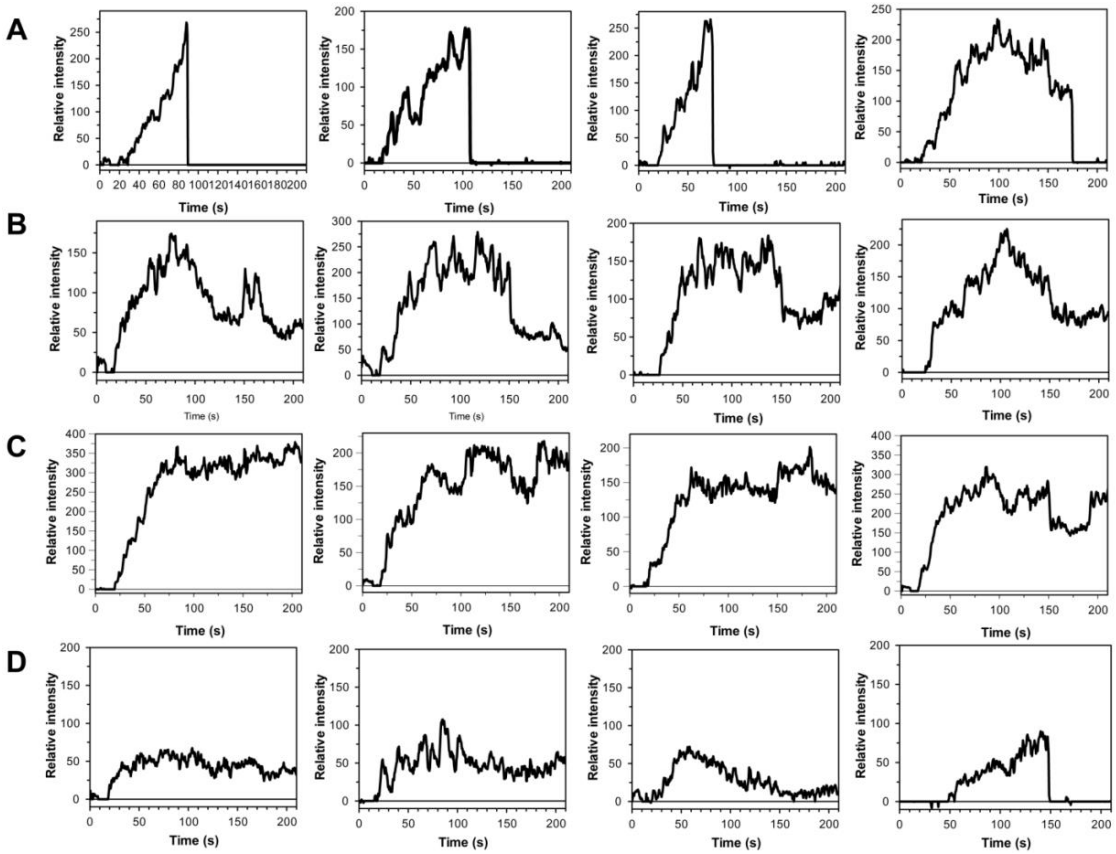

Figure 80. Four major populations of different types of unwinding events used for clustering.

A) Full drop: full unwinding followed by a decrease in intensity back to the zero, which corresponds to full unwinding and release of both complementary strands of the plasmid DNA. B) Half a drop: full unwinding with an intensity drop to approximately half of the maximum. This corresponds to the release of one of the plasmid strands from the bioPcrA/surface. C) No drop: full unwinding without a decrease in intensity (may fluctuate) due unwound plasmid remaining on the bioPcrA/surface. D) Partial unwinding: events where ΔI is significantly smaller than expected corresponding to the partial unwinding of the plasmid. This either remains on bioPcrA/surface or is released fully. The events in the figure are all from record 050412r05 in which pCER*oriD* 3094 bp plasmid was unwound.

0.5 nM Cy3b-bioPcrA(E449C) + 3094bp								
Record	Total number of events	Partial events (ΔI<100)	Full drop, all	Full drop, slow/steps	Full drop, instant	Half drop	No drop	Length of record after ATP (s)
090212r04	418	75(17.9%)	14 (3.3%)	13 (3.1%)	1 (0.2%)	128 (30.6%)	201 (48.1%)	149
050412r05	136	25 (18.4 %)	34 (25 %)	18 (13.2 %)	16 (11.8%)	44 (32.4%)	33 (24.3%)	185.4
130212r01	285	50(17.5%)	7 (2.5%)	4 (1.4%)	3 (1.1%)	73(25.6%)	155(54.4%)	128.5
0.5 nM unlabelled bioPcrA + 3094bp								
Record	Total number of events	Partial events (ΔI<100)	Full drop, all	Full drop, slow/steps	Full drop, instant	Half drop	No drop	Length of record after ATP (s)
050412r06	252	59 (23.4%)	69 (27.4%)	33 (13.1%)	36 (14.3%)	59 (23.4%)	67 (26.6%)	250
050412r08	148	28 (18.9%)	40 (27.0%)	12 (8.1%)	28 (18.9%)	23 (15.5%)	57 (38.5%)	219

Table 21. Clustering of single molecule plasmid unwinding events.

6.4. Discussion

PcrA function in plasmid replication, ssDNA binding and translocation and dsDNA unwinding has been extensively investigated previously using ensemble methods [51, 52, 54, 87, 88, 93, 157, 177]. With helicases such as PcrA, ensemble methods may miss important information due to averaging of the signal. These include processes such as pausing and reannealing of DNA and variation in the rate of unwinding between individual helicases. With PcrA, another interesting component of the PcrA plasmid unwinding is the interaction and possible changes in the interaction between PcrA and RepD during plasmid unwinding, which may not be observable using ensemble methods. The need to observe these kinds of processes has led to development of methods that enable observation of individual molecules. These methods include atomic force microscopy, electron microscopy, optical and magnetic trapping and fluorescence based assays on TIRFM [143, 178, 179]. Here, a single molecule method has been further developed to enable the observation of individual PcrA helicases unwinding complete plasmid in real time using TIRFM. The assay enabled the measurement of the PcrA oligomeric state during plasmid unwinding, its behaviour while unwinding such as the processivity and possible stalling and the rate of unwinding by individual PcrA helicases.

6.4.1. PcrA is a monomeric helicase

Most of the previous ensemble evidence suggests that PcrA is functional as a monomer, but requires other protein interactions for increased processivity. No definitive results have been produced to confirm the oligomeric state of PcrA while unwinding DNA. A monomer in solution does not discount dimers or higher oligomers being formed on binding to DNA. The single molecule plasmid unwinding assay used here with immobilised PcrA, gave an opportunity to understand the oligomeric state of PcrA. If PcrA is a monomer in solution before attachment to surface, the likelihood of PcrA forming dimers on biotin is low. Also, as no DNA is present during PcrA immobilisation, it cannot have an effect on the PcrA oligomeric state. The SEC-MALS experiments showed that wild-type PcrA and biotinylated PcrA are both monomeric in solution at micromolar concentrations. This meant that at low loading concentrations (nanomolar) of bioPcrA, the PcrAs were attached to surface as monomers and the unwinding events observed were unwound by monomeric PcrA.

The density measurements showed saturation of the field of view was observed at loading concentrations higher than 0.2 nM of Cy3B-bioPcrA(E449C) and the number of spots/objects observed had linear dependence with increasing loading concentrations when loading concentrations was varied from 0.01 nM to 0.2 nM (ASPT and SFDA tracking). But at loading concentrations below 0.5 nM ~90% of the spots had single photobleaching step (SFDA tracking). These PcrA helicases can be expected to monomers on the surface. This indicates that the unwinding events observed here are results of single monomeric PcrAs unwinding plasmids.

However, when comparing the plasmid unwinding event density with the density of Cy3B-bioPcrA(E449C) spots indicates that fraction of total Cy3B-bioPcrA(E449C) is unwinding plasmid DNA. In fact, the plasmid unwinding density is similar to density of Cy3B-bioPcrA(E449C) objects that have multiple step photobleaching (Section 6.2.3.). This could possibly

indicate that the plasmid unwinding events are result of PcrA molecules that are bound to streptavidin as dimer and hence have multistep photobleaching. This is unlikely as at the loading conditions the bioPcrA is monomeric. Also, to have the same density of multistep photobleaching objects and plasmid unwinding events, all the “dimeric” bioPcrAs would have to be active and this is unlikely.

6.4.2. Individual PcrA helicases unwinding complete plasmids

The single molecule plasmid unwinding assay enabled the measurement of processive unwinding of plasmids by PcrA. The plasmid unwinding rates observed were ~40-50 bp s^{-1} at 22 °C (in TIRF buffer), determined using three different lengths of plasmid DNA (2437 bp, 3094 bp and 3650 bp) (Table 18 and 19). Using the ensemble plasmid unwinding assay, PcrA had unwinding rate of ~27 bp s^{-1} at the same conditions [176]. The single molecule plasmid unwinding measurements indicated that the primary PcrA population actually unwinds plasmids faster than what has been observed in the ensemble assays. One likely reason for this could be the averaging of signal in ensemble assays, which would include the slower PcrA molecules. In the single molecule assay, the event duration (Δt) distribution shows “outliers”, which unwind DNA significantly slower. These outliers have less of an effect when a Gaussian fit is used to determine the mean Δt. The determination of the unwinding rate this way is possibly more accurate as the very slow events may be a result of anomalous or damaged PcrAs from the protein preparation. But there are other possibilities for these variations in rate such as there may be a small fraction of complexes pausing briefly when PcrA is in solution in ensemble assay. Whereas, with immobilised PcrA, premature dissociation of PcrA would not lead to loss of a fluorescent spot and might result in a short pause followed by re-association of a new PcrA close by to continue unwinding. This might be explained by the nucleotide-free PcrA having lower affinity to RepD-DNA and so it occasionally dissociates before binding to ATP. This would lead to longer unwinding times in solution PcrA in ensemble assay. The PcrA affinity

measurements using MDCC-PcrA(E449C) showed that PcrA·ATP has a ~6-fold faster binding to RepD-DNA than nucleotide-free PcrA (Sections 5.3 and 5.7).

The rate of unwinding between the individual PcrA helicases varied greatly, from approximately 15 to 150 bp s^{-1}, without obvious populations of speeds. This means that in the assay there are helicases unwinding DNA with whole magnitude difference in the rate of unwinding. There are several possibilities for the variation, which include fraction of PcrAs being damaged (slow unwinding), brief pausing or dissociation and re-association of certain PcrAs, variation in secondary structures formed on unwound ssDNA, suboptimal packing of Cy3B-SSB along the ssDNA, damaged plasmid DNA varying between individual plasmids and missing control elements from the reaction that would synchronise the PcrA unwinding rates. The missing component of the plasmid unwinding reaction, which would synchronise the PcrA unwinding rates, could be the DNA polymerase III. This has been shown to synthesise DNA *in vitro* at the rate of ~700 nt s^{-1} and addition of DNA polymerase III into reaction could increase the PcrA rate of unwinding [90]. DNA polymerase III would also remove one of the single-strand DNAs reducing the amount of possible tangling of ssDNA caused by secondary structures and the differences caused by variation in Cy3B-SSB ssDNA packing. One explanation for the faster unwinding rates, other than it being the actual PcrA unwinding rate, could be two PcrAs unwinding the same plasmid and together they would remove the effects of pausing and dissociation caused by low affinity and damaged DNA. The effect of damaged or nicked DNA could be tested and removed by treating the plasmid preparations with DNA ligase that should repair the nicked DNA. This would be an important and interesting test to be done in the future experiments.

The analysis of the start point of plasmid unwinding showed that it starts highly synchronised manner after addition of ATP and most events start in less than 2 s of PcrA binding to ATP. This indicates that the active PcrA·RepD-plasmid complex must be formed correctly before addition of

ATP or is formed very fast after binding ATP. The measurements with MDCC-PcrA(E449C) indicated that the ATP binding increases the PcrA affinity to RepD-DNA complex (Section 5.3.). As ATP is needed to initiate the plasmid unwinding, no ATP is added to the reaction until the PcrA·RepD-plasmid complex is formed. However, the addition of ATP solution may remove most of the unbound or weakly bound RepD-plasmid complex out from the flow cell. This would also explain why no events or very few fresh binding events are being observed.

In comparison to the almost immediate start point of plasmid unwinding in single molecule assay, the ensemble assay unwinding starts or is observed after ~25 s (Figure 27, Chapter 3). The DCC-SSB biosensor is known to have two ssDNA binding modes (~35 and ~65 base binding mode) with different fluorescent properties; it is likely that lag phase observed in the plasmid unwinding ensemble assay is caused partially by the DCC-SSB. The ~35 base binding mode is preferred at low concentration of ssDNA [121], which is the case at beginning of plasmid unwinding. This binding also has lower fluorescence change than the ~65 base binding mode. The single molecule plasmid unwinding signal relies on the Cy3B-SSB, for which the fluorescence signal is not dependent on the environment, nor whether SSB is binding to ssDNA in ~35 or ~65 base binding mode.. Hence, no lag phase is observed in single molecule plasmid unwinding assay. It should be noted that it can expected that when SSB is binding along ssDNA in ~35 base mode, larger number should be binding to the DNA reducing the fluorescence difference between ~35 and ~65 base binding modes.

6.4.3. PcrA processivity

The single molecule experiments showed that the bioPcrA unwinding processivity is approximately 3 kb, as full unwinding is observed with most events with plasmid 3094 bp and smaller. Plasmid longer than 3 kb showed increased proportion of unwound plasmid and with over 6 kb plasmid, only a small proportion of the plasmids were fully unwound. What caused these

partial unwinding events and why they increased with the increasing plasmid length? There are many possible explanations for this apart from the actual PcrA processivity being <3 kb, such as the DNA sequence variation between the plasmid lengths and the steric hindrance caused when PcrA unwinds longer plasmids and increased damage to longer plasmids. Also, longer plasmids are more likely to move out of evanescent field due to their increased size. The plasmids longer than 3094 bp have been constructed by inserting λDNA into the 3094 bp plasmid. These sequences may affect PcrA processivity or cause changes into DNA secondary structure that hinder PcrA unwinding. The attachment of PcrA to the surface may also cause hindrance while plasmid is unwound and this may be more of an issue when longer plasmids are unwound. Addition of DNA polymerase III into the unwinding reaction could increase the PcrA processivity by increasing its affinity or rate of unwinding. It could also possibly remove or reduce the effects of ssDNA secondary structures and becoming stuck on the surface.

One possibility for the observed similarity between the densities of multiple step photobleaching spots and unwinding event density is that two PcrAs may be required for the processive unwinding of complete plasmids. The affinity of bioPcrA to RepD-plasmid complex may not be tight enough to facilitate unwinding of long lengths of DNA. This possibly could be improved by having two PcrAs binding to same plasmid, whether or not as a dimer. These PcrA helicases could be bound to one streptavidin or two separate streptavidins close together. For example, if one PcrA dissociates from the plasmid, the other is still bound to it. It has been suggested that the processive unwinding in ensemble plasmid unwinding assay is a result of multiple PcrAs unwinding same plasmid. In this model, multiple PcrA are following the PcrA that is unwinding the plasmid. As it falls off, it is replaced by PcrA following it and this can be repeated multiple times during unwinding of single plasmid (“Helicase-Train” model) [170]. The ensemble plasmid unwinding assay is formed at high excess of PcrA over DNA. The MDCC-PcrA(E449C) binding experiments show that more than one PcrA is able to bind to *oriD* once it has been nicked by RepD, supporting the idea that PcrAs can follow each other on ssDNA even they might not form a

dimer (Section 5.6.). There can be a significant difference in the affinities between the PcrA free in solution and the immobilised PcrA. The PcrA affinity when immobilised to surface could be reduced to extent that two or three PcrAs are required for the efficient unwinding of plasmid DNA. Having said that, the binding measurement indicated increased affinity or at least increased rate of binding when PcrA is ATP bound and the actual affinity of PcrA to RepD-plasmid complex while unwinding may be significantly tighter than what was measured for RepD-plasmid binding without ATP using MDCC-PcrA(E449C).

6.4.4. Fate of the plasmid after unwinding

The clustering of events according to behaviour after unwinding showed that the most of the unwound plasmids remain in the evanescent field, either attached to the bioPcrA or close to it on the surface (Table 21). This may be caused by the plasmid unwinding stalling once reaching the *oriD*. As the reaction does not contain DNA polymerase III, no strand exchange can take place to terminate correctly The PcrA·RepD-plasmid-SSB complex stalls without dissociation or attaches to the surface. Addition of DNA polymerase III to the assay could increase the rate of unwinding observed with reduction of total intensity as fewer SSBs would be binding to ssDNA and it could change the way plasmid unwinding ends as the strand exchange could take place and one complete daughter plasmid would be formed. This would possibly increase the proportion of plasmids that are fully released after unwinding. Ideally, this would be something that should be tested in the future.

6.4.5. Limitations of the single molecule plasmid unwinding assay

The event density comparison with the density of Cy3B-bioPcrA(E449C) showed that only 10% of Cy3B-bioPcrA(E449C) on the surface is actively and processively unwinding plasmid DNA. This could be a result of low affinity of bioPcrA to RepD-plasmid complex, which could be

due to immobilisation or to PcrA and RepD being from different bacterial species. The effect of immobilisation could be possibly tested by immobilising the plasmid, but this would be successful only if the reduced affinity was directly caused by the immobilisation of PcrA.

The assay here was done with *B. stearothermophilus* PcrA and *S. aureus* RepD. Efforts have been made to produce PcrA and RepD from same species (*S. aureus*). In the future, repeating the experiments with PcrA and RepD from same species would be highly interesting and may give more accurate view of PcrA and RepD interaction. This could increase the PcrA affinity RepD-plasmid and so increase the number of plasmid unwinding events.

Another explanation for the relatively low event density, and possibly the most likely factor, is the washing off the RepD-plasmid complex from bioPcrA with the ATP buffer solution. This is also a major difference between the stopped-flow ensemble measurements where PcrA·RepD-plasmid complex is free in solution and not exposed to similar change of solution.

The event amplitude, ΔI, showed dispersion in the distribution (Figure 75B). Several reasons for this can be suggested such as the complex height above the surface, or multiple unwinding events observed very closely spaced. Alternatively, the events may be moving in and out of the evanescent field that affect the excitation and emission of the fluorescence. The intensity of the field decays exponentially from the surface and the attachment distance of the complex may vary, hence this could contribute to the intensity dispersion, as the intensity used to excite fluorophores varies depending on the depth of the complex. This variation can be caused by the difference in the PEGylation or angle on the flow cell. Both will affect the ΔI without changing the event duration. Some of the events may be multiple unwinding events close together, but as the experiments were repeated with 0.2 nM Cy3B-bioPcrA(E449C) loading concentration instead of 0.5 nM and the ΔI dispersion remained the same, this explanation does not seem likely. Another possibility could be the plasmids moving out of the evanescent field

in a manner, which affects more the ΔI than the Δt. For instance, once plasmid is unwound enough it can reach to outer layers of evanescent field leading to lower excitation and emission distorting linearity of intensity increase during plasmid unwinding. Again the Δt would not be affected by this as long as some increase in intensity is observed until whole plasmid is fully unwound. This could also explain why the events show reduction in the rate of intensity increase at the end of plasmid unwinding and the traces would fit well to single exponential increase. The amplitude of the fluorescence intensity may also be affected by the photobleaching and it can have different effect if there is variation in the excitation. The variation in excitation can be caused by various reasons such as the location and orientation of the plasmid unwinding reaction on the surface.

6.4.6. Summary

Biotinylated PcrA has been successfully used to develop a single molecule plasmid unwinding assay, which has enabled the observation of individual PcrA helicases unwinding full lengths of plasmid in real time by TIRFM. Fluorescent labelling of bioPcrA provided a method to determine the bioPcrA density on the surface and enhanced the control of focus when applying ATP to initiate the plasmid unwinding. The plasmid unwinding at single molecule level was measured on three lengths of plasmid (2437, 3094 and 3650 bp). The unwinding rate for plasmids fully visible in the TIRFM (2437 and 3094 bp) was 40-50 bp s^{-1} at 22 °C (Table 18 and 19). This is slightly increased compared to ensemble unwinding rate of ~30 bp s^{-1} at same conditions in ensemble measurements and may actually be faster when taking in account the temperature difference between the experiments. The DNA junction unwinding assay implies that the PcrA unwinding rate is halved by temperature drop from 30 °C to 22 °C, but it should be noted that the ensemble DNA junction unwinding is done with short linear DNA, which is vastly different circular plasmid DNA used in TIRFM measurements.

The single molecule plasmid unwinding experiments showed that the plasmid unwinding start almost immediately after ATP addition (Figure 73 and 79). The assay has shown PcrA processivity to be high and over 80% of plasmid are fully unwound once the unwinding has been initiated. The assay also indicates that the most of the unwound plasmid remain on PcrA or close to the location of unwinding once plasmid has been unwound. This may indicate stalling of the PcrA·RepD complex after unwinding as no DNA polymerase III is present to synthesise the leading strand and enable the strand exchange that completes leading strand synthesis of plasmid replication.

7. Overall discussion

This Chapter summarises the main aims and results within this thesis. It draws together all the experiments done and where possible, relates the results to previous work on PcrA and to its function in the DNA translocation and plasmid replication. The future possibilities for continuity of the project are also discussed.

7.1. Production of fluorescently labelled PcrA and RepD to investigate their function in plasmid replication

The role of PcrA in plasmid unwinding was investigated by creating several different fluorescent PcrAs, labelled with environmentally sensitive fluorophores. The labelling was achieved using site-directed mutagenesis to introduce cysteine residues at suitable locations on the surface of PcrA and subsequent labelling with fluorophores using maleimide chemistry. This proved to be a highly efficient and specific way to label PcrA and RepD, as the labelled species used in the experiments showed ~100 % labelling without significant non-specific labelling (Table 2, Chapter 3). The fluorescent proteins all showed ATPase activity and DNA unwinding activity similar to wild type PcrA (Figure 24 and Table 3, Chapter 3).

In the past, PcrA function has been studied using fluorophore labelled substrates or radioactivity and most of the transient kinetics data with PcrA has used labelled substrates such as mantATP/ADP, fluorophore-labelled DNA or a fluorescent biosensor. The benefit of labelling the substrate can be a fluorescent signal, which is usually simpler to achieve and in some cases easier interpret. With labelled enzyme this signal may be complex, as the enzyme often interacts with more than one substrate and goes through conformational changes. This complexity can often be overcome by further testing in particular focussing on partial reactions, as was achieved with most of the assays presented in this thesis.

7.2. PcrA binding and translocation on ssDNA shows site and sequence specificity

PcrA translocation on ssDNA was investigated using MDCC-PcrA(K138C). To understand the observed signal in ssDNA translocation, the MDCC-PcrA(K138C) binding to varying lengths of ssDNA was measured. This showed that the PcrA binds tighter to the middle of the ssDNA with higher fluorescence than to the ends of ssDNA (Figure 32, Section 4.2.1.), to which PcrA binds faster. This was indicated by the MDCC-PcrA(K138C) binding to the dT_{20} oligonucleotide, which showed phases for both binding modes (Figure 32 and 35, Chapter 4). This may be caused by the different conformations of PcrA when binding different parts of ssDNA. The hypothesis was confirmed by repeating measurements with DNA structures lacking the ssDNA ends (Figure 33, Section 4.2.1.). 'Removal' of ssDNA ends by making then double stranded, removed the end binding phase. Association and dissociation rate constant measurements using MDCC-PcrA(K138C) enabled the determination of PcrA affinity to different length of ssDNA. The results showed that PcrA affinity to short lengths of ssDNA (dT_{10}, K_d = 130 nM) is lower than to longer lengths of ssDNA (dT_{50}, K_d = 14 nM) (Table 6, Section 4.2.4.). The lower PcrA affinity to ends of ssDNA may have a biological importance in the cell for example in DNA repair and especially in RecA filament removal and PcrA locating them [94, 95].

Compared to previous ssDNA binding studies done with PcrA, a benefit of using labelled PcrA is the ability to observe signals with any length of ssDNA, as with 2-aminopurine-labelled oligos no signal was observed with oligos 30 bases and longer. This was because most of the PcrA binds too far from the fluorophore to affect its environment [51]. This is not the case with the MDCC-PcrA(K138C) as it shows signals with all lengths of ssDNA. Also, MDCC-PcrA(K138C) shows a signal with most DNA structures, as long as it has a ssDNA stretch on it.

The MDCC-PcrA(K138C) signal was used to measure PcrA translocation rate on ssDNA. Previous work has shown that PcrA movement on ssDNA is unidirectional [54], a finding which is supported by the MDCC-PcrA(K138C) translocation measurements, as the signal seen is dependent on PcrA moving uniformly to the end of ssDNA. This is observed as a decrease in fluorescence until PcrA reaches the end of the ssDNA. The rate of translocation was first determined (99 bases s^{-1}) on dT oligos (Figure 40, Section 4.3.1.). This is in good agreement with the previous measurements with labelled DNA carried out at the same conditions indicating that the MDCC-PcrA(K138C) is measuring ssDNA translocation accurately [51].

The advantage of using MDCC-PcrA(K138C) to measure ssDNA translocation was the possibility to do this with different sequences of ssDNA. This showed that when PcrA translocates on dA and dT oligos the rate of translocation is approximately ~250 bases s^{-1}, whereas with dC oligos the rate of translocation was over 500 bases s^{-1} at 30 °C (Table 7, Section 4.3.2.). This indicates that the PcrA rate of translocation is dependent on the sequence it is moving on, suggesting movement of the bases among the base binding pockets of PcrA limits the observed rate. Unfortunately, no translocation signal was observed with dG oligos. When random sequence oligos were used in the assay, the rate of translocation was determined as ~380 bases s^{-1}. This is as expected if there was a difference in the way PcrA translocates on dA/dT and dC/dG bases and is the first evidence showing that PcrA rate of translocation is sequence dependent. The reason for this could be PcrA having a lower affinity to dC bases that allows than faster movement on ssDNA. This property is most likely caused by the way the bases interact with base binding pocket of the PcrA. Interestingly, the speed of translocation on ssDNA is 5-8 times faster than the DNA unwinding rate. This implies that the separation of base pairs is rate limiting for PcrA moment, but the ATP hydrolysis remains as 1 ATP per base moved/unwound [87].

When comparing PcrA ssDNA translocation rate to closely related UvrD helicase, it is relatively similar. UvrD monomer has been shown to

translocation at the rate of ~190 bases s^{-1} at 25 °C on dT bases, [40]. Also, the rate of ssDNA translocation by UvrD has sequence dependence in the order dT>dC>dA>dG [40]. With PcrA this was observed to be dC>dT=dA, which is relatively surprising as PcrA and UvrD are structurally and functionally similar, having 42 % of sequence similarity. However, Tomko *et al*. 2007 experiments varied in the buffering conditions as they were done with 20 mM NaCl compared PcrA measurements which were done with either 150 mM NaCl or 200 mM KCl [39, 40, 142] and this could explain or add to the observed difference between PcrA and UvrD measurements.

7.3. PcrA-RepD-DNA complex formation at the initiation of plasmid unwinding

PcrA has been shown to be a poor helicase on its own and requires presence of Rep initiator protein for processive DNA unwinding [87, 88]. This was also shown here in the single molecule assay (Figure 74, Section 6.3.1.), as when RepD was not included the plasmid unwinding reaction, the unwinding event number was greatly reduced. The requirement of activating proteins emphasises the importance of having a control mechanism, as an unregulated helicase may have deleterious effect on the organism. Also, PcrA may have multiple functions in the cell, which consist of translocase and unwinding activities whereby binding partners can act as switches between these modes.

Before the work done as a part of this thesis, the interaction surface between PcrA and RepD had not been defined. The 2B subdomain of PcrA has been suggested as the most likely interaction site with the RepD [21], as it is not involved in the ATP hydrolysis or direct translocation on ssDNA. Also, this domain is known to show autoinhibition of PcrA helicase activity [180].

Here, the coumarin labelled PcrA mutants E447C, E449C, M450C and L453C, located on surface of the top of the 2B subdomain, showed a signal when binding to RepD-DNA complex on the stopped-flow measurements (Figure 46, Chapter 5). This supported the hypothesis that the PcrA-RepD

interaction surface is at the 2B domain. The fluorescent signal relating to RepD was only observed with the mentioned mutants on top of the 2B subdomain. Other labelled PcrA mutations did not show RepD-specificity and so are good controls for the RepD-specific signals. (Table 1, Chapter 3). This implies that the interaction of PcrA and RepD takes places once RepD is DNA bound. However, this cannot be fully confirmed by fluorescent signal experiments, as the possible interaction may not cause a large conformational change or is at a location which does not affect the environmentally sensitive fluorophore(s).

PcrA binding to the initiation complex was investigated using MDCC-PcrA(E449C). The MDCC-PcrA(E449C) signal is highly RepD-specific as the signal change was 5 times larger with DNA junction bound by RepD than with DNA junction 1 only (Figure 45, Section 5.2.1.). This enabled the determination of the association and dissociation kinetics of PcrA to and from DNA and RepD-DNA complexes in the presence and absence of a nucleotide. PcrA binding to RepD-DNA is faster when it is ATP-bound (with RepD-DNA junction 1 it was 6 μM^{-1} s^{-1} without ATP and over 25 μM^{-1} s^{-1} with ATP) and with RepD-DNA junction 1 the rate constant of binding is increased by almost 5-fold (Figures 47 and 50, Chapter 5) . Experiments repeated with non-hydrolysable ATP analogues were performed to observe the PcrA·ATP complex binding when no hydrolysis of the ATP takes place (Figure 52, Chapter 5). This showed that PcrA binding was faster without nucleotide, but not as fast as with ATP, which is hydrolysed when ssDNA is present.

MDCC-PcrA(E449C) binding to the RepD-DNA junction complex was biphasic indicating two processes of binding. The possible processes suggested included two conformations of PcrA (open and closed), two different binding sites on the dT-arm of the DNA junction or two different RepD-DNA complexes. These three possibilities were tested and the only condition where the biphasic nature of the binding signal was not observed was when PcrA was binding to RepD-DNA junction in presence of nucleotide (PcrA·ATP) (Figure 50, Section 5.3.1.). The X-ray crystal structure of PcrA with nucleotide (AMPPNP) shows that ATP binding causes a relatively small

structural change in PcrA where the 1A and 2A subdomains come closer together [21, 22] (Figure 2, Introduction). This change may be required for stabilising the structural change to one conformation (closed) when PcrA binds to DNA and so when PcrA is ATP bound, only one form of binding mode exist. When no ATP is present, the PcrA may fluctuate between these two modes of binding (open and closed). The structural change expected when PcrA binds to DNA, is the 2B domain folding over the 1B domain (closed conformation), as seen in the X-ray crystal structure of substrate bound PcrA (Figure 2B, Introduction) [21, 22] and this could be stabilised by the ATP. Figure 81 shows a kinetic scheme of the two PcrA conformations binding to RepD-DNA complex.

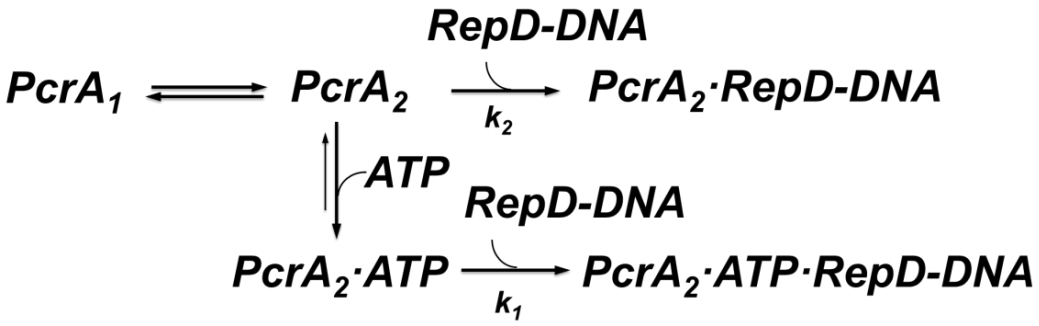

Figure 81. Model of PcrA conformation "locking" by ATP.

PcrA$_1$, PcrA conformation 1, open. *PcrA*$_2$, PcrA conformation 2, closed. k_1 is the binding rate constant 1 of the biphasic PcrA binding signal to RepD-DNA junction complex (no ATP). k_2 is the binding rate constant 2 of the biphasic PcrA binding signal to RepD-DNA junction complex (no ATP).When PcrA is ATP bound, it is "locked" into closed conformation. This increases the observed binding rate constant and removes the second binding phase observed when PcrA is nucleotide-free. The two conformations, open and closed, are shown in Figure 4, Section 1.2.2.

7.4. PcrA function in plasmid unwinding

7.4.1. In ensemble plasmid unwinding assays

An assay was developed using MDCC-PcrA(E449C) to measure PcrA activity in the plasmid unwinding using the stopped-flow apparatus. It measured the environmentally sensitive signal from the MDCC-maleimide. The assay showed rate of unwinding between 30 - 40 bp s^{-1} (Figure 60, Chapter 5). This is close to the rate of unwinding observed with the DCC-SSB plasmid unwinding assay, indicating that the assay is truly measuring plasmid unwinding. The signal was only observed when SSB was present. This may indicate the SSB requirement for processive plasmid unwinding by PcrA, but also SSB may be keeping the unwound DNA separated or physically activates PcrA. The activation by SSB seems unlikely as the DNA junctions are unwound without SSB in the reaction.

The signals observed with MDCC-PcrA(E449C) were different to those obtained with the DCC-SSB plasmid unwinding assay, as they did not have a lag phase at beginning of the signal (Figure 27, Chapter 3). The experiments suggest that the lag phase is partly a result of the DCC-SSB. The DCC-SSB has two main binding modes, the ~35 and ~65 base binding mode, where by the ~35 base binding dominates at low salt conditions and at a high protein to DNA ratio and the ~65 base mode dominates at high salt conditions [181-183]. Similarly, the DCC-SSB shows these binding modes and they have different fluorescent states, with the ~35 base mode having smaller fluorescence increase when binding to ssDNA [121]. This could mean that the lag phase is caused by the ~35 base mode binding, which may be preferred at the beginning of plasmid unwinding due to high SSB protein to DNA ratio. Another possible explanation is the presence of unlabelled SSB in the preparations which may have tighter affinity to the ssDNA than the labelled SSB. This would then bind to ssDNA at the start of plasmid unwinding and be observed as a lag phase [89].

7.4.2. Plasmid unwinding at the single molecule level

An assay to measure individual plasmid unwinding events using TIRFM was developed using biotinylated PcrA. Labelling of bioPcrA enabled visualisation of the bioPcrA on the surface of the flow cell and improved the control over the focus when performing the plasmid unwinding experiments. The determined unwinding rates varied between 40 to 50 bp s^{-1} at 22 °C for three lengths of plasmids that were small enough to remain in the evanescent field for the entire duration of the unwinding (2437, 3094 and 3650 bp) (Table 18 and 19, Chapter 6).

The PcrA showed a wide range of unwinding rates from 15 to 150 bp s^{-1}. This may be natural variation as it is possible, that PcrA function does not require tight control over the rate of unwinding or the control is introduced by other components of the plasmid replication complex that are missing from plasmid unwinding assay. The most likely component to have such an effect is the DNA polymerase III. Other possibilities for variation, which include fraction of PcrAs being damaged (slow unwinding), brief pausing or dissociation and re-association of certain PcrAs, variation in secondary structures formed on unwound ssDNA, suboptimal packing of Cy3B-SSB along the ssDNA and damaged plasmid DNA varying between individual plasmids. Generally, the rate of unwinding is faster than those observed for plasmid unwinding in ensemble experiments, which could be caused by the averaging of the slow unwinding PcrA helicases that may have been damaged during preparation.

Also, the distribution of amplitude varied greatly and showed relatively limited relation to the different sizes of plasmid. The variation could be caused by many factors, such as the two plasmids being unwound close together and seen as one event, the distance of the event from the surface (lower excitation, lower amplitude), the intensity variation over the field of view (though TIRF was adjusted to have the most even laser illumination possible), partial unwinding events being observed as full

unwinding events and also some events moving in and out of the evanescent field.

Full plasmid unwinding was observed with the 2437 and 3094 bp plasmids (Figures 83 and 84), whereas the 3650bp plasmid showed increased number of partial unwinding events (Figure 85) and the 6642 bp plasmid (Figure 86) had a high proportion of stalled unwinding events. This indicates majority of PcrAs unwind plasmids with a processivity ~3 kb. The clustering of 3094 bp plasmid unwinding showed that less than 20 % of the events are partial unwinding events. In other words, 80 % of the events were unwound to completion with a processivity above 3 kb.

Cy3B-bioPcrA(E449C) density on the surfaces was significantly higher than the density of plasmid unwinding events. This means that once PcrA does start to unwind, it is unlikely to dissociate before completion of unwinding. The difference in the Cy3B-bioPcrA(E449C) density and plasmid unwinding density could be an indication of low affinity by the surface bound bioPcrA to the RepD-plasmid complex. The PcrA binding to RepD-plasmid is tight in solution, but this may be weakened by the immobilization of PcrA (Section 5.7.). However, the evidence here indicates that addition of ATP should make the binding even tighter (Section 5.3.). In the assay, the ATP solution is added after incubation of RepD-plasmid complex with the bioPcrA. This may wash away many of the complexes from the bioPcrA, leading to a reduced number of unwinding events compared to the number of bioPcrA on the surface and the concentration of RepD-plasmid loaded on to surface. The affinity may be increased if the PcrA and RepD were from the same species, as in this study the PcrA is from *B. stearothermophilus* and the RepD is from *S. aureus*. Repeating the measurements with the *S. aureus* PcrA and RepD in the single molecule assay may increase of the number of events and possibly processivity of PcrA.

An interesting point highlighted by the single molecule plasmid unwinding assay was that the start of unwinding was almost instant once

ATP is added to the cell (Figure 79 and Table 20, Chapter 6). As with the MDCC-PcrA(E449C) plasmid unwinding assay, there is no lag phase in the plasmid unwinding. The Cy3B-SSB(W88C) is a different cysteine mutant than the DCC-SSB(G26C), which could also affect the binding, but as both have been tested and shown not to be significantly affected by the mutations or labels, this is unlikely [89, 146]. The great difference between DCC-SSB and Cy3B-SSB is the signal, as the Cy3B is not sensitive to environmental changes. As discussed with the MDCC-PcrA(E449C) plasmid unwinding assay the difference in the ssDNA biosensor may be the largest contributor the difference observed at the beginning of the plasmid unwinding. The single molecule plasmid unwinding supports the idea that the lag phase in the ensemble plasmid unwinding assay with DCC-SSB is caused by the different fluorescent states due to the different binding modes of DCC-SSB(G26C).

One important question addressed by the single molecule plasmid unwinding measurements using Cy3B-bioPcrA(E449C) was the oligomeric state of PcrA while unwinding plasmids. The loading of Cy3B-bioPcrA(E449C) at concentrations where individual objects were observed allowed photobleaching experiments to be used to probe the oligomeric state of the PcrA on the surface. This showed that over 90 % of the objects had a single photobleaching step only, which suggests that most of the Cy3B-bioPcrA(E449C) exist as monomers on the surface (Figure 71, Chapter 6). The loading of multiple PcrAs is possible even if PcrA is not forming a dimer, as the surface-bound streptavidin potentially has three free binding sites, but the formation of the multi-PcrA-streptavidin complexes is unlikely, as bioPcrA was shown to be a monomer at loading conditions using SEC-MALS (Figure 65, Chapter 6). This implies that the events seen are most likely showing unwinding by a monomeric PcrA. Hence, the single molecule assay using immobilised bioPcrA and plasmid-RepD complexes show that a single PcrA monomer is sufficient for processive plasmid unwinding. Although, in principle, conditions in the cell might allow multiple PcrA molecules to bind behind the unwinding complex, the presence of

both the DNA polymerase III and SSB make this much less likely and support the idea of a single monomeric PcrA as the functional unit *in vivo*.

7.5. PcrA helicase – a passive helicase

Helicases unwind and translocate on DNA at hugely varying rates, from a few to thousands of base pairs per second [6]. Helicases can be classified by their unwinding activity as “passive” or “active” [6, 61]. If a helicase is able to actively destabilize base pairs by lowering the activation energy of the base pairing, it can be considered as an active helicase. Alternatively, if a helicase is not able to lower the activation energy of base pairing but has to wait for the separation of base paring by the intrinsic thermal fluctuations before moving, it is seen as a passive helicase. With passive helicases, the base pair separation is a rate limiting step. The GC content of DNA will affect the rate of unwinding of a passive helicase, as more hydrogen bonds need to be broken to separate DNA. Generally, helicases that are unwinding fast with rates of thousands of base pairs per second are thought to be active helicases [184, 185].

A simple model to determine whether a helicase is passive or active in DNA separation exists. The model is based on comparison of helicase translocation rate on ssDNA and rate of dsDNA unwinding [61]. If a helicase is actively unwinding DNA, its translocation rate on ssDNA may be similar to the rate of unwinding dsDNA. An example is the Dda helicase, which has an unwinding rate over ssDNA translocation ratio of 0.96 making it likely to be an optimally active helicase [62]. If a helicase is passive, the translocation rate on ssDNA is significantly faster than the rate of dsDNA unwinding [61].

Table 22 summarises the results obtained for PcrA ssDNA translocation and dsDNA unwinding rates and unwinding rates. PcrA translocation on ssDNA is significantly faster than unwinding of dsDNA, varying from 4 to 8 times when comparing different assays done at same

conditions. This indicates that PcrA is a passive helicase or has similar activity to a passive helicase while unwinding plasmid DNA. At single molecule assay conditions, at 22 °C in TIRF buffer, the ssDNA translocation is ~130 bases s^{-1} and the plasmid unwinding ~40 bp s^{-1}. The V_{un}/V_{trans} ratio is 0.3. (For the ensemble conditions the V_{un}/V_{trans} ratio for PcrA is 0.13 when ssDNA translocation is calculated only from dT oligo translocation.) According to the model, helicases with a V_{un}/V_{trans} ratio >0.25 are seen as active and those showing V_{un}/V_{trans} ratios of 0.25 and below are classed as passive helicases. By this PcrA unwinds in manner of a passive helicase, a proposal which could be further tested by using DNA junctions and plasmids with varying GC content.

Type of DNA	Ensemble/ Single molecule	Rate of translocation	T(°C)	Buffer	RepD-plasmid complex formation	
					Time	T (°C)
ssDNA	Ensemble	130 bases s^{-1}	22	TIRF	-	-
ssDNA	Ensemble	240 bases s^{-1}	30	K200	-	-
Linear dsDNA 10-50 bp	Ensemble	50 bp s^{-1}	30	K200	5 min	30
Linear dsDNA 10-50 bp	Ensemble	24 bp s^{-1}	22	TIRF	5 min	30
Plasmid[§]	Ensemble	30 bp s^{-1}	30	K100/ K200	30 s	30
Plasmid*	Ensemble	27 bp s^{-1}	22	TIRF	10 min	30
Plasmid	Single molecule	40-50 bp s^{-1}	22	TIRF	10 min	30
Linear dsDNA 0.5-1.5 kb	Single molecule	>40 bp s^{-1}	22	TIRF	10 min	30

Table 22. Summary of PcrA translocation rates at different conditions and on different DNA.

§, the DCC-SSB plasmid unwinding assay Slatter et al. 2009, TIRF paper 2012. *, the experiments were performed at single molecule conditions by Toseland C.P. and Fili N.

How does this relate to PcrA's biological function? It could be that in plasmid unwinding the slow rate is required for correct function and correct replication of the plasmid. However, plasmid replication has been indicated to take place at a significantly faster rate than the observed plasmid unwinding and the DNA polymerase III holoenzyme has been shown to synthesise DNA *in vitro* at the rate of ~700 bases s^{-1} [90]. This could mean that the DNA polymerase III is the component that makes the PcrA move faster resulting in an active helicase. It is also possible that other protein partners exist for PcrA in the cell that make it behave more like an active helicase.

7.6. Project continuation

The novel fluorescent PcrA molecules prepared by site-directed mutagenesis and fluorophore labelling have enabled the development of new methods to study PcrA function and, of the 11 made, 10 showed fluorescent signals with at least one component of the plasmid replication complex. This led to the selection of the most significant and most easily interpretable signals, but some properties of signals were not investigated further due restrictions in time and the relevance of the process to this thesis. As an example, these included the MDCC-PcrA(K138C) signal with ATP and MDCC-PcrA(H53C) FRET pair with Cy3-labelled DNA junction. With aid of possible crystal structure of PcrA·RepD complex, these are avenues that could be addressed in the future and many possibilities exist for the labelling of the different PcrA cysteine sites developed here for FRET pairing with various components of the replication complex from ATP to other proteins, such as SSB and DNA polymerase.

PcrA is an essential helicase in Gram-positive bacteria and it seems likely that plasmid unwinding is not its only function and evidence to support

this exists [50, 94, 95]. The MDCC-PcrA(K138C) signal in ssDNA translocation may become a valuable tool for testing the endogenous function(s) of PcrA. UvrD has been shown to be involved and required for the removal of RecA filaments, which are toxic to cell genomic stability if their levels are not controlled tightly [186-188]. Similarly, PcrA has been shown able to dismantle RecA filaments and even though it is not an essential function for the organism, it may still be playing an important part in genomic stability and DNA repair [94, 95]. The evidence for PcrA dismantling RecA filaments was obtained from smFRET measurements where PcrA was shown to reel the ssDNA hydrolysing ATP and removing the RecA from the DNA. MDCC-PcrA(K138C) generated a fluorescent signal which relates to ssDNA translocation. It could possibly be used for further studies to observe the RecA filament removal in ensemble assays that has not been done before.

The plasmid unwinding assays reported here are all dependent on the presence of SSB. This may indicate that there is an interaction between PcrA and SSB. The possibility of an interaction between PcrA and SSB should be addressed. If an interaction was discovered, this could lead to further importance of SSB·PcrA interaction, which could show that SSB may be regulating its function. The other important component of plasmid replication is the DNA polymerase and how it affects PcrA function. The plasmid replication rates *in vitro* have been suggested to be ~700 nt s^{-1} for DNA polymerase III holoenzyme [90]. This is almost 20 times faster than the unwinding rate observed for PcrA. When plasmid replication occurs, they are expected to function as a complex or at least follow each other. This means that the DNA polymerase is either slowed down by PcrA or the translocation rate of PcrA is increased by the DNA polymerase.

One of the main questions of the PcrA function in plasmid replication is its interaction with RepD. Here, the evidence supports the location of the interaction to be the 2B subdomain, but still leaves many questions unanswered. The only method for determining the true form of interaction would be X-ray crystallography of PcrA and RepD in complex with DNA.

This could answer how RepD interacts with the DNA and explain many of the features at initiation, as well as during translocation and at the termination stage of plasmid replication.

8. References

1. Watson, J.D. and F.H. Crick, *The structure of DNA.* Cold Spring Harb Symp Quant Biol, 1953. **18**: p. 123-31.
2. Watson, J.D. and F.H. Crick, *Molecular structure of nucleic acids; a structure for deoxyribose nucleic acid.* Nature, 1953. **171**(4356): p. 737-8.
3. Watson, J.D. and F.H. Crick, *Genetical implications of the structure of deoxyribonucleic acid.* Nature, 1953. **171**(4361): p. 964-7.
4. Okazaki, R., et al., *Mechanism of DNA chain growth. I. Possible discontinuity and unusual secondary structure of newly synthesized chains.* Proc Natl Acad Sci U S A, 1968. **59**(2): p. 598-605.
5. Ogawa, T. and T. Okazaki, *Discontinuous DNA replication.* Annu Rev Biochem, 1980. **49**: p. 421-57.
6. Singleton, M.R., M.S. Dillingham, and D.B. Wigley, *Structure and mechanism of helicases and nucleic acid translocases.* Annu Rev Biochem, 2007. **76**: p. 23-50.
7. Lohman, T.M., E.J. Tomko, and C.G. Wu, *Non-hexameric DNA helicases and translocases: mechanisms and regulation.* Nat Rev Mol Cell Biol, 2008. **9**(5): p. 391-401.
8. Liu, Y., *Rothmund-Thomson syndrome helicase, RECQ4: on the crossroad between DNA replication and repair.* DNA Repair (Amst), 2010. **9**(3): p. 325-30.
9. Opresko, P.L., W.H. Cheng, and V.A. Bohr, *Junction of RecQ helicase biochemistry and human disease.* J Biol Chem, 2004. **279**(18): p. 18099-102.
10. Hickson, I.D., *RecQ helicases: caretakers of the genome.* Nat Rev Cancer, 2003. **3**(3): p. 169-78.
11. Shereda, R.D., D.A. Bernstein, and J.L. Keck, *A central role for SSB in Escherichia coli RecQ DNA helicase function.* J. Biol. Chem., 2007. **282**: p. 19247-19258.
12. Ashton, T.M. and I.D. Hickson, *Yeast as a model system to study RecQ helicase function.* DNA Repair (Amst), 2010. **9**(3): p. 303-14.
13. Rossi, M.L., A.K. Ghosh, and V.A. Bohr, *Roles of Werner syndrome protein in protection of genome integrity.* DNA Repair (Amst), 2010. **9**(3): p. 331-44.
14. van der Lelij, P., et al., *Warsaw breakage syndrome, a cohesinopathy associated with mutations in the XPD helicase family member DDX11/ChlR1.* Am J Hum Genet, 2010. **86**(2): p. 262-6.
15. Caruthers, J.M. and D.B. McKay, *Helicase structure and mechanism.* Curr Opin Struct Biol, 2002. **12**(1): p. 123-33.
16. Konola, J.T., K.M. Logan, and K.L. Knight, *Functional characterization of residues in the P-loop motif of the RecA protein ATP binding site.* J Mol Biol, 1994. **237**(1): p. 20-34.
17. Walker, J.E., et al., *Distantly related sequences in the alpha- and beta-subunits of ATP synthase, myosin, kinases and other ATP-requiring enzymes and a common nucleotide binding fold.* EMBO J, 1982. **1**(8): p. 945-51.

18. Story, R.M., I.T. Weber, and T.A. Steitz, *The structure of the E. coli recA protein monomer and polymer.* Nature, 1992. **355**(6358): p. 318-25.
19. Lee, J.Y. and W. Yang, *UvrD helicase unwinds DNA one base pair at a time by a two-part power stroke.* Cell, 2006. **127**(7): p. 1349-60.
20. Korolev, S., et al., *Major domain swiveling revealed by the crystal structures of complexes of E. coli Rep helicase bound to single-stranded DNA and ADP.* Cell, 1997. **90**(4): p. 635-47.
21. Velankar, S.S., et al., *Crystal structures of complexes of PcrA DNA helicase with a DNA substrate indicate an inchworm mechanism.* Cell, 1999. **97**(1): p. 75-84.
22. Subramanya, H.S., et al., *Crystal structure of a DExx box DNA helicase.* Nature, 1996. **384**(6607): p. 379-83.
23. Mackintosh, S.G., et al., *Structural and biological identification of residues on the surface of NS3 helicase required for optimal replication of the hepatitis C virus.* J Biol Chem, 2006. **281**(6): p. 3528-35.
24. Kim, J.L., et al., *Hepatitis C virus NS3 RNA helicase domain with a bound oligonucleotide: the crystal structure provides insights into the mode of unwinding.* Structure, 1998. **6**(1): p. 89-100.
25. He, X., et al., *The T4 phage SF1B helicase Dda is structurally optimized to perform DNA strand separation.* Structure, 2012. **20**(7): p. 1189-200.
26. Liu, H., et al., *Structure of the DNA Repair Helicase XPD.* Cell, 2008. **133**(5): p. 801-812.
27. Pike, A.C.W., et al., *Structure of the human RECQ1 helicase reveals a putative strand-separation pin.* Proceedings of the National Academy of Sciences, 2009. **106**(4): p. 1039-1044.
28. Bernstein, D.A. and J.L. Keck, *Domain mapping of Escherichia coli RecQ defines the roles of conserved N- and C-terminal regions in the RecQ family.* Nucleic Acids Res, 2003. **31**(11): p. 2778-85.
29. Lo, Y.H., et al., *The crystal structure of a replicative hexameric helicase DnaC and its complex with single-stranded DNA.* Nucleic Acids Res, 2009. **37**(3): p. 804-14.
30. Pape, T., et al., *Hexameric ring structure of the full-length archaeal MCM protein complex.* EMBO Rep, 2003. **4**(11): p. 1079-83.
31. Fass, D., C.E. Bogden, and J.M. Berger, *Crystal structure of the N-terminal domain of the DnaB hexameric helicase.* Structure, 1999. **7**(6): p. 691-8.
32. Singleton, M.R., et al., *Crystal structure of T7 gene 4 ring helicase indicates a mechanism for sequential hydrolysis of nucleotides.* Cell, 2000. **101**(6): p. 589-600.
33. Iwasaki, H., et al., *Mutational analysis of the functional motifs of RuvB, an AAA+ class helicase and motor protein for holliday junction branch migration.* Mol Microbiol, 2000. **36**(3): p. 528-38.
34. Yamada, K., et al., *Crystal structure of the Holliday junction migration motor protein RuvB from Thermus thermophilus HB8.* Proc Natl Acad Sci U S A, 2001. **98**(4): p. 1442-7.
35. Szczelkun, MarkÂ D. and MarkÂ S. Dillingham, *How to Build a DNA Unwinding Machine.* Structure, 2012. **20**(7): p. 1127-1128.

36. Soultanas, P., et al., *DNA binding mediates conformational changes and metal ion coordination in the active site of PcrA helicase.* J Mol Biol, 1999. **290**(1): p. 137-48.
37. Yang, Y., et al., *Evidence for a functional dimeric form of the PcrA helicase in DNA unwinding.* Nucleic Acids Res, 2008. **36**(6): p. 1976-89.
38. Cheng, W., et al., *E. coli Rep oligomers are required to initiate DNA unwinding in vitro.* J Mol Biol, 2001. **310**(2): p. 327-50.
39. Maluf, N.K., C.J. Fischer, and T.M. Lohman, *A Dimer of Escherichia coli UvrD is the active form of the helicase in vitro.* J Mol Biol, 2003. **325**(5): p. 913-35.
40. Tomko, E.J., et al., *A nonuniform stepping mechanism for E. coli UvrD monomer translocation along single-stranded DNA.* Mol Cell, 2007. **26**(3): p. 335-47.
41. Dillingham, M.S., *Superfamily I helicases as modular components of DNA-processing machines.* Biochem Soc Trans, 2011. **39**(2): p. 413-23.
42. Bernstein, D.A., M.C. Zittel, and J.L. Keck, *High-resolution structure of the E.coli RecQ helicase catalytic core.* EMBO J, 2003. **22**(19): p. 4910-21.
43. Marini, V. and L. Krejci, *Srs2: the "Odd-Job Man" in DNA repair.* DNA Repair (Amst), 2010. **9**(3): p. 268-75.
44. Korolev, S., et al., *Comparisons between the structures of HCV and Rep helicases reveal structural similarities between SF1 and SF2 super-families of helicases.* Protein Sci, 1998. **7**(3): p. 605-10.
45. Singleton, M.R., et al., *Crystal structure of RecBCD enzyme reveals a machine for processing DNA breaks.* Nature, 2004. **432**(7014): p. 187-93.
46. Ruiz-Maso, J.A., et al., *Genetic and biochemical characterization of the Streptococcus pneumoniae PcrA helicase and its role in plasmid rolling circle replication.* J Bacteriol, 2006. **188**(21): p. 7416-25.
47. Anand, S.P., et al., *Bacillus anthracis and Bacillus cereus PcrA helicases can support DNA unwinding and in vitro rolling-circle replication of plasmid pT181 of Staphylococcus aureus.* J Bacteriol, 2004. **186**(7): p. 2195-9.
48. Chang, T.L., et al., *Biochemical characterization of the Staphylococcus aureus PcrA helicase and its role in plasmid rolling circle replication.* J Biol Chem, 2002. **277**(48): p. 45880-6.
49. Bird, L.E., et al., *Characterisation of Bacillus stearothermophilus PcrA helicase: evidence against an active rolling mechanism.* Nucleic Acids Res, 1998. **26**(11): p. 2686-93.
50. Petit, M.A., et al., *PcrA is an essential DNA helicase of Bacillus subtilis fulfilling functions both in repair and rolling-circle replication.* Mol Microbiol, 1998. **29**(1): p. 261-73.
51. Dillingham, M.S., D.B. Wigley, and M.R. Webb, *Direct measurement of single-stranded DNA translocation by PcrA helicase using the fluorescent base analogue 2-aminopurine.* Biochemistry, 2002. **41**(2): p. 643-51.
52. Dittrich, M. and K. Schulten, *PcrA helicase, a prototype ATP-driven molecular motor.* Structure, 2006. **14**(9): p. 1345-53.

53. Dillingham, M.S., et al., *Defining the roles of individual residues in the single-stranded DNA binding site of PcrA helicase.* Proc Natl Acad Sci U S A, 2001. **98**(15): p. 8381-7.
54. Dillingham, M.S., D.B. Wigley, and M.R. Webb, *Demonstration of unidirectional single-stranded DNA translocation by PcrA helicase: measurement of step size and translocation speed.* Biochemistry, 2000. **39**(1): p. 205-12.
55. Dillingham, M.S., P. Soultanas, and D.B. Wigley, *Site-directed mutagenesis of motif III in PcrA helicase reveals a role in coupling ATP hydrolysis to strand separation.* Nucleic Acids Res, 1999. **27**(16): p. 3310-7.
56. Yu, J., T. Ha, and K. Schulten, *How directional translocation is regulated in a DNA helicase motor.* Biophys J, 2007. **93**(11): p. 3783-97.
57. Enemark, E.J. and L. Joshua-Tor, *Mechanism of DNA translocation in a replicative hexameric helicase.* Nature, 2006. **442**(7100): p. 270-5.
58. Toth, E.A., et al., *The crystal structure of the bifunctional primase-helicase of bacteriophage T7.* Mol Cell, 2003. **12**(5): p. 1113-23.
59. Labib, K., J.A. Tercero, and J.F. Diffley, *Uninterrupted MCM2-7 function required for DNA replication fork progression.* Science, 2000. **288**(5471): p. 1643-7.
60. Lohman, T.M., *Escherichia coli DNA helicases: mechanisms of DNA unwinding.* Mol Microbiol, 1992. **6**(1): p. 5-14.
61. Manosas, M., et al., *Active and passive mechanisms of helicases.* Nucleic Acids Res, 2010. **38**(16): p. 5518-26.
62. Byrd, A.K., et al., *Dda Helicase Tightly Couples Translocation on Single-Stranded DNA to Unwinding of Duplex DNA: Dda Is an Optimally Active Helicase.* J Mol Biol, 2012. **420**(3): p. 141-54.
63. del Solar, G. and M. Espinosa, *Plasmid copy number control: an ever-growing story.* Mol Microbiol, 2000. **37**(3): p. 492-500.
64. del Solar, G., et al., *Replication and control of circular bacterial plasmids.* Microbiol Mol Biol Rev, 1998. **62**(2): p. 434-64.
65. Scherzinger, E., et al., *Plasmid RSF1010 DNA replication in vitro promoted by purified RSF1010 RepA, RepB and RepC proteins.* Nucleic Acids Res, 1991. **19**(6): p. 1203-11.
66. Tomizawa, J., *Control of ColE1 plasmid replication: the process of binding of RNA I to the primer transcript.* Cell, 1984. **38**(3): p. 861-70.
67. Ehrenberg, M., *Hypothesis: hypersensitive plasmid copy number control for ColE1.* Biophys J, 1996. **70**(1): p. 135-45.
68. Tamm, J. and B. Polisky, *Characterization of the ColE1 primer-RNA1 complex: analysis of a domain of ColE1 RNA1 necessary for its interaction with primer RNA.* Proc Natl Acad Sci U S A, 1985. **82**(8): p. 2257-61.
69. Bruand, C., et al., *A fourth class of theta-replicating plasmids: the pAM beta 1 family from gram-positive bacteria.* Proc Natl Acad Sci U S A, 1993. **90**(24): p. 11668-72.
70. Yasueda, H., T. Horii, and T. Itoh, *Structural and functional organization of ColE2 and ColE3 replicons.* Mol Gen Genet, 1989. **215**(2): p. 209-16.

71. Scherzinger, E., et al., *Replication of the broad host range plasmid RSF1010: requirement for three plasmid-encoded proteins.* Proc Natl Acad Sci U S A, 1984. **81**(3): p. 654-8.
72. Khan, S.A., *Plasmid rolling-circle replication: highlights of two decades of research.* Plasmid, 2005. **53**(2): p. 126-36.
73. Baas, P.D., *DNA replication of single-stranded Escherichia coli DNA phages.* Biochim Biophys Acta, 1985. **825**(2): p. 111-39.
74. Velten, M., et al., *A two-protein strategy for the functional loading of a cellular replicative DNA helicase.* Mol Cell, 2003. **11**(4): p. 1009-20.
75. Kleanthous, H., C.L. Clayton, and S. Tabaqchali, *Characterization of a plasmid from Helicobacter pylori encoding a replication protein common to plasmids in gram-positive bacteria.* Mol Microbiol, 1991. **5**(10): p. 2377-89.
76. Erauso, G., et al., *Sequence of plasmid pGT5 from the archaeon Pyrococcus abyssi: evidence for rolling-circle replication in a hyperthermophile.* J Bacteriol, 1996. **178**(11): p. 3232-7.
77. Yasukawa, H., et al., *Rolling-circle replication of the plasmid pKYM isolated from a gram-negative bacterium.* Proc Natl Acad Sci U S A, 1991. **88**(22): p. 10282-6.
78. Bruand, C. and S.D. Ehrlich, *UvrD-dependent replication of rolling-circle plasmids in Escherichia coli.* Mol Microbiol, 2000. **35**(1): p. 204-10.
79. Iordanescu, S. and J. Bargonetti, *Staphylococcus aureus chromosomal mutations that decrease efficiency of Rep utilization in replication of pT181 and related plasmids.* J Bacteriol, 1989. **171**(8): p. 4501-3.
80. Iordanescu, S., *Specificity of the interactions between the Rep proteins and the origins of replication of Staphylococcus aureus plasmids pT181 and pC221.* Mol Gen Genet, 1989. **217**(2-3): p. 481-7.
81. Anand, S.P., A. Chattopadhyay, and S.A. Khan, *The PcrA3 mutant binds DNA and interacts with the RepC initiator protein of plasmid pT181 but is defective in its DNA helicase and unwinding activities.* Plasmid, 2005. **54**(2): p. 104-13.
82. Noirot, P., J. Bargonetti, and R.P. Novick, *Initiation of rolling-circle replication in pT181 plasmid: initiator protein enhances cruciform extrusion at the origin.* Proc Natl Acad Sci U S A, 1990. **87**(21): p. 8560-4.
83. Niedziela-Majka, A., et al., *Bacillus stearothermophilus PcrA monomer is a single-stranded DNA translocase but not a processive helicase in vitro.* J Biol Chem, 2007. **282**(37): p. 27076-85.
84. Thomas, C.D. and L.J. Jennings, *RepD/D*: a protein-DNA adduct arising during plasmid replication.* Biochem Soc Trans, 1995. **23**(3): p. 442S.
85. Thomas, C.D., D.F. Balson, and W.V. Shaw, *In vitro studies of the initiation of staphylococcal plasmid replication. Specificity of RepD for its origin (oriD) and characterization of the Rep-ori tyrosyl ester intermediate.* J Biol Chem, 1990. **265**(10): p. 5519-30.

86. Jin, R., M.E. Fernandez-Beros, and R.P. Novick, *Why is the initiation nick site of an AT-rich rolling circle plasmid at the tip of a GC-rich cruciform?* EMBO J, 1997. **16**(14): p. 4456-66.
87. Slatter, A.F., C.D. Thomas, and M.R. Webb, *PcrA helicase tightly couples ATP hydrolysis to unwinding double-stranded DNA, modulated by the initiator protein for plasmid replication, RepD.* Biochemistry, 2009. **48**(27): p. 6326-34.
88. Soultanas, P., et al., *Plasmid replication initiator protein RepD increases the processivity of PcrA DNA helicase.* Nucleic Acids Res, 1999. **27**(6): p. 1421-8.
89. Dillingham, M.S., et al., *Fluorescent single-stranded DNA binding protein as a probe for sensitive, real-time assays of helicase activity.* Biophys J, 2008. **95**(7): p. 3330-9.
90. Bruck, I., R.E. Georgescu, and M. O'Donnell, *Conserved interactions in the Staphylococcus aureus DNA PolC chromosome replication machine.* J Biol Chem, 2005. **280**(18): p. 18152-62.
91. Indiani, C., et al., *Translesion DNA polymerases remodel the replisome and alter the speed of the replicative helicase.* Proc Natl Acad Sci U S A, 2009. **106**(15): p. 6031-8.
92. Machon, C., et al., *RepD-mediated recruitment of PcrA helicase at the Staphylococcus aureus pC221 plasmid replication origin, oriD.* Nucleic Acids Res, 2009.
93. Arbore, C., L.M. Lewis, and M.R. Webb, *Kinetic Mechanism of Initiation by RepD as a Part of Asymmetric, Rolling Circle Plasmid Unwinding.* Biochemistry, 2012. **51**(17): p. 3684-93.
94. Park, J., et al., *PcrA Helicase Dismantles RecA Filaments by Reeling in DNA in Uniform Steps.* Cell, 2010. **142**(4): p. 544-555.
95. Anand, S.P., et al., *DNA helicase activity of PcrA is not required for the displacement of RecA protein from DNA or inhibition of RecA-mediated strand exchange.* J Bacteriol, 2007. **189**(12): p. 4502-9.
96. Takahashi, S., et al., *The rep mutation. VI. Purification and properties of the Escherichia coli rep protein, DNA helicase III.* Can J Biochem, 1979. **57**(6): p. 855-66.
97. Petit, M.A. and D. Ehrlich, *Essential bacterial helicases that counteract the toxicity of recombination proteins.* EMBO J, 2002. **21**(12): p. 3137-47.
98. Guarne, A., et al., *Structure of the MutL C-terminal domain: a model of intact MutL and its roles in mismatch repair.* EMBO J, 2004. **23**(21): p. 4134-45.
99. Arthur, H.M. and R.G. Lloyd, *Hyper-recombination in uvrD mutants of Escherichia coli K-12.* Mol Gen Genet, 1980. **180**(1): p. 185-91.
100. Atkinson, J., et al., *Localization of an accessory helicase at the replisome is critical in sustaining efficient genome duplication.* Nucleic Acids Res, 2010.
101. Veaute, X., et al., *UvrD helicase, unlike Rep helicase, dismantles RecA nucleoprotein filaments in Escherichia coli.* EMBO J, 2005. **24**(1): p. 180-9.
102. Lusetti, S.L. and M.M. Cox, *The bacterial RecA protein and the recombinational DNA repair of stalled replication forks.* Annu Rev Biochem, 2002. **71**: p. 71-100.

103. Khanna, K.K. and S.P. Jackson, *DNA double-strand breaks: signaling, repair and the cancer connection.* Nat Genet, 2001. **27**(3): p. 247-54.
104. Holthausen, J.T., C. Wyman, and R. Kanaar, *Regulation of DNA strand exchange in homologous recombination.* DNA Repair (Amst), 2010. **9**(12): p. 1264-72.
105. Kowalczykowski, S.C., et al., *Biochemistry of homologous recombination in Escherichia coli.* Microbiol Rev, 1994. **58**(3): p. 401-65.
106. Dupaigne, P., et al., *The Srs2 helicase activity is stimulated by Rad51 filaments on dsDNA: implications for crossover incidence during mitotic recombination.* Mol Cell, 2008. **29**(2): p. 243-54.
107. Radding, C.M., *Helical RecA nucleoprotein filaments mediate homologous pairing and strand exchange.* Biochim Biophys Acta, 1989. **1008**(2): p. 131-45.
108. Lakowicz, J.R., *Principles of Fluorescence Spectroscopy.* 2006.
109. Jablonski, A.Z., *Efficiency of Anti-Stokes Fluorescence in Dyes* Nature, 1933. **131**: p. 839-840.
110. Piston, D.W. and G.-J. Kremers, *Fluorescent protein FRET: the good, the bad and the ugly.* Trends in Biochemical Sciences, 2007. **32**(9): p. 407-414.
111. Roy, R., S. Hohng, and T. Ha, *A practical guide to single-molecule FRET.* Nature Methods, 2008. **5**: p. 507-516.
112. Tinoco, I., Jr. and R.L. Gonzalez, Jr., *Biological mechanisms, one molecule at a time.* Genes Dev, 2011. **25**(12): p. 1205-31.
113. Tan, L.P. and S.Q. Yao, *Intein-mediated, in vitro and in vivo protein modifications with small molecules.* Protein Pept Lett, 2005. **12**(8): p. 769-75.
114. Smith, M.E., et al., *Protein modification, bioconjugation, and disulfide bridging using bromomaleimides.* J Am Chem Soc, 2010. **132**(6): p. 1960-5.
115. England, P.M., *Unnatural amino acid mutagenesis: a precise tool for probing protein structure and function.* Biochemistry, 2004. **43**(37): p. 11623-9.
116. Chin, J.W., et al., *Addition of p-azido-L-phenylalanine to the genetic code of Escherichia coli.* J Am Chem Soc, 2002. **124**(31): p. 9026-7.
117. Algar, W.R., A.J. Tavares, and U.J. Krull, *Beyond labels: a review of the application of quantum dots as integrated components of assays, bioprobes, and biosensors utilizing optical transduction.* Anal Chim Acta, 2010. **673**(1): p. 1-25.
118. Webb, M.R., *Development of fluorescent biosensors for probing the function of motor proteins.* Mol Biosyst, 2007. **3**(4): p. 249-56.
119. Kerman, K., et al., *Peptide biosensors for the electrochemical measurement of protein kinase activity.* Anal Chem, 2008. **80**(24): p. 9395-401.
120. Brune, M., et al., *Mechanism of inorganic phosphate interaction with phosphate binding protein from Escherichia coli.* Biochemistry, 1998. **37**(29): p. 10370-80.

121. Kunzelmann, S., et al., *Mechanism of interaction between single-stranded DNA binding protein and DNA.* Biochemistry, 2010. **49**(5): p. 843-52.
122. Kunzelmann, S. and M.R. Webb, *A biosensor for fluorescent determination of ADP with high time resolution.* J Biol Chem, 2009. **284**(48): p. 33130-33138.
123. Kunzelmann, S. and M.R. Webb, *A fluorescent, reagentless biosensor for ADP based on tetramethylrhodamine-labeled ParM.* ACS Chem Biol, 2010. **5**(4): p. 415-25.
124. Eccleston, J.F., S.R. Martin, and M.J. Schilstra, *Rapid kinetic techniques.* Methods Cell Biol, 2008. **84**: p. 445-77.
125. Gutfreund, H., *Rapid-flow techniques and their contributions to enzymology.* Trends Biochem Sci, 1999. **24**(11): p. 457-60.
126. Coates, J.H., A.H. Criddle, and M.A. Geeves, *Pressure-relaxation studies of pyrene-labelled actin and myosin subfragment 1 from rabbit skeletal muscle. Evidence for two states of acto-subfragment 1.* Biochem J, 1985. **232**(2): p. 351-6.
127. Turner, D.H., et al., *Dimerization of proflavin by the laser raman temperature-jump method.* Nature, 1972. **239**(5369): p. 215-7.
128. Eccleston, J.F., J.P. Hutchinson, and D.M. Jameson, *Fluorescence-based assays.* Prog Med Chem, 2005. **43**: p. 19-48.
129. Gibson, Q.H., *Apparatus for the study of rapid reactions.* J Physiol, 1952. **117**(4): p. 49P-50P.
130. Eccleston, J.F., J.P. Hutchinson, and H.D. White, *Stopped-flow techniques*. Protein ligand interactions: structure and spectroscopy. A Practical Approach Series, ed. S.E. Harding and B.Z. Chowdry. 2001, Oxford, U.K.: Oxford University Press.
131. Jiang, Y., et al., *Sensing cooperativity in ATP hydrolysis for single multisubunit enzymes in solution.* Proc Natl Acad Sci U S A, 2011. **108**(41): p. 16962-7.
132. Skordalakes, E. and J.M. Berger, *Structure of the Rho transcription terminator: mechanism of mRNA recognition and helicase loading.* Cell., 2003. **114**(1): p. 135-46.
133. Zhang, W., et al., *Directional loading and stimulation of PcrA helicase by the replication initiator protein RepD.* J Mol Biol, 2007. **371**(2): p. 336-48.
134. Henn, A., et al., *Visualization of unwinding activity of duplex RNA by DbpA, a DEAD box helicase, at single-molecule resolution by atomic force microscopy.* Proc Natl Acad Sci U S A, 2001. **98**(9): p. 5007-12.
135. Axelrod, D., J.C. Dr. John, and Dr. H. William Detrich, III, *Chapter 7 Total Internal Reflection Fluorescence Microscopy*, in *Methods in Cell Biology*. 2008, Academic Press. p. 169-221.
136. Lakowicz, J.R., ed. *Topics Fluoresc. Spectrosc. 3*rd ed. 1992, Plenum Press, New York 289-342.
137. Hern, J.A., et al., *Formation and dissociation of M1 muscarinic receptor dimers seen by total internal reflection fluorescence imaging of single molecules.* Proc Natl Acad Sci U S A, 2010. **107**(6): p. 2693-8.
138. Ha, T., et al., *Initiation and re-initiation of DNA unwinding by the Escherichia coli Rep helicase.* Nature, 2002. **419**(6907): p. 638-41.

139. Honda, M., et al., *Single-Molecule Analysis Reveals Differential Effect of ssDNA-Binding Proteins on DNA Translocation by XPD Helicase.* Molecular Cell, 2009. **35**(5): p. 694-703.
140. Roy, R., et al., *SSB protein diffusion on single-stranded DNA stimulates RecA filament formation.* Nature, 2009. **461**(7267): p. 1092-7.
141. Johnson, D.S., et al., *Single-molecule studies reveal dynamics of DNA unwinding by the ring-shaped T7 helicase.* Cell, 2007. **129**(7): p. 1299-309.
142. Tomko, E.J., et al., *5'-Single-stranded/duplex DNA junctions are loading sites for E. coli UvrD translocase.* EMBO J, 2010. **29**(22): p. 3826-39.
143. Rothenberg, E. and T. Ha, *Single-molecule FRET analysis of helicase functions.* Methods Mol Biol, 2010. **587**: p. 29-43.
144. Myong, S., et al., *Spring-loaded mechanism of DNA unwinding by hepatitis C virus NS3 helicase.* Science, 2007. **317**(5837): p. 513-6.
145. Zhou, R., et al., *SSB Functions as a Sliding Platform that Migrates on DNA via Reptation.* Cell, 2011. **146**(2): p. 222-32.
146. Fili, N., et al., *Visualizing helicases unwinding DNA at the single molecule level.* Nucleic Acids Res, 2010.
147. Ashkin, A. and J.M. Dziedzic, *Optical trapping and manipulation of viruses and bacteria.* Science, 1987. **235**(4795): p. 1517-20.
148. Ashkin, A., et al., *Observation of a single-beam gradient force optical trap for dielectric particles.* Opt Lett, 1986. **11**(5): p. 288.
149. Cheng, W., et al., *Single-base pair unwinding and asynchronous RNA release by the hepatitis C virus NS3 helicase.* Science, 2011. **333**(6050): p. 1746-9.
150. Bustamante, C., W. Cheng, and Y.X. Mejia, *Revisiting the central dogma one molecule at a time.* Cell, 2011. **144**(4): p. 480-97.
151. Fuller, D.N., et al., *Measurements of single DNA molecule packaging dynamics in bacteriophage lambda reveal high forces, high motor processivity, and capsid transformations.* J Mol Biol, 2007. **373**(5): p. 1113-22.
152. Chemla, Y.R., et al., *Mechanism of force generation of a viral DNA packaging motor.* Cell, 2005. **122**(5): p. 683-92.
153. Smith, S.B., L. Finzi, and C. Bustamante, *Direct mechanical measurements of the elasticity of single DNA molecules by using magnetic beads.* Science, 1992. **258**(5085): p. 1122-6.
154. Strick, T.R., et al., *The elasticity of a single supercoiled DNA molecule.* Science, 1996. **271**(5257): p. 1835-7.
155. Lionnet, T., et al., *Real-time observation of bacteriophage T4 gp41 helicase reveals an unwinding mechanism.* Proc Natl Acad Sci U S A, 2007. **104**(50): p. 19790-5.
156. De Vlaminck, I. and C. Dekker, *Recent advances in magnetic tweezers.* Annu Rev Biophys, 2012. **41**: p. 453-72.
157. Toseland, C.P., et al., *The ATPase cycle of PcrA helicase and its coupling to translocation on DNA.* J Mol Biol, 2009. **392**(4): p. 1020-32.
158. Toseland, C.P. and M.R. Webb, *Fluorescence tools to measure helicase activity in real time.* Methods, 2010. **51**(3): p. 259-68.

159. Birnboim, H.C. and J. Doly, *A rapid alkaline extraction procedure for screening recombinant plasmid DNA.* Nucleic Acids Res, 1979. **7**(6): p. 1513-23.
160. Mashanov, G.I. and J.E. Molloy, *Automatic detection of single fluorophores in live cells.* Biophys J, 2007. **92**(6): p. 2199-211.
161. Ghosh, S.S., et al., *Use of maleimide-thiol coupling chemistry for efficient syntheses of oligonucleotide-enzyme conjugate hybridization probes.* Bioconjug Chem, 1990. **1**(1): p. 71-6.
162. Brune, M., et al., *Direct, real-time measurement of rapid inorganic phosphate release using a novel fluorescent probe and its application to actomyosin subfragment 1 ATPase.* Biochemistry, 1994. **33**(27): p. 8262-71.
163. Martinez-Senac, M.M. and M.R. Webb, *Mechanism of translocation and kinetics of DNA unwinding by the helicase RecG.* Biochemistry, 2005. **44**(51): p. 16967-76.
164. Okoh, M.P., et al., *A Biosensor for Inorganic Phosphate Using a Rhodamine-Labeled Phosphate Binding Proteinâ€* Biochemistry, 2006. **45**(49): p. 14764-14771.
165. Soultanas, P., et al., *Uncoupling DNA translocation and helicase activity in PcrA: direct evidence for an active mechanism.* EMBO J, 2000. **19**(14): p. 3799-810.
166. Lipps, H.J. and D. Rhodes, *G-quadruplex structures: in vivo evidence and function.* Trends Cell Biol, 2009. **19**(8): p. 414-22.
167. Paeschke, K., J.A. Capra, and V.A. Zakian, *DNA replication through G-quadruplex motifs is promoted by the Saccharomyces cerevisiae Pif1 DNA helicase.* Cell, 2011. **145**(5): p. 678-91.
168. Cadman, C.J. and P. McGlynn, *PriA helicase and SSB interact physically and functionally.* Nucleic Acids Res, 2004. **32**(21): p. 6378-87.
169. Rasnik, I., et al., *DNA-binding orientation and domain conformation of the E. coli rep helicase monomer bound to a partial duplex junction: single-molecule studies of fluorescently labeled enzymes.* J Mol Biol, 2004. **336**(2): p. 395-408.
170. Slatter, A.F., *Kinetic mechanism of the interaction of RepD and PcrA helicase during plasmid replication*, in *Department of Physical Biochemistry, MRC National Institute for Medical Research*. 2009, Univercity College London, UCL: London.
171. Jain, A., et al., *Probing cellular protein complexes using single-molecule pull-down.* Nature, 2011. **473**(7348): p. 484-8.
172. Lippincott-Schwartz, J., E. Snapp, and A. Kenworthy, *Studying protein dynamics in living cells.* Nat Rev Mol Cell Biol, 2001. **2**(6): p. 444-56.
173. Axelrod, D., *Total internal reflection fluorescence microscopy.* Methods Cell Biol, 1989. **30**: p. 245-70.
174. Axelrod, D., *Total internal reflection fluorescence microscopy in cell biology.* Traffic, 2001. **2**(11): p. 764-74.
175. Mattheyses, A.L., S.M. Simon, and J.Z. Rappoport, *Imaging with total internal reflection fluorescence microscopy for the cell biologist.* J Cell Sci, 2010. **123**(Pt 21): p. 3621-8.

176. Chisty, L.T., et al., *Monomeric PcrA helicase processively unwinds plasmid lengths of DNA in the presence of the initiator protein RepD.* Nucleic Acids Res, 2013.
177. Dou, S.X. and X.G. Xi, *Fluorometric assays for characterizing DNA helicases.* Methods, 2010. **51**(3): p. 295-302.
178. Bustamante, C., *In singulo biochemistry: when less is more.* Annu Rev Biochem, 2008. **77**: p. 45-50.
179. Ha, T., *Single-molecule fluorescence resonance energy transfer.* Methods, 2001. **25**(1): p. 78-86.
180. Cheng, W., et al., *The 2B domain of the Escherichia coli Rep protein is not required for DNA helicase activity.* Proc Natl Acad Sci U S A, 2002. **99**(25): p. 16006-11.
181. Lohman, T.M. and L.B. Overman, *Two binding modes in Escherichia coli single strand binding protein-single stranded DNA complexes. Modulation by NaCl concentration.* J. Biol. Chem., 1985. **260**: p. 3594-3603.
182. Bujalowski, W. and T.M. Lohman, *Escherichia coli single-strand binding protein forms multiple, distinct complexes with single-stranded DNA.* Biochemistry, 1986. **25**: p. 7799-7802.
183. Lohman, T.M. and M.E. Ferrari, *Escherichia coli single-stranded DNA-binding protein: multiple DNA-binding modes and cooperativities.* Annu Rev Biochem, 1994. **63**: p. 527-70.
184. Betterton, M.D. and F. Julicher, *Opening of nucleic-acid double strands by helicases: active versus passive opening.* Phys Rev E Stat Nonlin Soft Matter Phys, 2005. **71**(1 Pt 1): p. 011904.
185. Pyle, A.M., *Translocation and unwinding mechanisms of RNA and DNA helicases.* Annu Rev Biophys, 2008. **37**: p. 317-36.
186. Long, J.E., N. Renzette, and S.J. Sandler, *Suppression of constitutive SOS expression by recA4162 (I298V) and recA4164 (L126V) requires UvrD and RecX in Escherichia coli K-12.* Mol Microbiol, 2009. **73**(2): p. 226-39.
187. Flores, M.J., N. Sanchez, and B. Michel, *A fork-clearing role for UvrD.* Mol Microbiol, 2005. **57**(6): p. 1664-75.
188. Flores, M.J., V. Bidnenko, and B. Michel, *The DNA repair helicase UvrD is essential for replication fork reversal in replication mutants.* EMBO Rep, 2004. **5**(10): p. 983-8.

9. Appendix

9.1. Chapter 4 Appendix

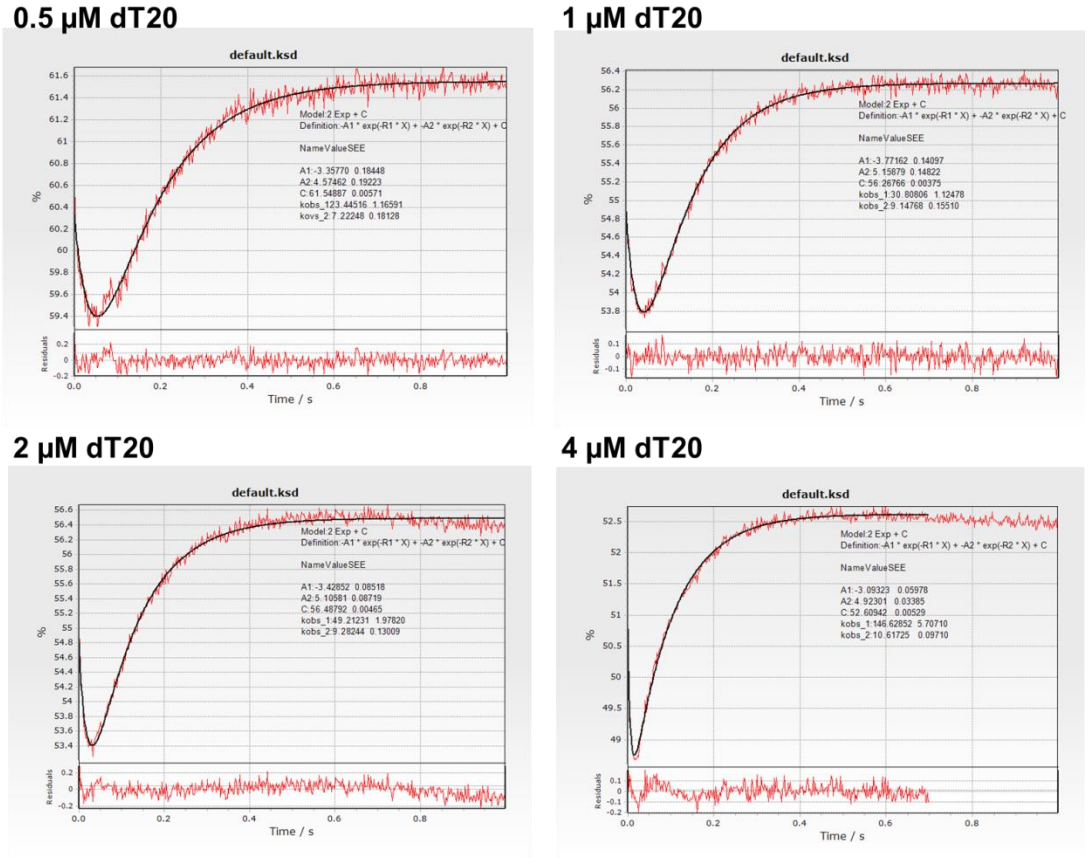

Figure 82. Fits of MDCC-PcrA(K138C) binding to dT_{20}.

The MDCC-PcrA(K138C) binding traces to dT_{20} fitted to double exponential fit. Y-axis:%, Intensity (a.u., arbitrary units). The traces were fitted using double exponential fit.

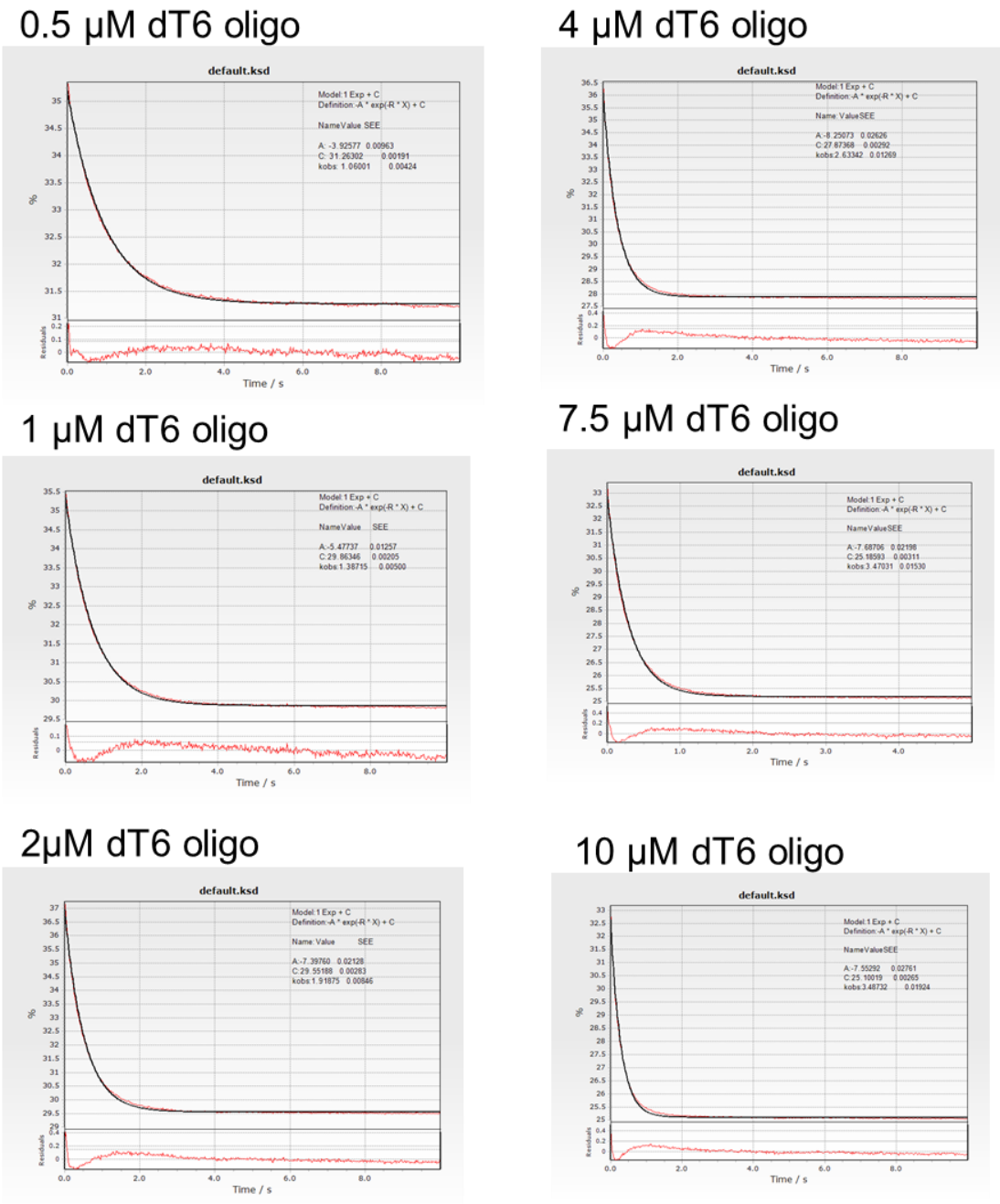

Figure 83. Fits of MDCC-PcrA(K138C) binding to dT_6.

The MDCC-PcrA(K138C) binding traces were fitted to single exponential decay for all the dT_6 concentrations measured. Y-axis:%, Intensity (a.u., arbitrary units). The traces were fitted using single exponential fit.

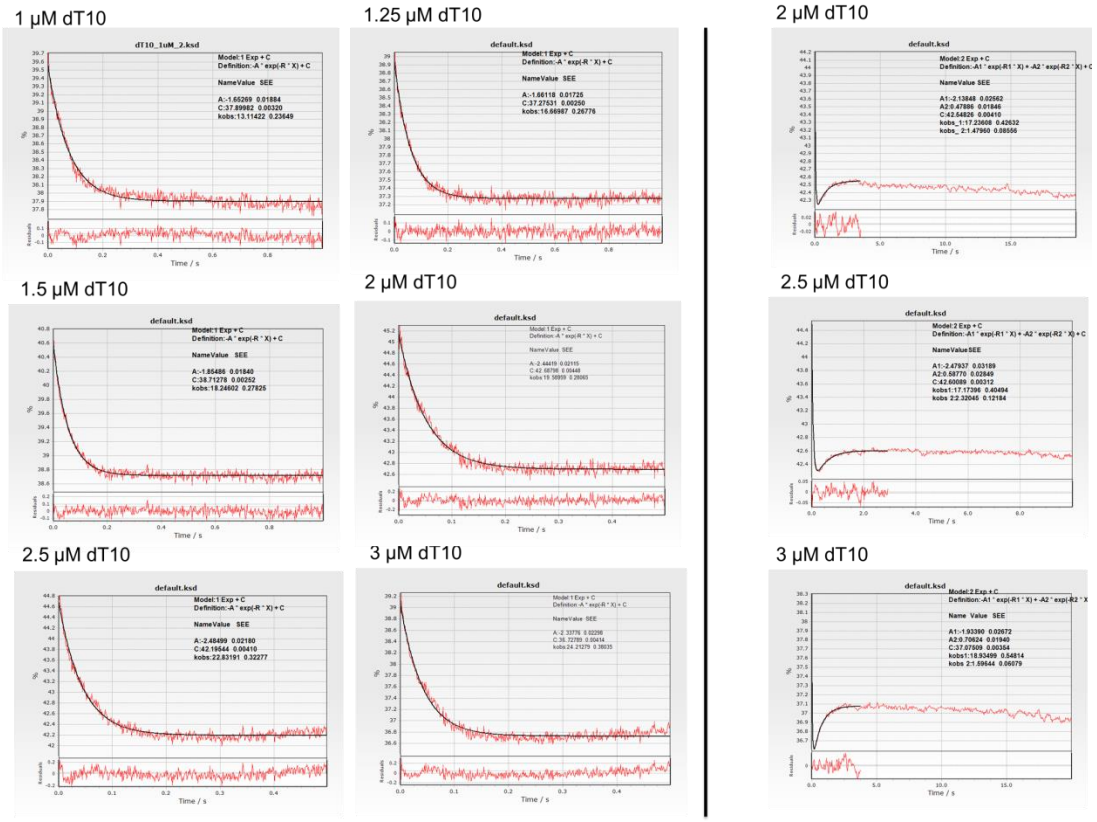

Figure 84. Fits of MDCC-PcrA(K138C) binding to dT_{10}.

The graphs on the left are single exponential fits of the End binding phase. The graphs on the right are showing the double exponential fit of MDCC-PcrA(K138C) binding to dT10. As the middle binding phase has small amplitude, the concentration dependence cannot be observed. Y-axis:%, Intensity (a.u., arbitrary units). The traces were fitted using single (left) double (right) exponential fit.

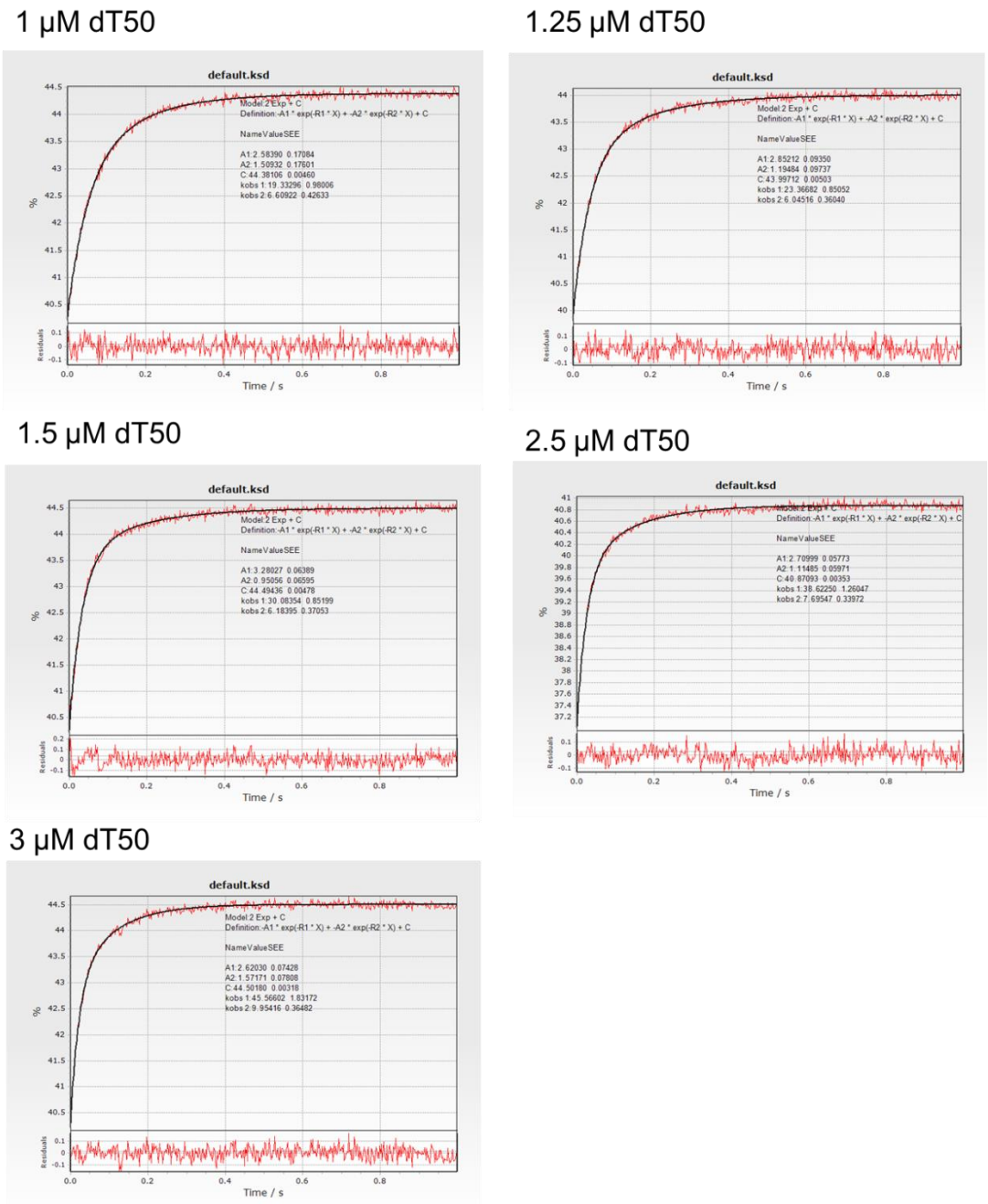

Figure 85. Fits of MDCC-PcrA(K138C) binding to dT_{50}.

The MDCC-PcrA(K138C) binding traces to varying dT_{50} concentrations fitted to double exponential. The second phase has not been used for analysis as it has does not show true concentration dependence and could be something like sliding on ssDNA. Y-axis:%, Intensity (a.u., arbitrary units). The traces were fitted using double exponential fit.

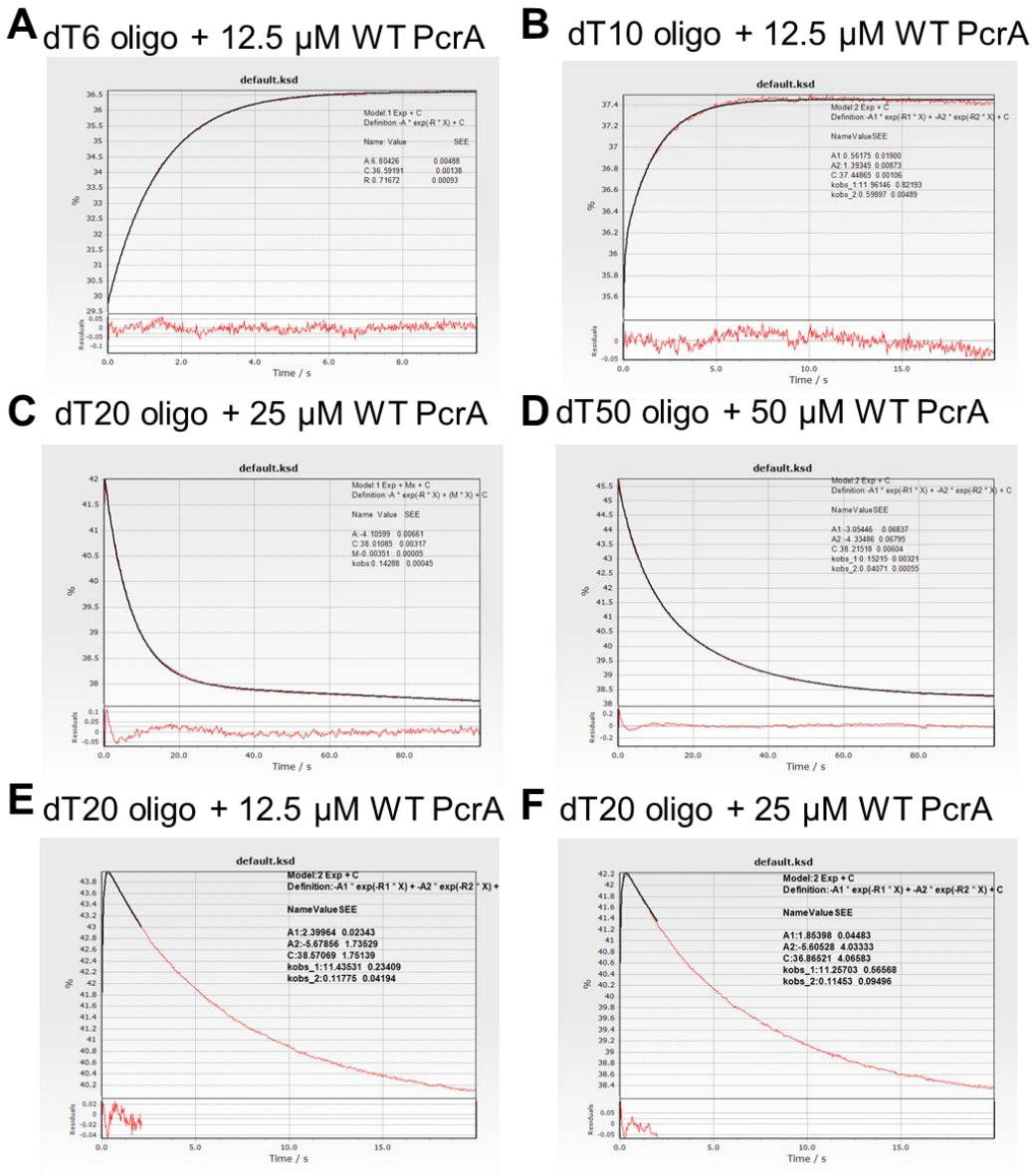

Figure 86. Fits of MDCC-PcrA(K138C) displacement by wild type PcrA.

Y-axis:%, Intensity (a.u., arbitrary units). The traces were fitted using single exponential fit with straight line.

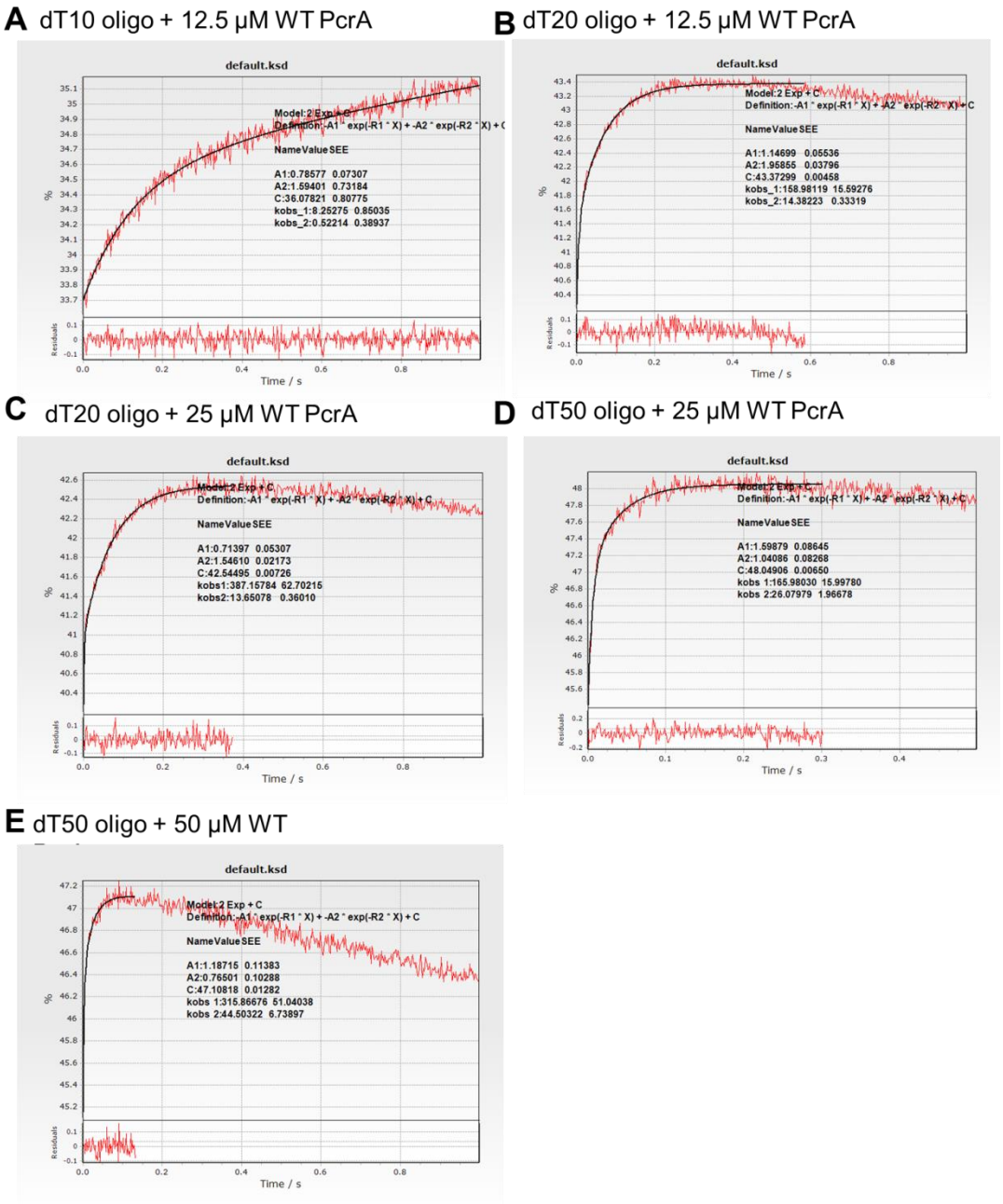

Figure 87. Fits to wild type PcrA binding phase in MDCC-PcrA(K138C) displacement assay.

Y-axis:%, Intensity (a.u., arbitrary units). The traces were fitted using double exponential fit. The first phase is the wild type PcrA binding to the ssDNA in close proximity to the MDCC-PcrA(K138C). The second phase is the actual dissociation of MDCC-PcrA(K138C) from dT_{10}.

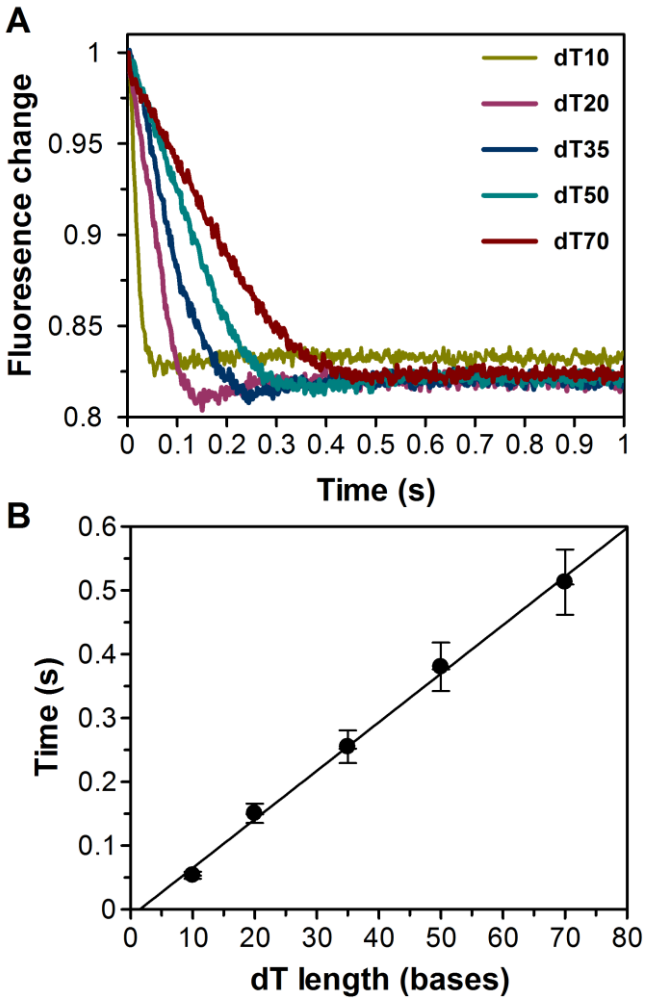

Figure 88. PcrA translocation rate at single molecule assay conditions.

A) Normalised traces for MDCC-PcrA(K138C) translocation on ssDNA with dT10 to dT70. B) The linear fit of translocation end time points against the number of bases in the oligos. The gradient of the linear fit is 0.0075 (SEM 0.0003). The measurements were done at 22°C in TIRF buffer with 100 nM MDCC-PcrA(K138C), 1 µM dT_x and 200 µM ATP.

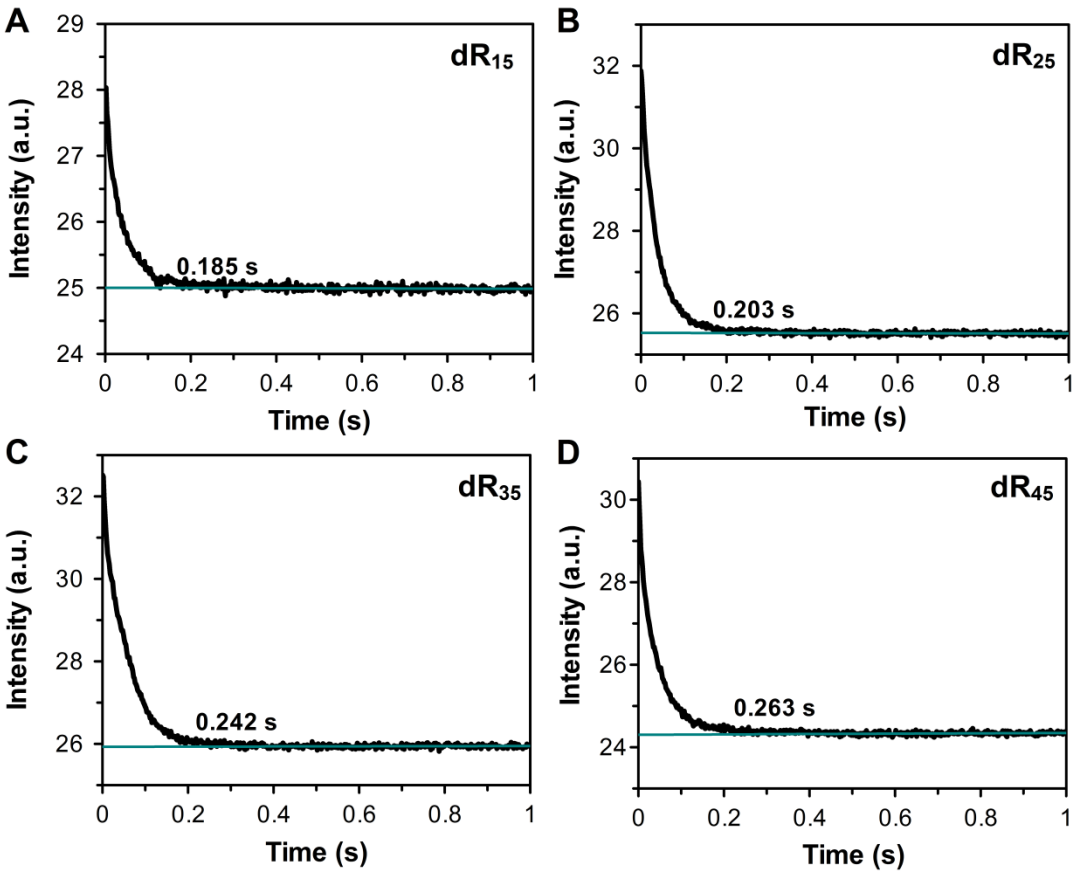

Figure 89. Fitting of MDCC-PcrA(K138C) translocation on random sequence oligos.

9.2. Chapter 5 Appendix

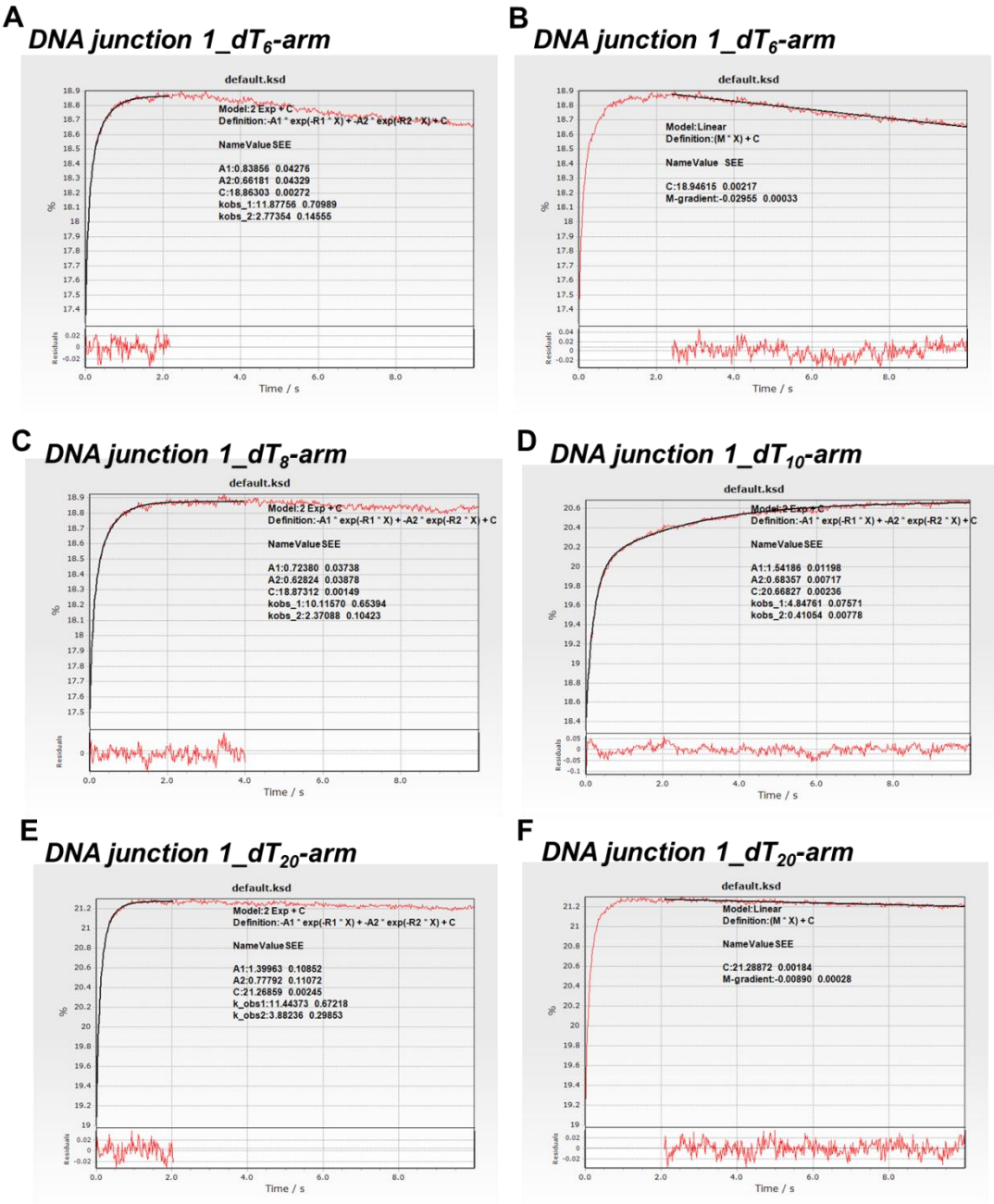

Figure 90. MDCC-PcrA(E449C) binding to RepD-DNA junction with varying dT_{arm} lengths.

Y-axis:%, Intensity (a.u., arbitrary units). The traces were fitted using double exponential fit (A and C to E)and linear regression (B and F).

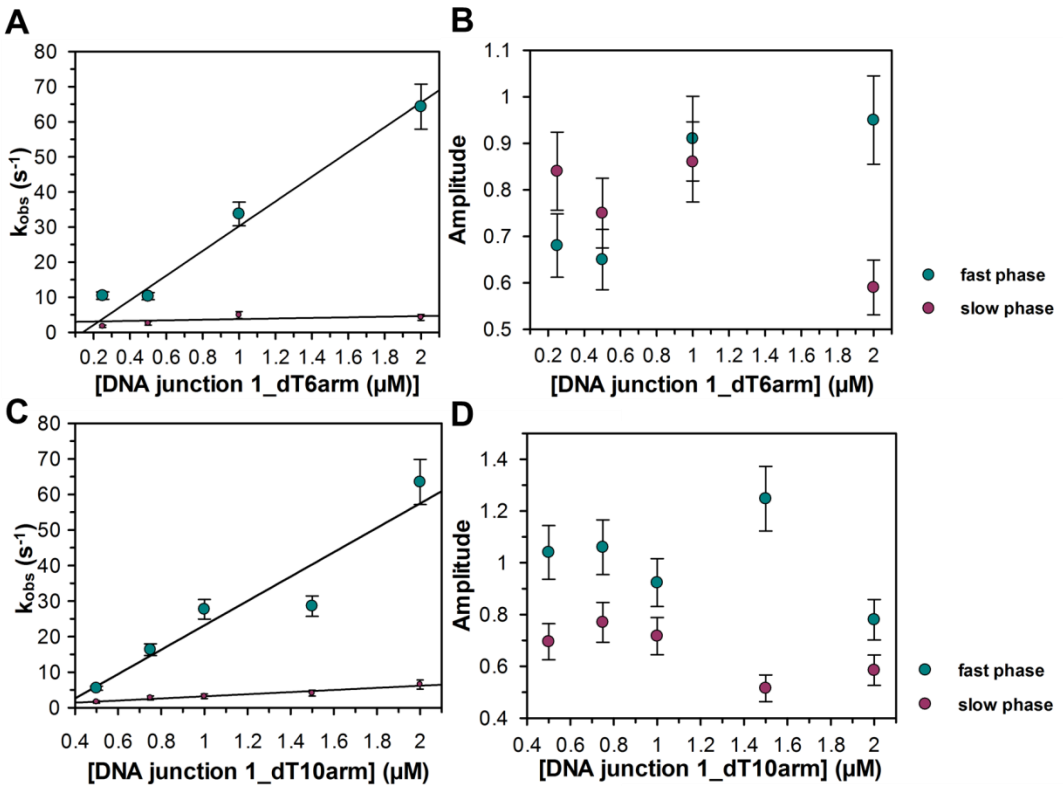

Figure 91. MDCC-PcrA(E449C) binding kinetics to DNA junctions with dT_6 and dT_{10}-arm without RepD.

The k_{obs} of PcrA binding to varying concentration of DNA junction 1_dT_{10}arm. The traces fit to double exponential. The fast phase has a gradient of 34.3 μM^{-1} s^{-1} and the slow phase 2.9 μM^{-1} s^{-1}. B) The amplitude change of fast and slow phase with varying DNA junction 1_dT_{10}arm concentration. C) The k_{obs} of PcrA binding to varying concentration of DNA junction 1_dT_{10}arm. The traces fit to double exponential. The fast phase has a gradient of 35.2 μM^{-1} s^{-1} and the slow phase 0.9 μM^{-1} s^{-1}. D) The amplitude change of fast and slow phase with varying DNA junction 1_dT_6arm concentration. Experimental conditions were same as in the Figure 45.

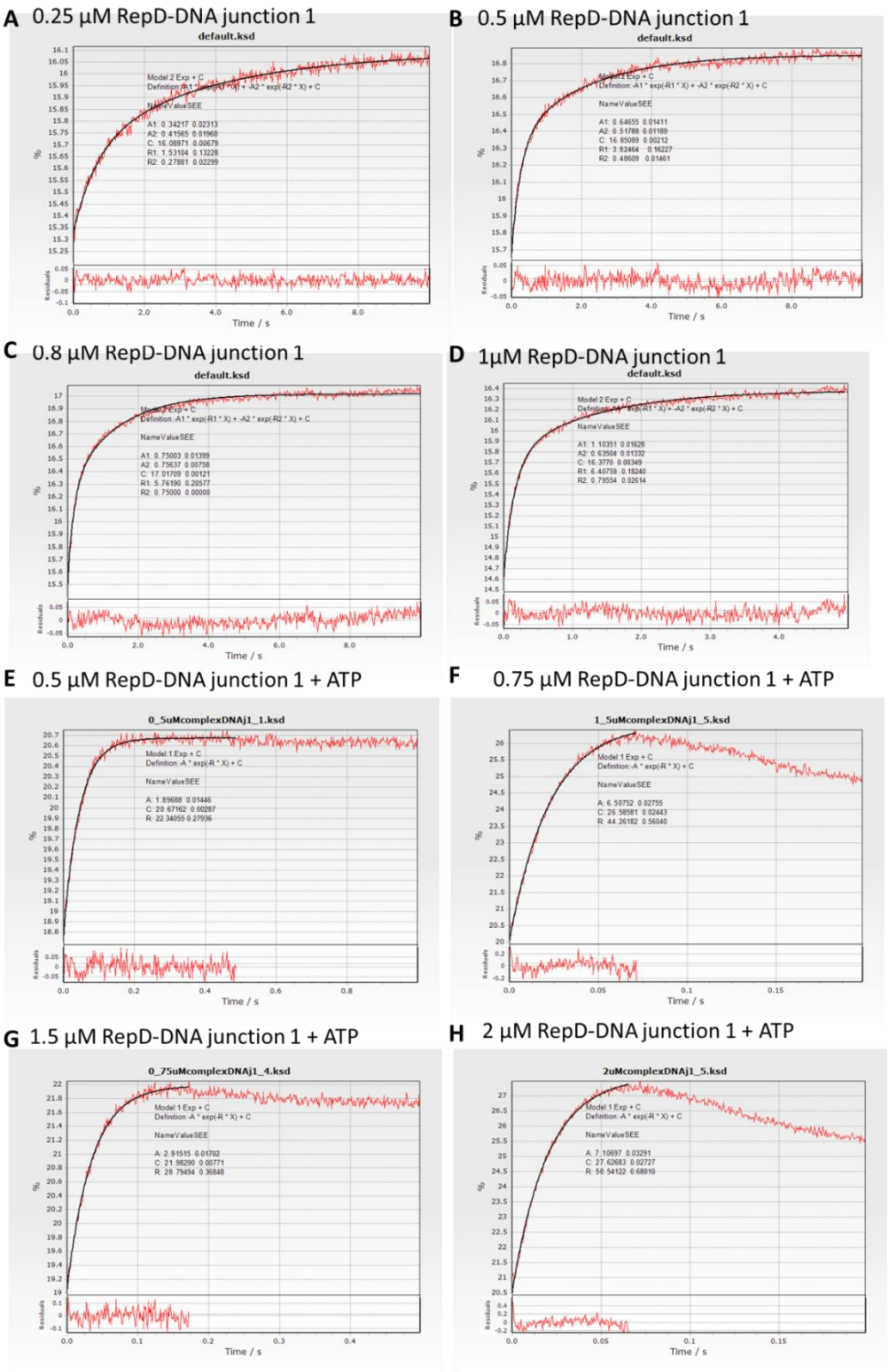

Figure 92. MDCC-PcrA(E449C) binding to varying concentration of RepD-DNA junction with and without ATP.

Y-axis:%, Intensity (a.u., arbitrary units). The traces were fitted using double exponential fit.

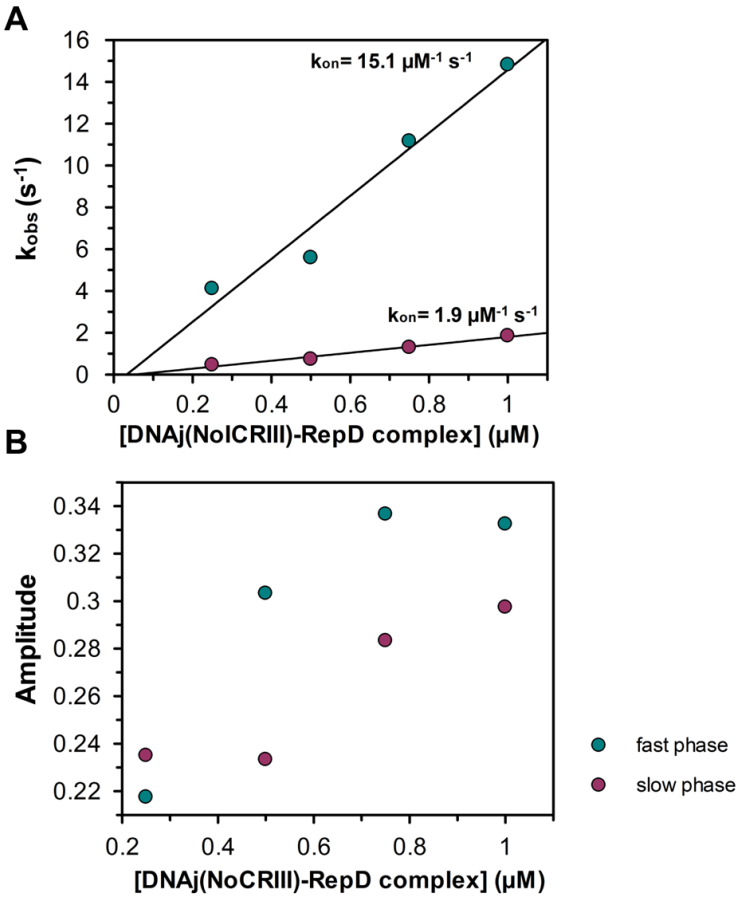

Figure 93. DNA junction (No ICRIII) bound to RepD.

A) PcrA binding kinetics to RepD-DNA junction (No ICRIII) complex with varying complex concentration. B) The signal amplitude change with increase concentration of RepD-DNA junction (No ICRIII) complex. Experimental conditions were same as in Figure 45.

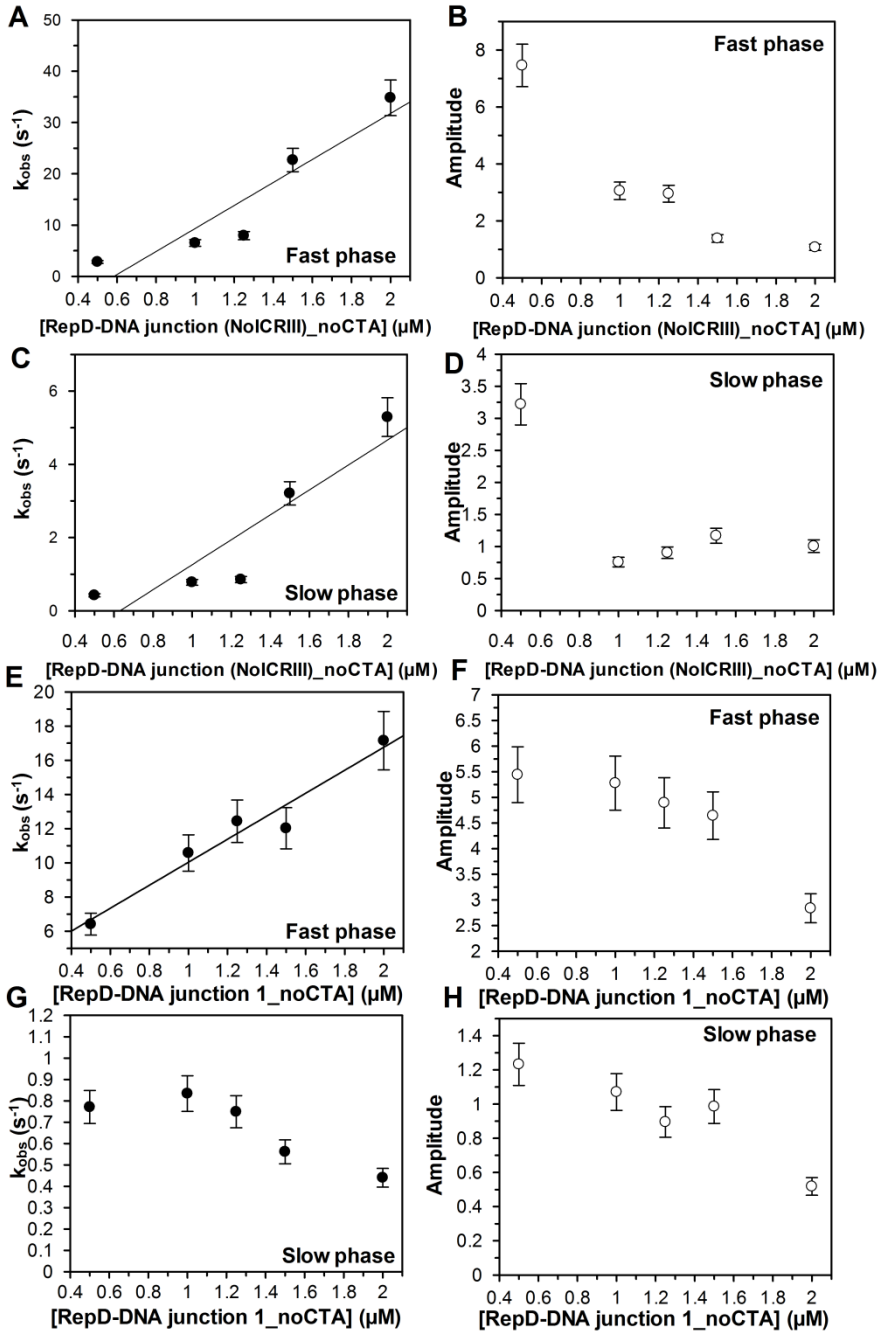

Figure 94. MDCC-PcrA(E449C) binding signal to DNA junctions without RepD-nicking site.

A) and C) are the observed rate constant dependence on the concentration of the RepD-DNA junction (no ICRIII, no CTA) for the fast and slow phase. B) and D) are the amplitude dependence on complex concentration for the RepD-DNA junction (no ICRIII, no CTA) fast and slow phase. E) and F) are the observed rate constant dependence on the concentration of the RepD-DNA junction (with ICRIII, no CTA) for the fast and slow phase. G) and H) are the amplitude dependence on complex concentration for the RepD-DNA junction (no ICRIII, no CTA) fast and slow phase. The experimental conditions are stated in Figure 45.

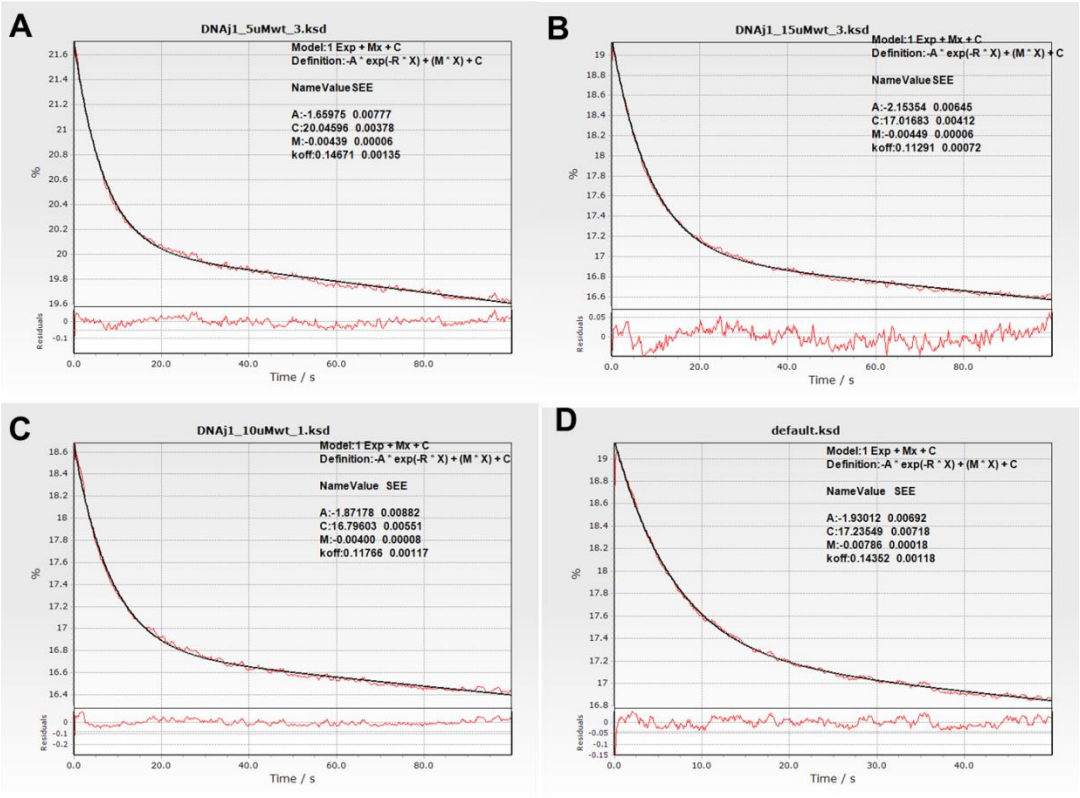

Figure 95. Fits of MDCC-PcrA(E449C) displacement from RepD-DNA junction 1.

A) 5 µM WT PcrA. B) 15 µM WT PcrA. C) 10 µM WT PcrA and D) 20 µM WT PcrA.

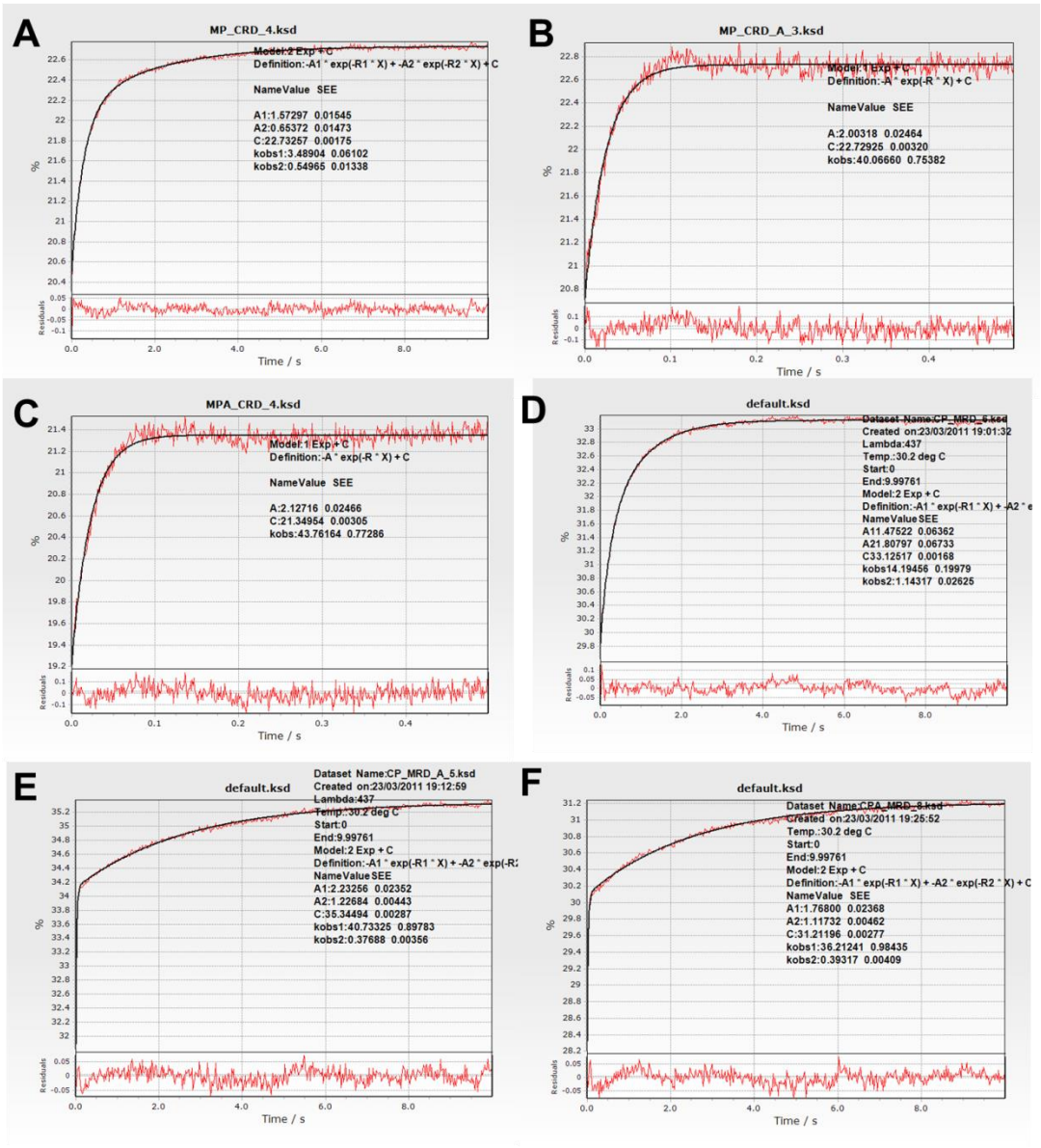

Figure 96.Fits for MDCC-PcrA(E449C) and Cy3-RepD/Cy3-PcrA(E449C) and MDCC-RepD FRET measurements with DNA junction 1 (bound to RepD).

A) Double exponential fit to MDCC-PcrA(E449C) mixed with Cy3-RepD-DNA junction 1. B) Single exponential fit to MDCC-PcrA(E449C) mixed with Cy3-RepD-DNA junction 1 with ATP. C) Single exponential fit to MDCC-PcrA(E449C)-ATP mixed with Cy3-RepD-DNA junction 1.D) Double exponential fit to Cy3-PcrA mixed with MDCC-RepD-DNA junction 1. E) Double exponential fit to Cy3-PcrA(E449C) mixed with Cy3-RepD-DNA junction 1 with ATP. F) Double exponential fit to Cy3-PcrA(E449C)-ATP mixed with MDCC-RepD-DNA junction 1. Y-axis:%, Intensity (a.u., arbitrary units). The traces were fitted using double exponential fit.

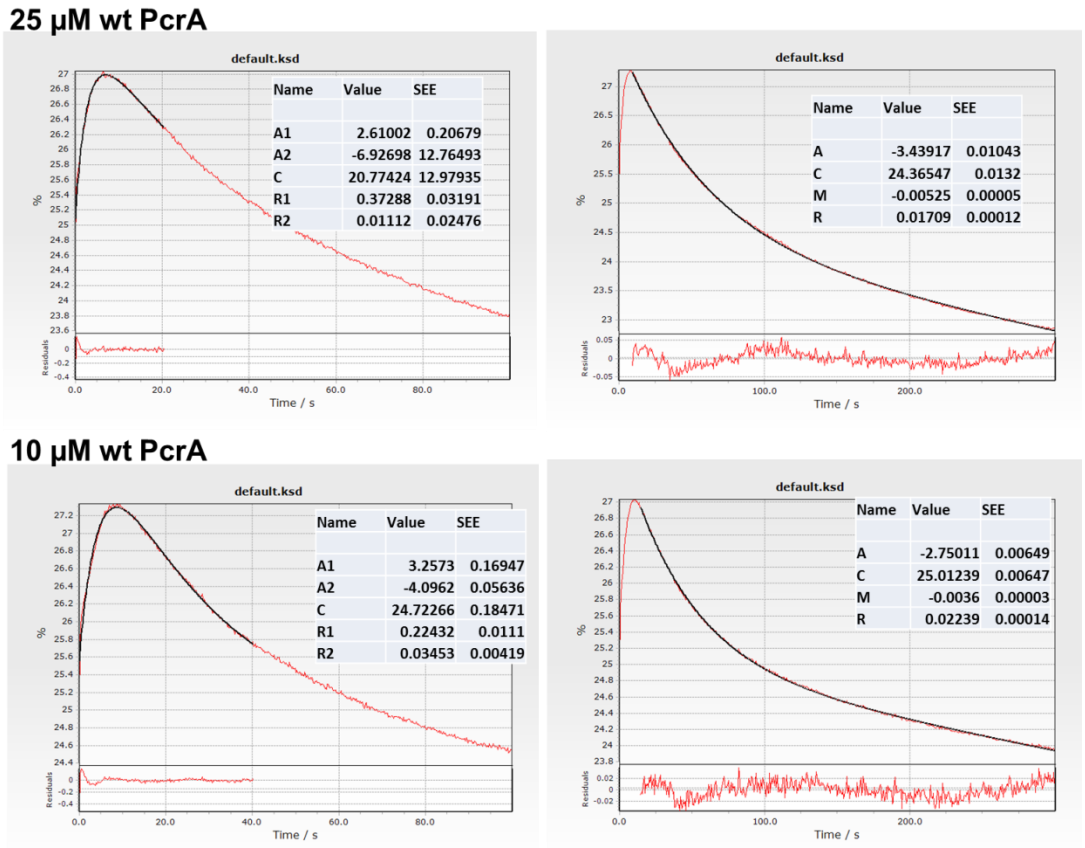

Figure 97. MDCC-PcrA(E449C) displacement assay traces from RepD-pCER*oriD* 3094 complex by wild type PcrA.

The fits on the left are done using double exponential and on the left by single exponential and slope. Y-axis:%, Intensity (a.u., arbitrary units). The traces were fitted using double exponential fit.

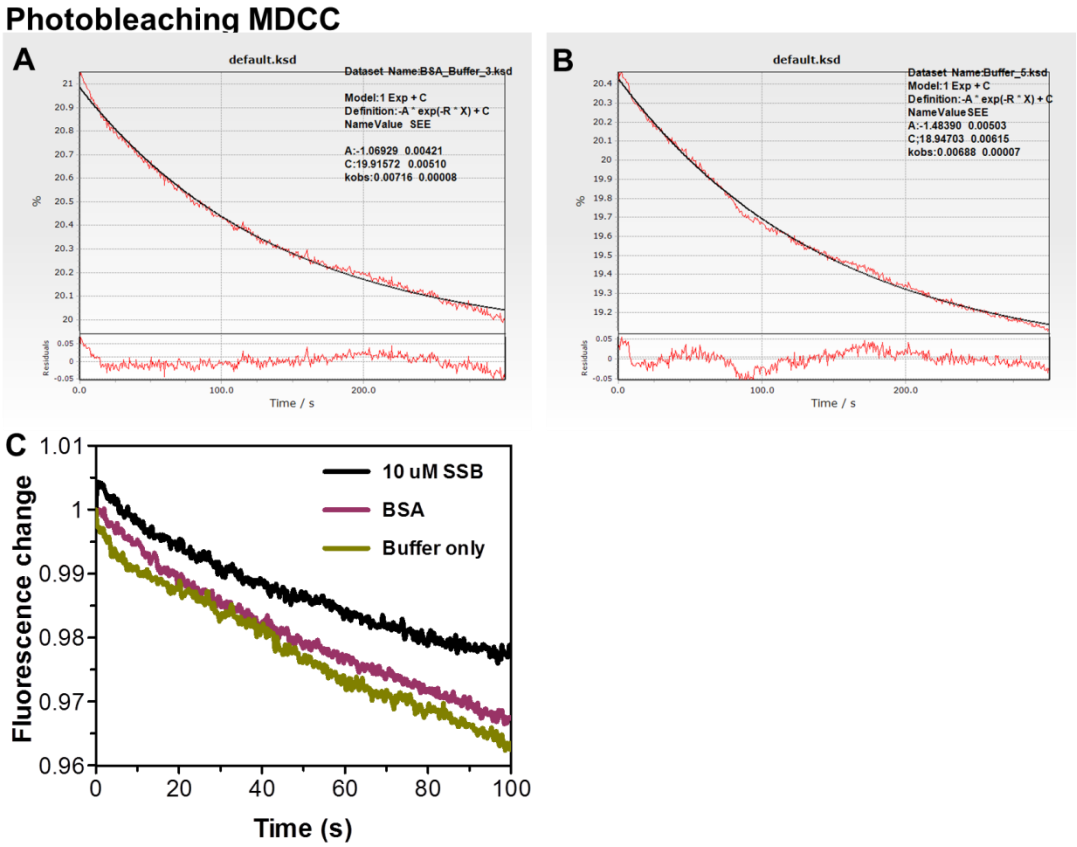

Figure 98. Photobleaching measurements of MDCC-PcrA(E449C) on stopped-flow instrument.

A) Single exponential fit of MDCC-PcrA(E449C) photobleaching inK200 buffer with 5 µM BSA. This has a k_{obs} of 0.007 s^{-1}. B) Single exponential fit of MDCC-PcrA(E449C) photobleaching inK200 buffer only. This also has a k_{obs} of 0.007 s^{-1}. B) Normalised photobleaching measurements MDCC-PcrA(E449C) in three conditions (only buffer, buffer with BSA and buffer with 10 µM SSB). These traces have also been fitted to single exponential and have k_{obs} between 0.007 and 0.011 s^{-1}. The experiments were done using the stopped-flow apparatus with 100 nM MDCC-PcrA(E449C) at 30 °C. The excitation was set to 436 nm and emission measured using 455 nm cut-off filter.

9.3. Chapter 6 Appendix

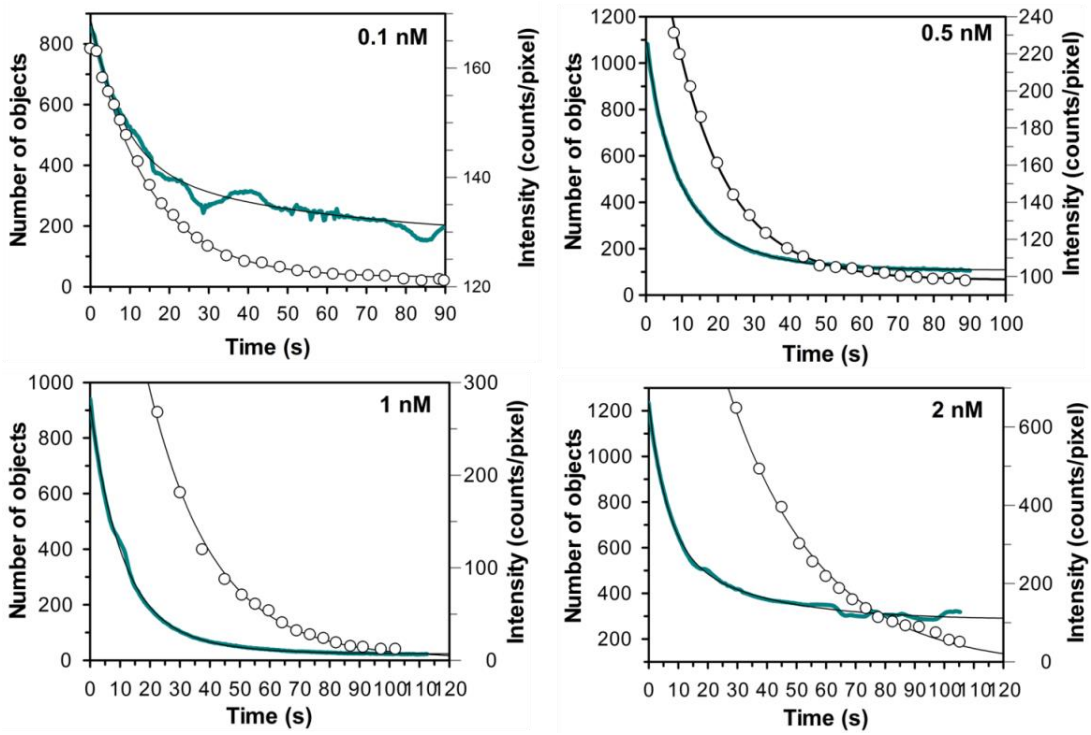

Figure 99. Extrapolation of Cy3B-bioPcrA(E449C) density on the flow cell surface.

The exponential decay of the intensity of total field of view is shown as blue trace and black is the fit of the intensity decay. The number of objects at each time point is shown as circles and the single exponential fit of object numbers is shown as black line. The sample preparation was done as in described in Methods Section 2.17.3. and the objects were tracked using ASPT by averaging five frames at each time point. The rate constant (k_c) was fixed to the rate constant determined from the rate of photobleaching of entire field of view and it varied from 0.036 to 0.066 s^{-1} between different records (0.1 nM k_c = 0.066 s^{-1}, 0.5 nM k_c = 0.053 s^{-1}, 1 nM k_c =0.036 s^{-1} and 2 nM k_c = 0.041 s^{-1}). The number of spots on the surface at the frame 1 is the value of the intercept on y-axis. As the area of record is known the object density can be calculated on the first frame of the record and results are shown in Table 16.

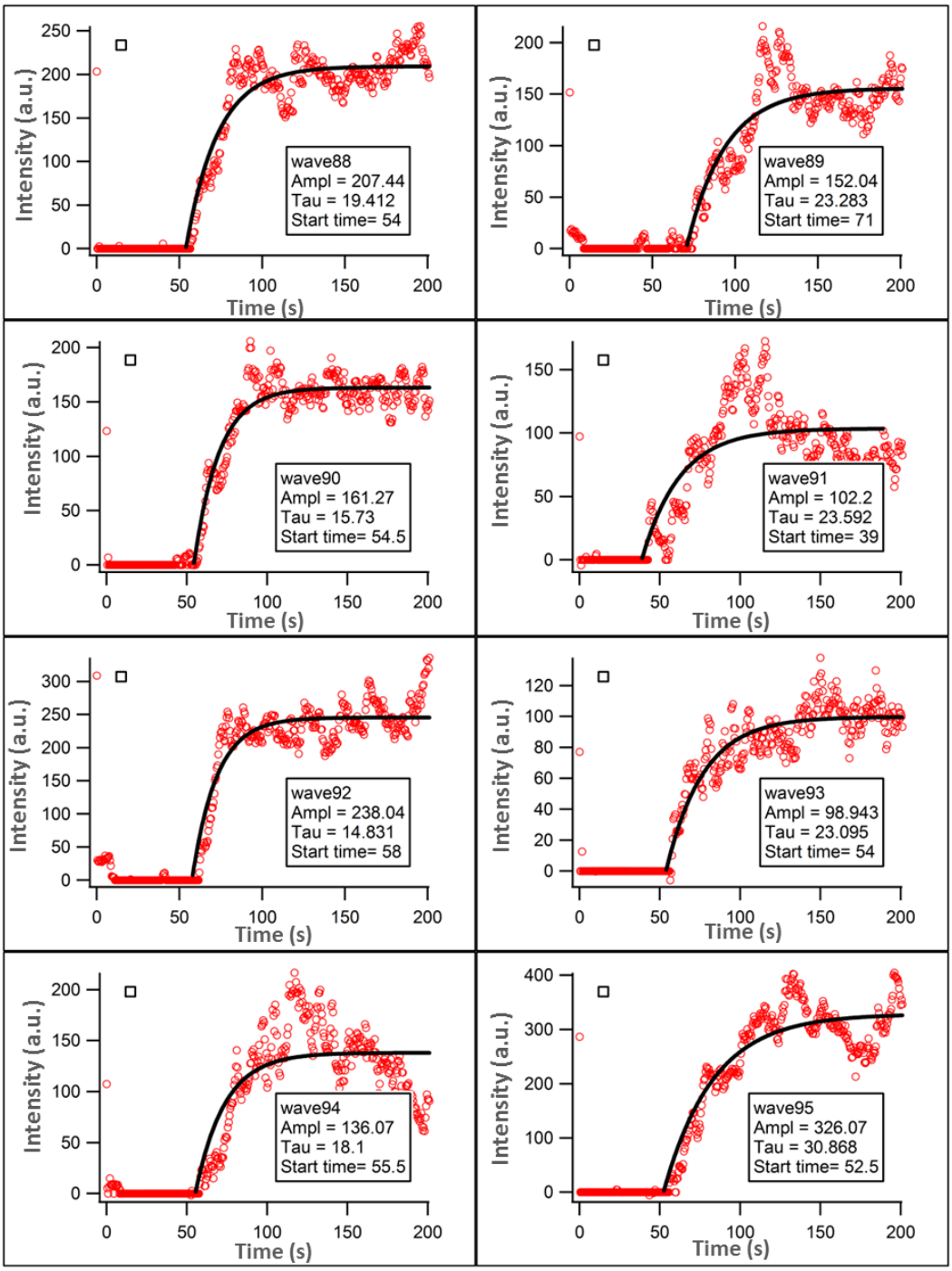

Figure 100. Individual unwinding events of pCER*oriD* 3094 bp.

The events were analysed using ASPT and the Δt and ΔI were determined by fitting a single exponential fit from start of record to defined point of time (75s and 150s) on Igor Pro programme. Between the two fitting times the results fitting better to Δt was used for final analysis. The fit produced an output file of Amplitude (ΔI), tau (1/4 of Δt) and start time of event /fit. These were used for determining the mean Δt and ΔI and the distribution of start time. The actual start time of event is calculated by deducting the time when ATP was added. For this record ATP was added at 49.61 s. In all of the graphs the x-axis is time (s) and y-axis is the fluorescence intensity (a.u.)

Measurements with 1.5 kb PCR product				Measurements with 3094 bp plasmid			
File	Events	Area (µm²)	Density of events	File	Events	Area (µm²)	Density of events
191109r44	59	465	0.13	090212r04	414	1743.7	0.24
191109r52	76	465	0.16	130212r01	273	1877.9	0.14
191109r49	72	465	0.15	130212r05	236	1896.1	0.12
		Average	**0.15**			**Average**	**0.17**
Measurements with 1.0 kb PCR product				**Measurements with 2437 bp plasmid**			
191109r06	77	465	0.17	090212r09	333	1743.7	0.19
191109r08	78	465	0.17	130212r08	294	1898.7	0.15
				220512r06	428	2985.5	0.14
		Average	**0.17**			**Average**	**0.16**

Table 23. Summary of single molecule plasmid unwinding event density analysis.

Event densities were determined for previous measurement done by Fili N. and Toseland C. with bioPcrA and linear DNA (PCR product) and to pCER*oriD* plasmid unwinding events by Chisty L.T.

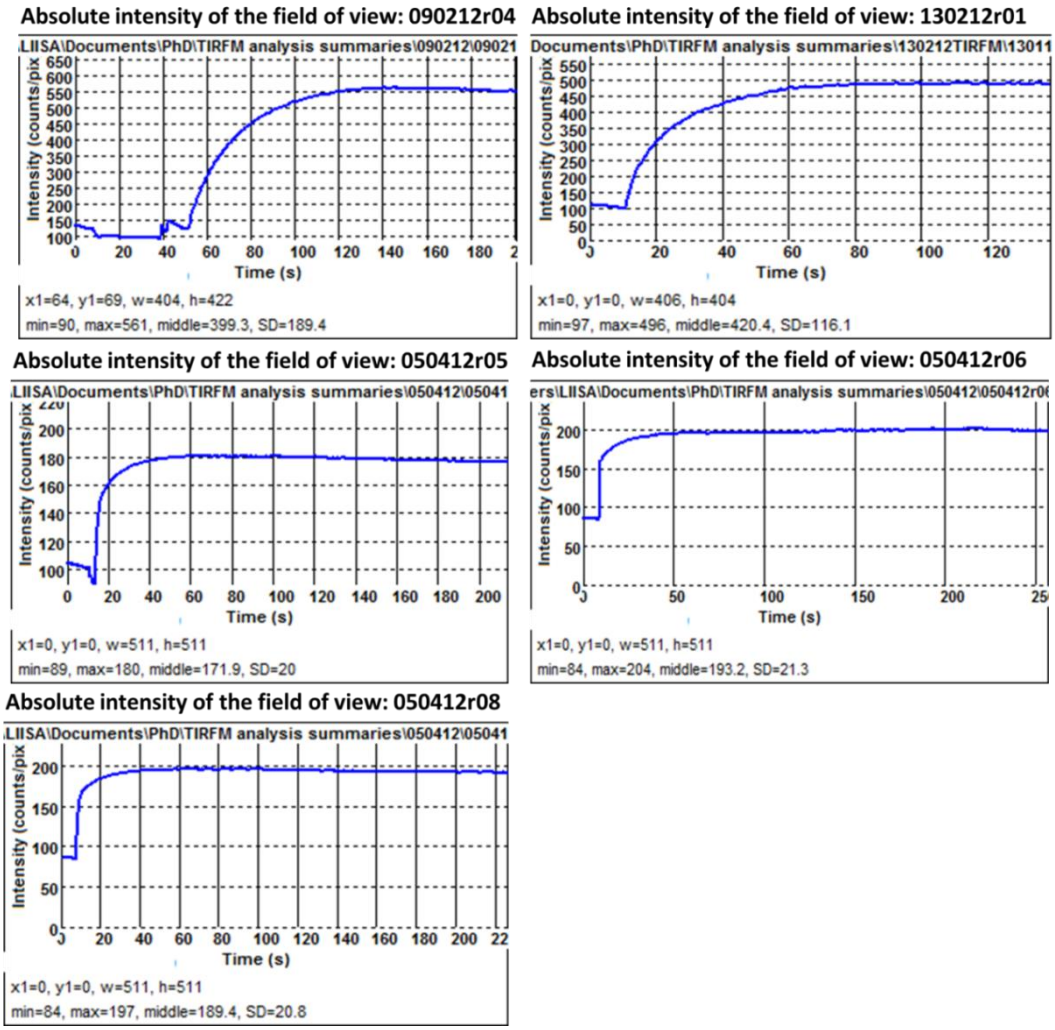

Figure 101. Absolute intensity change of the field of view during the recording.

0.5 nM Cy3B-bioPcrA(E449C): 090212r09, 130212r01 and 050412r05. 0.5 nM unlabelled bioPcrA 050412r06 and r08.

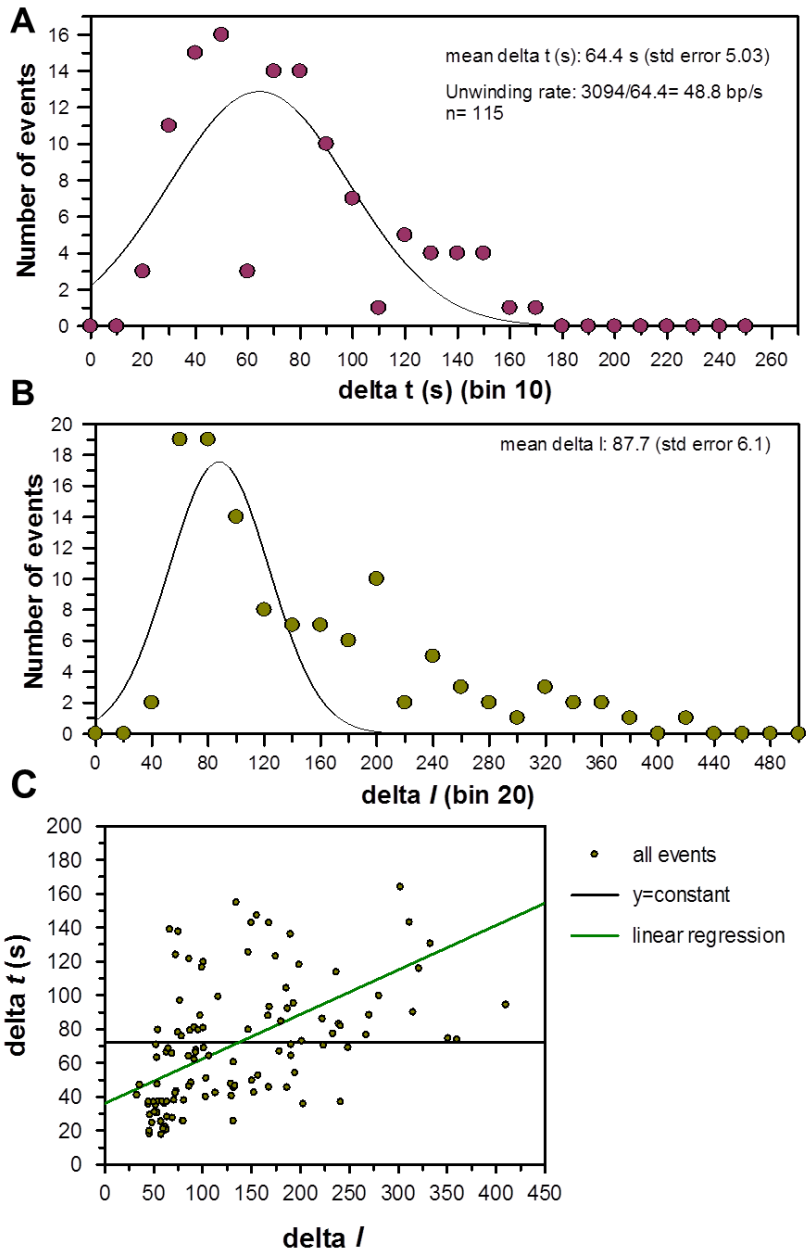

Figure 102. Distribution of unwinding events with 3094 bp plasmid with unlabelled bioPcrA.

The data were fitted to Gaussian distribution. C) Δt versus Δl plot of 3094 bp plasmid unwinding events with unlabelled bioPcrA. The data was fitted to linear regression and y=constant.

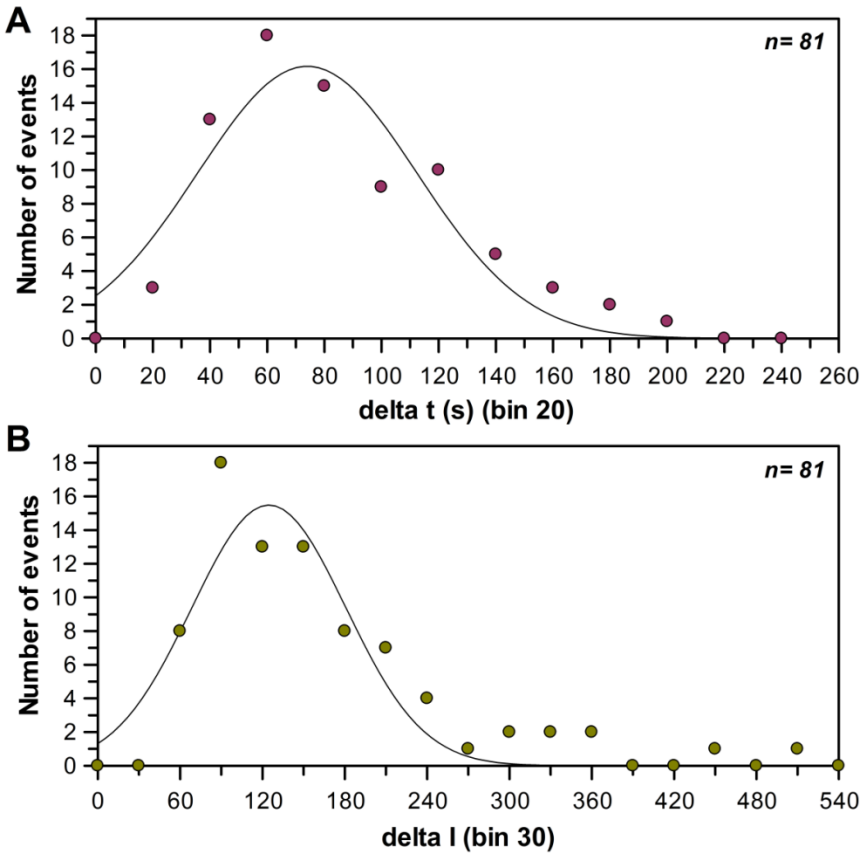

Figure 103. ΔI and Δt distributions of 3094 bp plasmid unwinding events with reduced Cy3B-bioPcrA(E449C) loading concentration.

A) Histogram of Δt distribution of events. The Gaussian fit has mean value of 74.0 s (SEM 4.3) that gives an unwinding rate of 41.8 +/- 2.4 bp s^{-1}. The variance of the fit is 38.4 (SEM 4.4). B) The histogram of ΔI distribution of events. The Gaussian fit has the mean of 124.7 (SEM 6.2). The variance of the fit is 56.1 (SEM 6.2). Record:040412r04